ABSTRACT

Title of Dissertation:	MARSH-ING THROUGH TIME: RESOLVING THE TEMPORAL AND SPATIAL VARIABILITY OF TIDAL MARSH SEDIMENT DISSOLVED ORGANIC CARBON SORPTION
	Hannah Morrissette, Doctor of Philosophy, 2021
Dissertation directed by:	Professor, Dr. Raleigh Hood Marine-Estuarine-Environmental Sciences

Tidal marsh ecosystems are among the most economically and ecologically valuable environments in the world, providing critical ecosystem services and a continuous exchange of carbon between these systems and their surrounding environments. Tidal marshes are an important overall net carbon sink, while simultaneously being a substantial source of dissolved organic carbon (DOC) to estuaries and the coastal ocean. The temporal and spatial variability in these carbon fluxes is large, difficult to measure, and currently considered to be one of the most daunting challenges to carbon exchange quantification. Sorption, despite being known as a dominant DOC exchange process at the sediment-water interface, is still

understudied in tidal marsh ecosystems, with exchange kinetics largely unquantified. This research combined observational data with sediment flux modeling to answer a suite of questions addressing sorption speed, its variability, and its impacts to DOC fluxes between sediments and adjacent waters.

Sediment flux models must incorporate sorption processes to more accurately simulate DOC fluxes between tidal marsh sediments and adjacent waters. Kinetics of these processes were quantified for the first time through a set of 24 hour sorption laboratory experiments, from which results showed that the majority of sorption processes occur rapidly, within 15 minutes of sediment exposure to water. Sorption rate parameters were determined through a numerical modeling study that simulated the laboratory experiments. These rates were used to parameterize a sediment flux model that included sorption processes formulated with varying degrees of complexity. The sorption kinetics of individual pools of DOC (colored and non-colored) were also measured, revealing that these separate pools sorb quickly but independently of one another, with preferential adsorption of humic colored DOC over time, and preferential desorption of native non-colored DOC over time. Sorption kinetics were also shown to be spatially variable within a marsh site, with adsorption decreasing with sediment depth and distance from the creek edge. This research provided important new information on sorption in tidal marsh sediments that allows these processes to be incorporated into models, which will, ultimately, facilitate efforts to simulate and quantify coastal carbon fluxes.

MARSH-ING THROUGH TIME: RESOLVING THE TEMPORAL AND SPATIAL VARIABILITY OF TIDAL MARSH SEDIMENT DISSOLVED ORGANIC CARBON SORPTION

by

Hannah Kay Morrissette

Dissertation submitted to the Faculty of the Graduate School of the
University of Maryland, College Park, in partial fulfillment
of the requirements for the degree of
Doctor of Philosophy
2021

Advisory Committee:
Dr. Raleigh Hood, Chair
Dr. Jeffrey Cornwell
Dr. William Nardin
Dr. Patrick Neale, Smithsonian Environmental Research Center
Dr. Maria Tzortziou, City University of New York
Dr. Karen Prestegaard, Dean's Representative

Acknowledgements

There are not enough words to capture the gratitude I feel towards the individuals and groups that have helped, guided, and encouraged me throughout my doctoral experience. Family, friends, and colleagues were continuously there for me, never faulting in support. It is with extreme appreciation that I thank the following:

My advisor, Dr. Raleigh Hood, for always allowing me to explore my ideas and interests to their fullest capacities.

My post-doctoral researcher, Dr. Drew Pinsonneault, who was always there with a piece of advice, a helping hand, or a great story, and never failed to make lab work a million times more fun.

My committee, with special thanks to Dr. Pat Neale, for providing constant advice, lab help, and theoretical discussions that improved the scope of the research.

My undergraduate advisors, Dr. Mel Zimmerman and Dr. Caroline Payne, for providing my first exposure to environmental science and always supporting my career.

My collaborators and site technicians, for providing guidance, logistical support, and help in the field/lab.

My lab group, and all the students of Horn Point, for providing the we-are-all-in-this-together attitude and well-deserved nights of fun.

My UMD writing group, for accountability and community through the final writing efforts.

The rest of my Horn Point family, who, for the last five years, have made me feel welcome, accepted, and appreciated.

And finally, my family and friends, who have graciously and unwaveringly listened to me rant about sediment carbon for years.

I could not accomplish half of the same things in life without this solid support team, and I leaned on all of you throughout my time here whether you knew it or not. A simple thank you is not enough, but I'll say it anyway – Thank you!

Table of Contents

List of Tables

List of Figures

Chapter 1: Introduction

Coastal wetlands, composed of many specific land cover types such as tidal marshes, mangrove forests, and seagrass beds, are some of the most ecologically and economically important ecosystems in the world. They cover an estimated 1.64×10^6 km^2 in global area (Davidson & Finlayson, 2018), providing disproportionately high levels of biodiversity and productivity for their relatively small areal extent (Najjar et al., 2018; Windham-Myers et al., 2018). Wetlands provide critical ecosystem services, such as habitat and food to thousands of aquatic and terrestrial species, regulation of coastal nutrient cycles, sequestration of atmospheric carbon, and protection from erosion and pollution (Canuel et al., 2012; Day et al., 2013; Windham-Myers et al., 2018).

Wetlands vary extensively in morphology (Bullock & Acreman, 2003; Morris et al., 2016; Pratolongo et al., 2019), composition (Bai et al., 2016; Pinsonneault et al., 2021, *in prep*; Yang et al., 2008), biodiversity (Groffman et al., 1996; Levin et al., 2001), nutrient availability (Bedford et al., 1999; Johnston et al., 2001), anthropogenic influence (Karstens et al., 2016), and extent (Davidson & Finlayson, 2018). The biogeochemical characteristics also vary dramatically in wetlands with depth of the sediment and the distance from adjacent waters. This variability includes changes in microbial community composition, redox potential, and hydrological influences (Han et al., 2020; Holden, 2005; Steinmuller et al., 2019; Thomas et al., 2009; Zhou et al., 2017). These differences in coastal wetland characteristics determine their functionality and importance for providing ecosystem services.

Several studies have attempted to quantify the value of wetland ecosystem services. Costanza et al. (1997) estimated that the global value of the wetland ecosystem services was almost $15 trillion, and more recently, Kirwan & Megonigal (2013) estimated these services to be worth $10,000 per hectare. Considering their substantial contribution to floral and faunal diversity and environmental health, losses of wetlands can have serious negative consequences, including extinction of species and decreased capacity for mitigation of climate change. With approximately 40% of the global population living on or near the coastline, these coastal wetland environments will continue to be under human-induced pressures that result in declines in their expanse and health. Yet, wetlands continue to adapt to multiple stressors such as land use change, sea level rise, decreased sediment supply, nutrient pollution, invasive species, and more. Enhancing our knowledge of biogeochemical cycling within these wetlands will lead to better understanding of the impact of these stressors on the important ecosystem services that wetlands provide.

As one of the most productive ecosystem types on earth, wetlands have a strong influence on the coastal carbon cycle, the dynamics of which are depicted in Figure 1.1 (from the Second State of the Carbon Cycle Report; SOCCR2, Windham-Myers et al., 2018). The processes that affect the wetland-atmospheric-estuarine carbon cycle are numerous and complex. They include allochthonous input from upland sources, autochthonous production via photosynthesis, atmospheric carbon sequestration, photochemical degradation, microbial respiration, organic matter remineralization, sorption, and others (Bauer et al., 2013; Cai 2011; Canuel et al.,

2012; Herrmann et al., 2015; Kleber et al., 2021; Mitsch et al., 2013; Najjar et al., 2018; Ward et al., 2017).

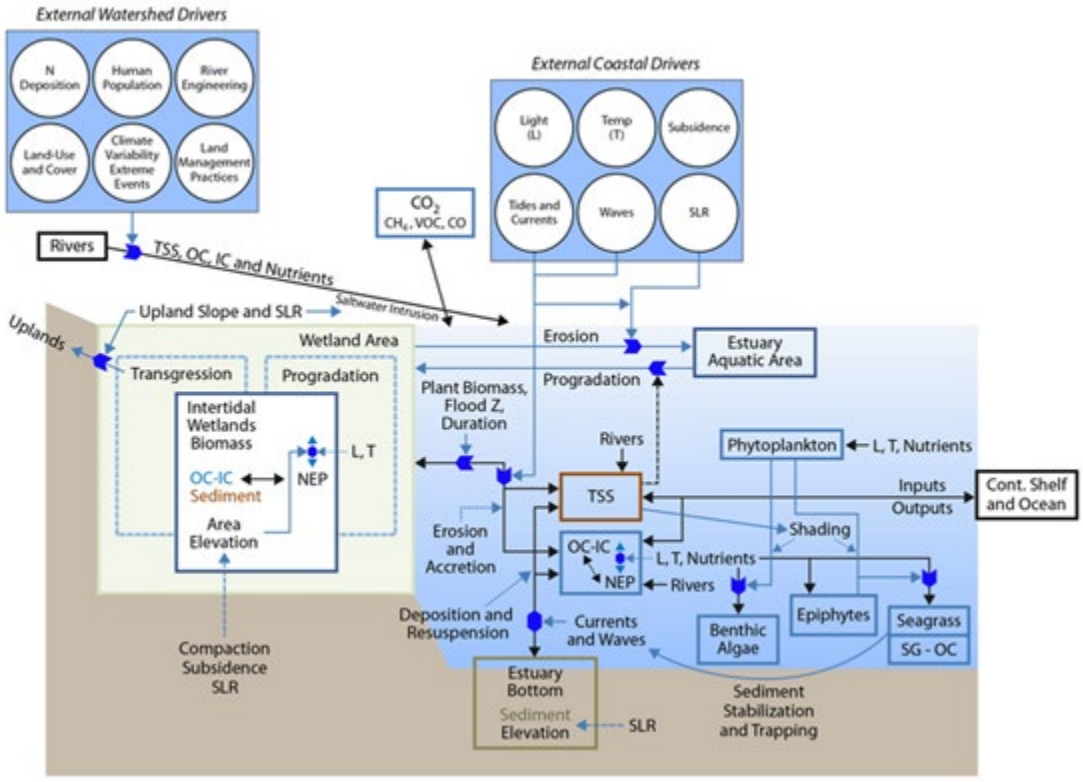

Figure 1.1 Conceptual diagram of coastal carbon dynamics from SOCCR2, 2018.

Tidal wetlands are a net carbon sink, but they are also a source of organic carbon to adjacent estuarine and coastal waters as depicted in Figure 1.2 for North America. Tidal wetlands pull carbon from the atmosphere, burying it into the sediments (Chmura et al., 2003; Herrmann et al., 2015; Mitsch et al., 2013; Nahlik & Fennessey, 2016; Najjar et al., 2018). They are extremely effective at carbon-capture, sequestering an estimated ~9 TgC yr^{-1} in North America alone (Windham-Myers et al., 2018), and up to 0.22 PgC yr^{-1} globally (Spivak et al., 2019). Wetlands are disproportionately efficient at sediment carbon sequestration and long-term

accumulation considering their limited extent (Chmura et al., 2003; Najjar et al., 2018; Pendleton et al., 2012; Windham-Myers et al., 2018). The sediment carbon accumulation leads to massive carbon stocks in wetland sediments, estimated to be as much as ~1.4 PgC in just the uppermost 1m of North American tidal wetland sediments alone (Windham-Myers et al., 2018).

Although wetlands are hotspots for net long-term carbon storage, they are particularly important sources of dissolved organic carbon to their surrounding estuarine and coastal waters (Barrõn & Duarte, 2015; Bauer et al., 2013; Cai 2011; Childers et al., 2000; Herrmann et al., 2015; Najjar et al., 2018; Tzortziou et al., 2008, 2011), resulting in as much as 80% of the annual lateral DOC and dissolved inorganic carbon (DIC) export to the ocean (Wang & Cai, 2004; Wang et al., 2016). The flux of DOC from wetland sediments to the surrounding waters varies daily, seasonally, and interannually, affecting downstream biogeochemistry and supporting coastal food webs (Bolan et al., 2011; Cai et al., 2019; Chen & Hur, 2015; Day et al., 2013; Najjar et al., 2018; Windham-Myers et al., 2018; Zhuang & Yang, 2018). Tidal cycles control hourly exchange, with different types of DOC released during ebbing vs. flooding tides (Tzortziou et al., 2008, 2011). Seasonally, DOC is continuously exported from marsh sediments, with peaks in flux observed during the breakdown of plant matter in late summer/early fall (Tzortziou et al., 2008). Significant interannual variability in DOC flux from marshes is also observed, often controlled by variability in freshwater flows that are exacerbated by storms (Windham-Myers et al., 2018).

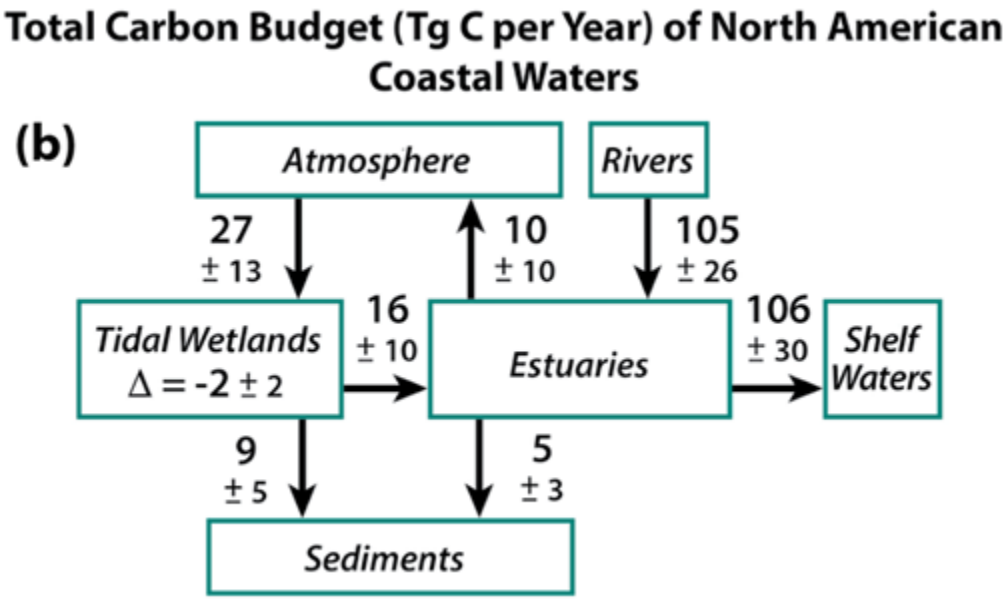

Figure 1.2 Total carbon budget estimated from many collated regional studies in North American coastal waters, taken from the SOCCR2 (2018).

Tidal marshes, in particular, are characterized by carbon sequestration and export, serving both as net sinks of carbon and important sources of DOC to adjacent waters (Figure 1.3) (Jordan & Correll, 1999; Najjar et al., 2018; Neubauer & Anderson, 2003; Tobias & Neubauer, 2009; Windham-Myers et al., 2018). Tidal marsh carbon accumulation rates have been estimated to be as high as 10.2 TgC yr^{-1} across global salt marshes (Ouyang & Lee, 2014). When analyzing the specifics of that carbon exchange, it has been shown that marsh sediments are important regulators of DOC quantity *and* quality, influencing the type of DOC that is exchanged over time (Clark et al., 2008; ◦Morrissette et al., *in prep*; Osburn et al., 2015; Pinsonneault et al., 2021; Tzortziou et al., 2008).

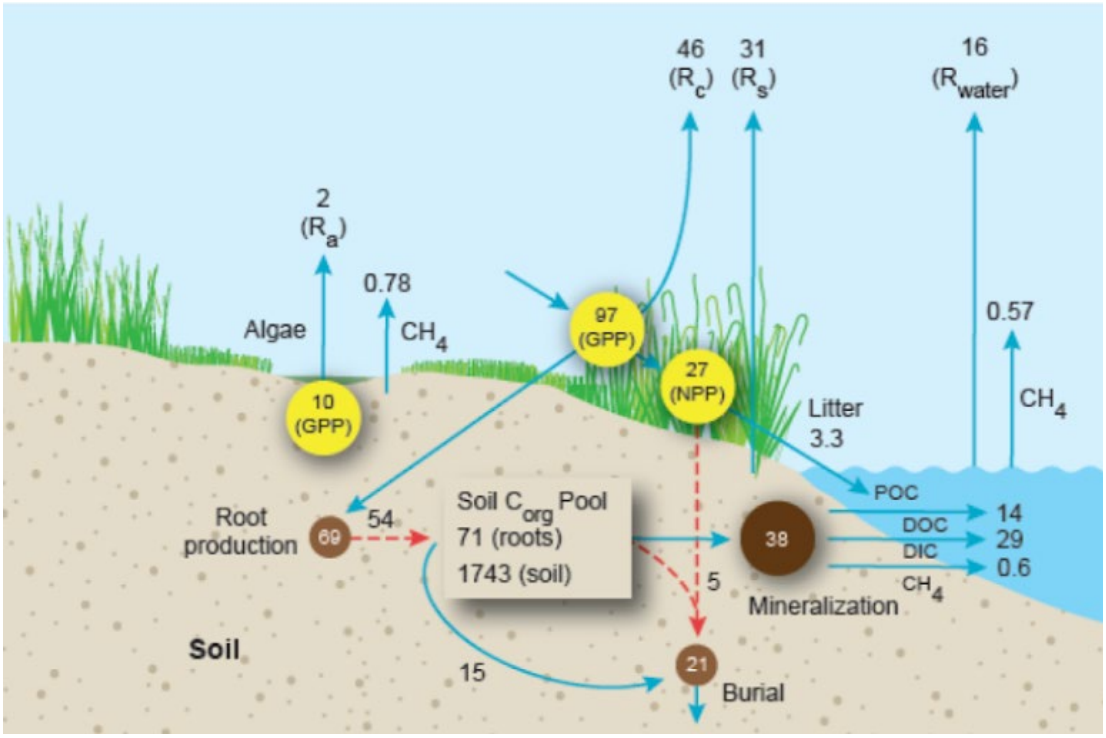

Figure 1.3 Detailed estimates of all carbon fluxes within the salt marsh ecosystem and between the atmosphere and surrounding waters, showing marshes as a specific lateral source of DOC, taken from Alongi (2020).

Colored dissolved organic matter (CDOM), or the fraction of DOM that absorbs light in the visible and UV wavelengths, affects water column light attenuation, productivity, and water quality (Osburn et al., 2015; Tzortziou et al., 2015; Wang et al., 2007). Marshes are known to be a net source of CDOM to adjacent waters, the composition of which is highly variable depending on source, microbial activity, currents, anthropogenic influence, and more. Optical properties can provide insights into CDOM composition, which has been a useful tool for tracking the DOC quality, fluxes, and transformations in estuarine and coastal waters (Fellman et al., 2010; McKnight et al., 2001; Stedmon & Nelson, 2014; Tzortziou et al., 2008).

There are many competing biotic and abiotic processes that influence DOM exchange between the water column and marsh sediments, some of which include microbial hydrolysis, diffusion, photochemical degradation, and sequestration. One abiotic process that has long been considered important for rapid carbon exchange in the sediments is abiotic sorption, which both releases (desorption) and captures (adsorption) carbon over time (Bader et al., 1960; Kalbitz et al., 2010; Kleber et al., 2021; Knobloch et al., 2021; Kothawala et al., 2008, 2009, 2012; [b]Morrissette et al., *in prep*; Pinsonneault et al., 2021; Qualls & Haines, 1992; Qualls & Richardson, 2003; Shaker et al., 2012; etc.). There have been many studies that have established the importance of sorption, and adsorption is now considered one of the most effective pathways of long-term carbon storage in marsh sediments (Bader, 1960; Keil & Mayer, 2014; Kleber et al., 2021; Kothawala et al., 2009), while desorption has been shown to be dominant over biologically-mediated degradation (hydrolysis) of particulate organic matter (Guggenberger & Kaiser, 2003; Qualls & Haines, 1992; Qualls & Richardson, 2003; Tavakkoli et al., 2014).

The kinetics of sorption are difficult to measure, with many studies suggesting that the processes are rapid (Gu et al., 1994; Guggenberger & Kaiser, 2003; Kothawala et al., 2009; McKnight et al., 1992; Pinsonneault et al., 2021; Qualls, 2000), but few studies have actually quantified rates of adsorption or desorption (Kaiser & Zech, 1998; [c]Morrissette et al., *in prep*; Qualls & Haines, 1992; Shaker et al., 2012). These few studies agree that abiotic sorption happens extremely quickly, with ~75% of the processes occurring within 15 minutes (Kaiser & Zech, 1998; [b]Morrissette et al., *in prep*), and equilibrium occurring within 30 minutes (Shaker et

al., 2012). Despite its proven importance, Pinsonneault et al. (2021) reported the results of the first sorption incubations on tidal marsh soils. These incubations were batch isotherms, measuring net DOC exchange due to adsorption and desorption over 24 hours to provide information on the impact of soil properties and initial conditions on sorption processes. Due to these results of the tidal marsh sorption isotherm incubations, it is now shown that marsh sediment characteristics such as salinity, mineral content, soil organic matter, and initial DOC concentration all affect DOC sorption (Pinsonneault et al., 2021). These isotherm results are consistent with kinetic sorption experiments from other types of soils that revealed rapid sorption kinetics (Kaiser & Zech, 1998; Shaker et al., 2012), which suggests that sorption processes in tidal marshes may be equally as fast.

Sorption processes almost certainly play an essential role in determining coastal carbon fluxes, stocks, and budgets. However, there are still large gaps in the understanding of sorption processes and kinetics, which make it impossible to predict how these processes will be altered under changing environmental conditions. Using a combination of laboratory experiments and sediment flux modeling, the research described in this dissertation addresses gaps in the understanding of sorption processes in tidal marsh sediments. Five dissertation chapters address the following principal questions:

Question 1: How does sediment flux model behavior change with the addition of sorption processes? Despite the evidence suggesting the critical role of sorption in coastal carbon cycling, sediment flux models do not yet include adsorption and desorption pathways in model formulations that simulate organic matter exchange

and transformation between the sediments and the water column. This chapter examined the impacts of adding sorption processes of varying levels of complexity to a well-developed and extensively applied sediment flux model (SFM; Di Toro, 2001). It was hypothesized that adding sorption into the model would increase DOC flux into the water column.

Question 2: How quickly does DOC sorption occur between marsh soils and the overlying water column, depending on sediment characteristics and initial conditions? Sorption kinetics had yet to be measured for tidal marsh sediments. This chapter reports some of the first kinetic sorption experiments on tidal marsh sediments that quantify the speed of the sorption processes and how they are influenced by the biogeochemical properties of the soil. It was hypothesized that tidal marsh sorption would be fast and controlled by salinity, DOC concentration, and mineral content.

Question 3: Can experimental simulations in a simplified model inform our understanding of sorption process complexity for SFM model parameterization? The experiments of the previous chapter were designed to provide sorption rate information for marsh sediments. This chapter describes the construction and parameterization of three "simplified" models that were designed to reproduce the kinetic sorption experiments and provide rate information. It was hypothesized that the simplified model would provide kinetic rates that can be used to parameterize the sorption formulations that were added to the SFM, and also provide additional insights into the dynamics of the sorption reactions.

Question 4: How do sorption kinetics vary with DOC composition? While previous chapters focused on bulk DOC fluxes, this chapter examined the kinetics and subsequent influences on sorption of two different DOC pools: colored DOC (CDOC) and non-colored DOC (NCDOC). It was hypothesized that the two pools would adsorb and desorb at different rates, and potentially in different directions, depending on the initial conditions.

Question 5: Which biological, chemical, or physical sediment characteristics control spatial variability in dissolved organic carbon sorption processes? The experimental and modeling work described in the other chapters of this dissertation focused on DOC kinetics of sediments from two different marshes. This chapter delves into the DOC kinetics of sediment samples taken from different locations within one marsh. It was hypothesized that vertical depth and distance from the creek edge would significantly influence sorption kinetics, and that spatial variations in the kinetics could be related to the biogeochemical properties of the sediments.

Chapter 2: The reparameterization of a sediment flux model to include sorption processes

Abstract

Adsorption and desorption of dissolved organic matter (DOM) in marsh sediments are important processes in coastal wetland systems which influence the ability of wetlands to abiotically regulate the coastal carbon cycle. However, current sediment flux models do not include these DOM transformations due to their poorly characterized interactions and lack of empirical data to validate these changes. To further the understanding and characterization of the influential processes on sediment DOM, multiple versions of a sediment flux model (SFM) were built with increasing complexity based on DOM reaction rate experiments. Model simulations were run under varying forcing conditions and compared with a 12.5-year time series of previous modeling studies in the Chesapeake Bay to determine the effect of the new formulations on carbon flux simulations. Results indicated that DOM sorption increased the sensitivity of the model's output to the input parameters. With time-varying forcing values, the addition of sorption processes reversed the bulk DOC flux to a continuous release of DOC into the water column from the sediments with fluxes highest in summer. It also increased the DOC efflux of each individual lability pool and showed that non-colored DOC (NCDOC) was always released to the water column at a higher magnitude than colored (CDOC). The addition of sorption more closely resembled what is observed of sediment-water column DOC flux in marsh ecosystems. These model formulations provided a new characterization of DOM

sediment biogeochemical processes which could be used to guide field or laboratory experiments.

Introduction

The export of organic carbon from estuaries into surrounding ocean environments is a large and important flux of the coastal carbon cycle (Clark et al., 2008; Herrmann et al., 2015; Najjar et al., 2018; Windham-Myers et al., 2018; Tzortziou et al., 2008, 2011; Wang & Cai 2004; Wang et al., 2016), with the most recent estimates reporting 0.1 PgC yr^{-1} for North American coastal waters (Windham-Myers et al., 2018) and up to 0.5 PgC yr^{-1} globally (Bauer et al., 2013; Cai, 2011). A substantial portion of that estuarine net flux is derived from coastal wetland lateral organic carbon export, which is a large source of dissolved organic carbon (DOC). Coastal wetlands are also hotspots for carbon sequestration (Chmura et al., 2003; Nahlik & Fennessey, 2016; Mitsch et al., 2013; Najjar et al., 2018), i.e., their sediment is composed of massive carbon stocks, much of which is in the upper 1m (estimated at ~1.9 PgC in North American wetland sediments; Windham-Myers et al., 2018) and therefore potentially available for exchange. These wetland sediments are a potentially important DOM source to estuaries and the coastal ocean (Bauer et al., 2013; Burdige, 2007; Maher & Eyre, 2010; Raymond & Spencer, 2015; Ward et al., 2017)

Sediment flux models track the transformation and transport of organic matter, nutrients, and other water constituents in many different environments over a wide range of time scales (Burdige et al., 2016; Di Toro, 2001). While a few models have integrated DOM flux from the sediments (Burdige et al., 2016; Yurova et al., 2008), only one three-dimensional coupled hydrodynamic-biogeochemical model has been modified to simulate wetland-estuary DOM exchanges and transformations

(Clark et al. 2017). This well-exercised sediment flux model (hereafter the SFM) simulates sediment organic matter and nutrient fluxes in a one-dimensional two-layer application (Di Toro, 2001; Brady et al., 2013; Testa et al., 2013). It was recently modified to incorporate dissolved organic matter (DOM) intermediary pools between particulate organic matter and its remineralized products (Clark et al., 2017). The addition of DOM to the SFM improved model performance for simulating estuarine nitrate flux, ammonium flux, and sediment oxygen demand over time (Brady et al., 2013; Clark et al., 2017; Testa et al., 2013), providing evidence that these DOM water column-sediment fluxes need to be included in order to improve model accuracy.

However, in this new version of the SFM, DOM was created only via biologically-mediated hydrolysis of particulate organic matter (POM), i.e., abiotic sorption processes were not included even though they are known to regulate organic matter fluxes in coastal sediments (Kleber et al., 2021; Kothawala et al., 2009; Liu & Lee, 2007; Pinsonneault et al., 2021; Qualls & Richardson, 2003; Spivak et al., 2019). Moreover, most sediment flux models (including the SFM) focus on estuarine and ocean sediment-water column exchanges and dynamics, and are not formulated for wetland ecosystems, even though wetland-estuarine DOM cycling is an important component of the coastal carbon cycle, as discussed above. More focus is needed on modeling the specific processes that are known to affect DOM pools and fluxes in wetland sediments.

Adsorption and desorption in marsh sediments are important processes that influence DOM exchanges in wetland systems (Kleber et al., 2021; [b,c,d]Morrissette et al., *in prep*; Pinsonneault et al., 2021). Sorption processes occur continuously in

sediments, the rates of which are rapid, and they are determined by physical and chemical factors (Dahlgreen & Marrett, 1991; Kaiser & Zech, 1998; Kothawala et al., 2009; [b]Morrissette et al., *in prep*; Qualls & Haines, 1992; Shaker et al., 2012). DOM desorption is the dominant transformation process that results in release of DOM from the marsh sediment, while adsorption is the reverse reaction that binds DOM (using several chemical pathways) to marsh sediments. It has been shown that hydrolysis, the biological degradation of POM, is a minor process compared to abiotic sorption (Qualls & Richardson, 2003). The magnitude of these sorption reactions vary over time and space due to variations in organic matter content, metal oxide concentrations, pH, flow, and sediment type (Clark et al., 2017; Groeneveld et al., 2020; Jardine et al., 1989; Kaiser & Guggenberger 2000, 2003; Kaiser et al., 1996, 2001; Keil et al., 1994; Kothawala et al., 2008, 2009, 2012; [b,d]Morrissette et al., *in prep*; Pinsonneault et al., 2021; Shields et al., 2016; Yurova et al., 2008).

In this study, sorption processes were incorporated into the SFM using several different formulations with increasing levels of complexity to 1) examine how the addition of these sorption processes influence model behavior, and 2) determine how the sorption rate parameters impact the model solutions. It is shown that incorporation of sorption processes into the SFM can significantly impact SFM simulation results, and that the magnitude of these impacts is strongly dependent upon the complexity of the sorption formulations and the magnitude of the rate parameters. It is also shown that the addition of sorption processes to the SFM using rate parameters derived from marsh soils could result in model-simulated fluxes that are more consistent with DOC fluxes observed in the field.

Methods

Four new model formulations for DOC adsorption and desorption were added to the Clark et al. (2017) version of the SFM, which built on previous formulations (see Brady et al., 2013; Testa et al., 2013 for full formulations) by including DOM as an intermediate state variable to explicitly simulate the breakdown of particulates through hydrolysis, before subsequent remineralization, to account for DOM in sediment flux budgets. This SFM formulation models DOM concentration and flux via temperature-dependent mass transfer between sediment layers and oxygen-dependent diffusion with the overlying water column. This formulation was implemented at three Chesapeake Bay stations (2 estuarine, 1 riverine), and validated with ammonium, nitrated, and sediment oxygen demand observational flux values (Boynton & Bailey, 2008). Four new models, which are listed below along with the original model (Clark et al., 2017 version) in order of increasing complexity, were coded to include additional processes of sorption between the intermediate DOM state variables and particulates, to increase the ways in which the pools can interact. They were named as follows with conceptual diagrams below:

1. *Hydrolysis* - original model formulation with hydrolysis of POM, no sorption processes
2. *Adsorption* - addition of the abiotic DOM to POM pathway of adsorption
3. *Desorption* - addition of the abiotic POM to DOM pathway of desorption

4. *Bound* - addition of sorption that occurred not only between POM and DOM, but also between DOM and "bound" pools in both sediment layers

5. *Organic/Inorganic* - addition of sorption that occurred between specified inorganic and organic "bound" pools

Model Formulations

Formulation 1: Hydrolysis

The original SFM formulation (Figure 2.1) from Clark et al. (2017) consists of an overlying water column which acts as a source or sink (J_{in}) of DOM and DIM to a thin, top aerobic layer of sediment (H_1, ~1mm, time-dependent), or as a source of POM to a thick deeper anaerobic layer of sediment (H_2, 10cm) (layer proportions in conceptual diagrams are not to scale). POM is converted to DOM in the deeper layer via biologically-mediated hydrolysis (K_h). DOM is converted to dissolved inorganic matter via remineralization (K_r) in both layers, and DOM and DIM can diffuse across layers (KL_{01}, KL_{12}) with the direction determined by the concentration gradient. POM, DOM, and DIM can also be lost from the deep layer via burial (W_2).

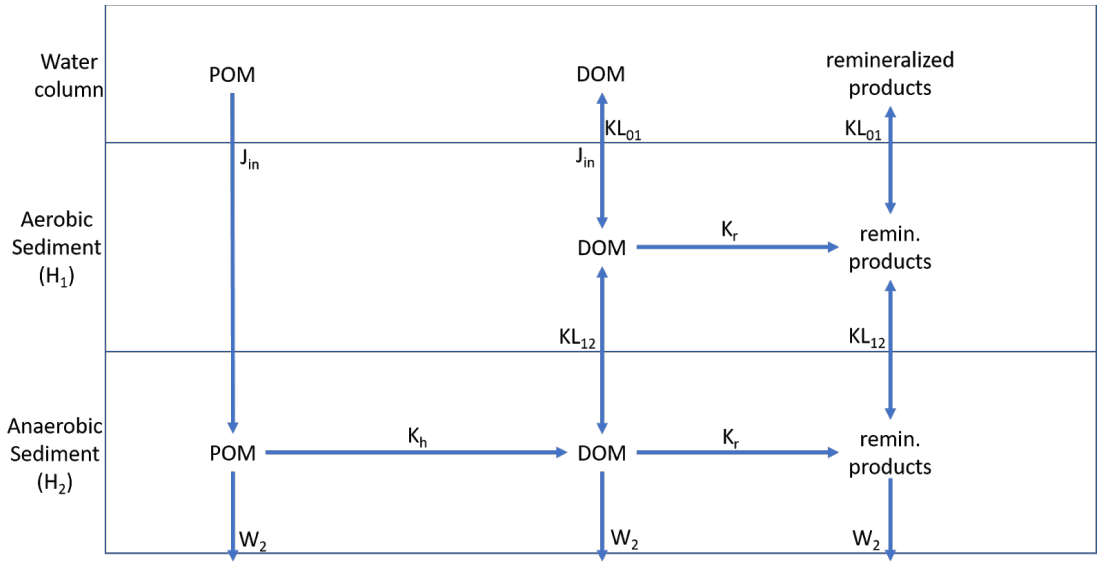

Figure 2.1. Conceptual diagram of formulation 1, adapted from Clark et al. (2017) and Di Toro (2001), depicting the major processes between organic and inorganic matter pools in the SFM.

Formulation 2: Adsorption

DOM can recombine with POM via a variety of processes, including adsorption, aggregation, and occlusion (Keil & Mayer, 2014). In formulation 2, an explicit pathway was provided that allows DOC to recombine with POC (red arrow in Figure 2.2). This pathway is referred to as "adsorption" even though it represents all processes that can cause a reentry of DOM into the POM pool.

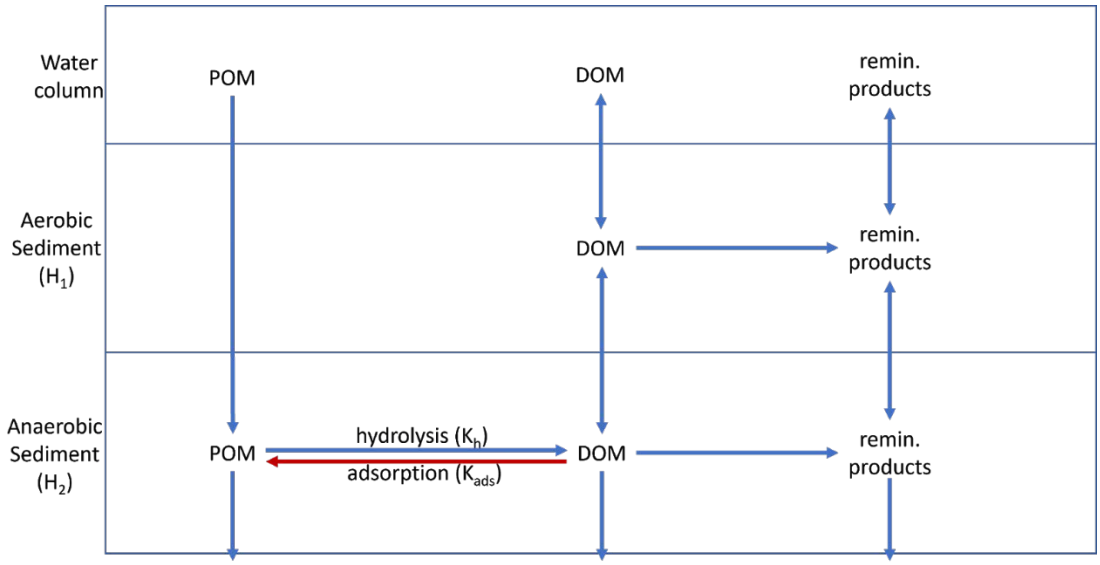

Figure 2.2: Conceptual diagram of SFM formulation 2.

Formulation 3: Desorption

With formulation 2, the model processes between the anaerobic sediment layer POC and DOC pools are simple reversible reactions; each direction encompassing a variety of different theoretical processes. Considering that the biotic and abiotic degradation of POC most likely have different rates, with desorption hypothesized to be dominant ([b]Morrissette et al., *in prep*; Qualls & Richardson, 2003), the second formulation separates these by adding in an explicit reaction for desorption (Figure 2.3). Red arrows in Figure 2.3 show the differentiation.

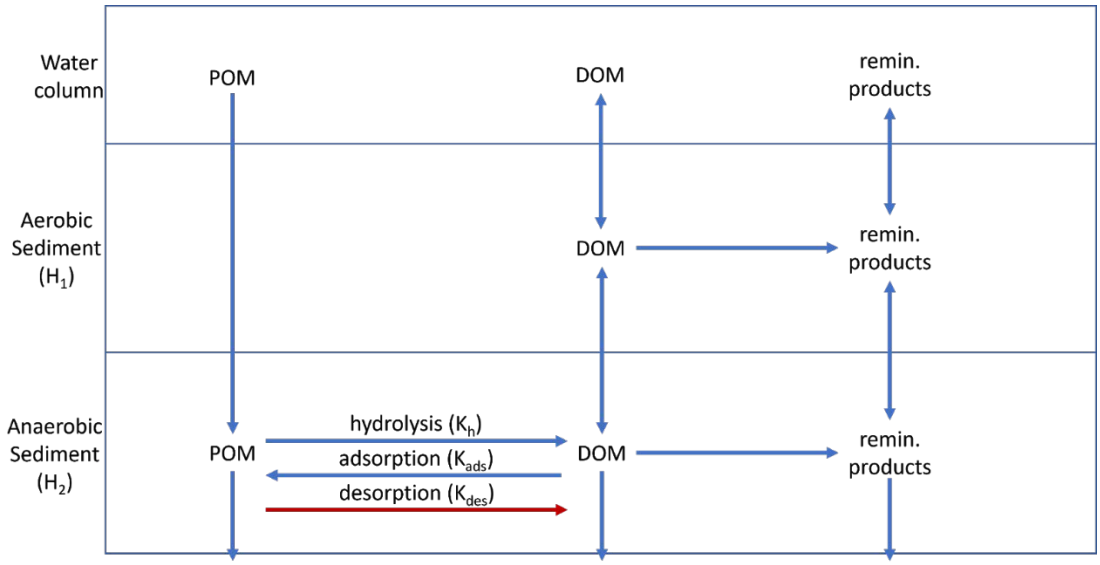

Figure 2.3: Conceptual diagram of SFM formulation 3.

Formulation 4: Bound

Here the DOC pools in both sediment layers can adsorb and desorb to and from a separate "bound DOC" pool in addition to the second layer POM (Figure 2.4). This formulation allows specification of different reaction rates for sorption processes that involves substrates other than POM, such as inorganic minerals or metals, and it lets adsorption and desorption happen in both sediment layers.

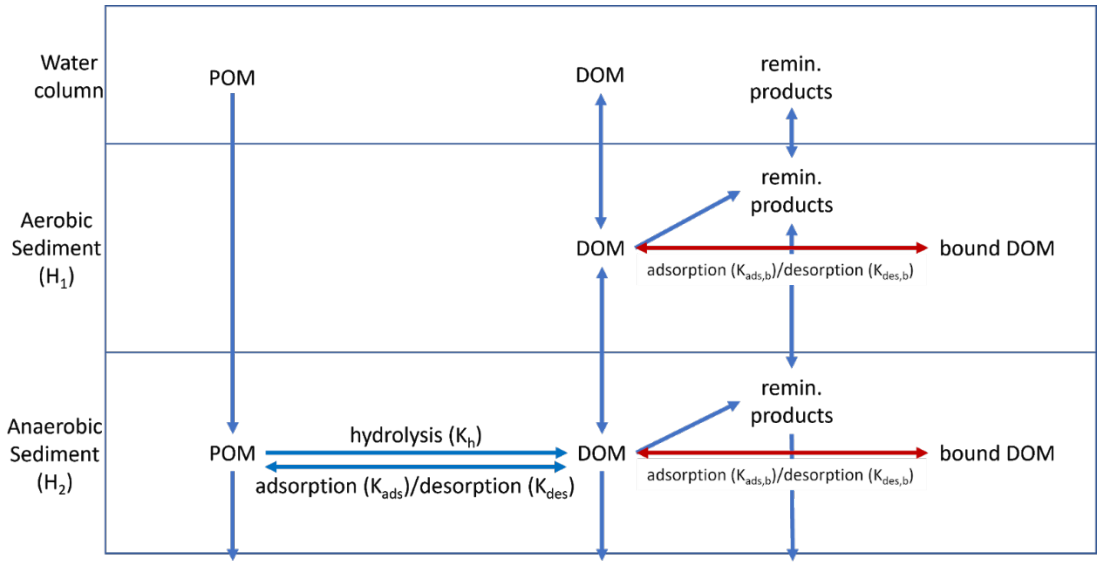

Figure 2.4: Conceptual diagram of SFM formulation 4.

Formulation 5: Organic/Inorganic

In this formulation, additional pathways were added to allow DOC adsorption to and desorption from either organic or inorganic substrates in both sediment layers (Figure 2.5). Sorption to/from POM and sorption to/from organic substrates are differentiated in the sense that the bound-to-organics pool cannot be hydrolyzed, and the adsorption to POM pathway can represent other processes such as aggregation and/or precipitation.

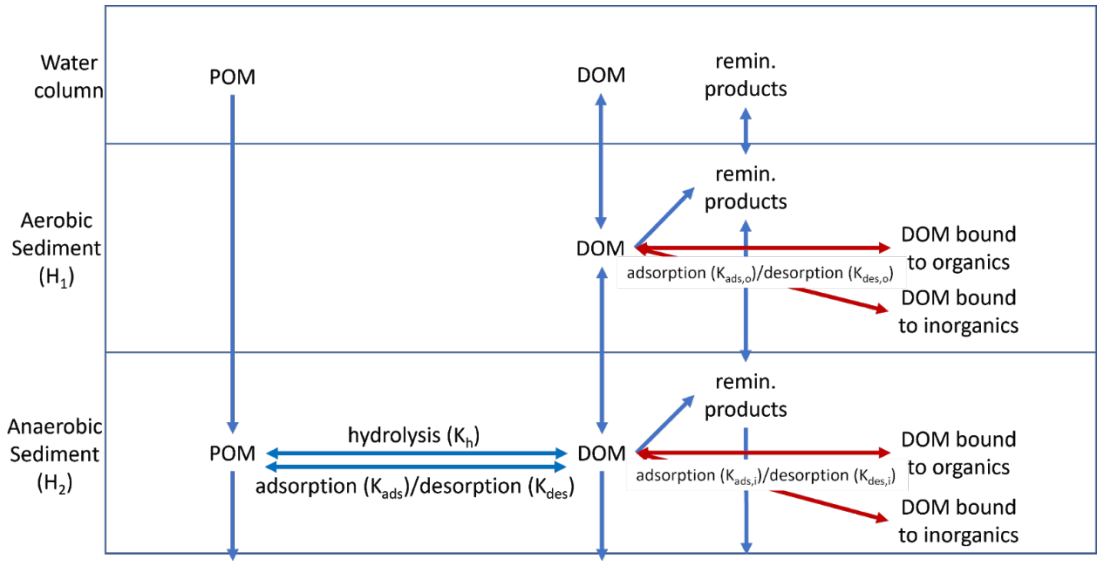

Figure 2.5: Conceptual diagram of SFM formulation 5.

Equations

The following subsections describe the general mathematical representations of the aforementioned sorption models (Figs. 2.1-5). In all equations, x represents lability levels of 1) labile, 2) semilabile, and 3) refractory pools. DOM represents the concentrations of colored (C) or non-colored (NC) dissolved organic carbon (DOC), nitrogen (DON), or phosphorus (DOP) (g m^{-3}). Refer to Appendix B for a fuller list of equations.

Formulation 1: Hydrolysis

DOM was formulated into the SFM as a change in concentration over time in both the aerobic and anaerobic sediment layers due to layer-specific reactions (Clark et al., 2017). Aerobic DOM concentration is calculated as:

(a) $RHS_{TMP} = -Krx * DOMx_{1,t-1} * H_1 + KL_{12}\left(DOMx_{2,t-1} - DOMx_{1,t-1}\right) - KL_{01}\left(DOMx_{1,t-1} - DOMx_{0,t-1}\right)$

(b) $DOMx_1 = DOMx_{1,t-1} + RHS_{TMP}\frac{DT}{H_1}$

where RHS_{TMP} is a temporary intermediate variable, Kr (d^{-1}), KL_{01} (m d^{-1}), and KL_{12} (m d^{-1}) are the remineralization rate, water column - aerobic layer diffusion coefficient, and the aerobic - anaerobic layer diffusion coefficient, respectively. Layer is denoted by subscript, with 0, 1, and 2 respectively representing the water column, aerobic layer, and anaerobic layer. H_1 (m) is aerobic layer depth. The change in anaerobic DOM concentration over time is calculated similarly to layer 2, with the addition of bottom layer specific interactions:

(c) $RHS_{TMP} = -Krx * DOMx_{2,t-1} * H_2 - KL_{12}\left(DOMx_{2,t-1} - DOMx_{1,t-1}\right) + Khx * POMx_{t-1} * H_2 - \omega_2 DOMx_{2,t-1}$

(d) $DOMx_2 = DOMx_{2,t-1} + RHS_{TMP}\frac{DT}{H_2}$

where Kh (d^{-1}) and ω_2 (m d^{-1}) are the hydrolysis and burial rate coefficients, and POMx is the particulate concentration (g m^{-3}). That POMx concentration is found via:

(e) $RHS_{TMP} = J_{POCx} * f_{POCx} - Khx * POMx_{t-1} * H_2 - \omega_2 POMx_{t-1}$

(f) $POMx = POMx_{t-1} + RHS_{TMP}\frac{DT}{H_2}$

where J_{POCx} (g m^{-2} d^{-1}) is the flux of POM being deposited into the sediments from the water column and f_{POCx} is the lability fractionation coefficient. Temperature dependency on the hydrolysis, remineralization, and diffusion coefficients (Kh, Kr, KL) is calculated through a temperature control parameter that is reaction-specific. Temperature control is calculated as:

(g) $Rx = Kx * \theta x^{T-20}$

where Rx represents one of the three above reactions, Kx is the specific version of each reaction based on lability and compound, θ is the temperature control parameter, and T is the sediment temperature (°C) at that time step. Full formulation of this model, and all equations related to carbon, can be found in Appendix B.

Formulation 2: Adsorption

Adsorption was first coded into the model (assuming a linear model of adsorption) to provide a reversible reaction between the particulate and dissolved organic matter pools. Previously, in the anaerobic layer, POM could just be biologically hydrolyzed, and DOM was not allowed to return to the POM pool. Second-layer DOM concentration ($DOMx_2$) was calculated as in Equations c & d above:

(1) $$RHS_{TMP} = -Krx * DOMx_{2,t-1} * H_2 - KL_{12}\left(DOMx_{2,t-1} - DOMx_{1,t-1}\right) + Khx * POMx_{t-1} * H_2 - \omega_2 DOMx_{2,t-1} - KDOMadsx * DOMx_{t-1} * H_2$$

(2) $$DOMx_2 = DOMx_{2,t-1} + RHS_{TMP}\frac{DT}{H_2}$$

where the main addition to the equation is the loss of DOM from KDOMads, the adsorption rate coefficient (d^{-1}).

For particulates, it is the reverse process of adding the amount gained from adsorption of DOM at the previous time step to the other fluxes associated with the POM pool ($g\ m^{-3}$) as in Equations e & f:

(3) $$RHS_{TMP} = J_{POCx} * f_{POCx} - Khx * POMx_{t-1} * H_2 - \omega_2 POMx_{t-1} + KDOMadsx * DOMx_{2,t-1} * H_2$$

(4) $$POMx = POMx_{t-1} + RHS_{TMP}\frac{DT}{H_2}$$

which calculates the current concentration of POM. The flux of DOM into the water column due to diffusion from sediment layer 1 ($DOMx_{0,flux}$, g m^{-2} d^{-1}) is calculated as:

(5) $DOMx_{0,flux} = KL_{01}(DOMx_1 - DOMx_0) * DT$

This equation is used in all following formulation for water column flux.

Formulation 3: Desorption

The next formulation of the model includes desorption, which combines with hydrolysis to increase the amount of POM transformed to the dissolved pool. The concentration of POM is calculated through a loss due to desorption:

(6) $RHS_{TMP} = J_{POCx} * f_{POCx} - Khx * POMx_{t-1} * H_2 - \omega_2 POMx_{t-1} - KPOMdesx * POMx_{t-1} * H_2 + KDOMadsx * DOMx_{2,t-1} * H_2$

(7) $POMx = POMx_{t-1} + RHS_{TMP} \frac{DT}{H_2}$

where KPOMdes (d^{-1}) is the new desorption rate coefficient, which is also then added to the previous to calculations of the current concentration of DOM:

(8) $RHS_{TMP} = -Krx * DOMx_{2,t-1} * H_2 - KL_{12}(DOMx_{2,t-1} - DOMx_{1,t-1}) + Khx * POMx_{t-1} * H_2 - \omega_2 DOMx_{2,t-1} - KDOMadsx * DOMx_{2,t-1} * H_2 + KPOMdesx * POMx_{t-1} * H_2$

(9) $DOMx_2 = DOMx_{2,t-1} + RHS_{TMP} \frac{DT}{H_2}$

Formulation 4: Bound

For the fourth formulation, the model includes the new "bound" DOM state variables in each sediment layer (DOMb), with adsorption and desorption fluxing between them and the free DOM pools. The concentrations of both free and bound

DOM in both layers are found by cumulative gains and losses. In the aerobic sediment layer:

(10) $RHS_{TMP} = -Krx * DOMx_{1.t-1} * H_1 - KDOMbadsx * DOMx_{1,t-1} * H_1 + KDOMbdesx * DOMbx_{1,t-1} * H_1 + KL_{12}(DOMx_{2,t-1} - DOMx_{1.t-1})$

(11) $DOMx_1 = DOMx_{1,t-1} + RHS_{TMP}\frac{DT}{H_1}$

where H_1 (m) is the depth of layer one (~1mm), Kr (d^{-1}) is the remineralization rate, KDOMbads/des (d^{-1}) are the sorption rate constants for the bound pool, and KL_{12} (m d^{-1}) is the diffusion rate parameter between the first and second sediment layer. The time- and depth-integrated first layer DOM concentration is equal to the initial input of organic matter from the water column to the first sediment layer, losing concentration to remineralization, adsorption to the bound pool, and diffusion to the water column or second sediment layer, and gaining concentration from desorption from POM and diffusion into that sediment layer. For aerobic-layer bound DOM:

(12) $RHS_{TMP} = KDOMbadsx * DOMx_{1,t-1} - KDOMbdesx * DOMbx_{1,t-1}$

(13) $DOMbx_1 = DOMbx_{1,t-1} + RHS_{TMP} * DT$

where the size of the pool changes only by adding concentration via adsorption and losing concentration via desorption to the free DOM pool in the first sediment layer. In the anaerobic sediment layer two, the free DOM concentration was calculated similarly to layer one (Eqs. 8-9):

(14) $RHS_{TMP} = Khx * POMx_{t-1} * H_2 - Krx * DOMx_{2,t-1} * H_2 - KDOMbads * DOMx_{2,t-1} * H_2 - KDOMadsx * DOMx_{2,t-1} * H_2 + KDOMbdesx * DOMbx_{2,t-1} * H_2 + KPOMdesx * POMx_{t-1} * H_2 - KL_{12}(DOMx_{2,t-1} - DOMx_{1,t-1}) - \omega_2 * DOMx_{2,t-1}$

(15) $DOMx_2 = DOMx_{2,t-1} + RHS_{TMP}\frac{DT}{H_2}$

except that there are different exchanges between layers. Diffusion occurs both ways across the border of layer one, and burial is present as a loss of DOM. Additionally, there is adsorption, desorption, and hydrolysis (Kh, d^{-1}) between the free DOM pool and the POM pool (no POM in layer one).

Second layer bound DOM is solved the same as in layer one (Eqs. 12-13):

(16) $RHS_{TMP} = KDOMbads * DOMx_{2,t-1} - KDOMbdesx * DOMbx_{2,t-1}$

(17) $DOMbx_2 = DOMbx_{2,t-1} + RHS_{TMP} * DT$

where the only reactions with the bound pool are adsorption and desorption.

Formulation 5: Organic/Inorganic

The final formulation separates the theoretical processes of sorption involving organic versus inorganic substrates. The equations are similar to those in formulation 4, except the "bound" processes are split into two directions. Aerobic layer one equations are as follows:

(18) $RHS_{TMP} = -Krx * DOMx_{1,t-1} * H_1 - KDOMoadsx * DOMx_{1,t-1} * H_1 + KDOModesx * DOMox_{1,t-1} * H_1 - KDOMiadsx * DOMx_{1,t-1} * H_1 + KDOMidesx * DOMix_{1,t-1} * H_1 + KL_{12}(DOMx_{2,t-1} - DOMx_{1,t-1})$

(19) $DOMx_1 = DOMx_{1,t-1} + RHS_{TMP}\frac{DT}{H_1}$

(20) $RHS_{TMP} = -KDOModesx * DOMox_{1,t-1} + KDOMoadsx * DOMx_{1,t-1}$

(21) $DOMox_1 = DOMox_{1,t-1} + RHS_{TMP} * DT$

(22) $RHS_{TMP} = -KDOMidesx * DOMix_{1,t-1} + KDOMiadsx * DOMx_{1,t-1}$

(23) $DOMix_1 = DOMix_{1,t-1} + RHS_{TMP} * DT$

where free DOM once again loses concentration via remineralization, adsorption (KDOMoads, KDOMiads, d^{-1}), and diffusion to sediment layer two, while gaining

from desorption (KDOModes, KDOMides, d^{-1}) and diffusion (from sediment layer two). The bound-to-organics pool (DOMo, g m^3) and bound-to-inorganics pool (DOMi, g m^3) loses concentration to desorption and gains from adsorption.

Anaerobic layer two equations involve the same processes as above with the addition of burial (W_2) as a loss and interactions with the particulate pool (KDOMads, KPOMdes, Kh):

(24) $$RHS_{TMP} = Khx * POMx_{t-1} * H_2 - Krx * DOMx_{2,t-1} * H_2 - KDOMoads * DOMx_{2,t-1} * H_2 - KDOMiadsx * DOMx_{2,t-1} * H_2 - KDOMads * DOMx_{2,t-1} * H_2 + KDOModesx * DOMox_{2,t-1} * H_2 + KDOMidesx * DOMix_{2,t-1} * H_2 + KPOMdesx * POMx_{t-1} * H_2 - KL_{12}\left(DOMx_{2,t-1} - DOMx_{1,t-1}\right) - \omega_2 * DOMx_{2,t-1}$$

(25) $$DOMx_2 = DOMx_{2,t-1} + RHS_{TMP}\frac{DT}{H_2}$$

(26) $$RHS_{TMP} = -KDOModes * DOMox_{2,t-1} + KDOMoads * DOMx_{2,t-1}$$

(27) $$DOMox_2 = DOMox_{2,t-1} + RHS_{TMP}\frac{DT}{H_2}$$

(28) $$RHS_{TMP} = -KDOMides * DOMix_{2,t-1} + KDOMiads * DOMx_{2,t-1}$$

(29) $$DOMix_2 = DOMix_{2,t-1} + RHS_{TMP}\frac{DT}{H_2}$$

Parameter Inputs

Each formulation used the same forcing values (boundary and initial conditions) for the R-64 Chesapeake Bay station as Clark et al. (2017). This station was chosen because it was the northernmost station on the Bay that was highlighted in Clark et al. (2017) and closest to sites sampled for observational values in kinetic laboratory incubations described in Morrissette et al. (*in prep*) and Pinsonneault et al. (2021). Forcing values, along with established rate parameters from the Clark et al.

(2017) formulation (and therefore the Brady et al. (2013) and Testa et al. (2013) versions), were kept the same throughout all model runs to ensure the only difference between outputs was the sorption rate parameters and subsequent interactions (Appendix B.1).

Three sets of rate parameters were chosen based on a range of sorption rate value output from a series of kinetic sorption experiments ([b]Morrissette et al., *in prep*). First, each formulation was run with "minimum" rate parameters for all sorption processes (reducing the rates by an order of magnitude for pools with decreased lability). These minimum rates were closest to the minimum rate outputs generated from the sorption experiments. A ratio close to the median ratio of desorption:adsorption rates from initial model output ([e]Morrissette et al., *in prep*) that recreated the kinetic sorption experiments was applied to the median adsorption value generated from those model results to obtain desorption rates, and converting to d^{-1} from hr^{-1}, "maximum" rates for sorption were calculated that were two orders of magnitude higher than the minimum rates. The sorption incubation experiments only focused on dissolved organic carbon, with the initial composition of colored DOC (CDOC) and non-colored DOC (NCDOC) being set as fractions of 35% and 65%, respectively, of the initialized DOC concentration. The rate parameters pertaining to nitrogen and phosphorus within the SFM were kept small and they are not discussed here (Table A.1).

All the models were coded in Fortran, then post-processed in Matlab. A new forward Euler solver was coded to calculate the concentrations of DOM and POM in all pools, which calculated the current flux of a state variable then added that

concentration to the previous time step's concentration, to provide the current concentration at that time step. A GitHub repository "SFM-DOMSorption-v0.9" with the model code and input files is available at https://github.com/hkmorrissette/SFM-DOMSorption-v0.9.

Results

The following sections showed the results of two tests; 1) *Sensitivity* - comparison of simulations generated by different model formulations using the minimum rate parameters and 2) *Rate Increase* - examination of the change in each simulation after increasing the rate parameters to the maximum values. For the Sensitivity test, each of the five formulations were run with the same rate parameters for each pool across all processes. For the Rate Increase test, only the carbon-related parameters were elevated, keeping the nitrogen and phosphorus rates the same as in the Sensitivity tests.

Sensitivity Test

Hydrolysis Formulation

With the hydrolysis formulation (processes outlined in Figure 2.1), DOC flux out of the sediment (positive DOC Flux (gC m^{-2} d^{-1}) value in Figure 2.6) was typically dominated by refractory fractions and annual peaks showed a steady pattern of small refractory flux out of the sediment during the summer every year with a maximum value of 1.86 x 10^{-3} gC m^{-2} d^{-1}. In contrast, DOC flux into the sediment was typically dominated by the labile and semilabile fractions with annual peaks again showing a steady pattern of flux into the sediment during summer every year

with a maximum flux value of -0.138 gC m^{-2} d^{-1}. Only three of the six pools are visible in Figure 2.6 (all NCDOC), because the CDOC and NCDOC pools (50% each of the net flux) of equal lability are the same over the time series. The labile pool dominated the maximum DOC flux into the sediments at 52.43%. Annual average net flux for this formulation was -0.023 gC m^{-2} d^{-1}.

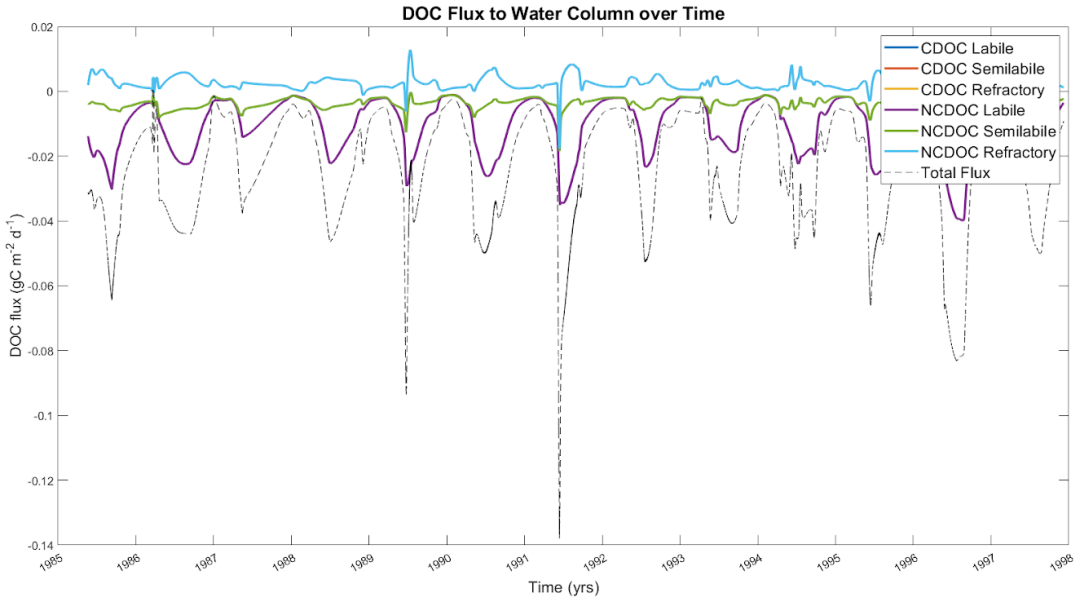

Figure 2.6. SFM DOC Flux between the water column and sediment from May 1985 to December 1997 for the hydrolysis formulation. Each color represents a different state variable related to DOC flux: Labile CDOC (dark blue), Semilabile CDOC (red), Refractory CDOC (yellow), Labile NCDOC (purple), Semilabile NCDOC (green), and Refractory (light blue). Net flux is depicted in the black dashed line over the course of the time series.

Adsorption Formulation

When the adsorption process was added to the model (Figure 2.7; processes outlined in Figure 2.2), the model behaved very similarly to the hydrolysis formulation. Flux into the water column was dominated by the refractory pool, flux into the sediment was dominated by labile and semilabile pools, net flux was into the sediment, and flux peaks - regardless of direction - occurred during the summer. The addition of adsorption (with minimum rates) into the model decreased the maximum flux towards the sediments slightly by 3.67 x 10^{-4} gC m^{-2} d^{-1}, or 0.27%. This decrease happened in both the CDOC and NCDOC fractions, but each lability pool was affected differently, i.e., labile and semilabile pool fluxes both decreased into the sediment by 2.30% and 0.03%, respectively, while refractory DOC pool flux decreased into the water column by 3.19%. Annual average DOC net flux was -0.022 gC m^{-2} d^{-1}.

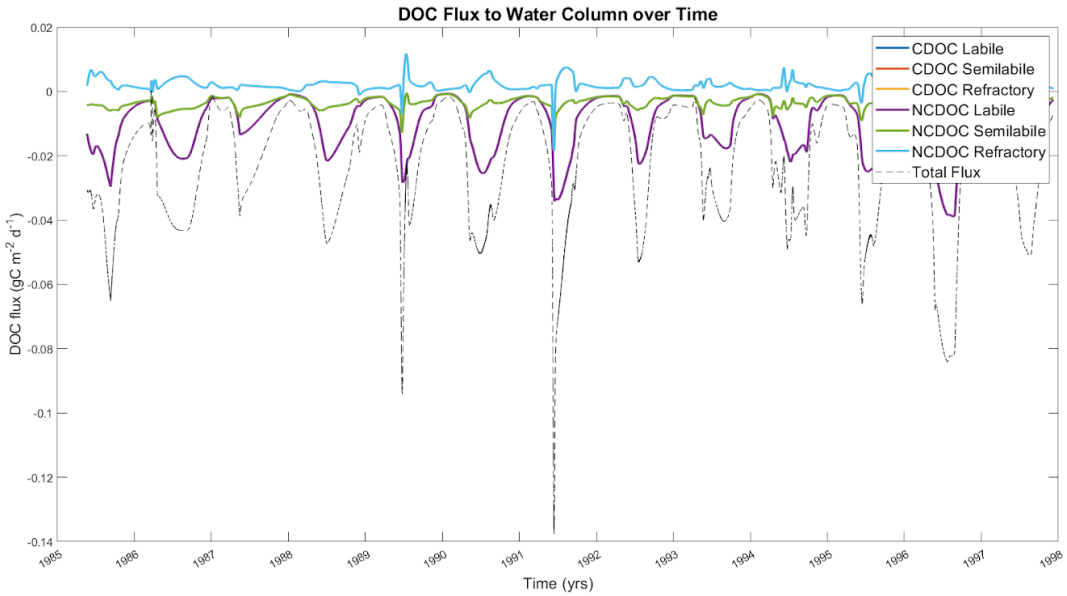

Figure 2.7. SFM DOC Flux between the water column and sediment from May 1985 to December 1997 for the adsorption formulation. Each color represents a different state variable related to DOC flux: Labile CDOC (dark blue), Semilabile CDOC (red), Refractory CDOC (yellow), Labile NCDOC (purple), Semilabile NCDOC (green), and Refractory (light blue). Net flux is depicted in the black dashed line over the course of the time series.

Desorption Formulation

There were dramatic changes in the fluxes when desorption was added to the model (Figure 2.8; processes outlined in Figure 2.3). The interannual peaks still occurred in summer, but the direction of the net flux changed. The colored and non-colored labile DOC pools were the only ones that fluxed into the sediments at any time, and both the semilabile and refractory pools fluxed consistently into the water column. Maximum fluxes increased by 99.75%, 521.17%, and 1.45 x 10^3% for labile, semilabile, and refractory pools, respectively. Net flux increased by 539.44% with the sediment acting as a net source of DOC over almost the entire time series, with the majority (72.23%) happening via the NCDOC pools. Average annual net DOC flux to the water column was 0.218 gC m^{-2} d^{-1}.

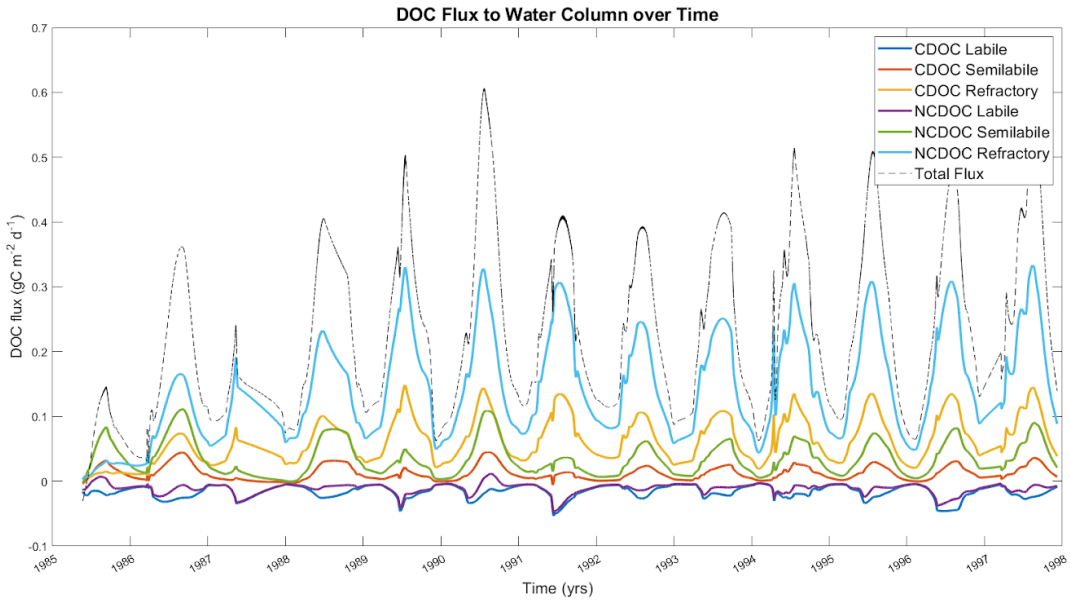

Figure 2.8. SFM DOC Flux between the water column and sediment from May 1985 to December 1997 for the desorption formulation. Each color represents a different state variable related to DOC flux: Labile CDOC (dark blue), Semilabile CDOC (red), Refractory CDOC (yellow), Labile NCDOC (purple), Semilabile NCDOC (green), and Refractory (light blue). Net flux is depicted in the black dashed line over the course of the time series.

Bound Formulation

Once the bound DOC pools were added to the formulation, net DOC flux into the water column increased by 8.25 x 10^{4}% as compared to the hydrolysis formulation (Figure 2.9; processes detailed in Figure 2.4). This showed that adding more pathways that generated higher concentrations of DOC in layer one increased the concentration gradient across the sediment-water interface and therefore the efflux to the water column. The relative fluxes among the different lability pools revealed the same patterns as seen with the desorption formulation; labile fractions had the

smallest fluxes out of the sediments, semilabile and refractory fractions had the largest fluxes out of the sediments, and all fluxes peaked in summer months. Similar to the desorption formulation, the NCDOC pools of each lability fraction had higher fluxes into the water column compared to their CDOC counterparts. The maximum flux of the three liabilities increased by 5.82 x 10^4%, 3.15 x 10^4%, and 1.71 x 10^5% for labile, semilabile, and refractory pools compared to the hydrolysis formulation. The annual average of DOC flux to the water column increased to 45.373 gC m^{-2} d^{-1}.

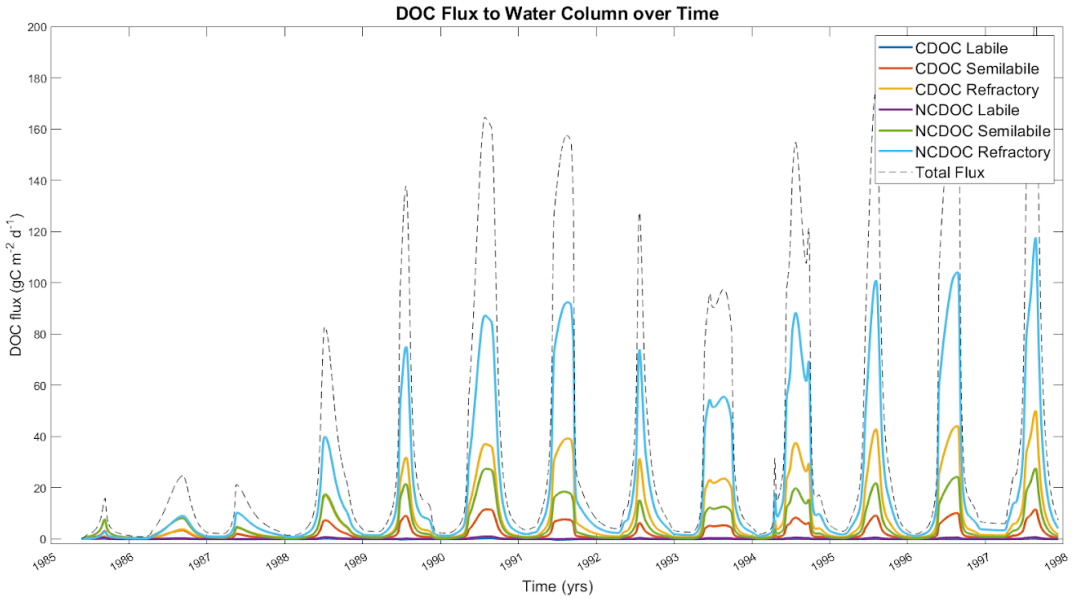

Figure 2.9. SFM DOC Flux between the water column and sediment from May 1985 to December 1997 for the bound formulation. Each color represents a different state variable related to DOC flux: Labile CDOC (dark blue), Semilabile CDOC (red), Refractory CDOC (yellow), Labile NCDOC (purple), Semilabile NCDOC (green), and Refractory (light blue). Net flux is depicted in the black dashed line over the course of the time series.

Organic/Inorganic Formulation

The flux patterns seen with the organic/inorganic model formulation were similar to the bound version: NCDOC fluxes (70.13% of net) were greater than CDOC fluxes and were overall the largest source of DOC to the water column (Figure 2.10; processes detailed in Figure 2.5). However, the maximum fluxes increased by another order of magnitude compared to the bound formulation, which showed, again, that adding more pathways and pools that generated higher concentrations of DOC in layer one increased the concentration gradient across the sediment-water interface and therefore the efflux. Maximum net flux increased from the hydrolysis version by 5.13 x 10^5%, with the three lability pools increasing by 6.21 x 10^4%, 3.15 x 10^5%, and 1.56 x 10^6%, respectively. The average net flux to the water column increased to 221.469 gC m^{-2} d^{-1}.

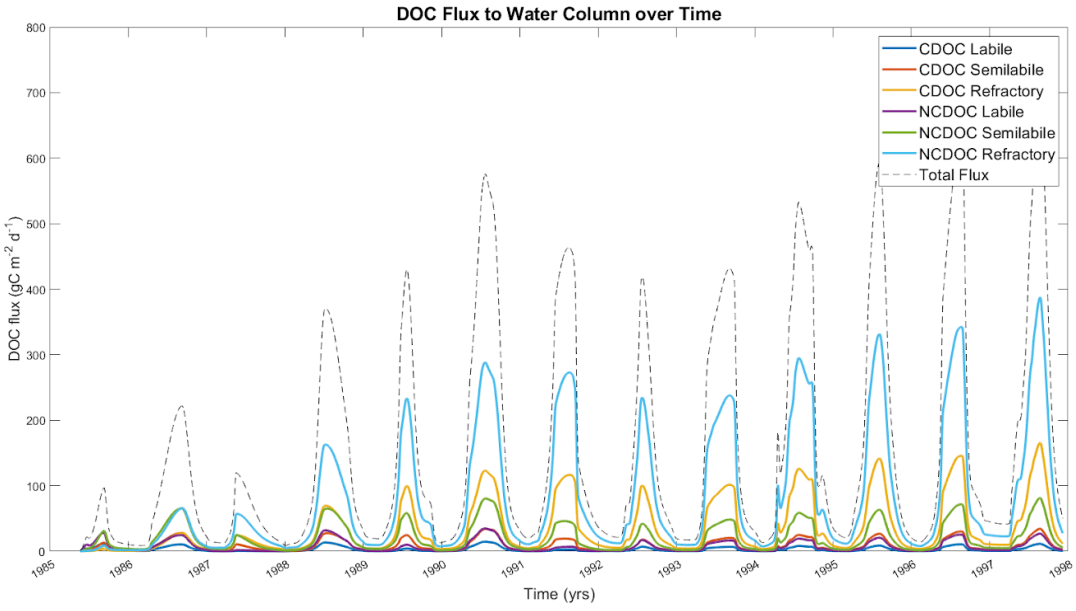

Figure 2.10. SFM DOC Flux between the water column and sediment from May 1985 to December 1997 for the organic/inorganic formulation. Each color represents

a different state variable related to DOC flux: Labile CDOC (dark blue), Semilabile CDOC (red), Refractory CDOC (yellow), Labile NCDOC (purple), Semilabile NCDOC (green), and Refractory (light blue). Net flux is depicted in the black dashed line over the course of the time series.

Output Comparison

Table 2.1. Quantification of change in the maximum flux between model formulations (positive values are increases in flux to the water column, negative values are increases in flux towards the sediment).

Model 1	**Model 2**	**DOC Pool**	**Change in max flux ($gC\ m^{-2}\ d^{-1}$)**	**Percent change (%)**
Hydrolysis	Adsorption	Total	3.670×10^{-4}	0.266
		Colored	1.830×10^{-4}	0.266
		Non-colored	1.830×10^{-4}	0.266
		Labile	1.832×10^{-3}	2.299
		Semilabile	1.850×10^{-5}	0.032
		Refractory	-1.130×10^{-3}	-3.193
Hydrolysis	Desorption	Total	0.744	5.390×10^{2}
		Colored	0.237	3.440×10^{2}
		Non-colored	0.507	7.350×10^{2}
		Labile	0.079	99.754
		Semilabile	0.192	5.212×10^{2}

		Refractory	0.515	1.451×10^3
Hydrolysis	Bound	Total	180.903	8.255×10^4
		Colored	52.824	4.821×10^4
		Non-colored	128.079	1.169×10^5
		Labile	10.050	5.824×10^4
		Semilabile	30.151	3.148×10^4
		Refractory	140.702	1.710×10^5
Hydrolysis	Organic/ Inorganic	Total	707.885	5.130×10^5
		Colored	211.492	3.065×10^5
		Non-colored	496.394	7.195×10^5
		Labile	49.485	6.211×10^4
		Semilabile	115.995	3.149×10^5
		Refractory	553.381	1.561×10^6

Table 2.2. Composition of pools in the maximum DOC flux in percentage for each formulation.

Model	**Total Max Flux (gC m^{-2} d^{-1})**	**Colored DOC (%)**	**Non-colored DOC (%)**	**Labile (%)**	**Semilabile (%)**	**Refractory (%)**
Hydrolysis	0.138	50.00	50.00	52.43	24.24	23.33
Adsorption	0.138	50.00	50.00	51.46	24.35	24.19

Desorption	0.606	27.77	72.23	0.03	24.46	75.51
Bound	180.903	29.18	70.82	5.56	16.67	77.78
Organic/ Inorganic	707.747	29.87	70.13	6.87	16.13	76.99

Rate Increase Test

For this test, adsorption and desorption reaction rates for carbon (listed in Appendix A.3) were increased to the maximum levels that were estimated based on the results of kinetic sorption experiments ([b]Morrissette et al., *in prep*) as described above.

Adsorption Formulation

Surprisingly, increasing the sorption rates by an order of magnitude to the maximum levels resulted in just a minor decrease in fluxes in all pools toward the water column. This resulted in an increase in net flux into the sediment by 3.69% (Figure 2.11). The labile, semilabile, and refractory pool fluxes increased to the sediment by varying degrees of 0.06%, 0.87%, and 12.81%, respectively, compared to the model run with the minimum rates. As with the hydrolysis and adsorption formulation that used minimum sorption rates, CDOC and NCDOC pools accounted for equivalent proportions of the net DOC flux. With the maximum rates the annual net flux average into the sediments increased to -0.026 gC m^{-2} d^{-1}.

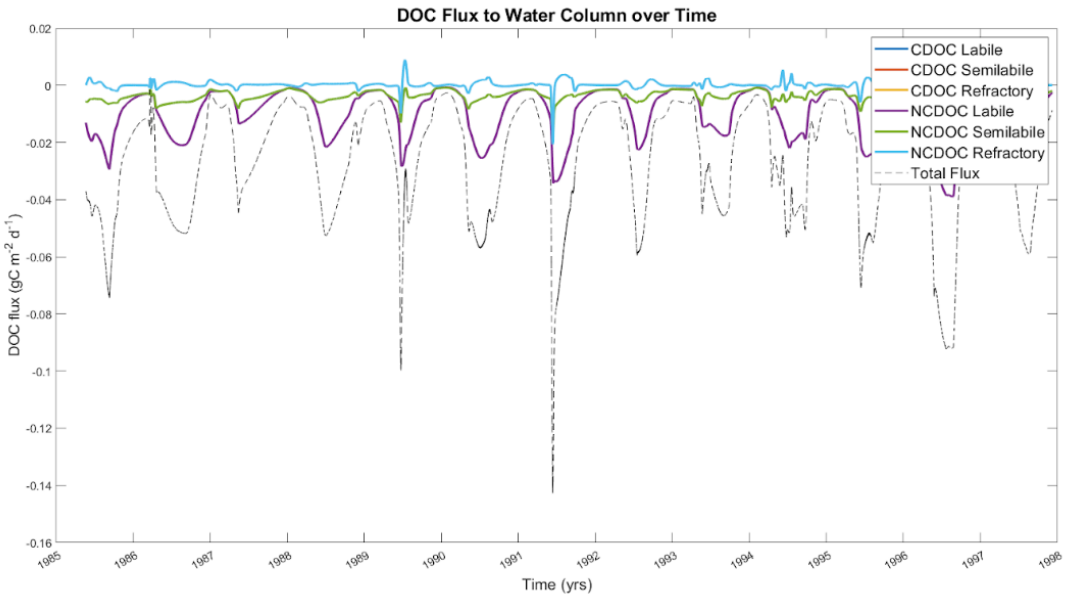

Figure 2.11. SFM DOC Flux between the water column and sediment from May 1985 to December 1997 for the adsorption formulation with maximum sorption rates. Each color represents a different state variable related to DOC flux: Labile CDOC (dark blue), Semilabile CDOC (red), Refractory CDOC (yellow), Labile NCDOC (purple), Semilabile NCDOC (green), and Refractory (light blue). Net flux is depicted in the black dashed line over the course of the time series.

Desorption Formulation

When the rates in the desorption formulation were elevated to the maximum values for both adsorption and desorption, the net flux to the water column decreased (annual average = 0.002 gC m^{-2} d^{-1}) and the net flux into the sediments increased by 92.50% compared to the model run with the minimum rates (Figure 2.12), which was opposite of expectation. The labile pool fluxes decreased toward the sediments, which was indicative of less adsorption, but they did not reverse directions. When adsorption was set to zero (results not shown), the net flux increased towards the

water column when compared to the run with minimum rates, indicating that desorption alone increased the flux as expected.

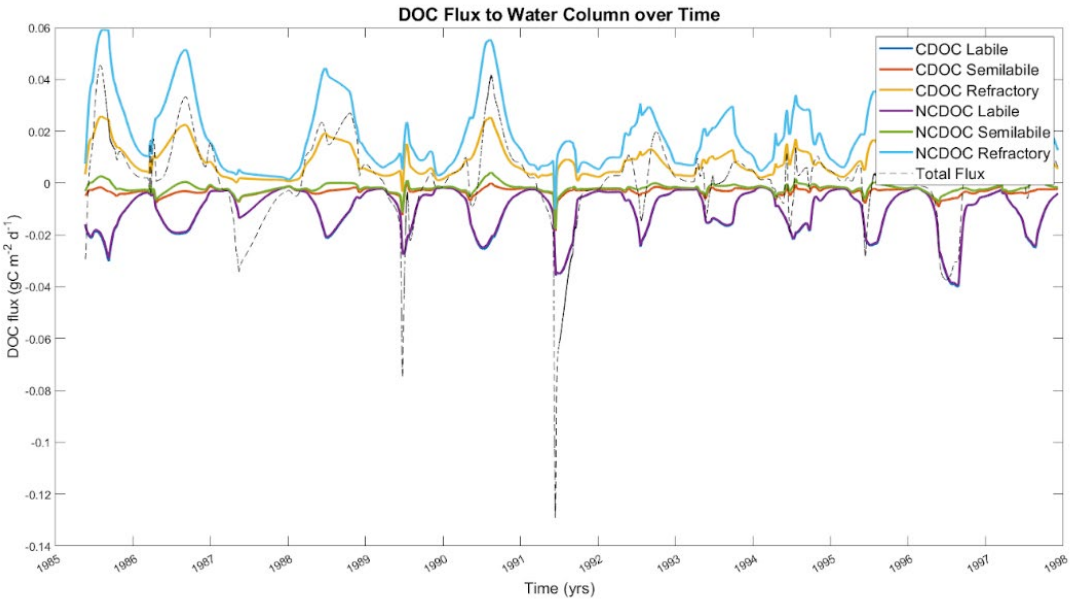

Figure 2.12. SFM DOC Flux between the water column and sediment from May 1985 to December 1997 for the desorption formulation with maximum sorption rates. Each color represents a different state variable related to DOC flux: Labile CDOC (dark blue), Semilabile CDOC (red), Refractory CDOC (yellow), Labile NCDOC (purple), Semilabile NCDOC (green), and Refractory (light blue). Net flux is depicted in the black dashed line over the course of the time series.

Bound Formulation

Increasing the rate parameters to the maximum values within the bound formulation resulted in an almost order-of-magnitude decrease in net flux to the water column (87.50%), and this effect was observed in all six DOC pools (Figure 2.13). The relative fluxes in the individual pools remained the same as with the minimum

rate parameters; labile fluxes were the smallest (2.77% of max flux), semilabile were intermediate (10.35% of max flux), and refractory fluxes were the largest (86.88% of max flux), with non-colored DOC fluxes constituting a larger fraction (71.11%) of the flux for all labilities. The average annual DOC flux decreased to 4.239 gC m^{-2} d^{-1}. When sorption reaction rates from the previous two formulations are set to zero, keeping sorption just between the bound pools and free DOC (results not shown), net efflux was decreased by another order of magnitude.

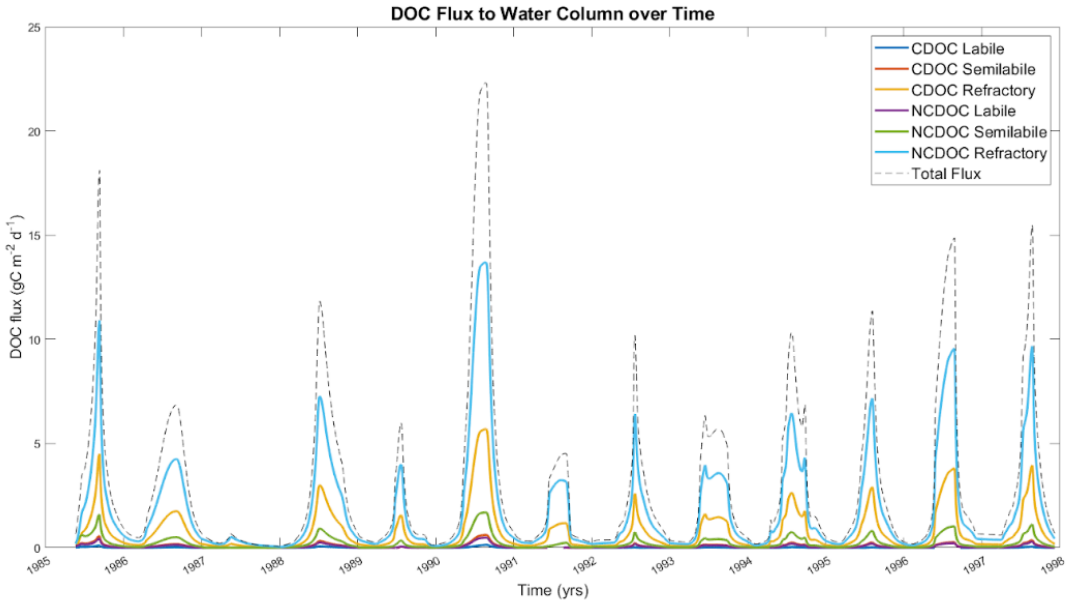

Figure 2.13. SFM DOC Flux between the water column and sediment from May 1985 to December 1997 for the bound formulation with maximum sorption rates. Each color represents a different state variable related to DOC flux: Labile CDOC (dark blue), Semilabile CDOC (red), Refractory CDOC (yellow), Labile NCDOC (purple), Semilabile NCDOC (green), and Refractory (light blue). Net flux is depicted in the black dashed line over the course of the time series.

Organic/Inorganic Formulation

As in the bound formulation response, application of the maximum rate parameters led to a decrease in maximum flux into the water column by 96.91% compared to the minimum sorption rate parameters (Figure 2.14). Refractory pools comprised the majority of the net flux out of the sediments (86.61%), with the NCDOC (71.12% of net flux) flux higher than the CDOC of the same lability. The labile, semilabile, and refractory pool fluxes to the water column decreased by 98.75%, 98.01%, 96.58%, respectively. The annual average of the DOC flux decreased by almost 2 orders of magnitude to 4.204 gC m^{-2} d^{-1}. Similarly to the bound formulation, when the POC - DOC desorption and adsorption rates were set to zero (not shown), net fluxes continued to be in the direction of the water column, but the magnitude of those fluxes decreased substantially.

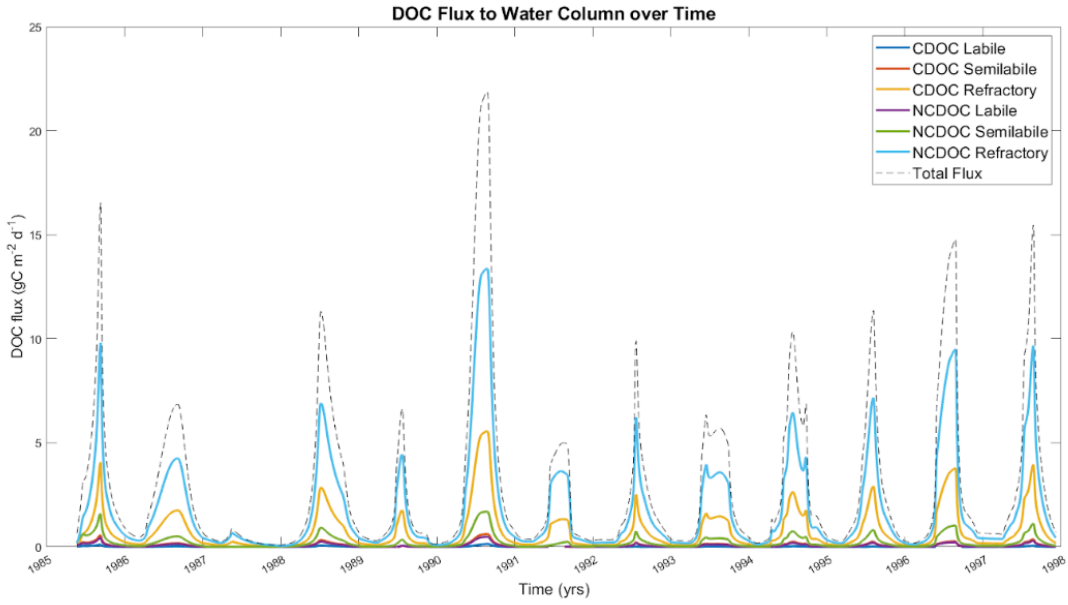

Figure 2.14. SFM DOC Flux between the water column and sediment from May 1985 to December 1997 for the organic/inorganic formulation with maximum

sorption rates. Each color represents a different state variable related to DOC flux: Labile CDOC (dark blue), Semilabile CDOC (red), Refractory CDOC (yellow), Labile NCDOC (purple), Semilabile NCDOC (green), and Refractory (light blue). Net flux is depicted in the black dashed line over the course of the time series.

Output Comparison

Table 2.3. Quantification of change in maximum flux between minimum and maximum rate model outputs (positive values are increases in flux to the water column, negative values are increases in flux towards the sediment).

Model 1	**Model 2**	**DOC Pool**	**Change in max flux (gC m^{-2} d^{-1})**	**Percent change (%)**
Adsorption minimum	Adsorption maximum	Total	-5.080×10^{-3}	-3.689
		Colored	-2.540×10^{-3}	-3.689
		Non-colored	-2.540×10^{-3}	-3.689
		Labile	-4.458×10^{-5}	-0.057
		Semilabile	-3.199×10^{-4}	-0.869
		Refractory	-4.685×10^{-3}	-12.806
Desorption minimum	Desorption maximum	Total	-0.561	-92.502
		Colored	-0.164	-97.198
		Non-colored	-0.396	-90.496
		Labile	-2.10×10^{-3}	-1.105×10^{3}
		Semilabile	-0.151	-97.335

		Refractory	-0.394	-82.299
Bound minimum	Bound maximum	Total	-158.593	-87.667
		Colored	-46.378	-87.797
		Non-colored	-112.214	-87.613
		Labile	-9.432	-93.851
		Semilabile	-27.842	-92.342
		Refractory	-121.317	-86.223
Organic/ Inorganic minimum	Organic/ Inorganic maximum	Total	-685.897	-96.913
		Colored	-205.113	-97.015
		Non-colored	-480.783	-96.869
		Labile	-48.788	-98.750
		Semilabile	-113.651	-98.010
		Refractory	-534.419	-96.580

Table 2.4. Composition of pools in the maximum DOC flux in percentage for each maximum rate output.

Model with Maximum Rates	**Total Max Flux (gC m^{-2} d^{-1})**	**Colored DOC (%)**	**Non-colored DOC (%)**	**Labile (%)**	**Semilabile (%)**	**Refractory (%)**
Adsorption	0.143	50.00	50.00	49.83	23.77	26.40

Desorption	0.046	10.18	89.82	2.59	4.53	92.89
Bound	22.311	28.89	71.11	2.77	10.35	86.88
Organic/ Inorganic	21.852	28.88	71.12	2.83	10.56	86.61

Discussion

The goal of this study was to examine how adding sorption processes of increasing levels of complexity to a widely used sediment flux model impacted the sediment flux simulations. A procedure of sequentially implementing models with increasing complexity was chosen to highlight the impacts of that complexity on the fluxes. By doing so, it was possible to parse out the effect of each new process on model output. In addition, the impact of varying the sorption rate parameters was examined. It was found that adding more complex representations of organic matter adsorption and desorption and increasing the rate parameters strongly affected model behavior.

Overall, the sediment flux model proved very sensitive to the addition of the sorption formulations. The first addition of adsorption did not drastically change the DOC flux patterns even though it created a pathway for DOC to adsorb to POC, which should promote retention of DOC in the sediments. In contrast, the addition of abiotic desorption dramatically changed the model behavior, i.e., it reversed the net flux of DOC from into the sediments to out of the sediments and into the water column. Given the larger importance of desorption as compared to hydrolysis, as discussed above (Guggenberger & Kaiser 2003, Qualls & Haines 1992, Qualls &

Richardson 2003, Tavakkoli et al. 2014), and the well-known fact that tidal marshes, despite being a carbon sink, are sources for DOC (Najjar et al., 2018; Windham-Myers et al., 2018; Tzortziou et al., 2008, 2012, 2015; etc.), adding sorption to the model resulted in fluxes that are more consistent with in situ marsh-specific sediment DOC observations ([b,c,d]Morrissette et al., *in prep*; Pinsonneault et al., *in prep*). Interestingly, adding more complexity to the sorption processes (the bound and organic/inorganic formulations) magnified this change by several orders of magnitude and resulted in a net DOC flux out of the sediments. These results are contrary to the idea that increasing the number of pools for DOC to sorb onto and stay in the sediment should decrease net flux out to the water column. Rather, when relatively slow sorption rates were used, the additional sorption pools and processes provided more DOC to the first sediment layer which resulted in increases in the DOC gradient between the sediment and water column which, in turn, drove larger net DOC flux to the overlying water column. Interestingly, the modeling study of Clark et al. (2017) showed that sediments could be sources of semilabile and refractory DOC, depending on initial conditions, at certain stations in the Chesapeake Bay, similar to the findings presented here. The results suggested that these fluxes could be more important than previously modeled.

Reaction rates for the model runs were chosen carefully. Rates in the SFM (Di Toro, 2001) for all other processes besides sorption-related parameters were kept the same as in previous formulations (Brady et al., 2013; Clark et al., 2017; Testa et al., 2013). Rates for all processes, regardless of being biotic or abiotic in nature, were reduced by an order of magnitude for each decrease in lability. Biologically, this is

due to the inherent definition that more refractory compounds are less biologically available. The same rationale that more refractory compounds have slower rates was also used for the selection of abiotic sorption rates, though the same assumption is not necessarily true, as more humic, refractory compounds may actually be sorbed preferentially ([c]Morrissette et al., *in prep*). This inherently has an effect on the individual break down of the movement of the pools shown in the results. However, as shown, the highest amount of desorption that occurred through all model runs was the refractory pools, followed by the semi-labile. Increasing their respective sorption rates would most likely increase the magnitude of the direction in which they are already fluxing. An increase in the adsorption rates alone in the 2nd formulation could potentially pull refractory pools into the sediments over time, but as that was the least-affected model from the original with the addition of adsorption, the changes might not be significant. Another set of runs with a reversal of the fastest rates could provide more definitive answers. Regardless, manipulating the sorption rates provided key information on how the magnitude of the fluxes could be modeled. When sorption rates were elevated to the maximum values the direction of the DOC fluxes remained largely unchanged, but the magnitudes of the fluxes dropped substantially. When sorption rates were increased in the bound and organic/inorganic formulations, fluxes to the water column decreased, indicating that adsorption of free DOC to those bound pools could override the increases in DOC concentration in the first sediment layer that were observed as compared to the simpler formulation where adsorption and desorption happen only in the second sediment layer.

When assessing the influences of formulation and rate changes on the individual CDOC and NCDOC pools and their three levels of lability, similar patterns were seen throughout the study. With the addition of each new formulation, refractory, semilabile, and labile pools always constituted the highest to lowest efflux, respectively. This is consistent with other observation and modeling studies, which have shown that labile DOC is quickly utilized and transformed to inorganic forms with the more refractory pools usually remaining, accumulating, and therefore driving fluxes out of the sediments (Burdige et al., 2016; Clark et al., 2017; Yurova et al., 2008). In addition, the NCDOC fluxes towards the water column were always higher than the CDOC towards the water column. Measurements of CDOC flux have shown it constitutes a larger fraction of the DOC export from the marsh over time (Clark et al., 2008; Tzortziou et al., 2008, 2015), but it is not known in what proportion CDOC and NCDOC are exported from the sediments specifically. However, recent studies of marsh sediment sorption have shown that while CDOC is a part of net DOC flux, highly colored, humic material is preferentially adsorbed to marsh sediments and NCDOC ultimately constitutes a higher portion of the net DOC efflux from the sediments to pore water over time ([c]Morrissette et al., *in prep*; Pinsonneault et al., *in prep*). For NCDOC to be the majority of the flux out of the sediments and CDOC to be the majority of the flux out of the entire marsh, NCDOC must be quickly transformed within the aqueous phase of the pore water or overlying water column after release from the sediments.

The addition of sorption processes to the SFM, combined with the use of high sorption rate parameters, resulted in net DOC flux out of the sediments that is

consistent with observations which have shown that tidal marshes, despite being a net carbon sink, are a net DOC source to their surrounding estuarine and coastal ocean environments (Clark et al., 2008; Najjar et al., 2018; Tzortziou et al., 2008, 2012; Windham-Myers et al., 2018). However, as the rest of the model was not modified from the Clark et al. (2017) version, which was parameterized based on estuarine observational data, there are undoubtedly more processes and initial conditions in addition to sorption that need to be altered to truly formulate the SFM as a marsh model. Sediment flux models like the SFM have not been formulated and parameterized to simulate marsh ecosystems. Rather, most have been validated with flux estimates from open-water stations (Boynton & Bailey, 2008; Brady et al., 2013; CBP; Clark et al., 2017; Di Toro, 2001; Testa et al., 2013) that are not representative of tidal marsh ecosystems.

Finally, it was important to emphasize the fact that, with the addition of sorption processes, the SFM generated larger fluxes out of the system for all DOC pools, not just refractory. This has major implications for the modification of sediment flux models moving forward. Sorption processes must be included in models like the SFM in order to capture DOC sediment fluxes from tidal marsh environments. At a minimum, models such as the SFM must include adsorption and desorption between the second sediment layer POC and free DOC, and they should be run with fast rate parameters derived from adsorption/desorption experiments. Given that the desorption, bound, and organic/inorganic formulations all represent the system as a net source of DOC, it is unclear what level of complexity is best. Here, a linear formulation for adsorption was used to model fluxes but some applications may

require the more complex, Langmuir formulation (ᶜMorrissette et al., *in prep*; Chapter 4). More research is needed to know which formulation captures each DOC pool's flux most effectively.

One desirable future use of sediment flux models is to capture and simulate the effects of climate change on marsh systems. However, more development is needed to provide models with accurate framework of marsh sediment flux before these changes are captured. Models are used extensively in other aspects of climate change: warming, open ocean circulation, atmospheric greenhouse gas levels, and sea level rise on the coastal ocean. In regards to sediment fluxes at the marsh-estuarine interface, the effects of climate change are numerous but highly complicated, most of which has yet to be captured through modeling studies. To do so, sediment flux models need to have dependencies on the very aspects that would change the most in the face of climate change, such as salinity levels, tidal inundation, and flooding inputs to the marsh. It is also important to note that the outputs of the sediment flux model presented here are based on the flux to and from the overlying water column, based on the transformation of DOC within the sediments. The DOC concentrations within the pore waters can be high, with Jug Bay and Taskinas (Chesapeake Bay watershed fresh and brackish tidal marshes, respectively) reporting values of up to 15-35 mg L^{-1} dependent on location within the marsh (Pinsonneault et al., *in prep*). While the likelihood of high amounts of exchange occurring with the pore waters within the sediments, future research is needed to have a better understanding of the pore water interactions that are not captured and still poorly quantified.

Conclusion

Sediment flux models are important tools that can be used to simulate nutrient, oxygen, and organic matter fluxes between sediments and the overlying water column in estuarine and coastal waters, and they are widely used both in research and to inform management actions. The addition of DOM to the SFM in previous work allowed the model to better simulate the flux of DOM into and out of the estuarine sediments over time. However, along with many other sediment flux models, the SFM did not include abiotic sorption processes which are known to be important in controlling DOM fluxes into and out of sediments. This, combined with the fact that the SFM was not developed and parameterized to simulate marsh sediments, suggested that SFM-simulated DOM fluxes into and out of sediments, through the lens of the marsh, could be significantly in error. This paper has provided the first assessment of how a sediment flux model behaved when sorption processes were added, how the model behavior changes when increasingly complex interactions were added, and how the increasing rate parameters changed flux output. It was found that model formulations that included desorption increased the net DOC flux towards the water column and that manipulating the rates within those formulations significantly affected the magnitude of these fluxes.

Chapter 3: Wetland soil biogeochemistry influences the kinetics of dissolved organic carbon sorption

Abstract

Sorption processes in the sediment-water column interface are observed to be rapid and dominant pathways of dissolved organic carbon (DOC) flux. However, kinetic data for sorption is sparse, because rates at short time scales are difficult to measure. For temperate tidal marshes, sorption rates are non-existent. In this study, sorption rate kinetic experiments were designed to constrain and validate new formulations of a sediment flux model coded to include explicit sorption pathways between particulate organic carbon and DOC pools. Batch incubations for marsh soil samples from Taskinas Creek (VA, USA) and Jug Bay Wetlands Sanctuary (MD, USA), were performed under four sets of initial conditions: stock solutions were permutations of two salinity treatments (0 psu, 35 psu) and two DOC concentrations (0 mg L^{-1}, 275 mg L^{-1}). All incubations were anaerobically performed at seven time points over 24 hours, focusing on short time scales. These results are the first DOC sorption kinetics data for tidal marsh sediments, revealing that 76% of total sorption occurred within the first 15 minutes. This agreed with other kinetic studies for different types of sediment, and also revealed distinct patterns of higher capacity for adsorption under high DOC concentrations and salinity, and higher capacity for desorption under low DOC concentrations and salinity, with differences in process magnitude between sediment types. These results provide a deeper understanding of the biogeochemical controls on sorption kinetics, whose rapidness suggests that it is

crucial to incorporate sorption processes into sediment flux models to accurately present DOC flux.

Introduction

As one of the most productive ecosystems on earth, wetlands have a strong influence on dissolved organic carbon (DOC) flux to their surrounding environments. Tidal marshes in particular are important sources of DOC to estuaries and coastal waters (Barrõn & Duarte, 2015; Bauer et al., 2013; Cai 2011; Childers et al., 2000; Herrmann et al., 2015; Najjar et al., 2018; Tzortziou et al., 2008; Tzortziou et al., 2011), resulting in as much as 80% of the annual lateral DOC and dissolved inorganic carbon (DIC) export to the ocean (Wang & Cai, 2004; Wang et al., 2016). Tidal marsh organic matter production and habitat also supports fisheries and other food webs as a vital ecosystem service (Day et al., 2013). Despite being a relatively small fraction of the total land surface on earth, tidal wetlands are disproportionately responsible for much of the coastal productivity, carbon fluxes, and sediment carbon accumulation (Chmura et al., 2003; Najjar et al., 2018; Pendleton et al., 2012; Windham-Myers et al., 2018).

Sorption is an established and important process that controls DOC retention and release within wetland sediments. Many experiments have proven the capability of sediments, particularly those that are minerally-dominated, of capturing DOC via adsorption (see Appendix C.1 for a list of relevant literature). While it is well established in the literature that iron and aluminum oxides, with large surface area and sorption capacity, promote adsorption of DOC in numerous environments, some studies have also shown that labile DOC is potentially stabilized and kept from degradation or utilization when it is adsorbed, making the desorption of that adsorbed material a very slow natural process (Gu et al., 1994; Guggenberger & Kaiser, 2003;

Kaiser & Guggenberger, 2000/2003, Keil et al., 1994; Wagai & Mayer, 2007; Wattel-Koekkoek & Buurman, 2004). However, laboratory incubations and in situ measurements suggest that adsorption and desorption are extremely fast processes (Gu et al., 1994; Guggenberger & Kaiser, 2003; Kaiser & Zech, 1998; Kothawala et al,. 2008; McKnight et al., 1992; Qualls 2000; Qualls & Haines, 1992; Shaker et al., 2012). This is very important because it means that desorption is a dominant process over microbial degradation/hydrolysis (Guggenberger & Kaiser, 2003; Qualls & Haines, 1992; Qualls & Richardson, 2003; Tavakkoli et al., 2014), and therefore an essential process to consider when thinking in terms of carbon flux models and budgets. Other kinetic studies indicate that adsorption and desorption are time-dependent and competitive, with adsorption initially happening rapidly and then slowing, and/or inducing desorption depending on the compounds (Koopal et al., 2019, Lilienfein et al., 2004; [b,c,d]Morrissette et al., *in prep*; Xing & Pignatello, 1996) Moreover, if sorption acts as a buffer for DOC flux in wetland sediments, as suggested by Qualls (2000) and Qualls & Richardson (2003), then there is even more need to account for this process.

Isotherm incubations are used to study the net exchange of DOM between sediments and their surrounding water. In most isotherm studies the incubations are run for 24 hours to measure the net change in DOC concentration in order to provide information on the net impact of sorption processes. These incubations inform many areas of study, including how optical properties of colored DOM show preferential adsorption and desorption (Kaiser & Guggenberger, 2000; Kothawala et al., 2012; Pinsonneault et al., *in prep*), the reversibility (or non-reversibility) of sorption (Gu et

al., 1994; Tavakkoli et al., 2014), how sorption affects soil properties (Kaiser et al., 2001; Kleber et al., 2021; Pinsonneault et al., *in prep*), and vice versa (Kaiser & Zech, 1998; Keil et al., 1994; Kleber et al., 2021; Kothawala & Moore, 2009; McKnight et al., 1992; Pinsonneault et al., 2021/*in prep*). However, very few of these incubations provide information about sorption rates. Pinsonneault et al. (2021) is the only set of isotherm incubations to be completed on wetland sediments, and Kaiser & Zech (1998) and Shaker et al. (2012) are two of only a few to report kinetic experiments. Both of the latter studies revealed the speed at which sorption occurs; with Kaiser & Zech (1998) reporting up to 75% of the process happening in the first 15 minutes, and 90% occurring by the end of 4 hours, and Shaker et al. (2012) showing equilibrium reached in less than 30 minutes regardless of initial conditions. They found similar controls on adsorption in their soils that Pinsonneault et al. (2021) saw in wetland sediments, such as the influence of mineral oxides and organic carbon concentration, so the probability of kinetics being as fast in wetland sediments was high.

It is important to understand how quickly adsorption and desorption occur in marsh soils for several reasons. Considering marshes are found to be sources of DOC, transformation and release rates of this DOC could have major implications in a changing climate. Marshes are exposed to changing conditions all the time, both gradually and rapidly. The impact of storms can happen within hours, increasing flow and runoff into marsh lands (Wilson et al., 2011) and potentially shocking the system with particulate and dissolved organic compounds. Salt intrusion is slowly increasing in coastal wetlands due to sea level rise, possibly changing the structure of the marsh sediments and their capacity for sorption. Long-term effects of salt intrusion have

been found to significantly affect DOC lability, subsequently altering biogeochemical processing, microbial activity, and sediment regulation of OC (Neubauer et al., 2013). Piecing together the consequences of the changes to marsh sediments in regard to DOC coastal cycling can inform predictive flux models.

This study addressed the kinetic data gap in tidal marsh DOC sorption rate measurements, reporting rates of sorption process completion for multiple marsh soil types and initial conditions derived from closed laboratory incubations. These measurements reaffirm the important role that sorption plays in the retention and release of DOC in tidal wetlands, and they can be used to help inform policy and management decisions for coastal wetlands moving forward.

Methods

Study Sites

The larger scope of this project included four study marsh sites in total: (1) Kirkpatrick Marsh in Edgewater, Maryland, U.S.A. (36°53'N, 76°33'W), (2) Jug Bay Wetlands Sanctuary in Lothian, Maryland, U.S.A. (38°46'N, 76°42'W), (3) Taskinas Marsh in Williamsburg, Virginia, U.S.A. (37°25'N, 76°43'W), and (4) Wachapreague Marsh in Wachapreague, Virginia, U.S.A. (37°32'N, 75°41'W) (Figure 3.1).

Figure 3.1. Map of the four study sites and the location of the Great Dismal Swamp. (From Pinsonneault et al. 2021).

Study sites were chosen that included a wide range of marsh characteristics such as salinity, percent organic matter (%SOM), marsh biodiversity, and sediment composition. This range was chosen to provide a more comprehensive view of how individual marsh characteristics influence sorption and provide insights into which marsh characteristics drive the observed variability patterns. This information can, in turn, provide data that is needed to formulate and parameterize numerical models. A detailed description of all four sites can be found in Pinsonneault et al. (2021).

Isotherm incubations were completed on all four sites with four salinity treatments, two of which are shown in Figure 3.2 (Pinsonneault et al., 2021).

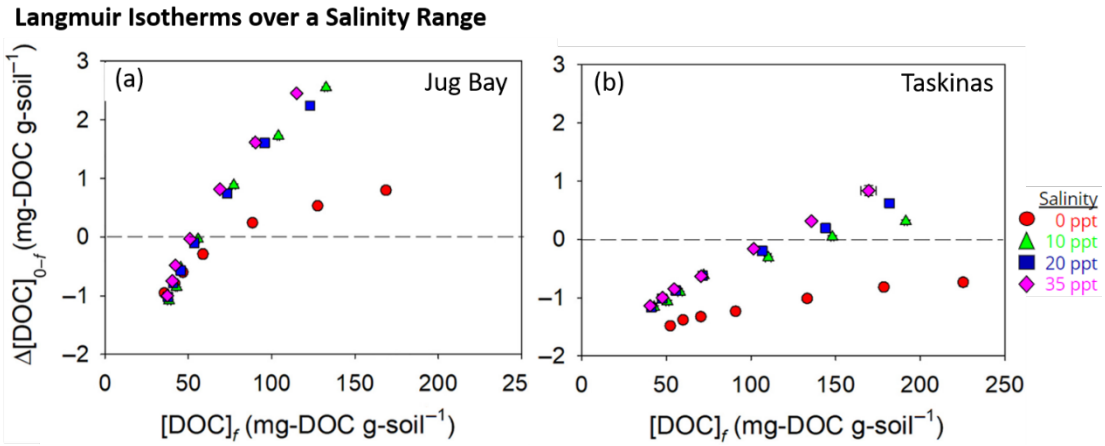

Figure 3.2. Traditional Langmuir isotherms across the four salinity treatments for (a) Jug Bay (JB) and (b) Taskinas (TA). Red circles, green triangles, blue squares, and purple diamonds reflect 0 psu, 10 psu, 20 psu, and 35 psu salinity treatments, respectively. Positive y-axis values indicate that net adsorption had occurred during the incubations, and negative y-axis values indicate that net desorption had occurred. (From Pinsonneault et al., 2021).

Experimental Design

The isotherm experiments (Pinsonneault et al., 2021) were completed to determine how much sorption took place over the course of 24 hours under a range of salinity and DOC concentration gradients. At the end of the incubations, the net sorption was measured and compared between soils. While the isotherm experiments were instructive as to how sediment composition affected net DOC exchange, they did not answer three questions that are key to modeling: 1) how fast are the sorption processes?; 2) how do the soil's sorption rates vary as a function of time?; and 3) how

much time is needed to reach steady state? The following kinetic experiments were designed to answer these questions and provide rate parameters that can be used to parameterize a sediment flux model with added sorption processes described in [a]Morrissette et al. (*in prep*).

It was not possible to do kinetic measurements on all of the isotherm experiments because the kinetic incubations required measurements at multiple time points over 24 hours. Therefore, soils from two of the four sites were chosen based on the maximum desorption and adsorption capabilities found from the isotherms (Jug Bay - maximum adsorption, Taskinas - maximum desorption) (Table 3.1). These soils were subjected to two end member salinity treatments (0 psu, 35 psu) and two end member DOC treatments (0 mg L^{-1}, 275 mg L^{-1}), and rates were measured at seven time points during that 24 hours (Table 3.1). Figure 3.3 depicts a breakdown of the experimental design for the stock solutions, inoculated at each time point. The fastest time points were chosen in close proximity because up to 75% of sorption has been shown to occur within the first fifteen minutes and 90% within the first hour after exposure to water (Kaiser & Zech, 1998).

Table 3.1. Individual parameters and their values for all treatments.

Parameter	Quantity	Values
Soils	2	Jug Bay - most adsorption; Taskinas - most desorption
Salinity	2	0 psu, 35 psu
Initial DOC Concentration	2	0 mg L^{-1}, 275 mg L^{-1}
Time	7	3.5 min, 10 min, 15 min, 1 hr, 6 hrs, 12 hrs, 24 hrs

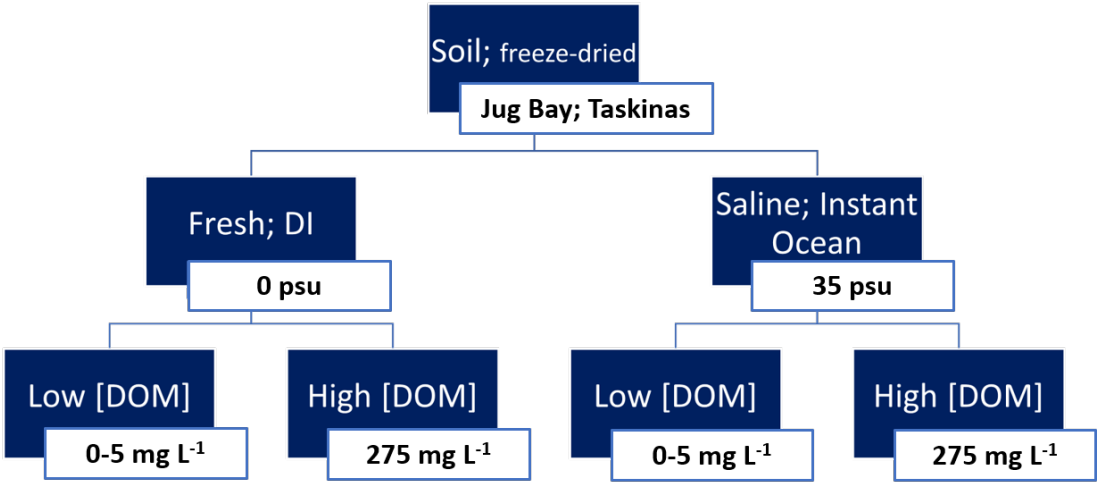

Figure 3.3. Conceptual model of experimental design. Two soils under eight treatments at seven timepoints equaling fifty-six total treatments. Incubations were conducted in triplicate for each time point.

Stock Creation

Following the protocol set forth in Pinsonneault et al. (2021), surface water was collected in August 2018 from the Jericho Ditch of the Great Dismal Swamp Wildlife Refuge, VA (36°41'45.03"N, 76°30'28.16"W) (Figure M.1) to create a concentrated DOC stock inoculant. The 120 L of highly colored water was concentrated further via reverse osmosis, filtered through 0.2 µm to remove particulates, and stabilized with sodium azide (NaN_3; 1 µM) to eliminate microbial activity. This stock solution was the fresh high DOC initial concentration. Instant Ocean was added to a sub-volume to reach 35 psu salinity. pH, salinity, and conductivity were measured for both solutions. A low DOC stock equivalent was made by adding an equivalent quantity of NaN_3 to the equivalent volume of DI water.

Hydrochloric acid (HCl) was added until the pH matched the concentrated stock solution, then Instant Ocean was added to a subset of the dilutant until the salinity and conductivity matched the high salinity concentrated DOC stock solution. This procedure produced four stock solutions: high DOC + no salt (HF), high DOC + salt (HS), low DOC + no salt (LF), and low DOC + salt (LS). Optical properties and total organic carbon were measured for all final stock solutions, and throughout the creation process to ascertain the effects of each preparation step on the DOC quantity and quality. Absorbance and slope ratio measurements, among other indicators of DOC composition, did not significantly differ throughout the process, meaning that the compounds within the stock solution remained consistent in source and chemical make-up. Concentrations did not differ significantly between steps except for post-reverse osmosis, when the DOC concentration was purposefully increased by three-fold.

Experimental Procedure

The experimental procedure and pre- and post-analyses followed Pinsonneault et al. (2021) to allow for direct comparison. This ensured that the incubation time was the only thing that differed between the isotherm and the kinetic incubations. The same cored, dried, and homogenized soils from the isotherm set of experiments were used here, being stored properly in a desiccator between incubations.

The aqueous phase of each soil slurry was measured for total organic carbon concentration and spectral properties. These included Emission-Excitation Matrices (EEMs), Humification Index (HIX), Freshness Index (β:α), Biological Index (BIX),

and Fluorescence Index (FI) on a FluoroMax 3 spectrofluorometer for information on the composition of the DOC compounds (as per Hansen et al., 2016; Helms et al., 2008). Absorbance was measured on a Thermoscientific spectrophotometer, providing information on the source of DOC. Total organic carbon (TOC) was measured on a Shimadzu TOC-L for the quantity of DOC throughout the incubations. Optical properties were measured to determine the quality of the DOC and how it shifted through time due to sorption, providing information on molecular weight, source, and partitioning between colored and non-colored fractions (CDOC; NCDOC). The detailed methods and results of these measurements can be found in the associated isotherm and optical manuscripts (ᶜMorrissette et al., *in prep*; Pinsonneault et al., 2021/*in prep*), as they were too numerous to include in this manuscript. Organic carbon measurements and the speed at which they abiotically transformed within the incubation periods are the focus of this study.

Isotherm Comparison

As previously mentioned, much of the experimental methods, equipment, measurements, and materials were kept the same between the isotherm incubations (Pinsonneault et al., 2021) and the kinetics of this manuscript. This was done for consistency: with a reduction in variability between incubations, the experiments can be directly compared in explanatory variables, net sorption processes, effects on the kinetics, etc. This process essentially ensured that, with minimized uncertainty, the kinetic incubations gave results on the speed of the same processes observed within the isotherms.

One measure of consistency was to fit the kinetic results to the isotherm curves, to confirm their fit within the extrapolated curves. The observed change in DOC concentration (Δ[DOC]) and post-incubation DOC concentration ($[DOC]_f$) data from the 24 hr kinetic incubation was added as end member points to the relevant Jug Bay and Taskinas isotherm curves (Figure 3.2) of Pinsonneault et al. (2021) to analyze the placement within the curves (see below). Only four curves from the isotherm experiments were plotted to match the kinetic data (Table 3.2). The confidence intervals were found using error propagation.

Table 3.2. Relevant isotherm experiment data and the comparison to the matching kinetic data.

Site	Salinity	[DOC] low - high	Relevant kinetic initial conditions
Jug Bay	0 psu	3.64 - 196.03 mg L^{-1}	JBLF - JBHF; 0 psu, 2.56 - 295.57 mg L^{-1}
Jug Bay	35 psu	3.47 - 198.27 mg L^{-1}	JBLS - JBHS; 35 psu, 3.51 - 279.50 mg L^{-1}
Taskinas	0 psu	2.57 - 200.53 mg L^{-1}	TALF - TAHF; 0 psu, 4.05 - 292.67 mg L^{-1}
Taskinas	35 psu	1.94 - 198.10 mg L^{-1}	TALS - TAHS; 35 psu, 4.14 - 280.43 mg L^{-1}

Error Propagation

Confidence intervals for the original isotherm curves were calculated via error propagation of the statistical uncertainty in the fitted parameters of the (non-linear) isotherm equation:

(1) $\Delta[DOC]0-f = \frac{(Qmax \times K \times [DOC]f)}{(1+(K \times [DOC]f))} - C0$

where $[DOC]_{0\text{-}f}$ is the change in DOC concentration subtracting final values from initial, Q_{max} is the maximum sorption capacity, K is the binding affinity, $[DOC]_f$ is the final DOC concentration in solution, and C_0 is the amount of desorbable carbon on the wetland sediments.

The derivatives of the equation with respect to Q_{max}, K, and C_0 are as follows:

(2) $\frac{dQmax}{dx} = \frac{K \times [DOC]f}{1+(K \times [DOC]f)}$

(3) $\frac{dK}{dx} = \frac{Qmax \times [DOC]f}{(1+(K \times [DOC]f))^2}$

(4) $\frac{dC0}{dx} = 1$

Placing the derivatives into the error propagation equation,

(5) $\sigma_x^2 \simeq \sigma_u^2(\frac{dx}{du})^2 + \sigma_v^2(\frac{dx}{dv})^2 + \ldots + 2\sigma_{uv}^2(\frac{dx}{du})(\frac{dx}{dv})$

where estimated variance (σ_x^2) is the square of the standard error (estimated from the non-linear fit of the isotherm equation to the incubation data), and estimated covariance is the product of the correlation and standard error of the parameters in question, the equation becomes:

(1) $\sigma_x^2 \simeq \sigma_{C0}^2(\frac{dx}{dC0})^2 + \sigma_{Qmax}^2(\frac{dx}{dQmax})^2 + \sigma_K^2(\frac{dx}{dK})^2 + 2\sigma_{Qmax,K}^2(\frac{dx}{dQmax})(\frac{dx}{dK}) +$

$2\sigma_{Qmax,C0}^2(\frac{dx}{dQmax})(\frac{dx}{dC0}) + 2\sigma_{C0,K}^2(\frac{dx}{dC0})(\frac{dx}{dK})$

where the root of the output (σ_x^2) gives the standard error (σ_x), which can be used to estimate the confidence interval for a particular $[DOC]_f$ value.

Statistical Analyses

Two-sample t-tests (assuming equal variances) were used to test the difference between sites for each initial condition and the percent of sorption completed over time, to analyze the effect the specific site, and to compare the different effects of salinity levels or DOC concentration within one site.

Results

Kinetic Incubations

Figures 3.4-5 shows the comparison between Jug Bay and Taskinas Δ[DOC] (mg L^{-1}) over time for four different sets of initial conditions (HF, HS, LF, LS). The graphs depicts either that net adsorption (negative Δ[DOC] (y-axis)) or net desorption (positive Δ[DOC] (y-axis)) occurred. The axis interpretation is the inverse of the axes on the isotherm plots (e.g. Fig. 2.2), which view DOC exchange from the soil's perspective. The Jug Bay core was characterized by 20% soil organic matter (%SOM), 7% total organic carbon (%TOC), 40 m^2 g^{-1} specific surface area (SSA), and 11 mg g^{-1} non-crystalline iron (NC-Fe). Taskinas differs from Jug Bay in each one of these categories, having 40 %SOM, 12 %TOC, 24 m^2 g^{-1} SSA, and 1.4 mg g^{-1} NC-Fe (Pinsonneault et al. 2021).

For Jug Bay sediments, when inoculated with the four sets of initial conditions, 77.75 ± 0.06% of the net exchange occurred within 15 minutes. Net adsorption occurred in the HF and HS incubations, and net desorption occurred in the LF and LS treatments, with no significant difference between LF and LS ($p = 0.967$, two-sample t-test). In contrast, there was a doubling of the amount of adsorption that

occurred between the HF and HS treatments, revealing that the effects of salinity on sorption were amplified under the high [DOC] conditions. The four incubations reached equilibrium at a Δ[DOC] of -53.8 ± 4.3 mg L^{-1}, -124.2 ± 0.6 mg L^{-1}, 34.1 ± 1.8 mg L^{-1}, and 34.0 ± 1.6 mg L^{-1}, for HF, HS, LF, and LS, respectively.

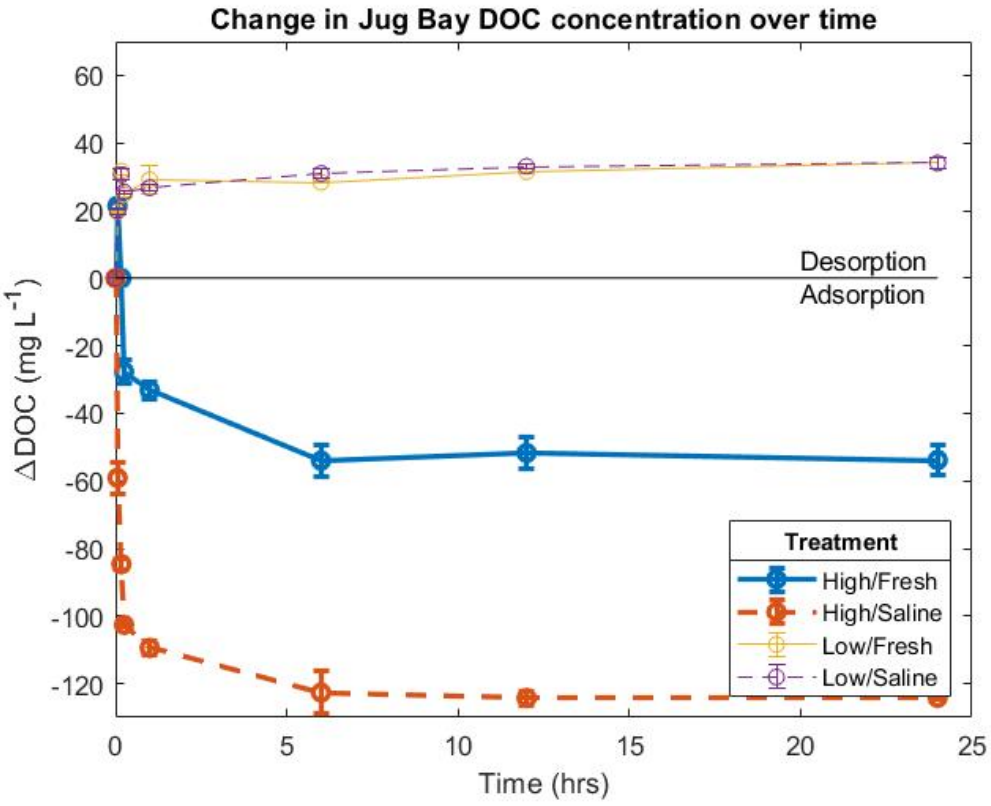

Figure 3.4. Jug Bay Δ[DOC] (final-initial) over time. Negative indicates net adsorption for that time point, while positive values indicate net desorption had occurred. The four different colors are each of the four stock solutions as highlighted in the methods section 2.3: HF (blue solid line); HS (red dashed line); LF (yellow solid line); LS (purple dashed line). Panel is over the full incubation time of 24 hours.

Taskinas sediments followed similar patterns in sorption processes with time (Figure 3.5). Again, in all cases, sorption happened quickly, with an average of 74.74

± 0.12% of sorption completed within 15 minutes, reaching relative equilibrium before 6 hours. For these sediments, however, there was more desorption such that the only treatment with net adsorption was HS. The magnitude of adsorption in the HS treatment was much lower, but the difference between it and HF was similar to the difference in the same treatments for Jug Bay. LF and LS were significantly different from one another for Taskinas ($p = 2.76 \times 10^{-7}$, two-sample t-test), indicating more of a response to the initial conditions. HF, HS, LF, and LS equilibrium values for the change in [DOC] were 25.9 ± 0.5 mg L^{-1}, -47.2 ± 3.9 mg L^{-1}, 50.3 ± 1.7 mg L^{-1}, and 33.5 ± 0.2 mg L^{-1}, respectively.

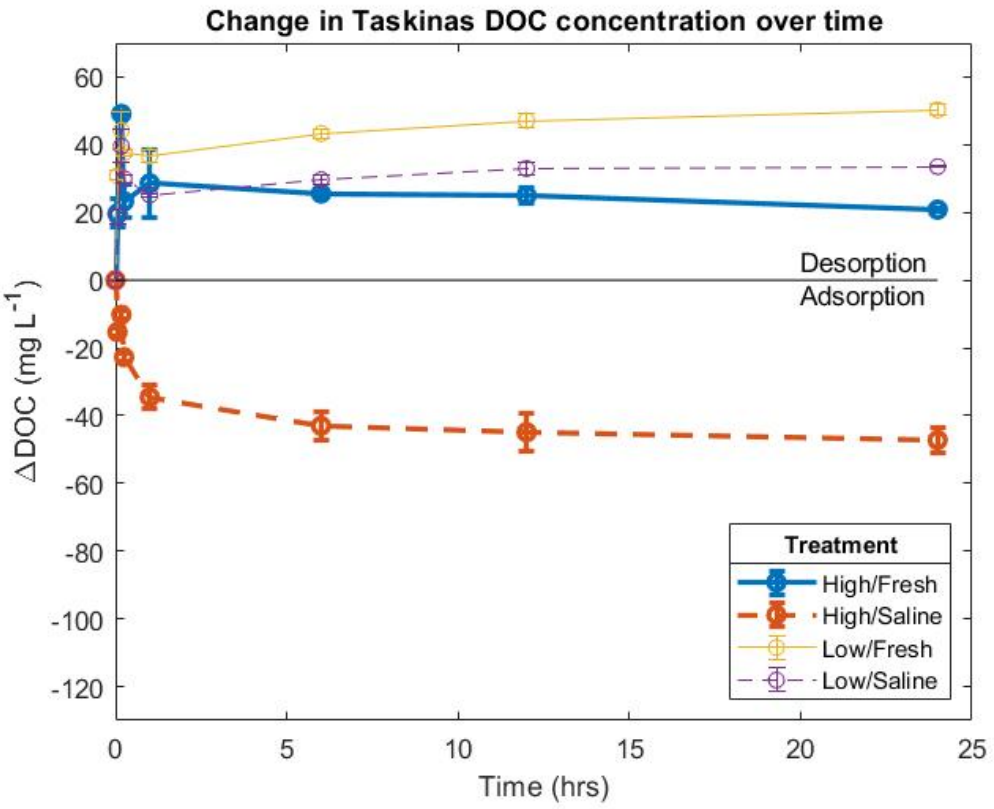

Figure 3.5. Taskinas Δ[DOC] (final-initial) over time. Negative indicates net adsorption for that time point, while positive values indicate net desorption had

occurred. The four different colors are each of the four stock solutions as highlighted in the methods section 2.3: HF (blue solid line); HS (red dashed line); LF (yellow solid line); LS (purple dashed line). Panel is over the full incubation time of 24 hours.

An average of 76.24 ± 0.09% and 83.54 ± 0.06% of total sorption across both Jug Bay and Taskinas was completed in the first 15 minutes and 1 hour, respectively, with 93.29 ± 0.03% of sorption happening out to 6 hours, thus ensuring that 24 hours was sufficient time for a sorption isotherm incubation of wetland sediments. Taskinas processes took slightly more time to reach equilibrium than Jug Bay based on percent completion of total exchange for each time point, but the difference was not statistically significant.

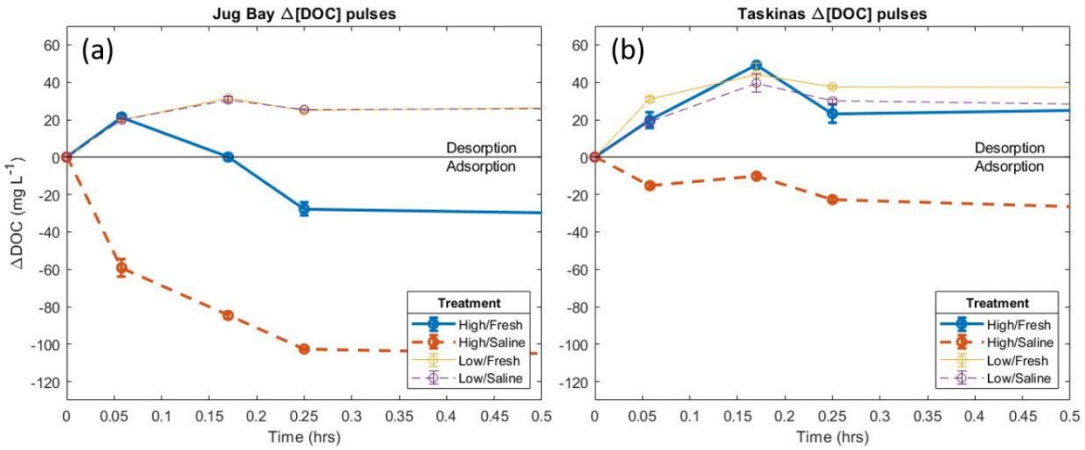

Figure 3.6. Kinetic Δ[DOC] (final-initial) over time. Negative indicates net adsorption for that time point, while positive values indicate net desorption had occurred. The four different colors are each of the four stock solutions as highlighted in the methods section 2.3. Panels are over the shortened time frame of the first 30 minutes.

Panels a-b of Figure 3.6 zoom in on the first 30 minutes of the incubations when most of the sorption fluxes occurred. These plots appear to reveal changes in the direction of the sorption in most of the treatments at both sites. This could represent a reversal of dominant sorption processes with time, i.e., desorption from the sediments followed by adsorption onto the sediments. Alternatively, the apparent initial desorption may have actually represented the immediate dissolution of freeze-dried DOC that had precipitated during the drying process, i.e., DOC became immediately present in solution upon re-wetting of precipitated DOC, followed by adsorption on the sediments. The relative importance of these two processes is unknown, since the amount of water retained in the core or the amount of DOC present in the pore water of the sediment core that may have precipitated out when the sediments were freeze-dried were both unknown.

Kinetic-Isotherm Comparison

Four sets of data from the traditional Langmuir isotherm experiments were chosen to be directly compared to the kinetic data: Jug Bay Fresh (JBF, 0 psu), Jug Bay Saline (JBS, 35 psu), Taskinas Fresh (TAF, 0 psu), and Taskinas Saline (TAS, 35 psu). The full range of [DOC] values for each of the four were plotted, then 8 points chosen from relevant kinetic data were graphed onto those curves. With the low [DOC] values, there were no significant differences between the isotherm and kinetic data points ($p = 0.995$, two-sample t-test). For the high [DOC] data points, the kinetic experiments' concentrated stock solution was, on average, 88.81 mg-DOC L^{-1} higher than the stock solution for the high initial [DOC] conditions of the isotherm experiments. So, rather than directly compare the highest value for each, the kinetic

points were checked against the original Langmuir isotherm curve confidence intervals solved for via error propagation. In Figure 3.7, the circled points for each set of initial conditions from the kinetic experiments are added onto the isotherm curves, and they are well within the calculated upper and lower limits of the standard error. The confidence interval for the Taskinas high salinity (purple triangles) incubation was not included. Due to it being more linear than the others and not indicating any approach in saturation, the non-linear fit was not able to obtain an acceptable value of Q_{max}. However, its fitted isotherm over the full range of values, extended out to the circled kinetic value, is included on Figure 3.7 to show its proximity to the fitted isotherm curve.

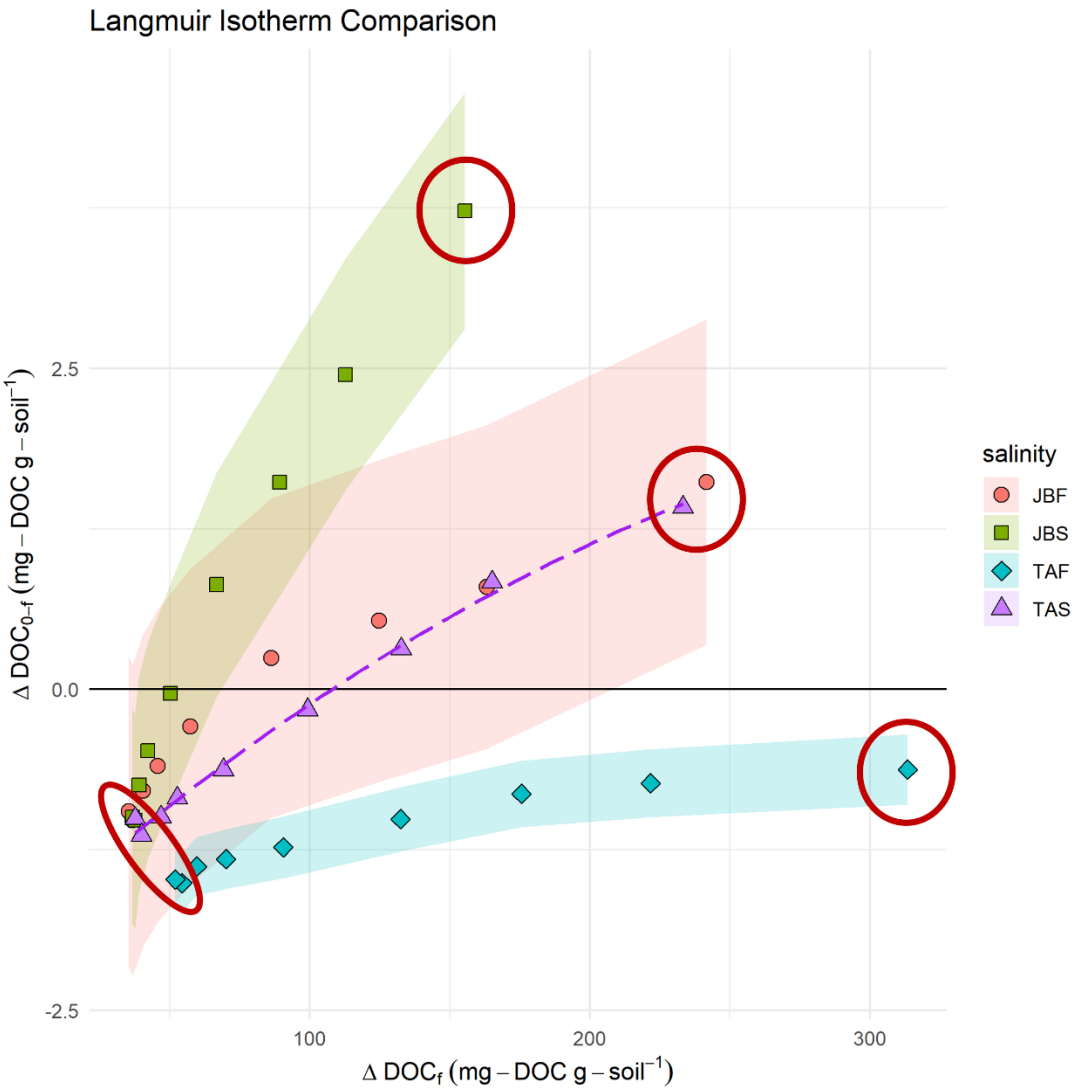

Figure 3.7. Isotherm curves plotted via $\Delta[DOC]_{0\text{-}f}$ (mg-DOC g soil^{-1}) versus $[DOC]_f$ (mg-DOC g soil^{-1}). Each color and shape represent salinity initial conditions (Jug Bay 0 psu = pink circle, Jug Bay 35 psu = green square, Taskinas 0 psu = blue diamond, Taskinas 35 psu = purple triangle). All seven of the [DOC] treatments from Pinsonneault et al. (2021) are plotted with the 24hr kinetic data points added (circled).

Discussion

The comparison between Jug Bay and Taskinas showed how sorption in two marsh soils can behave very differently when forced with the exact same initial conditions. With high [DOC], Jug Bay sediments adsorbed more than two times as much DOC than Taskinas sediments under both saline and fresh conditions. Under fresh conditions, desorption occurred from both sediments, but Taskinas released more DOC over time. These results were consistent with the isotherm experiments (Pinsonneault et al., 2021), which revealed much more net adsorption in the Jug Bay sediments and much more net desorption in the Taskinas sediments. This made sense when the biogeochemical properties of the sediments were compared: Jug Bay had higher amounts of mineral oxides, larger surface areas, and lower concentrations of organic matter, all of which promote adsorption of DOC. In contrast, Taskinas had higher amounts of organic matter, a lower presence of mineral oxides, and a subsequently smaller average surface area, all of which promote desorption of DOC (Kaiser et al., 1996; Kaiser & Guggenberger, 2003; Kaiser & Zech, 1998; Kothawala et al., 2009, 2012). Taskinas was also a brackish marsh, while Jug Bay was fresh. Thus, Taskinas sediments are likely not as susceptible as Jug Bay sediments to ionic shifts when they are exposed to saline conditions. Conversely, as the freshening of tidal marshes is seen as drivers in biogeochemical shifts (Kroeger et al., 2017; Portnoy 1999; Portnoy & Giblin, 1996), Taskinas could be highly susceptible to the fresh initial conditions, as it remains in the salinity range of 4-18 psu (Reay & Moore, 2009). The influence of these biogeochemical properties of sorption processes in the kinetic experiments was consistent with what has been seen in the literature, namely

that mineral presence, organic matter composition, and initial conditions of the solution have a strong influence on the magnitude and direction of sorption (Avneri-Katz et al., 2017; Groeneveld et al., 2020; Keil & Mayer, 2014; Kothawala et al., 2012; McKnight et al., 1992; Moore et al., 1992; Pinsonneault et al., 2021; Shields et al., 2016; Qualls, 2000, Wagai & Mayer, 2007).

These incubations were designed to isolate specific sorption processes on DOC concentrations with minimal outside influence, and for that reason, there are aspects of the closed, idealized, incubation that are not reflected in situ. For example, inoculating a fixed mass of sediment with a fixed volume of water in a closed tube does not allow for lateral diffusion, and is more representative of the introduction of an overlying water column to marsh sediments for vertical exchange of DOC or exchange with the pore waters. However, it is important to discuss that lateral exchange is most likely the smallest vector for DOC exchange to its adjacent waters. Lateral tidal influence directly on the sediments has been estimated to only have about 2.5 m of reach (Nuttle, 1988), and much of the tidal influence on marsh sediment-water column exchange occurs with the flooding tides inundating the sediments from above. Groundwater export has been found to be much smaller than other pathways of exchange (Czapla et al., 2020; Yelverton & Hackney, 1986), and most studies call for the focus of processes at the sediment surface-water column interface (French & Stoddart, 1992; Goni & Gardner, 2003). So, while groundwater could influence DOC sorption, it is only in the extent that it influences the pore waters. Thus, even though marshes are a known lateral source of DOC, it is most

likely not due to the importance of lateral transport, because the majority of any tidal marsh is not adjacent to the creek edge.

Kinetic experiments revealed sorption rates that were similar to those reported for terrestrial soils by Kaiser & Zech (1998) - 70% of sorption within 15 minutes and 90% in the first hour - and they demonstrated the importance of salinity levels and initial DOC concentrations on the direction and magnitude of sorption. The first time point of 3.5 minutes was the shortest measurable time interval, yet the speed of sorption was such that even these first time points revealed significant fluxes. Equilibrium took longer to reach than the 15-30 minutes reported by Shaker et al. (2012), but the majority of the processes over both sites and all initial conditions (84%) were completed by one hour into the incubations, indicating that monitoring short time frames is crucial for capturing sorption reactions.

Most of the ΔDOC curves in Figure 3.6 reveal what appears to be an initial spike of desorption that is followed by adsorption. There were four possible explanations for this apparent reversal in sorption processes. There could have been: 1) immediate dissolution of precipitated non-adsorbed freeze-dried DOC followed by adsorption of this DOC on the sediments; 2) different rates of adsorption and desorption, with desorption occurring faster and therefore dominating the sorption processes early in the incubation, and adsorption occurring slower and therefore having greater influence later in the incubation; 3) competing influences of the initial conditions, with the lack of salt providing an environment more conducive to desorption, but the very high [DOC] ultimately overwhelming the system and forcing the DOC to adsorb onto the sediments; and/or 4) preferential sorption of separate

DOC fractions onto the sediments, replacing and subsequently releasing previously sorbed DOC into solution. It is likely that the first option dominated the initial appearance of DOC in the first two time points of the experiments, but the other three processes may have also been occurring in tandem. Unfortunately, the relative contribution of each is unknown. The contribution of two different DOC fractions, colored and non-colored DOC pools, to the fluxes at each time point are analyzed in [c]Morrissette et al. (*in prep*).

The process of freeze-drying the cores does lead to an unknown amount of DOC dissolution (consequences discussed in Kaiser et al. 2001), however, these experiments followed that procedure for a number of reasons. The overarching goal of the set of incubations was to get equivalent material for comparative studies, to reduce variability and differences between experimental setup as much as possible. Using a different, more realistic procedure, such as incubations on fresh, intact cores, would lead to more unmeasured variations in pore water DOC concentrations, microbial activity, and starting amount of DOC in the incubation. With freeze-drying there was some precipitated DOC, however, processing all the soil in a similar fashion provided a more uniform set of samples with which to work.

The results in this chapter highlight the importance of the influence of salinity and organic matter content on sorption processes and thus, potential retention of carbon in marsh sediments. It was clear that high initial DOC concentration and high salinity primarily drove the reduction in desorption. The magnitudes differed between locations, but the pattern remained the same. This indicates the speed and direction of the net sorption process can be estimated based on initial conditions, while the

sediment characteristics can modulate the magnitude of these processes. The influences of short and long-term salinity changes on marsh systems have been studied in the last few decades due to concerns about the impacts of increased storm frequency and intensity, more severe droughts, and salt intrusion as a result of sea-level rise (SLR) (Armitage et al., 2019; Charles et al., 2019; Costanza et al., 2008; Glick et al., 2013; Grace & Ford, 1996; Herbert et al., 2018; Kirwan & Megonigal, 2013; Moffett et al., 2015; Morris et al., 2002; Neubauer, 2013; Nicholls et al., 1999; and more). These studies have shown that there is a potential for recovery under short-term salinity changes as compared to long-term (Herbert et al., 2018). However, sustained increases in salt levels decrease net ecosystem production, plant biomass, and the subsequent ability of marshes to store organic carbon and accrete sediment to combat SLR (Charles et al., 2019, Herbert et al., 2018, Neubauer et al., 2013, Weston et al., 2011). The kinetic incubations, with a maximum of 24-hour exposure of sediments to higher salinity levels, fall under acute interactions, but nonetheless provide vital information on how both freshwater and brackish marsh sediments respond to rapid changes in salinity and DOC concentration.

While the kinetic experiments revealed some rapid DOC fluxes and oscillations within minutes of sediment disturbance, the net DOC fluxes were more well behaved and predictable in ideal conditions. Since the net DOC fluxes reached equilibrium within 24 hours and reacted similarly to the initial conditions across all incubations, it should be possible to model these processes as a function of just a few variables. The chemistry that drives the specifics of adsorption and desorption is complicated (Kleber et al., 2021), but salinity, [DOC] gradient between the sediment

and water, and the number of adsorption sites (mineral concentrations) largely control DOC flux due to sorption, and they can and should be added to the sediment flux models. The addition of these processes to models such as the SFM (Di Toro, 2001; [a]Morrissette et al., *in prep*) would allow simulation of DOC fluxes from marshes with different sediment characteristics and over a wide range of salinities.

Following the patterns in bulk DOC tidal marsh sediment kinetics, the next step was to investigate sorption kinetics and their relation to the contribution of DOC pools of different sources, and how sorption kinetics change with distance from creek edges and depth. [c]Morrissette et al. (*in prep*) utilized optical measurements of absorbance, spectral slope ratio, and mixing models to determine the relative contribution of separate DOC pools, colored and non-colored (CDOC; NCDOC), over time. With key sediment characteristics, such as mineral composition and soil organic matter, being observed to vary within one marsh to the same degree as separate marshes entirely, [d]Morrissette et al. (*in prep*) performed similar kinetic incubations to determine the spatial variability in sorption kinetics across a tidal salt marsh. This suite of kinetic sorption incubations ties biogeochemical influence with temporal and spatial variability.

Conclusion

It is well-established that sorption processes are a dominant pathway for DOC exchange in wetland sediments (Bader et al., 1960; Kaiser & Zech, 1998; Kalbitz et al., 2000; Kleber et al., 2021; Kothawala et al., 2009; Pinsonneault et al., 2021). This study presents evidence that adsorption and desorption within tidal marsh sediments happens within minutes. Not only were the processes quick, but the concentration of

DOC that exchanged between the solution and the sediments was considerable, at times exceeding 100 mgC L^{-1}. The adsorption magnitude was positively related to the increases of DOC present in solution, salinity levels, and adsorption capacity. This information potentially affects the way in which marsh sediments are regarded as DOC regulators, with sorption being important for coastal policy and management when mitigating the effects of coastal sediment disturbances.

Yet, despite the prevalence and importance of these sorption processes, predictive sediment flux models do not yet include sorption processes and the rates have remained relatively unknown. The sorption kinetic incubations presented in this paper reveal how fast sorption could occur under different sets of initial conditions and how the speed and magnitude changed between sediments with different biogeochemical characteristics. These results are the first reported kinetic results within a tidal marsh ecosystem. It is crucial to incorporate sorption processes into sediment flux models to accurately represent DOC flux, because the processes allow sediments to release or retain large quantities of DOC very rapidly following a disturbance. This need is particularly acute given both short and long-term threats to wetland systems from climate change.

Chapter 4: Sorption kinetics models to inform rate parameters

Abstract

The quantification of the coastal dissolved organic carbon flux is often challenging due to the dynamic nature of many interrelated processes. Sediment flux models, useful tools for simulating nutrient, oxygen, and organic matter fluxes for sediment-water column interactions, do not always account for dissolved organic matter (DOM) specifically, often implicitly represented in background processes. For the sediment flux models that do include explicit DOM fluxes, they do not include the crucial abiotic processes of sorption, observed to be prevalent and rapid in many sediment-water column organic matter exchanges. This study formulated "simplified" numerical models to simulate adsorption and desorption processes from laboratory kinetic experiments in order to determine sorption rate parameters. The models provided a range in rate parameters from fitting linear first-order and non-linear ordinary differential equations to the kinetic change in DOC concentration curves over time. Output from three versions of the models suggested that the linear model was unable to simulate the non-linear sorption curves with linear equations, that saturation of adsorption sites was a concern and therefore a necessary inclusion in the equations, and that time-dependent rates should be incorporated in models that attempt to simulate short time scales of DOM flux due to rapid rates and oscillating exchanges. Sorption rates provided from this research were used to inform a sediment flux model with newly incorporated DOM sorption processes. Applicable sorption

rates offer a deeper understanding of dissolved organic matter interactions within wetland sediments and should be further implemented.

Introduction

Quantifying coastal carbon flux is both challenging, due to the extensive amount of interaction between and within coastal ecosystems, and necessary, considering the importance of coastal carbon cycling in the global carbon cycle. Models such as the Sediment Flux Model (SFM; Brady et al., 2013; Di Toro, 2001; Testa et al., 2013) attempt to accurately simulate observed nutrient and carbon exchange and transformation within coastal sediments, but dissolved organic carbon has only recently been added to the SFM (Clark et al., 2017). This was done due to the increasing number of studies that show that DOC is a large and important component of the coastal carbon budget but is often not considered in sediment-water column flux models (Burdige et al., 2016; Clark et al., 2017).

Tidal wetlands (with a focus on marshes for this study) are generally carbon sinks, pulling carbon from the atmosphere (Chmura et al., 2003; Chmura, 2013; Herrmann et al., 2015; Laffoley & Grimsditch, 2009; Mcleod et al., 2011; Weston et al., 2013) and burying it into their sediments. Tidal wetlands have one of the most naturally efficient carbon-capture processes sequestering ~9 TgC per year just in North America (Windham-Myers et al., 2018). In addition, tidal wetlands are known sources of dissolved inorganic and organic carbon (DIC & DOC) to their neighboring environments with fluxes that vary substantially over tidal, seasonal, and annual cycles (Clark et al., 2008; Childers et al., 1993; Herrmann et al., 2015; Najjar et al., 2018; Tzortizou et al,. 2008, Tzortziou et al., 2011). They provide as much as 80% of the total annual carbon lateral flux to coastal ocean ecosystems, which is estimated to be ~16 TgC per year (Windham-Myers et al., 2018; Wang & Cai, 2004; Wang et al.,

2016). When this carbon flux, DOC in particular, enters downstream marine ecosystems, it significantly affects biogeochemical cycling (Bolan et al., 2011; Cai et al., 2019; Chen & Hur, 2015; Day et al., 2013; Najjar et al., 2018; Windham-Myers et al., 2018; Zhuang & Yang, 2018).

Sorption has long been theorized to be an important suite of abiotic processes that both release carbon (desorption) and capture carbon (adsorption) in the sediment (Bader et al., 1960; Kalbitz et al., 2010; Kleber et al., 2021; Knobloch et al., 2021; Kothawala et al., 2008; [b]Morrissette et al., *in prep*; Pinsonneault et al., 2021; Qualls & Haines, 1992; Qualls & Richardson, 2003; Shaker et al., 2012; Wattel-Koekkoek & Buurman 2004; etc.). The kinetics of adsorption and desorption in sediments have been shown to be rapid, with the majority of the processes occurring in one hour or less after an introduction to water (Kaiser & Zech, 1998; [b,c,d]Morrissette et al., *in prep*; Shaker et al., 2012). However, information on how the sorption rates change over time in response to the sediment's biogeochemical characteristics is still lacking, and these processes are still missing from sediment flux models like SFM.

The SFM is a rate-based model that relies on parameters that determine how fast processes occur in the sediments to accurately represent interacting inorganic and organic matter pools in sediments and the overlying water column. The processes of DOC flux in sediments that are accounted for in the SFM include hydrolysis of particulate organic matter (POM), mineralization, burial, and diffusion. In order to include the above-mentioned sorption processes in the SFM, rate parameters ([e]Morrissette et al., *in prep*) must be specified, but this rate information is not currently available. This study described efforts to formulate a suite of simplified

numerical models to simulate the exact 0-dimensional conditions as in the kinetic dissolved organic carbon sorption experiments detailed in [b]Morrissette et al. (*in prep*). This was done to provide insights into the dynamics of the sorption processes in marsh sediments, and to provide rate parameters that are needed to include sorption processes in the full SFM.

Methods

The subsequent sections describe the formulation and parameterization of a suite of carbon-based zero-dimensional models that simulated the laboratory kinetic sorption incubations detailed in [b]Morrissette et al. (*in prep*) with the following assumptions:

1. Anaerobic Conditions
2. No diffusion (incubations were enclosed environments)
3. No bacterially-mediated processes (incubations were sterilized with sodium azide)
4. No precipitation/coagulation (tested separately)
5. No photobiological processes (stored/performed in the dark)

The model formulations assumed that the DOC fluxes in the laboratory incubations were driven by adsorption and desorption processes. It should be noted, however, that immediate dissolution of dried DOC upon re-wetting of the soil was a potential additional process that may have occurred as a consequence of experimental conditions. The potential influence of this process is discussed further below.

Figure 4.1 shows a conceptual diagram of the exchange of DOC pools during the incubations, also described in [c]Morrissette et al. (*in prep)*. In the left panel (Figure 4.1a), two pools were separated at time 0 with carbon associated with the sediment ($C_{wetland}$) and surrounding water (Dismal Swamp DOC; $DOC_{DismalSwamp}$). Following inoculation (Figure 4.1b), the pools exchanged between adsorbing onto the sediments and desorbing into solution, with both pools present in solution and on the sediment in differing amounts depending on time and initial conditions ([b]Morrissette et al., *in prep*). However, even though it was clear multiple pools of DOC were involved in the total DOC exchange ([c]Morrissette et al., *in prep*), only the bulk DOC pools, Cs (sediment-associated) and DOCw (solution-associated), were modeled here. Figure 4.2 shows the simplified conceptual model where at time 0 (Figure 4.2a), Cs and DOCw were separated and exchange occurred over time with sorptive flux of the bulk DOC (Figure 4.2b).

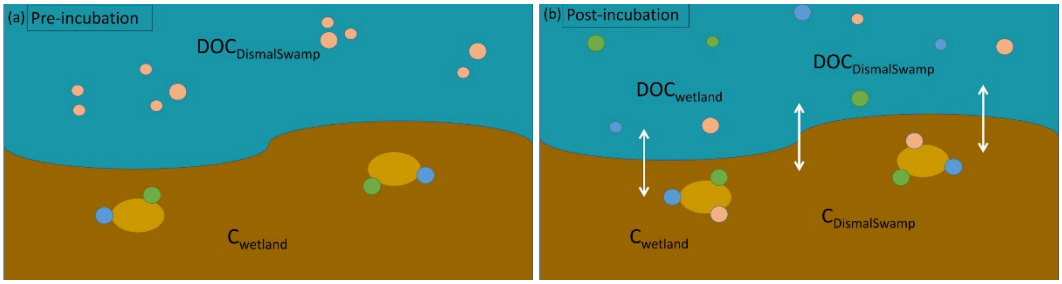

Figure 4.1a-b. Conceptual diagrams of the closed incubation experiments with (a) pre and (b) post exchange tracking of multiple carbon pools of separate origin.

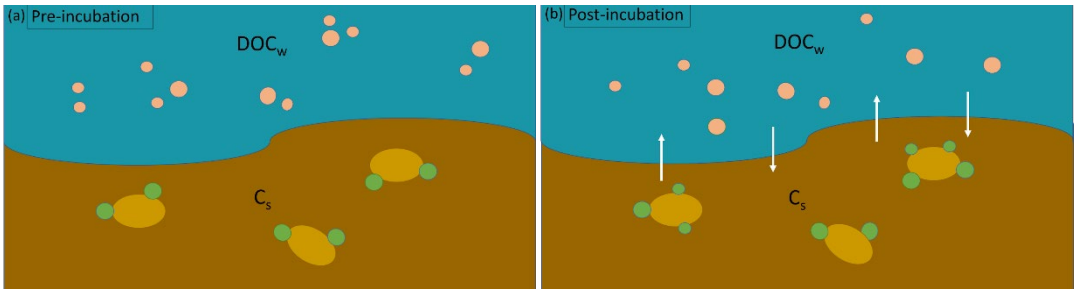

Figure 4.2a-b. Conceptual diagrams of the closed incubation experiments with (a) pre and (b) post exchange tracking of the bulk carbon pools.

The experiments were modeled mathematically using a system of two equations that simulated the flux of DOC in the closed experiments due to adsorption and desorption (Eq. 1 & 2). These equations were solved analytically, then they were subsequently modified and solved numerically to provide more realistic simulations of the experiments. These versions were referred to as the *Linear*, *Langmuir*, and *Time-Dependent* models.

Linear Model

Equations

Assuming first order ordinary differential equations (ODEs) for the above exchange (Figure 4.2), a mathematical representation of the sorption experiments was formulated as follows:

(1) $\frac{dCs}{dt} = -kdes \times Cs \; + \; kads \times DOCw$

(2) $\frac{dDOCw}{dt} = kdes \times Cs \; - \; kads \times DOCw$

where each equation represents the change in organic carbon mass over time in either the solution (DOC*w*) or sediment (C*s*). Both pools have an associated rate parameter; desorption (kdes) associated with the sediment pool, and adsorption (kads) associated with the solution pool. The solution pool loses mass from adsorption (leaving solution to attach to sediments) and gains from desorption (coming off of sediments into solution), whereas for the sediment pool the opposite is true. Equations were mass-specific since the volume of solution was constant. Parameter descriptions can be found in Table 4.1.

Analytical Solution and Fitting

Equations 1 & 2 are linear first order ODEs with constant coefficients (kdes; kads). Following a well-known process for solving a homogeneous system through substitution of the unknowns and finding the roots of the equation (Herman, 2018), a generic solution for each equation was calculated:

(3) $Cs(t) = \frac{kads}{kdes} C2 - C1\, e^{-(kads+kdes)\times t}$

(4) $DOCw(t) = C2 + C1\, e^{-(kads+kdes)\times t}$

where C_1 and C_2 are generic constants, the value of which depends on initial conditions of the incubations. At t = 0:

(5) $Cs(0) = \frac{kads}{kdes} C2 - C1$

(6) $DOCw(0) = C2 + C1$

considering $e^0 = 1$. These reduced equations were solved in terms of C_1 and C_2:

(7) $C1 = DOCw(0) - (\frac{Cs(0)+DOCw(0)}{1+kads/kdes})$

(8) $C2 = \frac{Cs(0)+DOCw(0)}{1+kads/kdes}$

which could then be re-inserted into equations 3 & 4, and simplified to be:

(9) $Cs(t) = \frac{1}{kads+kdes}\left[Cs(0)\left(kads + kdes\, e^{-(kads+kdes)t}\right) + DOCw(0)kads\left(1 - e^{-(kads+kdes)t}\right)\right]$

(10) $DOCs(t) = \frac{1}{kads+kdes}\left[Cs(0)kdes\left(1 - e^{-(kads+kdes)t}\right) + DOCw(0)\left(kdes + kads\, e^{-(kads+kdes)t}\right)\right]$

Using the "fitnlm" function in Matlab 2020a, time (t) was provided along with values for DOCw(0) and Cs(0) (Cs at time 0 was taken from the native desorbable carbon (C_0) pool calculations performed, explained, and listed in Pinsonneault et al. (2021)). Initial guesses for kads and kdes were passed to the function, which used the input parameters to fit a curve to the observational DOCw data and estimate best parameter coefficients for kads and kdes as the relative unknowns. Initial data points that created a sorption "spike" were omitted during the fitting process, as the model could not capture the directional shift. When analyzing the sorption isotherms from Pinsonneault et al. (2021; Fig. 4.3), it is apparent that regardless of the initial concentration of DOC in solution, the range of isotherm values per salinity level could be fit with one curve from one equation – meaning that the isotherm curves themselves were predictable over a range of DOC concentrations. For this model, that results in the fact that one set of kads and kdes parameters should be able to be applied to both the high [DOC] and low [DOC] kinetic results within one site, and should differ between the fresh and saline initial conditions since the isotherms vary significantly with salinity level. The fitting function essentially split the process in

half, simultaneously evaluating the best fit estimates for the high [DOC] and low [DOC] sets of data and resulting in one set of coefficients. This process was repeated for all sites.

Table 4.1. Linear Model parameters, descriptions, and units. Values of each parameter for $time_0$ were scenario-dependent (Appendices E-F).

Parameter	**Description**	**Unit**
kdes	Desorption rate coefficient	hr^{-1}
kads	Adsorption rate coefficient	hr^{-1}
Cs(t)	Mass of organic carbon adsorbed on sediments	mg
DOCw(t)	Mass of DOC free in solution	mg

Langmuir Model

Based on the incubation results from Pinsonneault et al. (2021) (Figure 4.3), the projection of the isotherm curves indicated the possibility of saturation, especially at lower salinity. Since the stock inoculant for the kinetics incubations ([b,c]Morrissette et al. *in prep*.) that led to this work had an even higher concentration of DOC, adsorption saturation on the Taskinas and Jug Bay sediments theoretically could have occurred. A version of the model was therefore formulated that included a saturation coefficient that allowed sorption to slow or stop when approaching the limit of available adsorption sites over time.

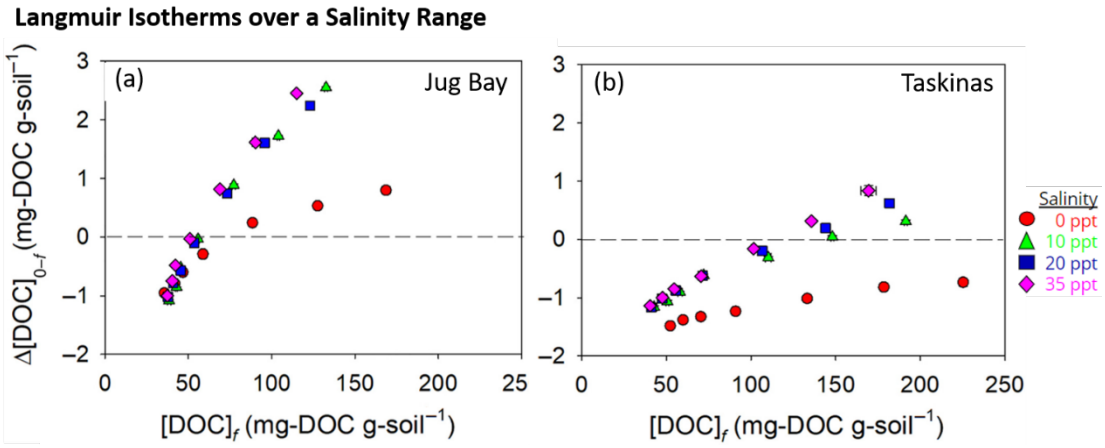

Figure 4.3a-b. Adapted from Pinsonneault et al. (2021). Langmuir isotherms for (a) Taskinas and (b) Jug Bay. Red circles, green triangles, blue squares, and purple diamonds represent four different salinity treatments of 0, 10, 20, and 35 psu, respectively. Positive values indicate adsorption, negative values indicate desorption has occurred.

Equations

Saturation was introduced into equations 1 & 2 as follows:

(11) $\frac{dCs}{dt} = -kdes \times Cs + kads_2 \times DOCw \times S$

(12) $\frac{dDOCw}{dt} = kdes \times Cs - kads_2 \times DOCw \times S$

where $kads_2$ is a second-order rate constant with units of mg^{-1} hr^{-1} by definition, and the adsorption terms were multiplied by the saturation coefficient (S; mg). S was calculated as:

(13) $S = Qmax - Cs$

where Q_{max} (mg) is the maximum adsorption capacity for the sediment and Cs (mg) is the mass on the sediment. Adding the saturation coefficient, assuming a monolayer adsorption scheme, controls the rate of adsorption based on the adsorption capacity of

the sediments. If Q_{max} increases or Cs decreases, the rate of adsorption could increase due to a larger S, and if the opposite occurs, the rate of adsorption could slow or stop. As with the linear model, initial rapid exchanges of DOC that often occurred in the experiments could not be simulated by this Langmuir model, so these initial data points were omitted during fitting.

Initial Values

Since the sediment samples used in the incubations were the same as Pinsonneault et al. (2021), fixed parameter values for Q_{max} and Cs at time 0 were used from their fitted Langmuir isotherms. DOCw at time 0 was always set to be the pre-incubation observed TOC value from laboratory analysis. Initial values for all the simulations can be found in Appendix E. The fitting scheme, using "ode23" in Matlab 2020a, performed best-fit analysis as in the analytical solution, simultaneously analyzing high and low [DOC] data sets for one set of rate coefficients.

Table 4.2. Langmuir Model additional parameters, descriptions, and units. As with the linear model, values at $time_0$ are scenario-dependent (Appendix E).

Parameter	**Description**	**Unit**
S	Saturation coefficient	mg
Q_{max}	Maximum adsorption capacity	mg
$kads_2$	Saturation adsorption rate coefficient	$mg^{-1}\ hr^{-1}$

Time-Dependent Model

A third model was formulated with a time-dependent desorption rate to capture the initial rapid exchanges of DOC that often occurred in the incubations. As mentioned above, this model assumed that these initial fluxes were due to sorption processes even though it was possible that they were due to re-wetting the freeze-dried DOC.

Initial Values

In this third version of the model, the linear sorption model equations (Eq. 1 & 2) were used, but the desorption rate was initialized to be an order of magnitude higher (kdes_max) when time was less than or equal to 0.17 hours (10 min) to allow capture of the initial peak in observed DOC in solution. The adsorption rate (kads) was initialized to be half that of the slow desorption rate (kdes_min). The two-compartment numerical model used a time step of 1.44 minutes and was fitted to the experimental data to derive rate parameters by minimizing a cost function (*modCost* in the R-package "FME"). An iterative process was used in which best-guess rate parameters were inputs in the fitting scheme to produce best-fit rate parameters, which were then cycled back as input values until the model fit errors were reduced as much as possible. This method was different from the other two models considering that the goal was only to show that a time-dependent sorption parameter could capture the oscillations in the observational data that the other versions could not. Rates for the H and L initial conditions were fit separately. All other initial values were the same as the Langmuir model (Appendix E).

Table 4.3. Time-dependent Model additional parameters, descriptions, and units. Values of each parameter were scenario-dependent (Appendix F).

Parameter	Description	Unit
kdes_max	Quick initial desorption rate coefficient	hr^{-1}
kdes_min	Slow desorption rate coefficient	hr^{-1}
kads	Adsorption rate coefficient	hr^{-1}

Analysis

The analytical solution for the linear model was calculated in Matlab 2020a using the "nlmfit" function. The Langmuir numerical model was coded and analyzed in Matlab 2020a using the "ode23" function. The time-dependent model was coded, analyzed, and assessed in RStudio, using the "deSolve" package for solving ODEs and "FME" for parameter calibration. Additional packages within RStudio of "dplyr", "tidyr", "patchwork", and "ggplot2" were used for data manipulation and graphing. A GitHub repository "Kinetic-Sorption-Incubation-Models" with the model code and input files is available here: https://github.com/hkmorrissette/Kinetic-Sorption-Incubation-Models.

Root mean square error (RMSE), model efficiency (MEF; Stow et al., 2009), average absolute error (AAE), adjusted R^2, and Spearman rank correlation values were calculated to assess model performance. RMSE is shown on the following graphs in the results section and ranked tables can be found in Appendix G. As described previously, "peaks" in the data were omitted for the linear and Langmuir

models before calculating these model performance metrics, whereas the analyses for the time-dependent model used all the data.

Results

In the following, for brevity, the solutions are reported and discussed only for the four sets of initial conditions (HF, HS, LF, and LS) for the Jug Bay experiments described in [b]Morrissette et al. (*in prep*). These results can be taken as representative of all the model fits to the experiments described in [b]Morrissette et al. (*in prep*; see Appendices I-L). The model comparison graphs show the full time series of observed data for reference, even though not all of the data was included when fitting the linear and Langmuir models.

Linear Solution

The fits to Jug Bay kinetic data followed either exponential decay functions or hyperbolic saturations functions depending on the parameter values (Eqs. 3 & 4, example fitting in Appendix H). When DOC was initially high the experiment was dominated by adsorption over time and the analytical solution captured this decay, while the opposite was true when DOC was initially low (Appendix I). Figure 4.4 shows the analytical fits to the observed data for all initial conditions of Jug Bay kinetic experiments. Most of the analytical solutions provided poor fits to the observed data, signifying that the simplest analytical solution alone cannot capture the sorption incubation results.

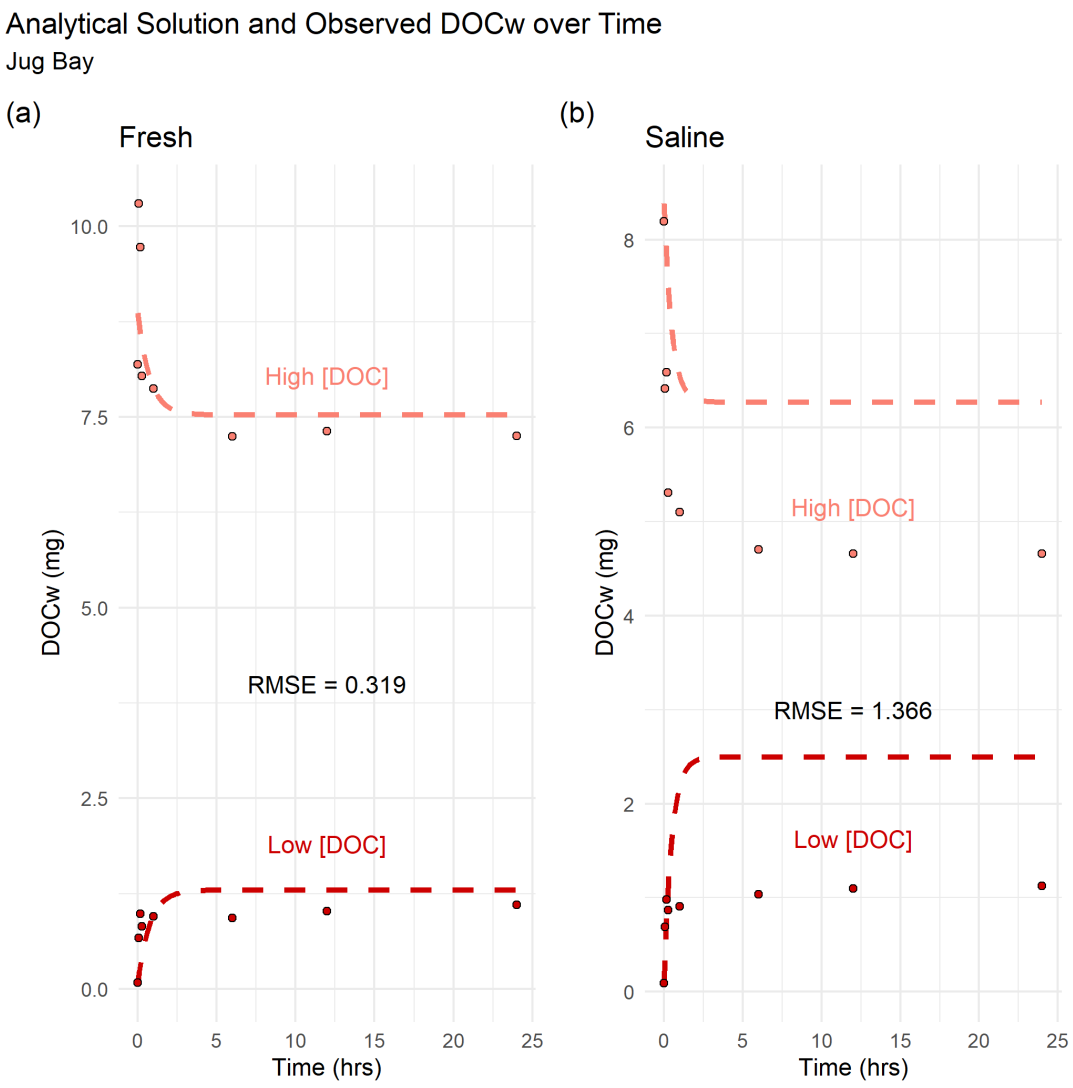

Figure 4.4. Analytical (*Linear*) solution (dashed line) to the observed (points) Jug Bay DOC mass in solution over time: a) JBHF (pink), JBLF (red); b) JBHS (pink), JBLS (red).

Langmuir Solution

Introducing a saturation coefficient to the ODEs drastically altered the model fits (Figure 4.5) with, overall, improved fits seen throughout. Occasionally, the inflection points of the curves sharpened slightly compared to the linear model. The

remaining fits for the rest of the experimental scenarios (Appendix J) depicted a similar pattern of a majority improvement from the analytical fits, suggesting that saturation is a major concern and needed to be included in the equations to improve the fits to the observed data.

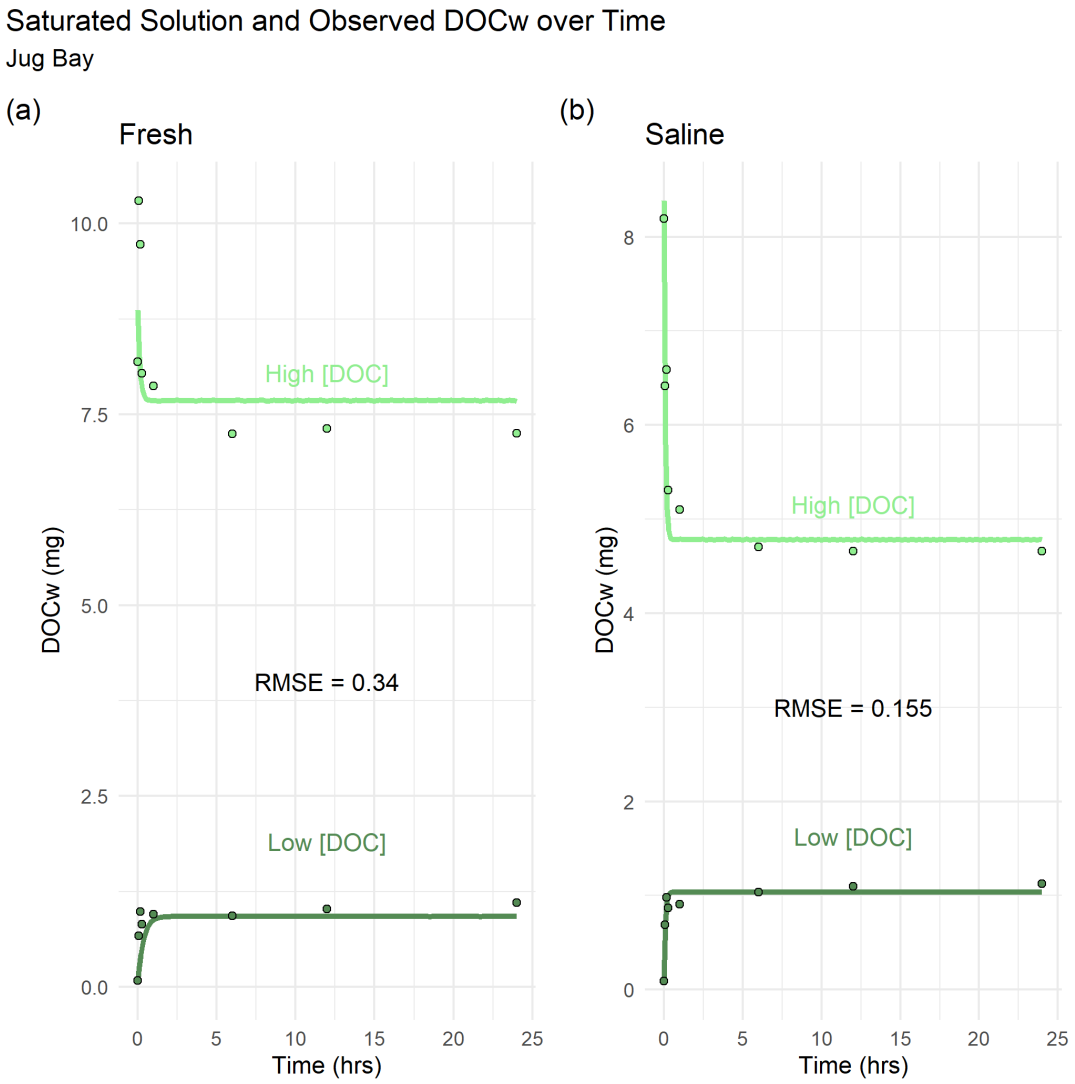

Figure 4.5. Numerical *Langmuir* model solution (green solid line) to the observed (solid points) Jug Bay DOC mass in solution over time: a) JBHF (light green), JBLF (dark green); b) JBHS (light green), JBLS (dark green).

Time-Dependent Solution

Incorporating a time-dependency in the desorption rate parameter allowed the model to capture the rapid initial changes in DOC at the first two time points (<10 minutes). However, although the time-dependent model was able to simulate the initial peaks in the data (Figure 4.6), it also resulted in fits that had much sharper inflection points. Some of the experiments had more than one directional switch, revealing an oscillation in the DOC flux. These oscillations were not captured by the model because it was coded to allow for only one change in the desorption rate over time. The model could capture these oscillations if the desorption rate is allowed to change more than once (not shown). The remaining fits for the rest of the experimental scenarios are found in Appendix K.

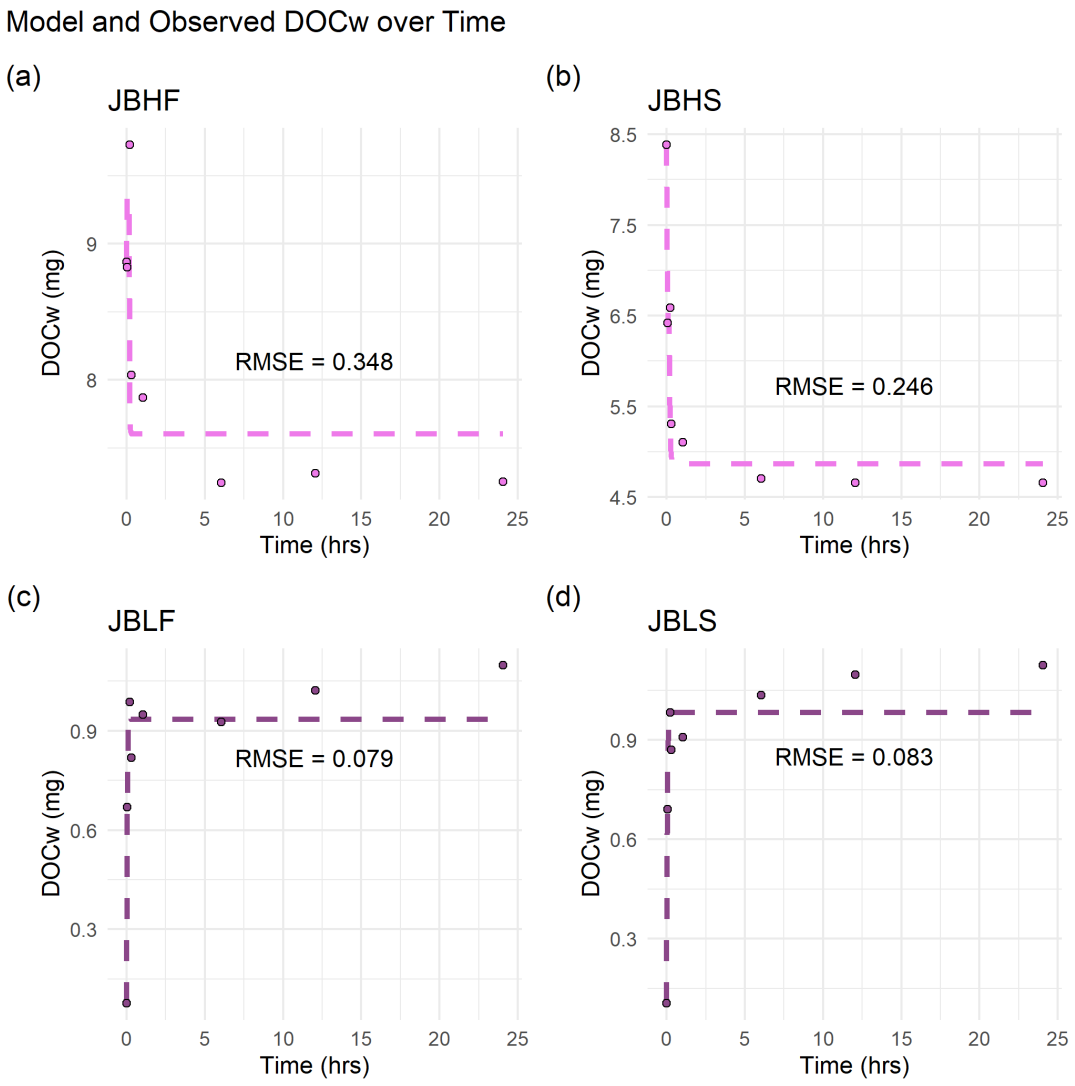

Figure 4.6. Numerical *Time-dependent* model solution (purple dashed line) to the observed (black solid points) Jug Bay DOC mass in solution over time: a) JBHF; b) JBHS; c) JBLF; d) JBLS.

Model Comparison

Figure 4.7 shows all three of the previous models' best solutions plotted against the observations. For Jug Bay, the Langmuir model fit the best to the saline data (without including the initial peaks in the data), and the time-dependent

desorption model had the best fit for both fresh experiments. Overall, the patterns seen in the remaining fits for the rest of the comparisons (Appendix L) depict relatively poor fits for the linear model outputs and markedly improved fits for the Langmuir and time-dependent model outputs, with the Langmuir capable of fitting better over the course of the 24 hours and the time-dependent capable of fitting better over the course of 15 minutes.

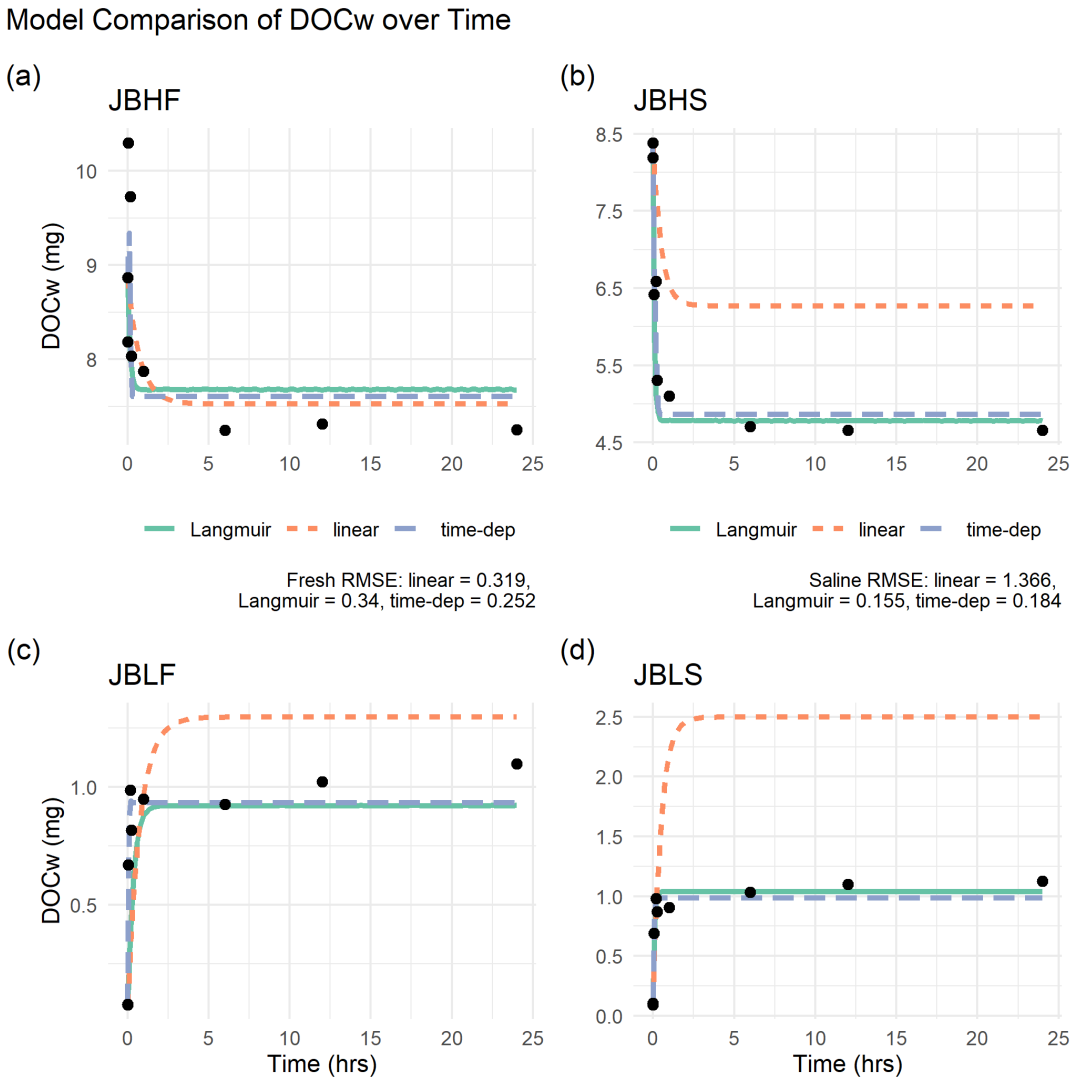

Figure 4.7. Model comparison with the graphs of Figures 4.4-6 plotted together. The *Linear* model is plotted in orange dotted lines (calibrated to reduced data set), the

Langmuir model in green solid lines (calibrated to reduced data set), and the *Time-Dependent* model in purple dashed lines (calibrated to full data set).

Rate Analysis

The linear and Langmuir kinetic models with the omitted data and the time-dependent model with the full data set, for all 32 initial condition scenarios, were compared for main statistical features. A summary of the maximum, minimum, mean, and median rate values for the adsorption and desorption rate parameter sets is listed in Table 4.4. The median values of both the desorption (kdes) and adsorption (kads) parameters were much smaller than the mean, indicating that the maximum values skew the mean of the dataset, and the majority of the rates were smaller (Table 4.4). Also, the magnitudes of the maximum and minimum values were reduced, perhaps mitigated, in the Langmuir kinetic output compared to the linear or time-dependent.

Table 4.4. Statistical summary of model-generated rate constants (hr^{-1}). The product $kads_2 * Q_{max}$ is the maximum adsorption rate of the Langmuir model (hr^{-1}) which can be compared with the linear adsorption rate (kads).

	Linear		**Langmuir**		**Time-dependent**		
	kdes	kads	kdes	kads ($kads2 * Q_{max}$)	kdes_max	kdes_min	kads
max	1.36	3417.0	65.47	18.31	868.96	238.13	65.44
min	-577.5	-0.01	0.31	0.21	0.61	0.00	0.01
mean	-36.07	218.03	5.87	4.03	62.50	19.94	11.82
median	0.33	1.88	0.98	1.13	14.17	7.73	7.86

The median rate parameters derived from this study for the linear and Langmuir models were comparable to rates previously published by Kaiser & Zech (1998) on European forest soils, i.e., they also reported fast sorption reactions that mostly occurred within 15 minutes to four hours.

Discussion

Sorption, having been proven to be a relevant and dominant abiotic process in wetland sediment carbon flux, was included in the SFM to allow for a more realistic sediment flux simulation ([a]Morrissette et al., *in prep*). However, sorption process rate data were needed to parameterize the improved SFM. This need motivated a series of sorption incubation experiments that could provide these data ([b]Morrissette et al. *in prep*). A simplified 0-dimensional model was constructed to simulate these experiments and calculate the adsorption and desorption rates. This linear model omitted several aspects of the SFM that were not relevant to the closed-environment laboratory experiments, such as oxygen, diffusion, biological activity, etc. Additionally, unlike the SFM, DOC in the linear model was not partitioned by lability levels which means that the derived rate parameters could not, necessarily, be directly applied. Nonetheless, the linear model provided important insights into the magnitude of these rate parameters and how they might change over time and space.

All versions of the models started with two ordinary differential equations that could be solved analytically (Herman, 2018). The solution to these equations with constant rate parameters produced a simple non-linear exponential decay or hyperbolic saturation response that could simulate adsorption and desorption over

time, however, this simplest version of the model could not always accurately capture the DOC mass in solution at steady state.

The comparison of three versions of the simplified model provided insights into which mathematical expression of sorption best reproduced the experimental observations. When all the time points were included (not shown), the time-dependent model always gave the best fits to the data, revealing the necessity of changing the rate constants to capture rapid initial fluxes in DOC concentrations. Tuning the linear and Langmuir models to the full data sets produced poor fits that gave too much weight to the first 3-10 minutes of the incubations. If the DOC flux oscillates over short time scales like this in nature, then these models may be inadequate when they are applied with constant rate parameters. On the other hand, when the models are fitted to the data without the initial oscillating time points, the performance of the linear and Langmuir models improved, with better fits resulting from the Langmuir model when compared to the linear, which showed that the saturated equations are adequate for modeling DOC sorption processes over longer time scales in the SFM.

However, it should be emphasized that the soil cores were freeze-dried, leading to the possibility that the initial increases in DOC were caused by re-wetting of precipitated DOC in the samples. It is impossible to know the extent of this occurrence, but it is likely incorrect to assume that the entire flux of DOC in the first few time steps of the experiments was due to sorption alone. On the other hand, the fact that oscillations in DOC concentrations were observed beyond 10 minutes in some of the experiments clearly suggests that sorption processes are also involved.

Also, adsorption has been theorized to rapidly decrease over time (Kleber et al., 2021; Koopal et al., 2019; Xing & Pignatello, 1996) due to complicated internal biogeochemical processes inside of the particles themselves, indicating an interesting set of dynamics between adsorption and desorption with equally dynamic rates. Regardless of the processes that caused the initial flux of DOC into solution, rapid adsorption and desorption were still occurring throughout the incubations, with an average of 71.7% ± 0.27 of the processes occurring within the first 15 minutes of the incubations across all experiments, matching the magnitudes of rates derived from previous experiments (Kaiser & Zech, 1998; Shaker et al., 2012).

It should also be noted that the Langmuir model consistently and drastically improved the fits to the observational data over the longer time scales when compared to the linear. This indicates that the potential for saturation was present, and that the experiments could not be accurately simulated without the saturation coefficient. Even though DOC concentrations in natural systems are much lower - recent values report an average DOC concentration of 5-6 mg L^{-1} across four years of sampling at Taskinas Marsh (Knobloch et al., 2021) and a maximum of 6.0 mg L^{-1} at Jug Bay (Logozzo et al., 2021) – Pinsonneault et al. (2021) found evidence of potential saturation in some of the isotherm curves, especially under fresh conditions. It therefore seems most appropriate to use the saturated Langmuir equations with constant rate coefficients in the SFM, given that it is generally applied at multi-annual time scales, even though it is possible that rapid sorption processes can potentially give rise to oscillations in DOC flux.

The model fits to the data provided a wide range of sediment sorption responses under different initial conditions and salinity levels that subsequently gave a wide range of wetland sorption reaction rates (Xu, 2016). This led to the question of how these rates should be used to inform the SFM. One thing was clear: the sorption rates derived from this study were 2 to 100 times faster than those that have been applied in previous SFM studies ([a]Morrissette et al., *in prep*). Moreover, when these faster rates were used in the SFM they gave very different simulation results that may be more consistent with DOC fluxes that are observed in marsh systems ([b,c,d]Morrissette et al., *in prep*). Above all, it seems clear that sorption processes should be included in all sediment flux models that track sediment carbon flux in order to properly capture the fast reactions that can occur, especially if they are being used to simulate fluxes in response to perturbations.

Conclusion

Three "simplified" numerical models were formulated to determine sorption rate parameters and to provide insights into adsorption and desorption processes in laboratory kinetic experiments. The linear model was unable to fit most of the non-linear sorption data under initial conditions that produced both net adsorption and net desorption, where the former defined an exponential decay and the latter a hyperbolic saturation. The improved fits via the Langmuir model revealed that saturation is most likely a concern and therefore does need to be considered for implementation in other models. Introduction of a time-dependency in the sorption rate in the linear model allowed the model to fit rapid initial oscillations in DOC concentrations that were observed in some experiments. This parameter time-dependency may be required in

models that seek to simulate sediment flux following a disturbance and/or when/where oscillations in DOC flux occur over time as was also observed in some experiments, with the caveat that it is likely the initial rapid oscillations were partly or wholly due to a methodological artifact.

Obvious next steps for model development include adding a salinity and/or spatial dependence to the sorption processes and perhaps more sophisticated ways to simulate time-dependence to capture sediment carbon flux variability more accurately. These kinds of improvements will provide more accurate predictive sediment carbon flux models that are needed to determine more accurate carbon budgets for the marsh-estuarine complex and simulate the impacts of released/retained carbon to the surrounding environments.

Chapter 5: Optical properties as tools to track distinct dissolved organic carbon pools during sorption kinetics

Abstract

The quantity and quality of colored dissolved organic matter (CDOM) is observed as an important driver of many biogeochemical processes, affecting food webs and biological activity. It is also an important proxy for water quality, but the details of its coastal sediment-water column exchange, and that of its non-colored counterpart (NCDOM), are largely understudied. Due to recent studies suggesting that sorption processes affect CDOM and NCDOM in different capacities, this study used optically distinct sources of DOC to provide information on separate colored DOC (CDOC) and non-colored DOC (DOC) exchange via sorption over time. This was done using optical mixing models on sorption absorbance outputs from a set of laboratory kinetic experiments. Results revealed that CDOC was controlled by initial conditions, being rapidly adsorbed from solution over time with high DOC concentrations and salinity, and desorbed from the sediment over time under low DOC concentrations and salinity. NCDOC, unaffected by initial conditions, rapidly and consistently desorbed from the sediment over time. The separate pools moving independently throughout the 24-hour time series suggested that highly humic colored material was preferentially adsorbed over time, replacing native CDOC and NCDOC on the sediments and subsequently leading to a higher native DOC concentration in solution over time. These data could be important for coastal management decisions and carbon flux modeling under high levels of DOC input to marsh ecosystems.

Introduction

Colored dissolved organic matter (CDOM) is the fraction of DOM that absorbs light in visible and UV wavelengths. The quality and quantity of CDOM affects light attenuation, primary productivity, microbial activity, and nutrient cycling, being a vital proxy for water quality monitoring (Osburn et al., 2015; Tzortziou et al., 2015; Wang et al., 2007). Because CDOM can be tracked with optical measurements, it is an important proxy for dissolved organic carbon (DOC) cycling in the riverine-wetland-estuarine-coastal ocean complex carbon cycle (Fellman et al., 2010; McKnight et al., 2001; Stedmon & Nelson, 2014; Tzortziou et al., 2015). Some optical properties of CDOM can also be measured via remote sensing, even in complex and dynamic coastal waters (Aurin & Dierssen, 2012; Brezonik et al., 2015; Cao & Tzortziou, 2021; Vantrepotte et al., 2015), allowing large scale synoptic quantification of CDOM variability.

Despite being a major sink of carbon as a whole worldwide, tidal marshes are known to be a source of dissolved inorganic and organic carbon (DIC, DOC) to estuarine and coastal ocean waters (Jordan & Correll, 1999; Najjar et al., 2018; Neubauer & Anderson, 2003; Tobias & Neubauer, 2009; Windham-Myers et al., 2018). Tidal marshes are also a net source of the colored fraction of DOC (CDOC) to adjacent waters with the magnitude of the fluxes varying significantly with seasonal, tidal, floral, and anthropogenic influence (Clark et al., 2008; Gao et al., 2011; Osburn et al., 2015; Tzortziou et al., 2008, 2011, 2015; Wang et al., 2007). The quality of this marsh-derived CDOC has been reported to be composed of highly humic, complex, aromatic, more refractory compounds with a high molecular weight (Clark et al.,

2008; Osburn et al., 2015; Tzortziou et al., 2008, 2011), and this CDOC has been shown to significantly affect downstream food webs and biogeochemistry (Bolan et al., 2011; Cai et al., 2019; Chen & Hur, 2015; Day et al., 2013; Najjar et al., 2018; Windham-Myers et al., 2018; Zhuang & Yang, 2018).

The processes that control DOM exchange between the water column from marsh sediments are numerous, including sequestration, photodegradation, plant leaching, microbial activity, and tidal flushing. Sorption is an abiotic process that is considered to be one of the most important mechanisms involved in long-term carbon storage within the sediments (adsorption; Bader, 1960; Kleber et al., 2021), and it is also involved in the release of carbon into the overlying water column at rates that are much more rapid than microbial degradation (desorption; Qualls & Richardson, 2003). Sorption processes have also been shown to be dominant and rapid in controlling bulk DOC fluxes between sediments and adjacent water in forest and tidal marsh soils (Kaiser & Zech, 1998; [b,d]Morrissette et al., *in prep*; Pinsonneault et al., 2021; Shaker et al., 2012), but how the individual colored and non-colored dissolved organic matter (NCDOC) fractions sorb over time is largely unknown.

It is important to understand how CDOC and NCDOC separately sorb over time, and how these kinetics affect the quality of the DOC compounds that are exchanged between marsh sediments and adjacent waters, in order to inform carbon budgets and simulation models. Recent isotherm and kinetics studies provide new insights into how the CDOC and NCDOC pools move between water and sediment in marsh soils ([c]Morrissette et al., *in prep*; Pinsonneault et al., *in prep*). Pinsonneault et al. (*in prep*) found a net, preferential adsorption of CDOC and a net desorption of

NCDOC after 24 hours in isotherm incubations, and they showed that the magnitude of the exchanges was regulated by key soil and site characteristics, such as iron content and salinity. The results reported here build on Pinsonneault et al. (*in prep*) by tracking the movement of CDOC and NCDOC pools due to sorption over the course of 24 hours and thus provide the first insights into the sorption kinetics of these pools.

Methods

Stock Solutions

120 liters of surface water from the Jericho Ditch (36°41'45.03"N, 76°30'28.16"W) of the Great Dismal Swamp National Wildlife Refuge (GDS) (Figure M.1) was collected. Collections were performed in April 2018, August 2018, and November 2019. This location was chosen, as previously described ([b]Morrissette et al. *in prep*, Pinsonneault et al. 2021), for its optical characteristics, particularly its extremely low spectral slope ratio (S_R) when compared to other sources, making it useful in tracking DOC pools (Helms et al., 2008). This water has a naturally high concentration of colored, humic DOC that was concentrated further through the process of reverse osmosis. Each collection of 120 L of surface water was cycled through the Growonix GX600 machine, removing the permeate and recirculating the retentate until only 40 L of concentrated stock remained for a final DOC concentration of 217 mg L^{-1}, 275 mg L^{-1}, and 204 mg L^{-1} for the three collections, respectively. The purpose of this was to obtain a concentrate of DOC that would expose the sediments in the experiments to a level that was at about an order of magnitude higher than natural pore water DOC concentrations at these sites. This

ensured that at least some net adsorption would be observed within each set of incubation conditions.

The stock solution was then filtered down through a 10 μm pore size Whatman Polycap 75 HD disposable filter capsule, followed by a similar filter of 5 μm pore size, then 0.2 μm pore size Whatman Polycap 36 TC polyethersulfone membrane capsule to remove particulates. Sodium azide (NaN_3) was added to the solution to a concentration of 1mM to inhibit microbial activity. This stock was then divided into two parts, with one part kept fresh and the other made saline with the addition of Instant Ocean until the solution was 35 psu.

To get a stock with low initial DOC concentrations, deionized water was brought to the same concentration of sodium azide. Despite the fact that microbial activity in the DI water was expected to be nonexistent, this was to ensure the non-concentrated stock had the same chemical properties as the concentrated GDS stock. Hydrochloric acid (HCl) was added to the DI water to reduce the pH to match the GDS stock, then a subset of the DI water was made saline via an addition of Instant Ocean until levels reached 35 psu. This process created four stock solutions:

1. High initial [DOC], low salinity (HF)
2. High initial [DOC], high salinity (HS)
3. Low initial [DOC], low salinity (LF)
4. Low initial [DOC], high salinity (LS)

All stock solutions were kept in the dark at 4°C for the duration of the experiments.

Measurements

Batch incubations on homogenized sediment cores from Taskinas Marsh

(37°25'N, 76°43'W) and the Jug Bay Wetland Sanctuary (38°46'N, 76°42'W) were performed under 95% nitrogen (N_2) and 5% hydrogen (H_2) atmosphere in a Coy Laboratory Products anaerobic chamber at seven incubation times of 3.5 min, 10 min, 15 min, 1 hr, 6 hrs, 12 hrs, and 24 hrs. The detailed methodology is described in Pinsonneault et al. (2021) and [b]Morrissette et al. (*in prep*). Considering how highly colored the GDS solutions were, post-incubation filtered supernatants were diluted by a factor of 10 with the appropriate dilutant (HF with LF, HS with LS) before being measured for total organic carbon concentration and spectral properties.

Absorbance scans on a Thermo Scientific Evolution 220 UV-Vis spectrophotometer were performed on every pre- and post-incubation sample. Scans were 2 nm intervals between wavelengths of 270-750 nm with deionized (DI) water as reference. Triplicate scans were run for each sample, with DI blanks between every sample. CDOM absorption coefficients ($a_{CDOM}(\lambda)$) were calculated from the optical density (OD) and path length (l, which was 1 cm = 0.01 m for measurements in this manuscript):

(1) $$aCDOM(\lambda) = \frac{2.303 * OD}{l}$$

which is then further multiplied by a factor of 10 to account for dilution. pH (Thermo Orion 3 Star pH meter), salinity (WTW multi 340i probe), and conductivity were also measured on all samples.

Spectral slope was calculated from the non-linear fit (Matlab, *nlinfit*) of absorbance spectra for the full scan, 270-700 nm, to the equation:

(2) $$aCDOM(\lambda) = aCDOM(440)e^{-S(\lambda-440)}$$

where S (nm^{-1}) is the spectral slope. Slopes over the smaller wavelength intervals of

275-295 nm ($S_{275-295}$) and 350-400 nm ($S_{350-400}$) were estimated by linear regression of $\ln(aCDOM(\lambda))$ vs. λ (Matlab, *regress*). These slopes are useful as measures of CDOM source and diagenetic state. Slope ratio (S_R) was subsequently calculated as the ratio of the two:

(3) $S_R = \frac{S275-295}{S350-400}$

As an aromatic content proxy, specific ultraviolet absorbance at 280 nm (SUVA 280) was measured as the absorbance value at the 280 nm wavelength divided by the concentration of DOC per sample.

(4) $SUVA_{280} = \frac{aCDOM(280)}{[DOC]}$

Fluorescence for each sample triplicate was measured on a Horiba Jobin Yvon FluoroMax-3 spectrofluorometer to obtain excitation-emission matrices (one replicate only) and fluorescence indices, i.e., fluorescence (FI), freshness (β:α), biological (BIX), and humification (HIX). Excitation intervals were 5 nm and emission intervals were 2 nm. Raw data was processed with Datamax software. The correction for the inner filter effect on spectra was applied as in Murphy et al. (2013). All FI, β:α, BIX, and HIX were analyzed and interpreted as in Helms et al. (2008) and Hansen et al. (2016). The parallel factor analyses (PARAFAC) of the excitation-emission matrices (EEMs) are reported in Pinsonneault et al. (*in prep*).

DOC Exchange

Optical properties were used to distinguish DOC pools following a procedure similar to that described by Clark et al. (2019) and modified by Pinsonneault et al. (*in prep*). This approach considered the DOC pool to be partitioned into colored CDOC

and non-colored (NCDOC) fractions. The CDOC fraction was determined by reference to a specific absorbance, *a*doc(λ)* (m^2 g^{-1}). The CDOC fraction in any given absorbance scan is estimated based on the equation:

(5) $a(\lambda) = CDOC \times a^{*}doc(\lambda)$

where CDOC (mg L^{-1}) is determined using a non-negative least-squares fit (Matlab, *lsqnonneg*) of *a(λ)* vs *a*doc(λ)* for wavelengths between 270-600 nm. For *a*doc(λ)*, the initial solution (GDS), called a*pre, and the post-incubation results of similar incubations from Pinsonneault et al. (*in prep*), termed a*post (see Results), were considered. Once CDOC is determined, NCDOC is estimated as:

(6) $NCDOC = DOCtot - CDOC$

where DOC_{tot} is the total observed DOC in solution per sample and time point.

Statistical Analyses

Two-sample t-tests (assuming equal variances) were used to test differences in absorbance scans between high/low, fresh/saline, and site, and the differences in percent sorption completed between CDOC vs. NCDOC per and between site.

Results

Optical properties differed between the Dismal Swamp surface water collections for the isotherm, kinetic, and spatial incubations (Pinsonneault et al., *in prep*, [b,d]Morrissette et al., *in prep*) due to seasonal influences (collected in April 2018 - S_R = 0.8; August 2018 - S_R = 0.76; and November 2019 - S_R = 0.77, for the HS pre solution, respectively), so details of the absorbance and spectral slope ratios of the

pre-incubation samples between sets of experiments differed slightly. However, a similar general trend of compositional shift over time was observed in all experiments.

Jug Bay absorbance spectra (Figure 5.1) show that absorbance decreased over time in the HF and HS experiments (HF = 25.76% decrease; HS = 62.86% decrease), consistent with CDOC adsorbing onto the sediments (bulk DOC exchange can be found in [b]Morrissette et al. (*in prep*)). Final absorbance values at 270 nm (time 7) for JBHS were significantly lower (55.62%; $p = 1.11 \times 10^{-15}$, two-sample t-test) in magnitude than JBHF, which agreed with the higher total amount of adsorption in the JBHS experiments. For LF and LS, absorbance was very small (no added DOC), but there was an increase in absorbance over time (24.70% and 36.45%, respectively), consistent with net desorption. The LF and LS spectral scans were not significantly different for Jug Bay ($p = 0.47$, two-sample t-test).

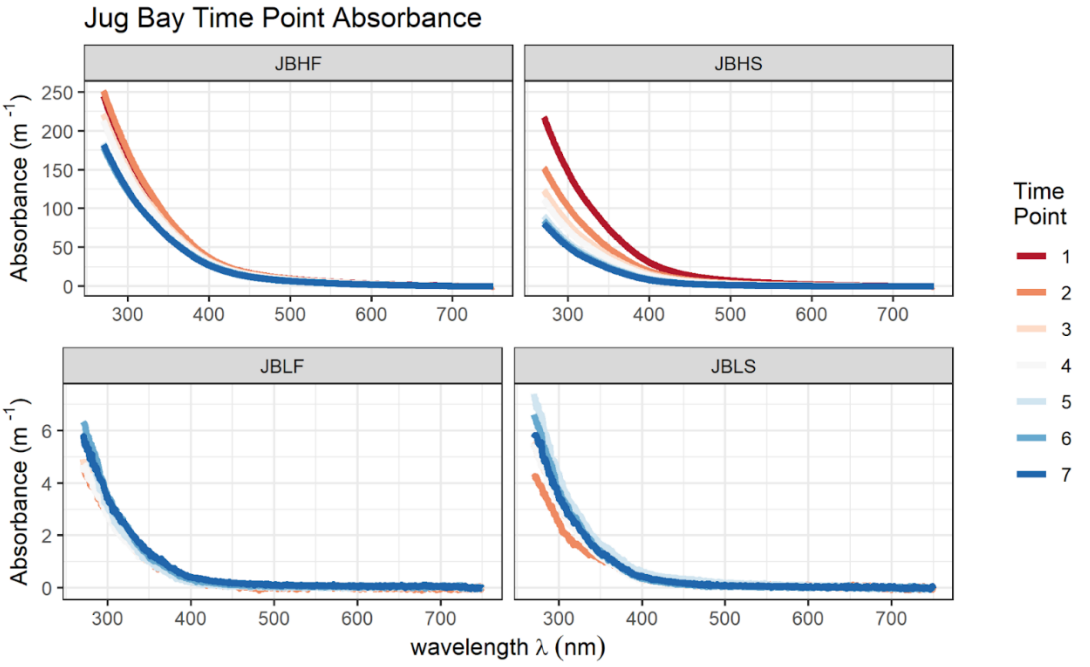

Figure 5.1. Jug Bay absorbance spectra of each post-incubation sample (averages, n=3 for every time point). The four panels are the sets of initial conditions, and the colors represent the 7 incubation time points (1 = 3.5 min, 2 = 10 min, 3 = 15 min, 4 = 1 hr, 5 = 6 hrs, 6 = 12 hrs, 12 = 24 hrs).

Taskinas absorbance spectra (Figure 5.2) follow the same patterns as Jug Bay - absorbance decreased over time in the HF (8.43%) and HS (25.41%) sets of initial conditions and increased in the LF (61.64%) and LS (62.55%) experiments - but the magnitude of change within each set of spectra was lower for HF/HS and higher for LF/LS, showing less adsorption and more desorption over time than Jug Bay. HS was still significantly lower (37.49%; $p = 3.24 \times 10^{-7}$, two-sample t-test) in absorbance at 270 nm than HF, and with Taskinas the LF and LS spectra were significantly different as well (59.41%; $p = 1.52 \times 10^{-16}$, two-sample t-test).

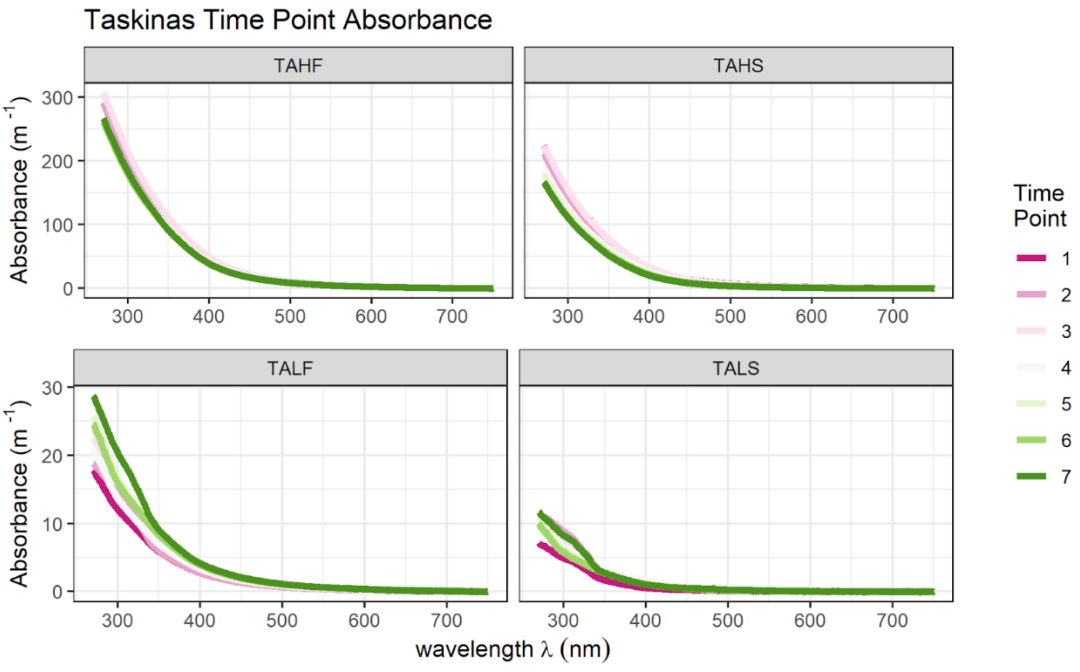

Figure 5.2. Taskinas absorbance spectra of each post-incubation sample (averages, n=3 for every time point). The four panels are the sets of initial conditions, and the colors represent the 7 incubation time points (1 = 3.5 min, 2 = 10 min, 3 = 15 min, 4 = 1 hr, 5 = 6 hrs, 6 = 12 hrs, 12 = 24 hrs).

Jug Bay and Taskinas slope ratios (S_R, Figures 5.3-4) for HF and HS experiments mirror the movement of DOC. Rapid shifts in S_R within the first few minutes matched the rapid exchange of CDOC and NCDOC. The overall increase in S_R for Jug Bay over 24 hours (by 2.25% and 1.19% for HF and HS, respectively) indicated a shift to CDOC of a lower molecular weight, matching the removal of very humic CDOC of high molecular weight from the Dismal Swamp stock solutions (Hansen et al., 2016; Helms et al., 2008). Taskinas had less overall increase in S_R over time, even decreasing slightly by the end of the 24 hours (by 2.76% and 3.51% for HF and HS, respectively), indicating that less CDOC was removed in the Taskinas incubations. The time courses of S_R for LF and LS were not shown due to the shape of the curves being influenced by the small amount of absorbance coming from the dilutant. Values presented here fall within the range reported by Helms et al. (2008), who showed a S_R range of 0.69 to 0.84 for the Great Dismal Swamp (Feb 2006 sample, fresh, %HMW = 88.7) and samples from Great Bridge, VA (May 2004-Oct 2005, brackish, avg. %HMW = 74.9), respectively. Jug Bay and Taskinas spectral slopes ($S_{275\text{-}295}$) were also calculated over time and can be found in Appendix O.

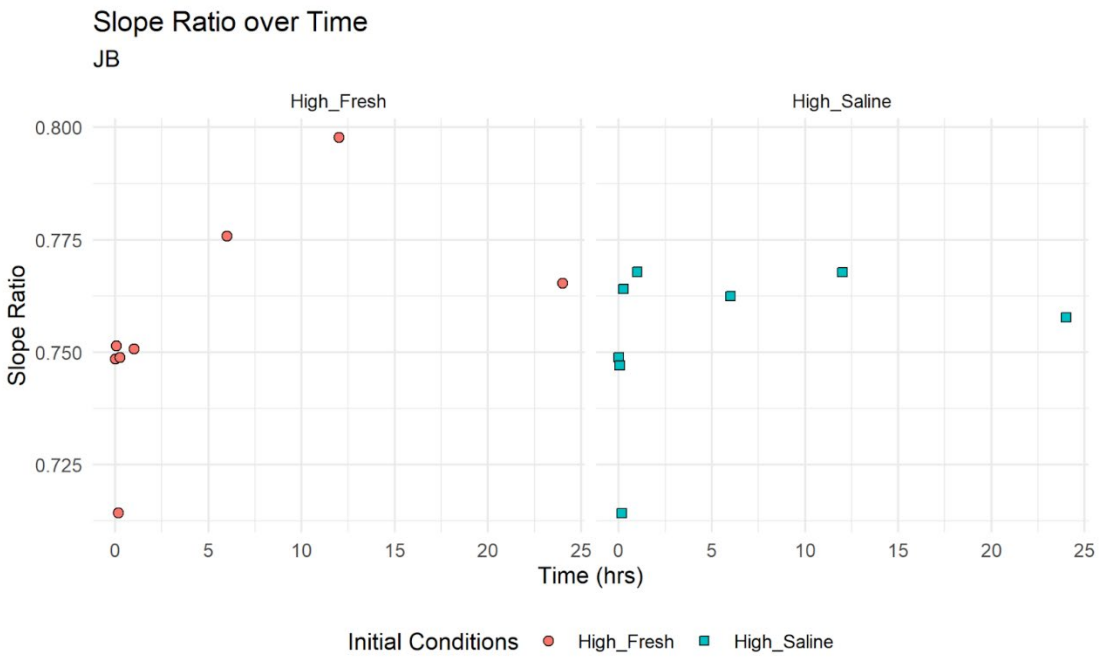

Figure 5.3. Jug Bay slope ratio over time for HF (orange circles) and HS (blue squares) initial conditions.

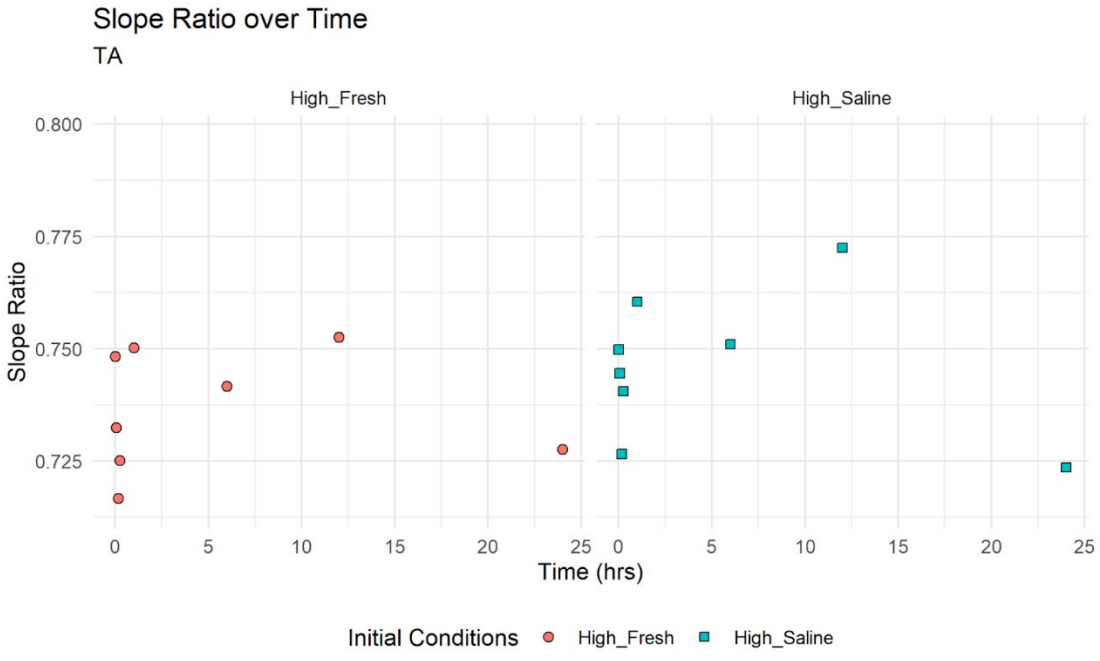

Figure 5.4. Taskinas slope ratio over time for HF (orange circles) and HS (blue squares) initial conditions.

Other spectral characteristics were measured over time to compare to literature values and analyze the change in composition over time. Values for the final indices fit within the average range reported in literature values for wetland waters, which are 1.2-2.3 for FI (Hansen et al., 2016; Jaffe et al., 2004; Wang et al., 2014), and 0.4-1.0 for β:α and BIX (Hansen et al., 2016; Wang et al., 2014). Literature ranges for HIX values are much larger, within which the LF and LS experiment values fit: 0.6-5.0 (Guo et al., 2013; Hunt & Ohno, 2007; Ohno, 2002). The HIX values for HF and HS experiments were much higher (>10), matching the Great Dismal Swamp's naturally highly colored, highly humic composition. SUVA 280 almost always decreased over time for all sites and depth segments, except for TALF, which corroborated the shift in composition of DOC to a higher percentage of NCDOC over time.

Table 5.1. Average ± standard deviation of values at time 7 (24 hrs) for freshness, biological, fluorescence, and humification indices and delta (Δ) values for SUVA 280 after 24 hrs per site and set of initial conditions.

Site	Freshness Index (β:α)	Biological Index (BIX)	Fluorescence Index (FI)	Humification Index (HIX)	ΔSUVA 280
range	0.376 - 0.832	0.382 - 0.895	1.737 - 2.286	0.862 - 20.295	--

JBHF	0.475 ± 0.07	0.481 ± 0.07	1.908 ± 0.06	12.388 ± 2.99	-0.667 ± 0.03
JBHS	0.484 ± 0.00	0.488 ± 0.00	1.932 ± 0.03	12.597 ± 1.57	-1.750 ± 0.04
JBLF	0.818 ± 0.17	0.882 ± 0.23	2.286 ± 0.44	1.055 ± 0.48	-7.557 ± 0.52
JBLS	0.832 ± 0.08	0.895 ± 0.09	1.990 ± 0.05	0.862 ± 0.40	-9.623 ± 1.08
TAHF	0.376 ± 0.00	0.382 ± 0.00	1.737 ± 0.01	16.725 ± 0.49	-0.393 ± 0.10
TAHS	0.416 ± 0.00	0.421 ± 0.00	1.827 ± 0.01	20.295 ± 0.10	-3.300 ± 0.03
TALF	0.561 ± 0.03	0.565 ± 0.03	1.759 ± 0.01	3.522 ± 0.03	0.150 ± 0.10
TALS	0.643 ± 0.06	0.662 ± 0.08	1.953 ± 0.02	3.523 ± 0.29	-0.237 ± 0.28

The partitioning of the quantity of CDOC in the sample was based on how closely the sample spectra matches the a^*_{DOC} spectra, after scaling to obtain a best fit (Equation 3). Statistically, this was estimated using a least squares non-negative analysis of the GDS pre-incubation absorbance as the independent variable and each post-sample absorbance as the dependent variable, the fitted coefficient being the CDOC.

To subsequently analyze the partition of CDOC and NCDOC in solution per time point, several a*doc values were compared. Even though the quality of DOC changed throughout the time series, the kinetics incubations only tested two initial DOC concentrations, which was insufficient for a regression analysis to provide an a*doc value from the post-incubation solutions based on the method of Clark et al.

(2019). Given the change in slope ratio from the initial, the post-incubation samples at each time point are inferred to consist of some combination of $CDOC_{DismalSwamp}$ from the stock solution and native wetland sediment $CDOC_{wetland}$. Pre-incubation optical measurements of the stock solutions were the only spectra with a CDOC derived from a single source. Nevertheless, a*pre provided an acceptable basis to partition the CDOC fraction, as it gave consistently good fits to the incubation spectra using Equation 3. (JB a*pre avg. $R^2 = 0.946$, TA a*pre avg. $R^2 = 0.966$; Appendix P). Values for a*post from Pinsonneault et al. (*in prep*) were also tested, but the fits to the incubation spectra were not better than a*pre. Also, due to the aforementioned minor differences in optical properties of the Dismal Swamp stock solutions used for a*pre, it could not be assumed that the a*post values from the isotherm incubations were also applicable to the kinetic spectra.

Analyzing the partitioning of CDOC vs NCDOC in the post-incubation samples using the a*pre (GDS) specific absorbance revealed several patterns. Figure 5.5 shows the concentration of both pools in the post-incubation sample at every incubation time point for Jug Bay. For the incubations with high initial [DOC], CDOC was quickly adsorbed, losing 75.06 mg L^{-1} for a 27.51% decrease over time. When salinity was compounded with high [DOC], a larger loss of CDOC was seen over time, with 195.92 mg L^{-1} being removed for a 71.75% loss. With low initial [DOC], CDOC stayed at a low concentration in solution throughout the time series, showing a minor amount of desorption, gaining 3.97 mg L^{-1} and 4.12 mg L^{-1} over time for LF and LS incubations. NCDOC was always a net gain in solution over time, increasing on average by 34.77 mg L^{-1} for HF, LF, and LS incubations. HS NCDOC

was not included in this average because it increased by ~2x more than the rest; 78 mg L^{-1} over time.

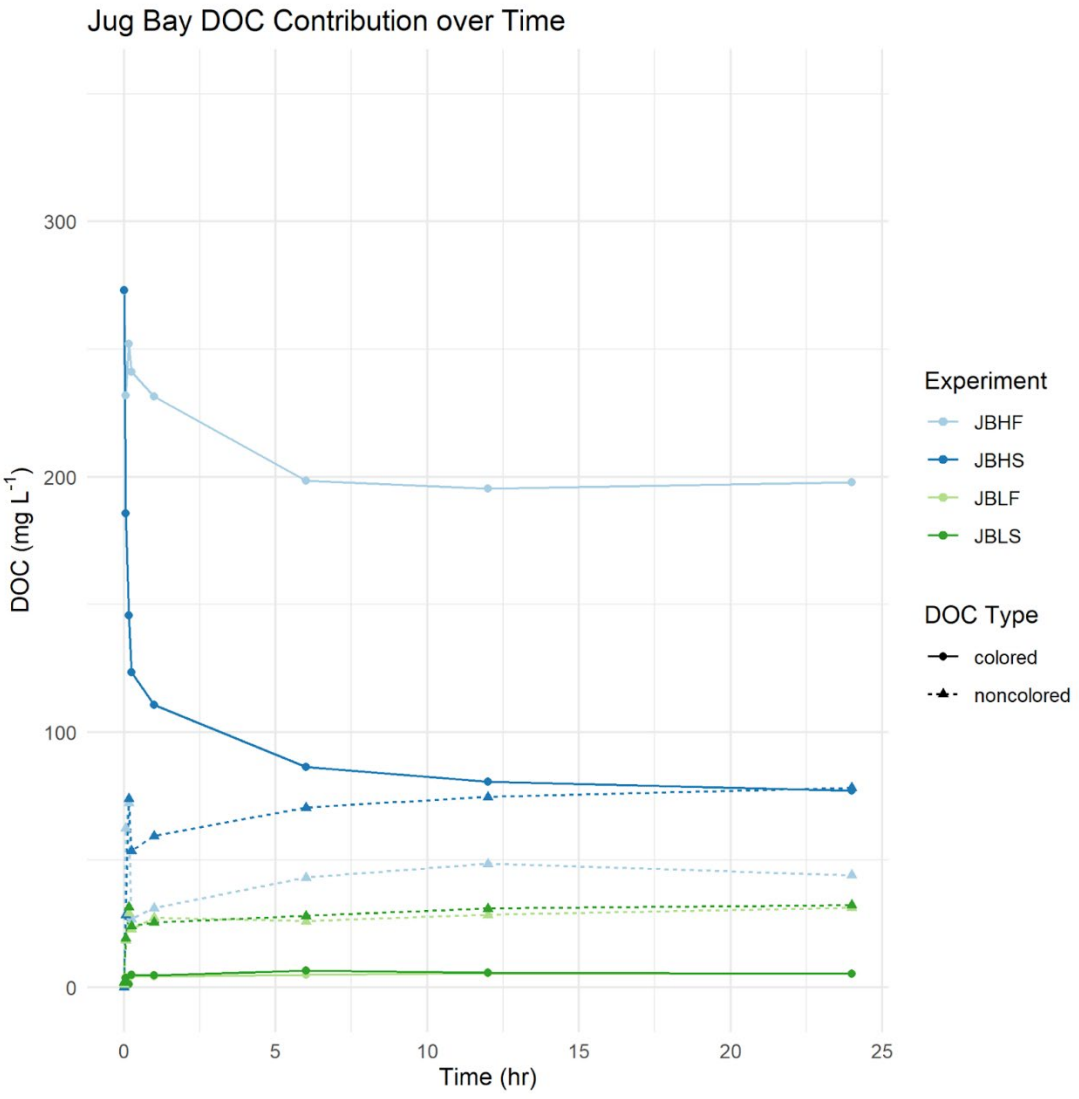

Figure 5.5. Jug Bay DOC concentration of each pool at every incubation time point. Colors indicated one of the four sets of initial conditions (light blue = JBHF, dark

blue = JBHS, light green = JBLF, dark green = JBLS), and the line type was associated with the DOC pool type (solid = colored, dashed = non-colored).

Due to rapid exchange processes in Figure 5.5, focusing on the first hour gives a better, more detailed picture of those initial interactions (Figure 5.6). For NCDOC, all four sets of initial conditions showed a rapid release of NCDOC in the first 10 minutes, followed by a slight "re-adsorption" of a smaller amount, then ended the time series as a net desorbed pool. While it was probable that some of this rapid desorption was an artifact of the experiments' methodology - soil cores were freeze-dried, leading to free pore water DOC precipitating then immediately dissolving upon re-wetting of the sediment - the rest of the sorption processes continued over time regardless of the spike indicating that most sorption occurred at longer time scales. A bit of that signature was also captured in the JBHF colored pool in the first few minutes. CDOC and NCDOC exchanged at different rates within Jug Bay overall, based on percent of total sorption completed within 15 minutes and 1 hour (Table 5.2), with NCDOC being significantly faster over all initial conditions (percent sorption completed of CDOC vs NCDOC for each initial condition set, two-sample t-tests, each with $p < 0.05$). However, speed did not significantly differ between specific initial conditions.

Table 5.2. Percent sorption completed 15 minutes and 1 hour into the Jug Bay incubations for the CDOC and NCDOC pools of each initial condition.

Initial Conditions	DOC Pool	15 minutes	1 hour

HF	CDOC	60.09%	68.20%
	NCDOC	81.91%	84.90%
HS	CDOC	76.40%	82.86%
	NCDOC	79.30%	84.20%
LF	CDOC	68.58%	71.57%
	NCDOC	75.62%	85.57%
LS	CDOC	73.98%	74.70%
	NCDOC	81.96%	84.96%
Average across conditions	**CDOC**	**69.76%**	**74.33%**
	NCDOC	**79.70%**	**84.91%**

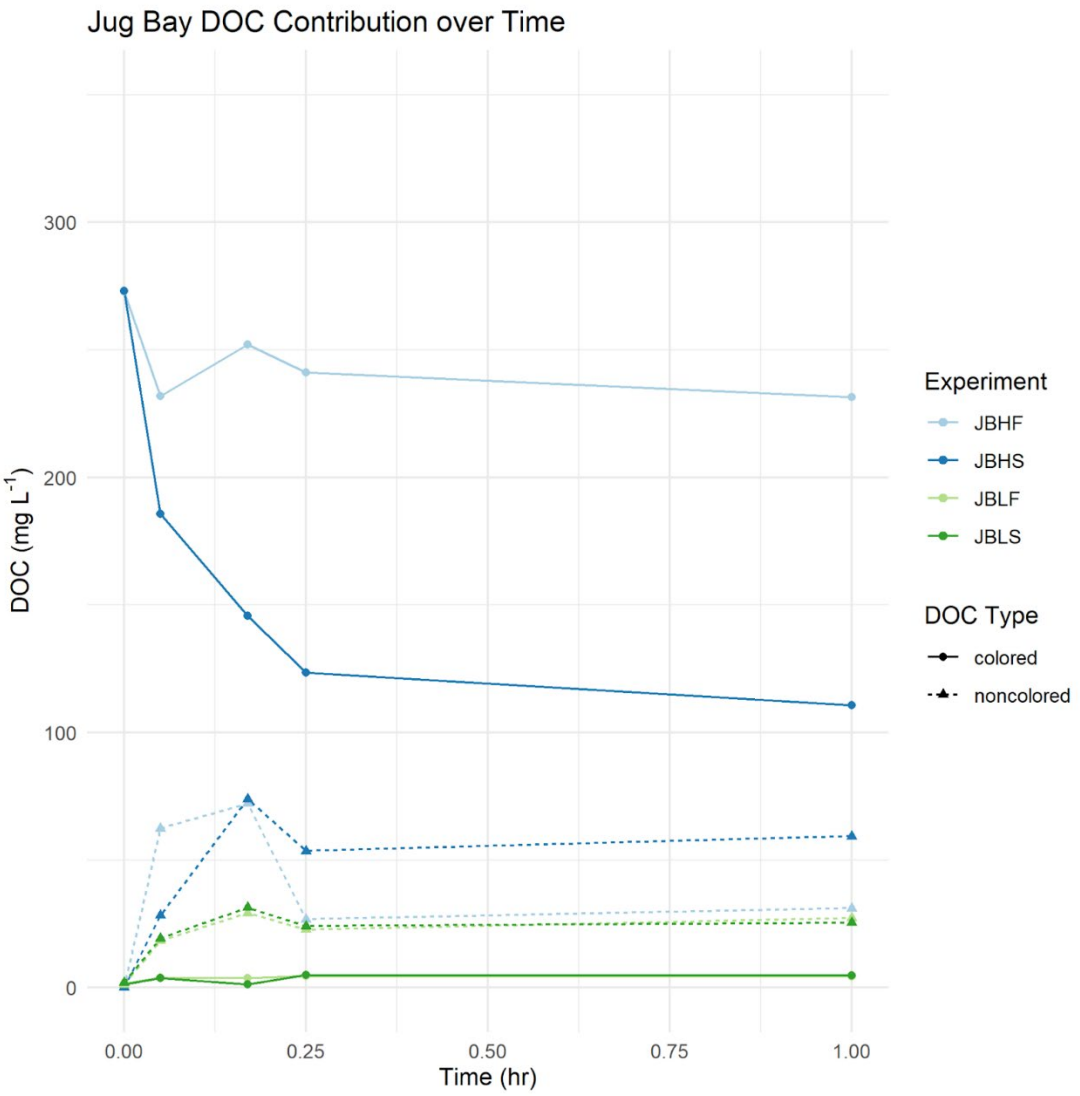

Figure 5.6. Jug Bay DOC concentration of each pool for the first hour of incubations. Colors indicated one of the four sets of initial conditions (light blue = JBHF, dark blue = JBHS, light green = JBLF, dark green = JBLS), and the line type was associated with the DOC pool type (solid = colored, dashed = non-colored).

Figure 5.7 reveals the same patterns as percentage of the contribution of each DOC type. Across all sets of initial conditions, CDOC decreased and NCDOC

increased in percentage of the total DOC in solution; 18.19%, 50.33%, 40.71%, and 25.26% net switch for HF, HS, LF, and LS, respectively. Higher total percentages of CDOC in the top two panels matched the relative amount of DOC placed into the incubation. Time 0 was removed from the low [DOC] experiments because there was no DOC in solution.

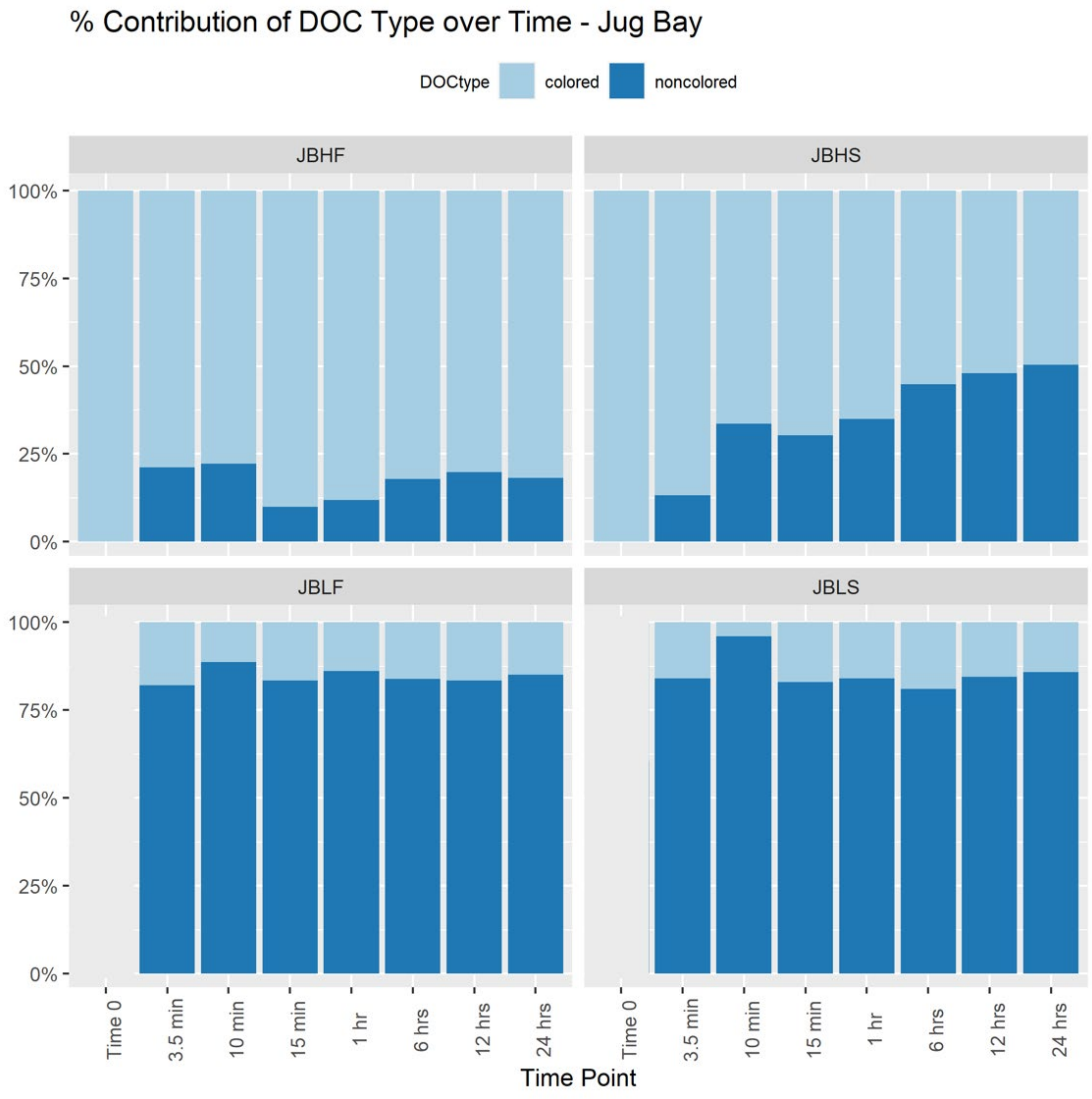

Figure 5.7. Percent contribution of Jug Bay DOC pools in each post-incubation solution. Colors indicated DOC type (light blue = colored, dark blue = non-colored),

and each of the four panels was a set of initial conditions (top left = HF; top right = HS, bottom left = LF; bottom right = LS).

Taskinas samples revealed similar patterns of DOC contribution with CDOC adsorption in the high initial [DOC] experiments, CDOC desorption with low initial [DOC], and a release of NCDOC across all incubations (Figure 5.8-9). 1.01 mg L^{-1} and 162.58 mg L^{-1} of CDOC were removed from solution for the HF and HS incubations, while 29.09 mg L^{-1} and 6.34 mg L^{-1} of CDOC were added to solution in the LS and LS incubations over time. An average of 28.25 mg L^{-1} of NCDOC was released into solution over time for HF, LF, and LS incubations, with HS, as for Jug Bay, releasing much more over time: 132.22 mg L^{-1}. Zooming into the first hour of the incubations, a spike in NCDOC in solution in the first 10-15 minutes is again revealed. CDOC for Taskinas, however, also increased in solution through the first 15 minutes of all incubations before being drawn down into net adsorption (HF & HS) or desorption (LF & LS) at the end of the 24 hours (Figure 5.9). The percent completions of CDOC and NCDOC sorption processes (Table 5.3) were not statistically significant from each other or for most sets of initial conditions (exception being high vs. low [DOC] comparisons) for Taskinas, unlike Jug Bay. Percentage plots of the Taskinas DOC contribution over time show the decrease in proportion of CDOC and increase in NCDOC over time (Figure 5.10), but with a lower magnitude of adsorption and higher magnitude of desorption than Jug Bay. The net exchange between the two pools led to a 10.72%, 56.70%, and 5.11% CDOC

decrease and NCDOC increase over time for HF, HS, and LS incubations. LF CDOC slightly increased, by 0.57%, matching the positive ΔSUVA 280.

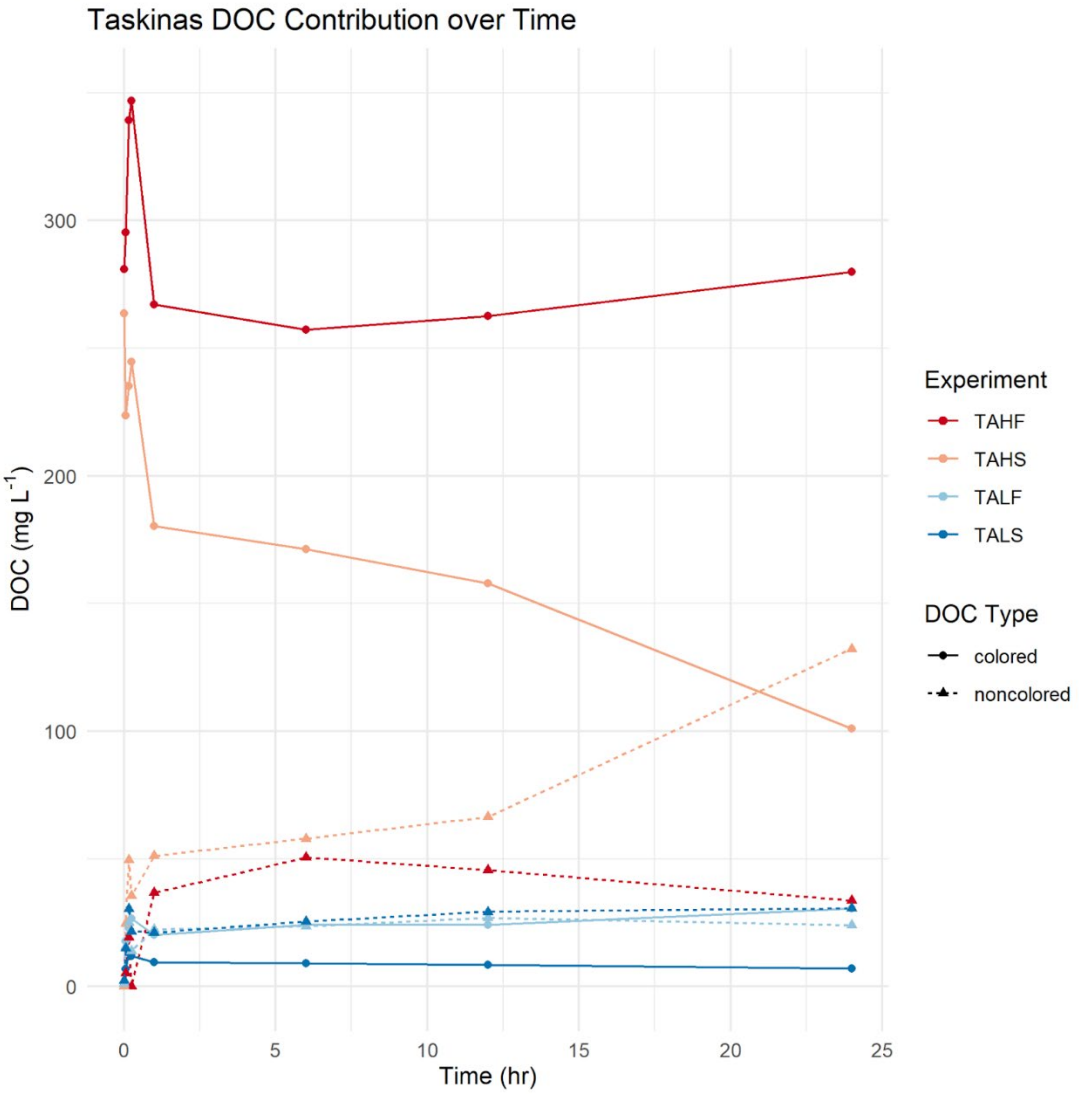

Figure 5.8. Taskinas DOC concentration of each pool at every incubation time point. Colors indicated one of the four sets of initial conditions (red = TAHF, pink = TAHS, light blue = TALF, dark blue = TALS), and the line type was associated with the DOC pool type (solid = colored, dashed = non-colored).

Table 5.3. Percent sorption completed 15 minutes and 1 hour into the Taskinas incubations for the CDOC and NCDOC pools of each initial condition.

Initial Conditions	DOC Pool	15 minutes	1 hour
HF	CDOC	36.98%	81.72%
	NCDOC	36.37%	71.13%
HS	CDOC	29.78%	61.18%
	NCDOC	39.72%	49.44%
LF	CDOC	60.51%	75.69%
	NCDOC	68.80%	85.08%
LS	CDOC	73.25%	86.64%
	NCDOC	78.70%	79.77%
Average across conditions	**CDOC**	**50.13%**	**73.31%**
	NCDOC	**55.90%**	**71.35%**

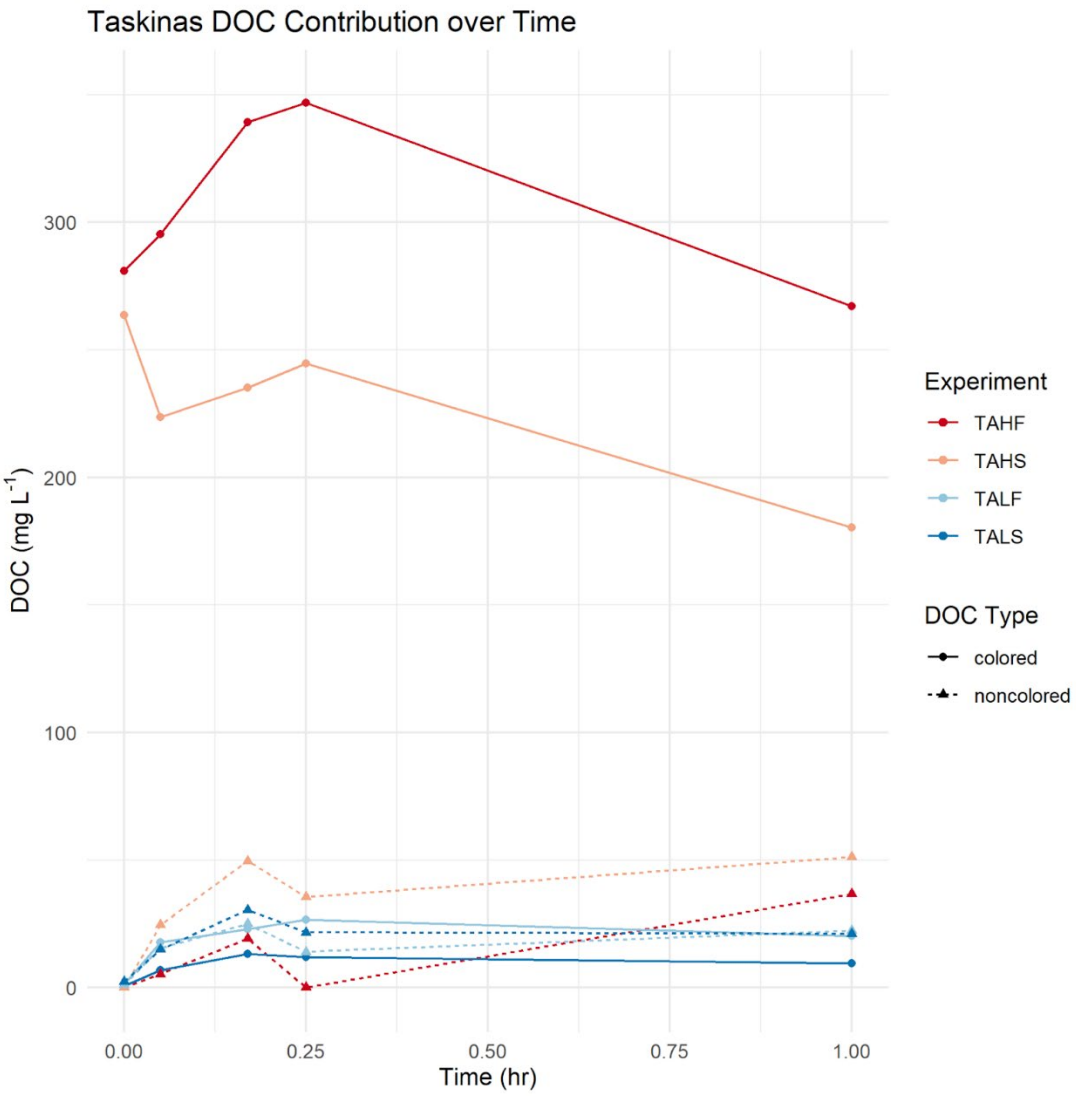

Figure 5.9. Taskinas DOC concentration of each pool for the first hour of incubations. Colors indicated one of the four sets of initial conditions (red = TAHF, pink = TAHS, light blue = TALF, dark blue = TALS), and the line type was associated with the DOC pool type (solid = colored, dashed = non-colored).

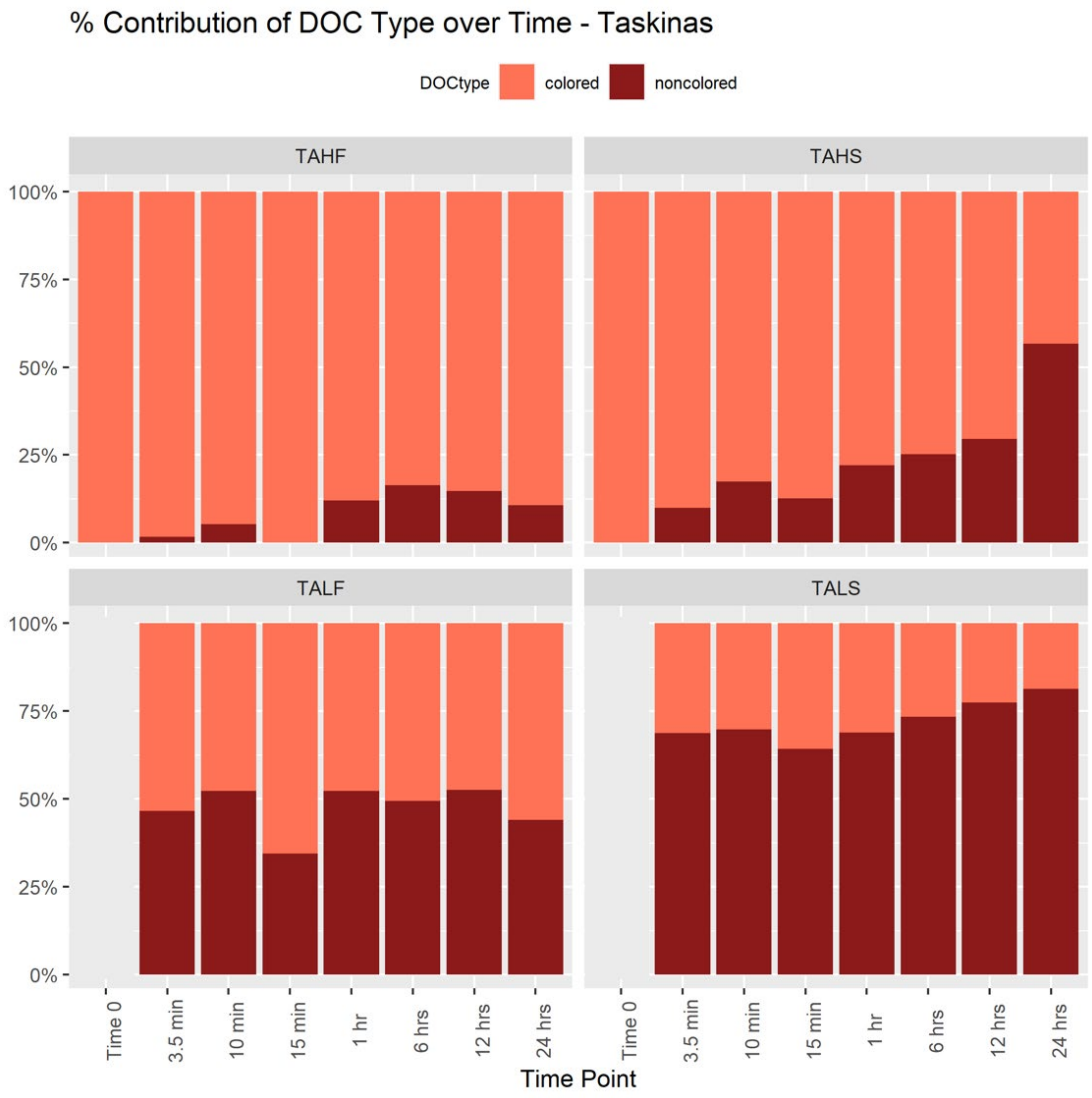

Figure 5.10. Percent contribution of Taskinas DOC pools in each post-incubation solution. Colors indicate DOC type (pink = colored, red = non-colored), and each of the four panels is a set of initial conditions (top left = HF; top right = HS, bottom left = LF; bottom right = LS).

HF and HS %CDOC and %NCDOC at each time point were not statistically significant between the two sites (two-sample t-tests, each with $p > 0.05$), even though the CDOC concentrations at those same time points were significantly

different (two-sample t-tests, each with $p < 0.05$). The percentages of pool contributions in the LF and LS experiments across all time points were significantly different (two-sample t-tests, each with $p < 0.05$), although there would be more noise with the smaller overall DOC concentration being more impacted by shifts between the pools over time. Speeds of the processes for the individual pools were also significantly different between sites for the first 15 minutes of the incubations. Jug Bay CDOC and NCDOC sorption processes were significantly faster than Taskinas at 15 minutes ($p < 0.05$, two-sample t-test), but not at 1 hour or later. Within Jug Bay alone, NCDOC sorption was significantly quicker than CDOC ($p < 0.05$, two-sample t-test), with the caveat that some immediate NCDOC processes were most likely not attributable to sorption.

Discussion

As seen in Pinsonneault et al. (*in prep*), optical properties of the four pre-incubation stocks differed from post-incubation solutions absorbance measurements even in the case of net adsorption, indicating that some amount of DOC exchange with the sediments had occurred (Figure 5.11). A similar inference of DOC exchange was concluded form the results of the bulk DOC variation in the time-series incubations ([b]Morrissette et al., *in prep*). The conceptual diagrams below show the separation of the DOC associated with the Dismal Swamp stock solution ($DOC_{DismalSwamp}$) and with the sediments ($DOC_{wetland}$) before inoculation (Figure 5.11a). Once inoculation had occurred, $DOC_{wetland}$ desorbed from the sediments and $DOC_{DismalSwamp}$ adsorbed onto the sediments within the closed incubation, and that

exchange was seen at every time point within the suite of kinetic experiments (Figure 5.11b).

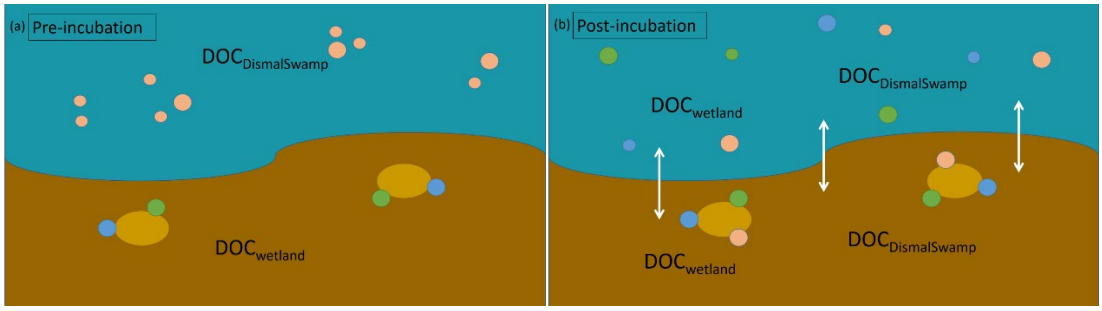

Figure 5.11a-b. Conceptual diagrams of the closed incubation experiments with (a) pre and (b) post exchange tracking of multiple DOC pools of separate origin.

The optical measurements of absorbance and slope ratio indicated that not only did the quantity of DOC change over time, but the *quality* of DOC in solution also shifted throughout the time series. This change in composition at every time point within the kinetic incubations both supported the findings from Pinsonneault et al. (*in prep*) that exchange occurred within 24 hours, and showed that the exchange was rapid and consistent over time. Moreover, the bulk DOC isotherms were fit to a standard isotherm curve with little error for the full range of initial conditions (Pinsonneault et al., 2021), which indicated that the speed of the shift was not likely regulated by variables such as sorption capacity or binding affinity. Rather, it appeared that individual pools within the bulk DOC sorbed at different rates within the bulk movement.

DOC Exchange

Uptake of CDOC was consistent with changes in the spectral absorbance scans over time (Figures 5.2-3), showing adsorption with a reduction in magnitude of CDOC absorbance over the course of the incubations, even at the time points where adsorption was not the dominant process for the bulk DOC incubations. In addition, the change in slope ratio (Figures 5.4-5) over time indicated that CDOC composition changed at each time point, starting out with a lower slope ratio indicative of highly humic, high molecular weight Dismal Swamp material. The slope ratios shifted to higher values over time indicating a larger fraction of lower molecular weight material in the CDOC in solution due to desorption of sediment CDOC and/or the removal of Dismal Swamp CDOC from solution. Since both the storage of the stock solutions and the incubations themselves were in the dark, the shift in composition was not due to photobleaching.

While it is difficult to fully break down the exact chemical interactions taking place, this work showed that the sediments of both Jug Bay and Taskinas preferentially, and quickly, adsorbed the introduced $CDOC_{DismalSwamp}$ while consistently releasing native $CDOC_{wetland}$ and NCDOC. This has implications for the connectivity of ecosystems, with forested uplands being a known - and even increasing - source of flushing colored material into rivers, streams, and coastal wetland ecosystems (Clark et al., 2008; Dalva & Moore, 1991; Pumpanen et al., 2014; Worrall et al., 2002) Due to the similarities in DOC composition between the Great Dismal Swamp surface water and forested catchments, these results indicate that this foreign DOC may be preferentially taken up by marsh soils, replacing the

DOC previously adsorbed on the sediments. Thus, not only might it be possible to predict what type of compounds will be released to downstream environments during these events, but how quickly and why.

CDOC vs. NCDOC

As shown in Pinsonneault et al. (2021), the CDOC fraction determined the direction of the standard isotherm curve, while NCDOC behaved independently. Figures 5.6 and 5.9 highlight the differences between the two pools, showing that the CDOC fraction in the HF and HS experiments was being taken up by the sediments, always ending in net adsorption, with a higher quantity being adsorbed in the HS incubations than HF, consistent with the fact that more net adsorption occurs under the compounded effects of higher [DOC] and higher salinity at both marsh locations (Pinsonneault et al., 2021). In the LF and LS experiments, where no initial DOC was added to the incubations, the small CDOC signature that accumulated in solution over time revealed desorption from the sediment. NCDOC - regardless of soil type, biogeochemical characteristics, and initial conditions - desorbed over time from the sediment. This desorption of NCDOC from the sediments, even when CDOC was simultaneously adsorbing onto the sediments, matches what was found in the isotherm experiments (Pinsonneault et al., *in prep*).

The apparent preferential adsorption of highly humic, inherently refractory material within these incubations seemingly contradicts the results of Chapter 2, in which the sediment flux model released more refractory material into the water column over the entire time series for every formulation's DOC flux output. However, it is necessary to note that this cannot be directly compared, as the

incubations do not provide information on the *biological* lability of the compounds exchanged over time. Since microbial activity was reduced with the addition of sodium azide, the adsorbed CDOC or desorbed NCDOC in solution could be labile or refractory, and was not analyzed in depth here. Also, the patterns do match in the sense of CDOC to NCDOC proportions, with NCDOC being the more likely fraction to desorb and be released to the water column from the sediments, and, conversely, CDOC being the fraction that is quickly adsorbed and more likely to remain on the sediments. More research is needed to analyze the addition of microbial processes in combination with sorption on the quality and quantity of DOC sediment-water column exchange.

These kinetic experiments revealed the temporal dynamics of the sorption for each individual pool. Within the first few minutes, NCDOC was very quickly released into solution, followed by some re-adsorption, before steadily increasing in concentration for the rest of the incubation. As noted above, however, this initial oscillation can be partly attributed to an artifact of the experimental procedure of freeze-drying the sediment cores: free DOC in the pore water before freeze-drying just exists in the solid phase, not sorbed to anything, and can be immediately released into solution upon re-wetting of the sediment. It is likely that the initial increases in NCDOC in solution are the result of a combination of desorption of DOC from the sediments and the immediate dissolution of this “free” DOC. It is not possible to determine the relative importance of these two processes from these data. Regardless of what combination of processes determined the initial flux, the kinetic experiments suggest that the rapid NCDOC interactions dominated the initial peaks in the bulk

DOC graphs (Figures N.1-2), while CDOC controlled the final net sorption process. These results are also consistent with the patterns seen in the bulk DOC movement; a) more adsorption occurred in the HF and HS incubations, b) more desorption occurred for LF and LS incubations, and c) less CDOC was drawn up in the Taskinas soils than Jug Bay.

Comparing the CDOC and NCDOC contribution within the post incubation solution to only the absorbance values of the pre stock solution most accurately matched the CDOC signature. Attributing all the starting DOC to $CDOC_{DismalSwamp}$ led to the assumption that all NCDOC accumulating in solution past the first time point was from marsh soil desorption. Since the absorption spectra of purely native wetland CDOC was unknown in these experiments, there is some amount of uncertainty when it comes to the overall ratio of CDOC and NCDOC in the final solutions, but several iterations of the process using different specific-absorbance spectra as mentioned above resulted in insignificant changes to their concentrations and the patterns of mixing. Regardless, the wetland spectral properties of the previous isotherm experiments are known (Pinsonneault et al., *in prep*), and that set of incubations also saw a net increase in NCDOC in solution after 24 hours. Since the overall pattern of kinetics match the net findings of the isotherms, and the partitioning based on other absorbance spectra does not significantly change the post-incubation CDOC concentration, this method was deemed appropriate and the conclusions reliable.

Analyzing the rates between pools and sites, based on the percentage of completed sorption processes per time point, it became apparent that the speed of the

sorption processes must be also related to sediment biogeochemistry. Since there was almost never a significant difference between how fast CDOC and NCDOC sorption approached the final value between any of the initial conditions within each site (exception for high [DOC] vs. low [DOC] at Taskinas, $p = 0.022$, two-sample t-test), DOC concentration and salinity could not predict speed of the individual pools. The most significant differences occurred between sites within 15 minutes of incubation, and between CDOC and NCDOC at Jug Bay. The causation of the differences in these situations can possibly be explained by sediment characteristics, namely iron content and soil organic matter. It was difficult to parse out the specific differences in speed for desorption and adsorption processes within this particular study (see [e]Morrissette et al., *in prep*). NCDOC release into sediments was significantly faster than CDOC at Jug Bay, but not all of the release could be attributed to the sorption process alone, as previously discussed. Speed of adsorption was apparent, however, in JBHS, having the highest percent completion of sorption processes of any other CDOC pool across both sites.

It is important to emphasize that while the changes in bulk DOC concentrations over time showed an equilibrium being reached after the first few hours, breaking the DOC down into the CDOC and NCDOC fractions revealed that these pools were consistently desorbing or adsorbing over time with the pools moving sometimes oppositely, sometimes in tandem - CDOC was desorbed or adsorbed depending on initial conditions and NCDOC desorbed over time - which combined to determine equilibriums in the bulk DOC fluxes (Appendix N) for all incubations.

Conclusion

A focus on tracking the movement of DOC from wetland sediments in recent research has resulted in a better understanding of the retention and release of DOC compounds under specific environmental conditions, and the quality and quantity of DOC that is exchanging within the marsh-estuarine complex (Clark et al., 2008; Osburn et al., 2015; Pinsonneault et al., 2021; Tzortziou et al., 2008, 2011, 2015; Wang et al., 2007). This is important for quantifying the existing carbon stocks and net annual DOC exchange within wetland ecosystems. The changes in the optical properties of DOC reported previously and in this manuscript suggested that tidal marshes may adsorb upland DOC, release different compounds at ebbing tide versus flooding tide (Tzortziou et al. 2008), and alter DOC composition (Pinsonneault et al., *in prep*). However, the biogeochemical interactions that control the sorption of colored vs. non-colored DOC, and how fast they occur, were unknown. The sorption isotherm experiments with tidal marsh soils (Pinsonneault et al., 2021) provide the first insights into the biogeochemical controls on CDOC vs. NCDOC regulation within these marsh sediments, and the kinetic incubations reported here reveal how fast they occur.

Our findings show that the sorption kinetics of bulk DOC was regulated by the sum of the movements of different pools: individual CDOC and NCDOC pools adsorbed and desorbed in distinct, separate directions over time. Highly humic, colored fractions of DOC were preferentially adsorbed or kept on the sediments, displacing the wetland DOC and leading to higher amounts of native NCDOC in solution. The rapid release and/or dissolution of NCDOC, desorbing over time for all

sets of initial conditions, along with the accelerated adsorption of CDOC under HS conditions, dominated the rapid bulk DOC movement within the first few time steps (<15 min), while CDOC across all incubations, affected by the initial conditions, controlled the net sorption process over the course of 24hrs, demonstrating the separation of two distinct pools moving within the incubation. Speed of the CDOC and NCDOC sorption processes are most likely determined by certain sediment characteristics that differ significantly between Jug Bay and Taskinas, particularly elevated iron content at JB and soil organic matter at TA. While this set of experiments forced the incubations with a DOC concentration that was an order of magnitude higher than the Jug Bay or Taskinas marshes typically experience, it indicates that under the conditions of high DOC input to these ecosystems, native DOC can be replaced with the introduced DOC. This has implications for the effects on downstream environments of tidal marsh ecosystems, such as seagrass beds, estuaries, or the coastal ocean.

Chapter 6: Resolving the spatial variability in tidal marsh dissolved organic carbon sorption kinetics

Abstract

Sorption processes in wetland sediment pore waters are an integral part of organic matter transformations and fluxes that have been observed in many studies. Previous research showed that salinity, DOC concentrations, and sediment characteristics have significant influences on sorption processes, and that the sediment characteristics also significantly differ not only between different marshes but also within lateral and vertical gradients within one marsh site. Hypothesizing that vertical depth and distance from the creek edge would differ in sorption capability, a set of incubations were designed to parse out the spatial resolution of DOC kinetics. Taskinas Creek (VA, USA) marsh soils, chosen for high particle size and composition variability within the marsh, were cored at the creek edge, intermediate marsh, and high marsh, and were separated at 0-5cm and 30-40cm depths. Anaerobic sorption kinetic laboratory incubations at seven time points over the course of 24 hours revealed that spatial variability played a large role in DOC sorption kinetics. Adsorption decreased significantly with distance from the creek edge and with depth, while desorption (in lower magnitude) increased significantly with distance from the creek edge and depth. Analyses between samples showed that sorption kinetics varied as significantly between segments within one marsh as between cores from separate marsh systems. Resolving the spatial variability in sorption kinetics further informed the factors that most affected the net changes and fine scale interactions in dissolved

organic carbon biogeochemical transformations, and it is recommended that spatial variability be taken into consideration when quantifying carbon flux estimates.

Introduction

Coastal wetlands ecosystems, covering an estimated 1.64 x 10^6 km^2 globally (Davidson & Finlayson, 2018), occupy coastal regions with a range of ecosystem types. These wetlands vary extensively in morphology (Bullock & Acreman, 2003; Morris et al., 2016; Pratolongo et al., 2019), composition (Bai et al., 2016; Pinsonneault et al., 2021, *in prep*; Yang et al., 2008), biodiversity (Groffman et al., 1996; Levin et al., 2001), nutrient availability (Bedford et al., 1999; Johnston et al., 2001), anthropogenic influence (Karstens et al., 2016), and extent (Davidson & Finlayson, 2018). These differences in coastal wetland characteristics determine their functionality and importance for providing ecosystem services.

All coastal wetland ecosystems are complex with the biogeochemical characteristics of sediment cores varying dramatically with depth and distance from adjacent waters. For example, cores reveal marked vertical and horizontal zonation of microbial communities and redox potential (Thomas et al., 2009; Zhou et al., 2017). In addition, metal presence in cores matches spikes in pollution (Aguinaga et al., 2019; Callaway et al., 1998), and hydrological processes that control water level affects the sediment biogeochemistry (Han et al., 2020; Holden 2005; Steinmuller et al., 2019).

Tidal marsh sediments play a major role in the coastal carbon cycle along these spatial gradients. Marsh sediments are known to be sources of dissolved organic and inorganic carbon (DOC, DIC) along tidal boundaries (Pinsonneault et al., *in prep*; Tzortziou et al., 2011) and they also provide long-term storage of organic carbon at depth (Bernal & Mitsch, 2008; Mitsch et al., 2013; Steinmuller et al., 2019).

These marsh sediment-water column carbon exchanges are known to be controlled and mediated by some of the aforementioned sediment and pore water characteristics through their influence on sorption. Adsorption is positively correlated with metal oxide concentrations, DOC loading, and specific surface area (SSA) (Groeneveld et al., 2020; Gu et al., 1994; Kaiser & Guggenberger, 2000; Kaiser et al., 1996; Kalbitz et al., 2005; Keil & Mayer, 2014; Kothawala et al., 2009, 2012; Pinsonneault et al., 2021), while being inversely related to soil organic matter (%SOM), pH, and autochthonous organic matter (Groeneveld et al., 2020; Kaiser & Zech, 1998). Preferential adsorption of terrestrial-like material, highly humic and aromatic compounds, and hydrophobic fractions of DOC has also been shown to occur in marsh soils (Groeneveld et al., 2020; Kaiser et al., 1996; Kaiser & Zech, 1998; [c]Morrissette et al., *in prep*; Pinsonneault et al., *in prep*).

The spatial and temporal variability of marsh sediment characteristics, coupled with knowledge of how these characteristics separately affect sorption processes, can be used to infer spatial variability in sorption processes. However, few studies have been conducted that explicitly measure the spatial variability of sorption processes in marsh soils, and no studies exist that examine the combined effects of space and time. Lilienfein et al. (2004) found that adsorption capacity increased with marsh soil age, referring to age as stratified depth of cores. Pinsonneault et al. (2021) determined, in a sorption study that compared separate marsh sites, that adsorption increased in locations with higher metal oxides and SSA. These lateral and vertical variations between and within wetland sites are very likely to influence the impact of sorption on carbon fluxes.

In this study, the influence of vertical depth and distance from the creek edge on DOC sorption kinetics in a Chesapeake Bay mesohaline marsh system is examined. It is shown that vertical depth and distance from the creek edge have a strong influence on DOC sorption magnitude and speed, and that these spatial variations can be explained by changes in the biogeochemical characteristics of the soils.

Methods

Incubations

The experiments described in this study employed the same methodology as described in [b,c]Morrissette et al. (*in prep*) for sediment collection, incubation procedure, stock preparation, and pre/post analyses. For this study, three 0-40cm sediment cores were taken from Taskinas Marsh (Williamsburg, Virginia, U.S.A., 37°25'N, 76°43'W) (Figure M.1), representing the marsh creek edge (C), intermediate marsh (I; 3m from creek edge), and high marsh (M: 30m from the creek edge) (Figure 6.1) to reveal horizontal spatial variability in the sorption kinetics. Taskinas Marsh was chosen from the sites of the larger effort ([b]Morrissette et al., *in prep*, Pinsonneault et al., 2021) due to its representative nature of the Chesapeake Bay. More of the Bay's wetland ecosystems are characterized as organic, tidal brackish marshes than fresh, microtidal, and highly mineral in composition as in Jug Bay. In addition, two depth segments (0-5 cm and 30-40 cm) were taken from the three separate cores to reveal vertical variability in sorption kinetics. As in [b]Morrissette et al. (*in prep*), sorption incubations were performed under anoxic,

abiotic conditions at seven different time points of 3.5 minutes, 10 min, 15 min, 1 hr, 6 hrs, 12 hrs, and 24 hrs, and four sets of initial conditions were used: high initial [DOC], fresh (HF); high initial [DOC], saline (HS); low initial [DOC], fresh (LF); low initial [DOC], saline (LS).

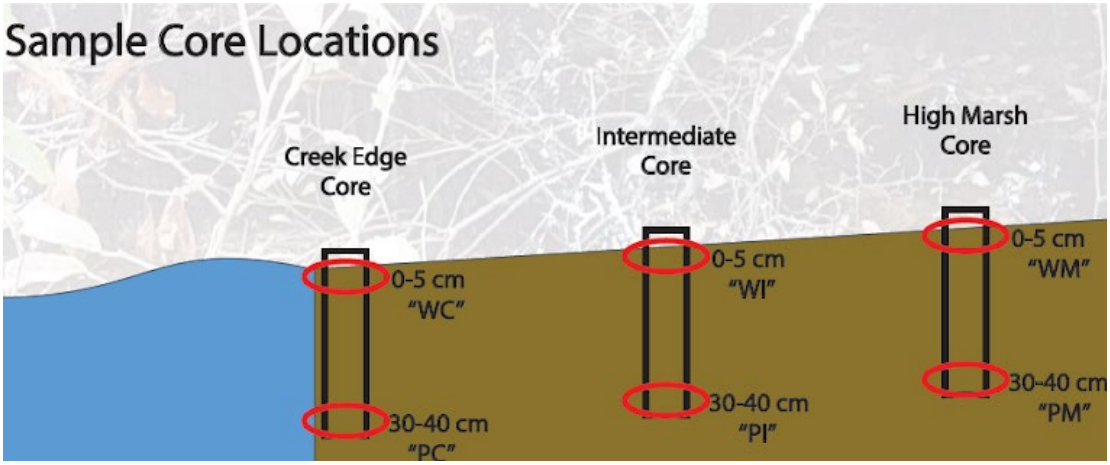

Figure 6.1. Conceptual diagram of the six core sections of Taskinas marsh studied in the spatial experiments: Shallow Creek Edge (WC); Shallow Intermediate (WI); Shallow High Marsh (WM); Deep Creek Edge (PC); Deep Intermediate (PI); Deep High Marsh (PM).

Analyses

Sediment characteristic measurements were made by the Canuel lab at the Virginia Institute of Marine Science and the Megonigal lab at the Smithsonian Environmental Research Center. These measurements included loss on ignition (LOI), percent soil organic matter (%SOM), specific surface area (SSA), total organic carbon, (TOC), grain size, mineral composition and concentration (non-crystalline iron and aluminum - NC Fe and NC Al), bulk density, percent total nitrogen and organic matter (%TN and %TOC), carbon to nitrogen ratio (C:N), $\delta^{15}N$, and $\delta^{13}C$

(Canuel & Pondell, unpublished data; for methodological details see Pinsonneault et al., *in prep*). These soil characteristic measurements were compared to the results of the spatial incubations to determine how distance and depth in the marsh influenced the physical and chemical characteristics of the marsh soils, and how changes in these characteristics drove the variability in the sorption processes.

Optical analyses of absorbance, fluorescence, specific ultraviolet absorbance at 280 nm (SUVA 280), CDOM pool partitioning, spectral slope ($S_{275\text{-}295}$), and slope ratio (S_R) were performed following the methods described in [c]Morrissette et al. (*in prep*). All statistical analyses were done using R Studio. CDOM optical indices of freshness (β:α) biological (BIX), fluorescence (FI), and humification (HIX) were analyzed and interpreted following Hansen et al. (2016).

Statistical measurements were completed as in Chapters 3 & 5. A single factor ANOVA was performed on either the outputs of bulk DOC sorption or CDOC/NCDOC concentration over time for each incubation within a site to analyze differences between the four sets of initial conditions. A two-way ANOVA was used to determine the significance of soil characteristic differences between core and depth within the core. A three-way ANOVA was used to determine the significance of site, initial condition, and type of DOC on percent sorption completed. Two-sample t-tests (assuming equal variances) were used to test differences in concentration outputs between sites per initial condition, differences in absorbance scans between high/low, fresh/saline, and site, and the differences in percent sorption completed between CDOC vs. NCDOC per and between sites.

Results

Bulk DOC

The patterns of adsorption and desorption of bulk DOC over time (ΔDOC, Figure 6.2) were similar to those reported in Pinsonneault et al. (2021) and [b]Morrissette et al. (*in prep*), i.e., the reaction rates were rapid and the magnitudes of the net adsorption/desorption were strongly influenced by salinity and initial DOC concentration (Figure N.1-2). DOC adsorbed more onto, or desorbed less from, the sediment when forced with high salinity and high initial DOC concentrations, and desorbed more from the sediment when forced with low initial DOC concentrations and low salinity. Most of the reactions (75.05 ± 0.09%) occurred within the first hour, which is consistent with the reaction speeds reported in previous studies (Kaiser & Zech, 1998; [b]Morrissette et al., *in prep*; Shaker et al., 2012). Table 6.1 illustrates the differences in sorption reaction speed at each site. On average, the reaction speeds were slightly slower in the shallow samples, with 59.95 ± 0.11% and 74.45 ± 0.08% of the processes occurring by 15 minutes and 1 hour, respectively, in the shallow samples, and 63.65 ± 0.09% and 75.66 ± 0.08% occurring by 15 minutes and 1 hour, respectively, in the deep samples (Table 6.1).

Table 6.1. Percent (%) of sorption processes completed by 15 minutes and 1 hour, respectively, for each spatial site.

Site	Description	15 min	1 hr
WC	Shallow, Creek Edge	60.01 ± 0.07	79.76 ± 0.04
WI	Shallow, Intermediate	57.20 ± 0.13	68.02 ± 0.12

WM	Shallow, High Marsh	61.54 ± 0.12	75.57 ± 0.06
PC	Deep, Creek Edge	56.41 ± 0.16	71.90 ± 0.14
PI	Deep, Intermediate	70.37 ± 0.06	84.57 ± 0.07
PM	Deep, High Marsh	64.17 ± 0.05	70.51 ± 0.02
All spatial		**61.62 ± 0.10**	**75.05 ± 0.09**

Figure 6.2 also shows that adsorption decreased in the shallow samples in cores that were further away from the creek edge and the influence of water and tides, whereas the opposition was true for desorption. Similar patterns were observed in the deep samples with generally less adsorption and more desorption. Across the shallow segment gradient, the equilibrium ΔDOC values for the HF, HS, LF, and LS initial conditions increased by 215.80%, 84.73%, 91.23%, and 85.78%, respectively, from creek edge to high marsh. The differences across the deep segments were less pronounced, with the HF and HS equilibrium ΔDOC values decreasing slightly by 5.57% and 32.22%, and the LF and LS values increasing by 17.71% and 17.35%. The difference in the amount of sorption between the shallow and deep samples of the same core was most prominent in the creek edge core, with the HF, HS, LF, and LS initial conditions increasing in equilibrium ΔDOC values from shallow to deep by 315.72%, 100.38%, 61.84%, and 56.30%, respectively.

The shallow creek edge and deep high marsh samples had the largest difference in equilibrium ΔDOC values across all initial conditions of and permutations of segment comparison (Table 6.2). A list of the equilibrium ΔDOC values after 24 hours, along with the maximum or minimum ΔDOC across the entire time series is shown in Table 6.2. The HS initial condition always had the maximum

amount of adsorption across sites, while the LF (HF for PC) initial condition had the maximum amount of desorption across sites. When grouped together, the differences in the equilibrium ΔDOC for each set of the initial conditions were significant (each with $p < 0.05$, single factor ANOVA) within each site, across shallow sites with space, and between shallow vs. deep sites with depth, but they were not significantly different (each with $p > 0.05$, single factor ANOVA) across the deep segments. However, when examined individually, HS was the only initial condition that was consistently significantly different within and between every site. HF was only significantly different from LF and LS in the segments of the creek edge core, and the LF and LS conditions were significantly different from each other in the WI, WM, and PI segments. These differences were often revealed in the first few time steps (Figure 6.3). The compounding effects of high salinity and initial [DOC] were similar over all sites, with an average ΔDOC difference between HS and HF time series of 54.06 ± 8.13 mg L^{-1}, or average 143.31% increase in desorption from HS to HF. The standard deviations for the HF and HS incubations were much more variable than the LF and LS incubations due to: 1) higher inherent variability associated with the measurement of a calculated difference, and 2) each triplicate was its own incubation, allowing for slight variations in DOC or sediment composition that are exacerbated with the significantly higher amount of exchange with high [DOC] initial conditions.

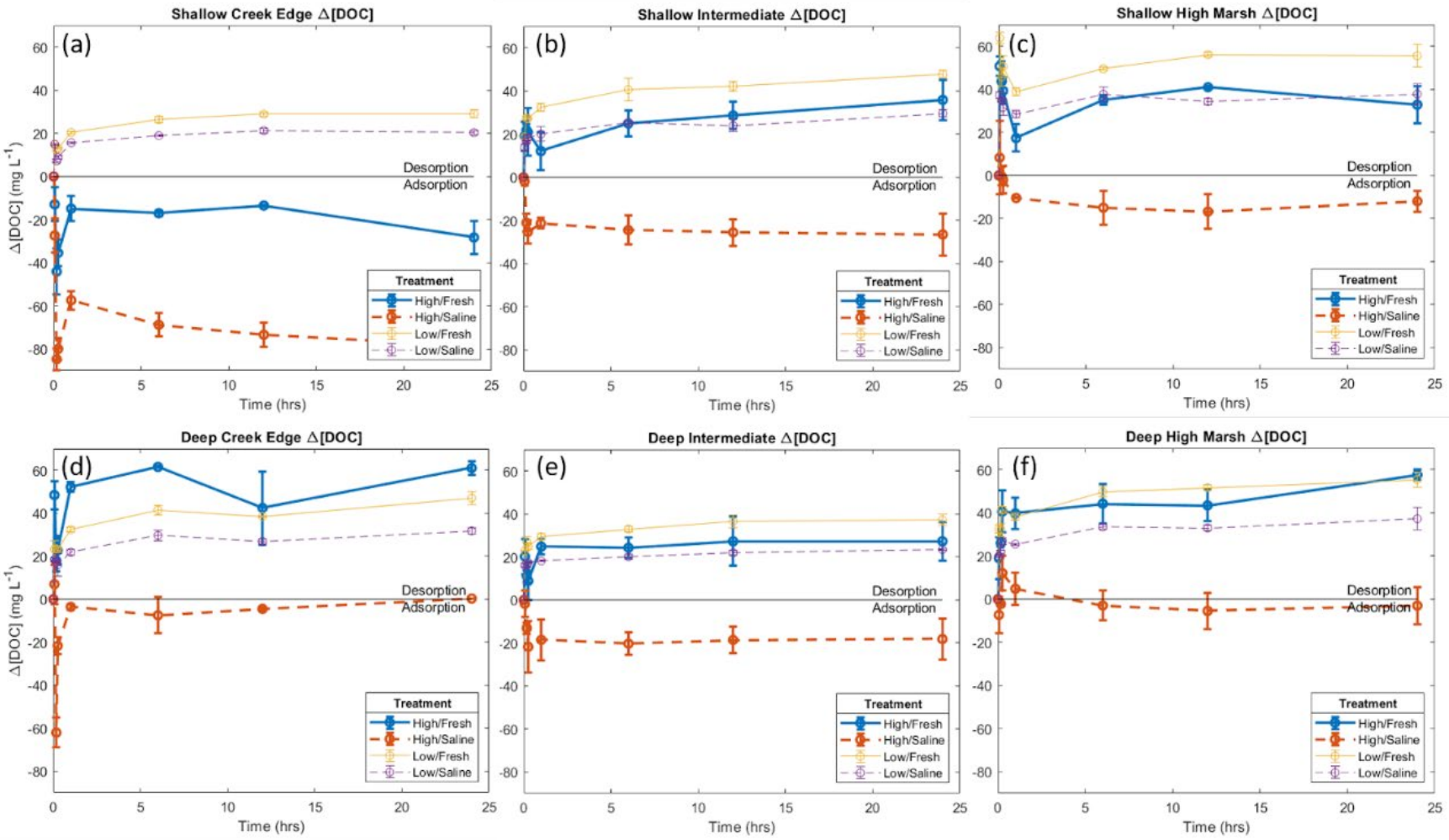
Shallow Creek Edge Δ[DOC]
(a)
Shallow Intermediate Δ[DOC]
(b)
Shallow High Marsh Δ[DOC]
(c)
Deep Creek Edge Δ[DOC]
(d)
Deep Intermediate Δ[DOC]
(e)
Deep High Marsh Δ[DOC]
(f)
Δ[DOC] (mg L-1)
Time (hrs)
Desorption
Adsorption
Treatment
High/Fresh
High/Saline
Low/Fresh
Low/Saline

Figure 6.2. Bulk Δ[DOC] (final-initial) over time for the six subplots within Taskinas marsh: a) WC; b) WI; c) WM; d) PC; e) PI; f) PM. The four colored lines represent the four sets of initial conditions: HF (blue solid line); HS (red dashed line); LF (yellow solid line); LS (purple dashed line). Positive values indicate net adsorption has occurred at that time point, while negative values indicate net desorption at that time point.

Table 6.2. Average equilibrium ΔDOC after 24 hrs (mg L^{-1}) and the maximum/minimum ΔDOC values across the whole time series (mg L^{-1}) per site and set of initial conditions.

Site	Average ΔDOC after 24 hrs (mg L^{-1})	Maximum +ΔDOC (desorption) per site (mg L^{-1})	Maximum -ΔDOC (adsorption) per site (mg L^{-1})
WCHF	-28.3 ± 7.64		
WCHS	-78.6 ± 1.1		-84.70 ± 5.10
WCLF	29.06 ± 1.69	29.06 ± 1.69	
WCLS	20.32 ± 0.98		
WIHF	35.80 ± 9.34		
WIHS	-21.10 ± 2.97		-25.57 ± 6.22
WILF	47.74 ± 1.90	47.74 ± 1.90	
WILS	29.55 ± 1.73		
WMHF	27.90 ± 3.25		
WMHS	-12.00 ± 4.74		-12.25 ± 1.77
WMLF	55.57 ± 5.22	63.82 ± 2.62	
WMLS	37.75 ± 4.88		
PCHF	61.05 ± 3.32	61.55 ± 0.35	
PCHS	0.30 ± 0.14		-62.10 ± 6.93
PCLF	47.03 ± 3.02		
PCLS	31.76 ± 1.42		
PIHF	27.33 ± 8.93		
PIHS	-18.20 ± 9.59		-21.80 ± 11.89
PILF	37.20 ± 2.53	37.20 ± 2.53	
PILS	23.44 ± 0.32		
PMHF	57.65 ± 2.47	57.65 ± 2.47	

PMHS	-3.05 ± 8.56		-5.47 ± 8.52
PMLF	55.36 ± 3.49		
PMLS	37.27 ± 5.31		

Zooming into the first 30 minutes of the spatial incubations (Figure 6.3) to look at the rapid sorption processes, the results show similar patterns, again, to the kinetic bulk DOC results reported in [b]Morrissette et al. (*in prep*), i.e., initial desorption spikes were observed in many of the experiments. The only set of initial conditions that did not cause an initial desorption spike within the first few minutes was the HF and HS experiments within the WC segment, which were the two experiments that had the highest magnitude of adsorption occur over the course of the incubation. All of the other incubations revealed rapid apparent desorption at the first measurement time point, and in most of these incubations this desorption was followed immediately by adsorption. As discussed in [b]Morrissette et al. (*in prep*), these initial oscillations in the ΔDOC time series are most likely the combination of rapid initial desorption combined with the immediate dissolution of freeze-dried DOC upon re-wetting.

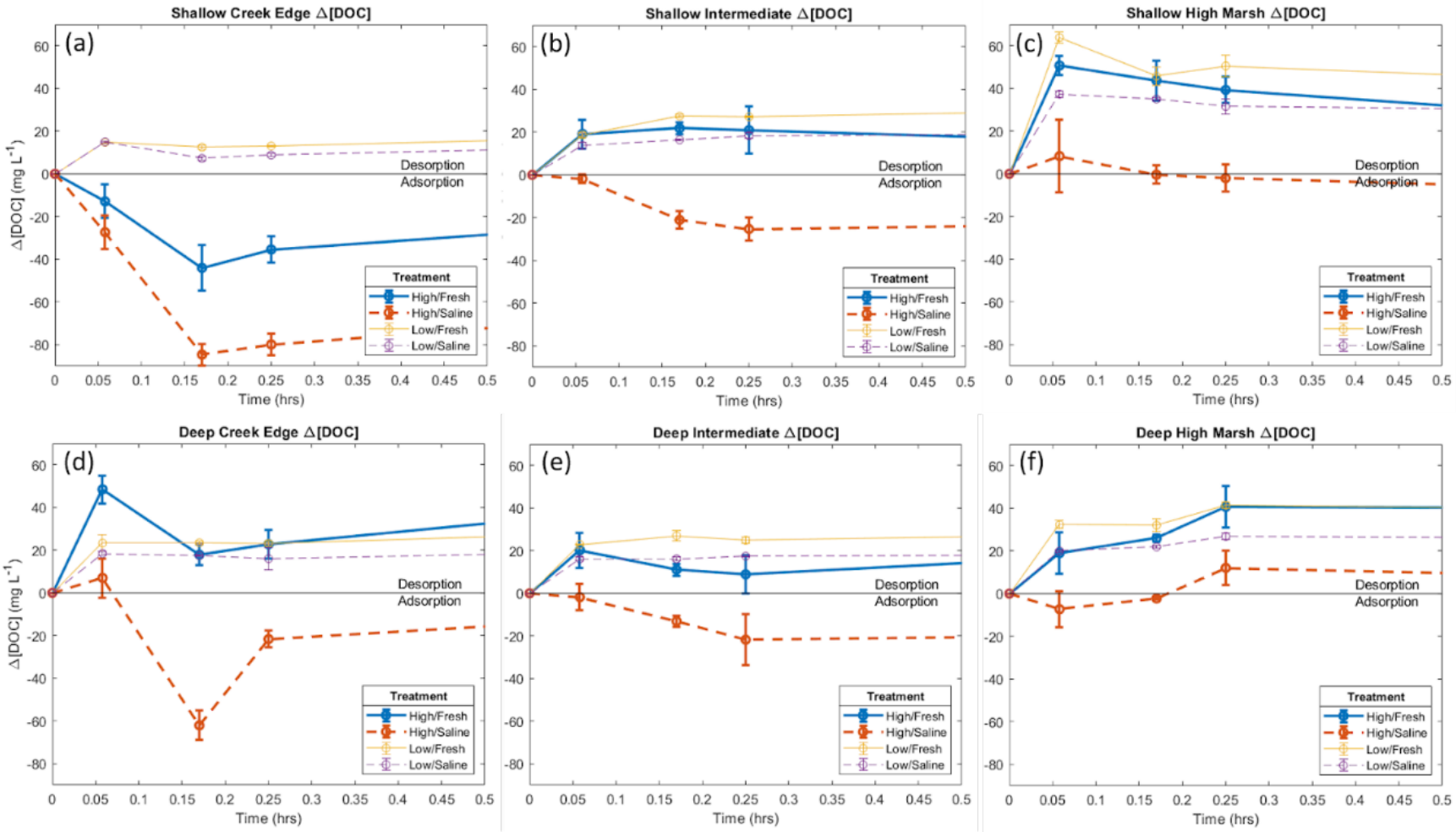
Shallow Creek Edge Δ[DOC]
(a)
Shallow Intermediate Δ[DOC]
(b)
Shallow High Marsh Δ[DOC]
(c)
Deep Creek Edge Δ[DOC]
(d)
Deep Intermediate Δ[DOC]
(e)
Deep High Marsh Δ[DOC]
(f)
Δ[DOC] (mg L-1)
Time (hrs)
Desorption
Adsorption
Treatment
High/Fresh
High/Saline
Low/Fresh
Low/Saline

Figure 6.3. Bulk Δ[DOC] (final-initial) over the first 30 minutes for the six subplots within Taskinas marsh: a) WC; b) WI; c) WM; d) PC; e) PI; f) PM. The four colored lines represent the four sets of initial conditions: HF (blue solid line); HS (red dashed line); LF (yellow solid line); LS (purple dashed line). Positive values indicate net adsorption has occurred at that time point, while negative values indicate net desorption at that time point.

Spectral Properties

Spectral absorbance measurements revealed changes in the amount of DOC in the sample that absorbs light (colored DOC; CDOC). Final absorbance at the 270 nm wavelength (time 7, 24 hrs) decreased in magnitude between the HF to HS experiments by an average of 53.92 m^{-1} across all sites, and an average of 13.66 m^{-1} between LF and LS experiments. Within one site, the average final-initial absorbance for the HF, HS, LF, and LS initial conditions across all sites was -10.76 m^{-1}, -39.18 m^{-1}, 6.88 m^{-1}, and 0.23 m^{-1}, with the negative values revealing adsorption of CDOC and the positive values revealing desorption of CDOC (Figures 6.4-5), i.e., HF and HS both showed a decrease in absorbance over time, indicating a net uptake of CDOC by the sediments, while the reverse was true for the LF and LS experiments. Where net adsorption occurred (mainly for HS), the decreases in absorption spectra magnitude were significantly greater (each with $p < 0.05$, two-sample t-test) than where net desorption occurred. All differences between spectra were statistically significant, and these patterns were the same for all six samples.

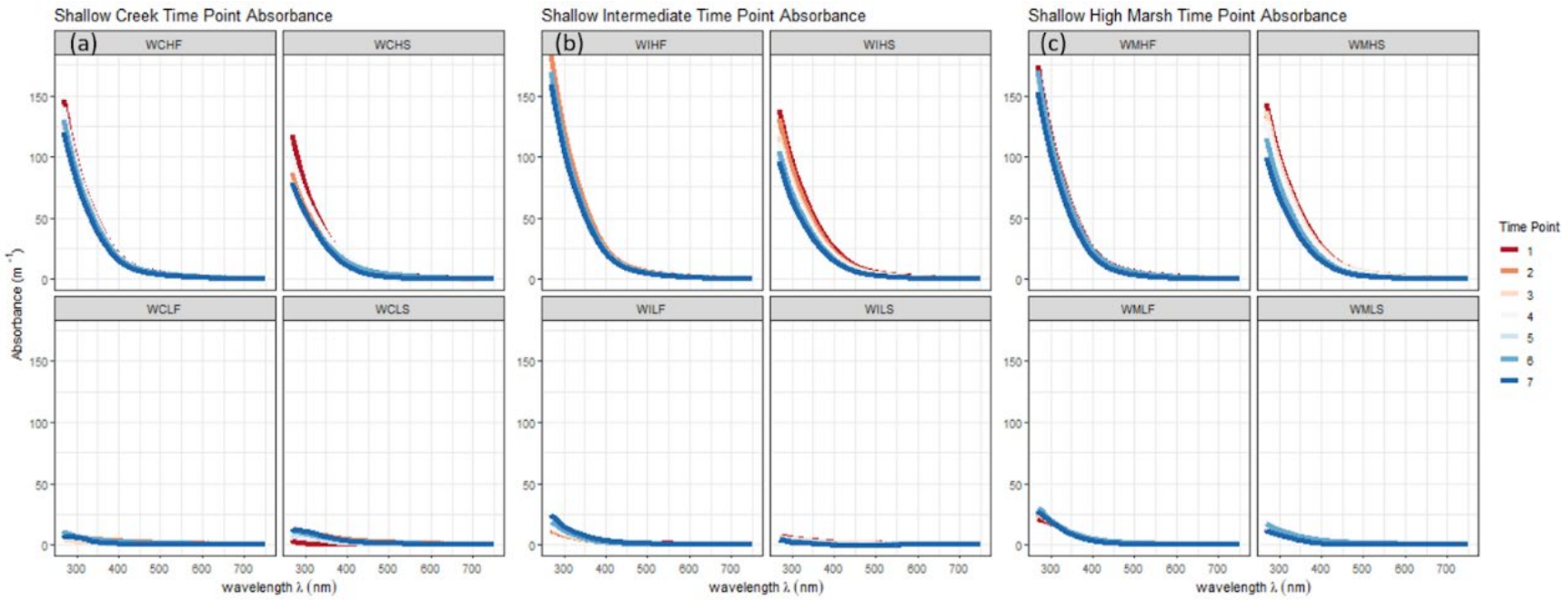

Figure 6.4. Shallow segment absorbance spectra of each post-incubation sample. The four panels are the sets of initial conditions (top left = HF; top right = HS, bottom left = LF; bottom right = LS), and the colors represent the 7 incubation time points (1 = 3.5 min, 2 = 10 min, 3 = 15 min, 4 = 1 hr, 5 = 6 hrs, 6 = 12 hrs, 12 = 24 hrs).

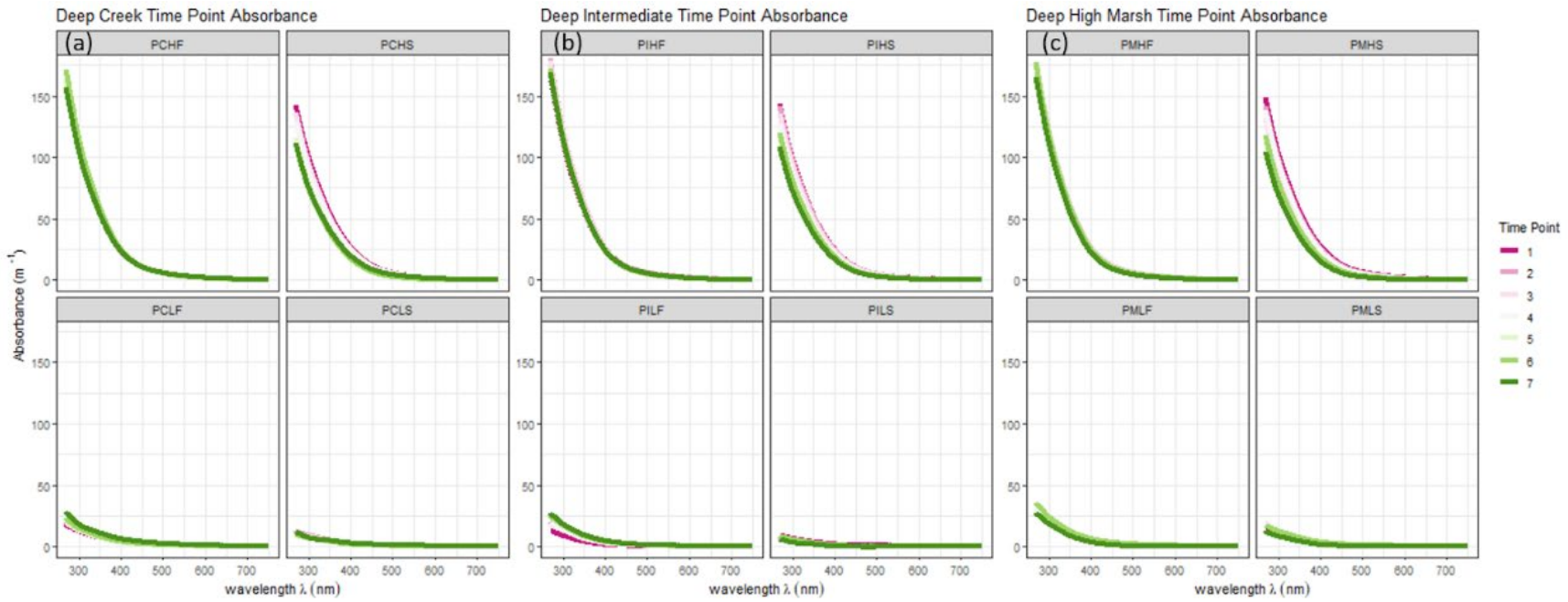

Figure 6.5. Deep segment absorbance spectra of each post-incubation sample. The four panels are the sets of initial conditions (top left = HF; top right = HS, bottom left = LF; bottom right = LS), and the colors represent the 7 incubation time points (1 = 3.5 min, 2 = 10 min, 3 = 15 min, 4 = 1 hr, 5 = 6 hrs, 6 = 12 hrs, 12 = 24 hrs).

Slope ratios (S_R) (Spectral slopes ($S_{275-295}$) found in Appendix Q) for HF and HS experiments demonstrate compositional shifts in DOC over time (Figures 6.6-7). Initial rapid changes in S_R within the first few minutes indicated rapid exchange of foreign (Dismal Swamp) and native (associated with the soils) CDOC and NCDOC. HS experiments typically had higher S_R measurements, with a final-initial average increase over time by 0.0513 across all sites, which was consistent with a shift from higher to lower CDOC molecular weight in the final solution. Shallow segments increased less than deeper segments, with increases of 0.0830 and 0.0197, respectively. For HF conditions across all sites, the slope ratio decreased by 0.0399 on average. Post-incubation S_R values fit within reported ranges in literature for wetland waters of 0.76 - 1.79 (Helms et al., 2008). However, WC and PC S_R, reported below, had a slight shift from the patterns reflected across all other sites (Appendix Q). The slope ratio for WC HF and HS experiments both decreased over time, while they both increased over time for PC. The time series of S_R for LF and LS were not shown due to the shape of the curves being influenced by the small amount of absorbance coming from the dilutant.

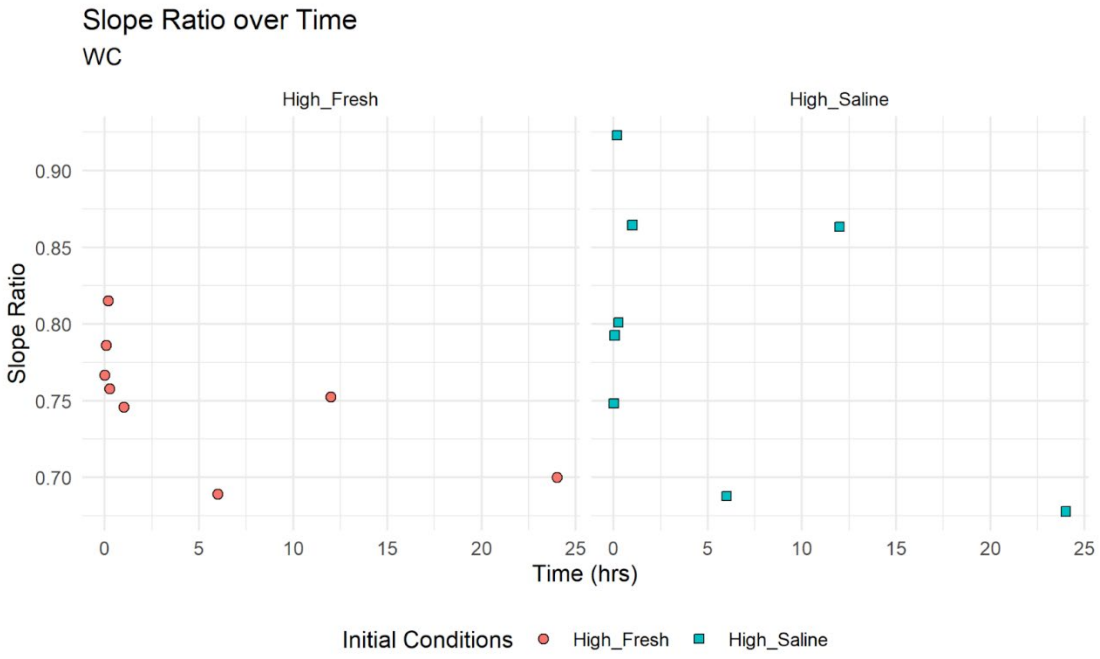

Figure 6.6. WC slope ratio over time for HF (orange circles) and HS (blue squares) initial conditions.

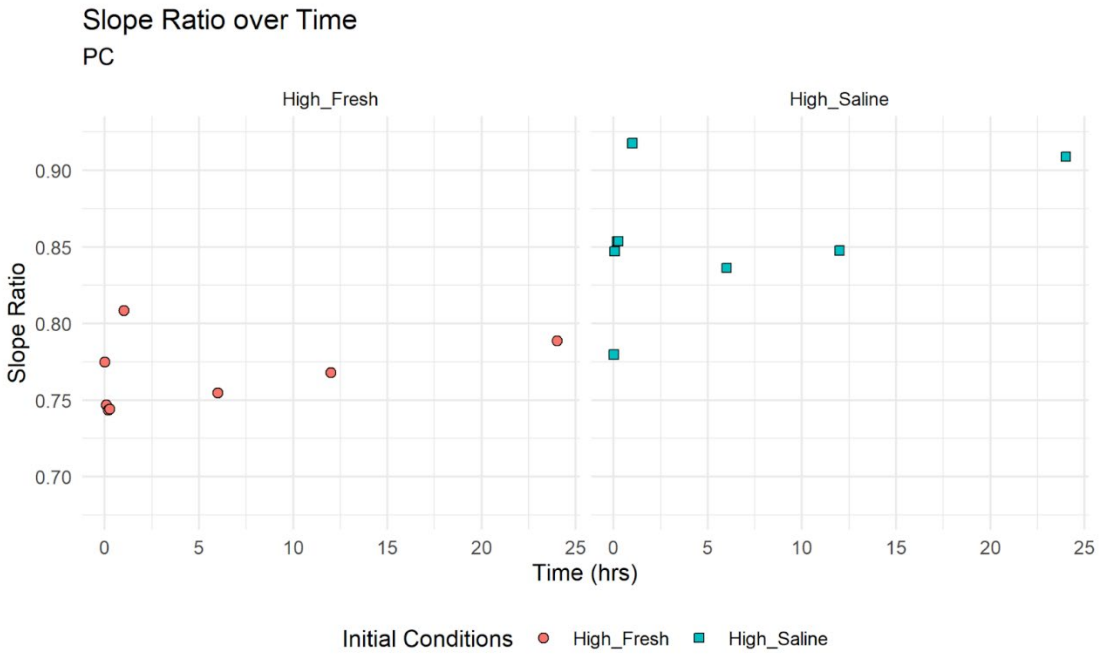

Figure 6.7. PC slope ratio over time for HF (orange circles) and HS (blue squares) initial conditions.

Other spectral characteristics were measured over time to compare to literature values and analyze the change in composition over time (Table 6.3). Values for the final indices fit within the average range reported in literature values for wetland waters, which are 1.2-2.3 for FI (Jaffe et al., 2004; Hansen et al., 2016; Wang et al., 2014), and 0.4-1.0 for β:α and BIX (Hansen et al., 2016; Wang et al., 2014). Literature ranges for HIX values are much larger, within which the LF and LS experiment values fit: 0.6-5.0 (Guo et al., 2013; Hunt & Ohno, 2007; Ohno 2002). The HIX values for HF and HS experiments were much higher (>10), matching the Great Dismal Swamp's highly colored, highly humic composition. SUVA 280 almost always decreased over time for all sites and depth segments, which indicated a shift in composition of DOC to a higher percentage of NCDOC over time.

Table 6.3. Average time 7 values for freshness, biological, fluorescence, and humification indices and delta (Δ) values for SUVA 280 after 24 hrs per site and set of initial conditions.

Site	Freshness Index (β:α)	Biological Index (BIX)	Fluorescence Index (FI)	Humification Index (HIX)	ΔSUVA 280
range	0.384 - 1.141	0.389 - 1.310	1.625 - 2.214	1.683 - 25.253	--
WCHF	0.414 ± 0.01	0.420 ± 0.01	1.854 ± 0.01	17.912 ± 0.93	-0.656 ± 0.25
WCHS	0.595 ± 0.01	0.601 ± 0.01	2.093 ± 0.03	14.497 ± 0.25	-0.563 ± 0.62
WCLF	0.714 ± 0.11	0.779 ± 0.12	2.025 ± 0.08	1.683 ± 0.06	-2.879 ± 0.81

WCLS	1.141 ± 0.12	1.310 ± 0.21	2.214 ± 0.04	1.846 ± 0.19	0.831 ± 0.21
WIHF	0.400 ± 0.01	0.408 ± 0.01	1.760 ± 0.01	17.103 ± 0.51	-0.898 ± 0.08
WIHS	0.548 ± 0.02	0.553 ± 0.03	2.047 ± 0.01	21.079 ± 1.93	-1.395 ± 0.08
WILF	0.609 ± 0.02	0.613 ± 0.02	1.625 ± 0.05	3.198 ± 0.15	-0.115 ± 0.41
WILS	0.915 ± 0.08	0.965 ± 0.10	2.047 ± 0.01	4.127 ± 0.36	-1.075 ± 0.18
WMHF	0.424 ± 0.03	0.434 ± 0.02	1.767 ± 0.02	16.821 ± 1.35	-0.711 ± 0.18
WMHS	0.579 ± 0.02	0.585 ± 0.02	2.025 ± 0.03	16.309 ± 0.91	-1.060 ± 0.25
WMLF	0.626 ± 0.05	0.642 ± 0.05	1.721 ± 0.01	4.415 ± 0.26	-1.924 ± 0.69
WMLS	0.987 ± 0.08	1.050 ± 0.08	2.000 ± 0.03	3.798 ± 0.12	-0.176 ± 0.11
PCHF	0.394 ± 0.01	0.397 ± 0.01	1.755 ± 0.02	18.562 ± 1.34	-6.040 ± 0.14
PCHS	0.557 ± 0.01	0.560 ± 0.01	2.038 ± 0.01	19.910 ± 1.45	-0.719 ± 0.14
PCLF	0.772 ± 0.15	0.816 ± 0.17	1.639 ± 0.05	2.912 ± 0.29	0.680 ± 0.11
PCLS	1.128 ± 0.05	1.266 ± 0.05	1.949 ± 0.04	3.005 ± 0.17	-0.414 ± 0.10
PIHF	0.384 ± 0.00	0.389 ± 0.00	1.754 ± 0.01	20.589 ± 0.75	-0.635 ± 0.11
PIHS	0.496 ± 0.03	0.504 ± 0.02	2.021 ± 0.01	25.253 ± 2.80	-1.228 ± 0.28
PILF	0.498 ± 0.03	0.508 ± 0.03	1.640 ± 0.03	4.906 ± 0.11	0.653 ± 0.40
PILS	0.735 ± 0.06	0.764 ± 0.08	1.957 ± 0.02	6.060 ± 0.15	-0.717 ± 0.21

PMHF	0.391 ± 0.01	0.396 ± 0.01	1.757 ± 0.02	20.797 ± 2.14	-0.704 ± 0.15
PMHS	0.497 ± 0.02	0.504 ± 0.01	2.005 ± 0.01	22.000 ± 1.89	-0.986 ± 0.27
PMLF	0.430 ± 0.07	0.437 ± 0.07	1.688 ± 0.01	6.734 ± 1.47	-1.931 ± 0.64
PMLS	0.664 ± 0.09	0.675 ± 0.08	2.009 ± 0.05	5.813 ± 1.00	-0.043 ± 0.16

DOC Pools: CDOC vs. NCDOC

Partitioning DOC into two distinct pools of colored DOC (CDOC) and non-colored DOC (NCDOC) demonstrates the ability of the sediments to preferentially draw CDOC out of solution and release NCDOC into solution over time (Figure 6.8). The methods of partitioning CDOC and NCDOC at each time point involved a least squares non-negative analysis of pre vs. post absorption spectra, providing consistently good fits across sites, as described in [c]Morrissette et al. (*in prep*) (WC avg. $R^2 = 0.914$, WI avg. $R^2 = 0.924$, WM avg. $R^2 = 0.969$, PC avg. $R^2 = 0.965$, PI avg. $R^2 = 0.963$, PM avg. $R^2 = 0.968$, Appendix R).

The results presented in Figures 6.8-13 reveal similar changes in CDOC and NCDOC contributions over time as observed in previous incubations ([c]Morrissette et al., *in prep*). For all six sites, the HF and HS experiments always had a net adsorption of CDOC over time with an average loss of 22.86 mg L^{-1} and 85.18 mg L^{-1}, respectively, from solution after 24 hours. Shallow segments had significantly (each with $p < 0.05$, two-sample t-test) more adsorption of CDOC (HF = -38.70 mg L^{-1}, HS = -103.79 mg L^{-1}) than deep segments (HF = -7.02 mg L^{-1}, HS = -66.58 mg L^{-1}). In the LF and LS experiments, the sediments were a net source of CDOC to solution,

releasing an average of 26.72 mg L^{-1} and 10.66 mg L^{-1}, respectively, over all six segments. The deep samples released more CDOC on average; 32.58 mg L^{-1} for HF (vs. 20.87 mg L^{-1} for shallow) and 10.74 mg L^{-1} for LS (vs. 10.57 mg L^{-1} for shallow). NCDOC desorbed into solution from the sediments over time for every initial condition across all sites with an average of 53.86 mg L^{-1}, 58.78 mg L^{-1},17.60 mg L^{-1}, and 18.12 mg L^{-1}, released for HF, HS, LF, and LS, respectively.

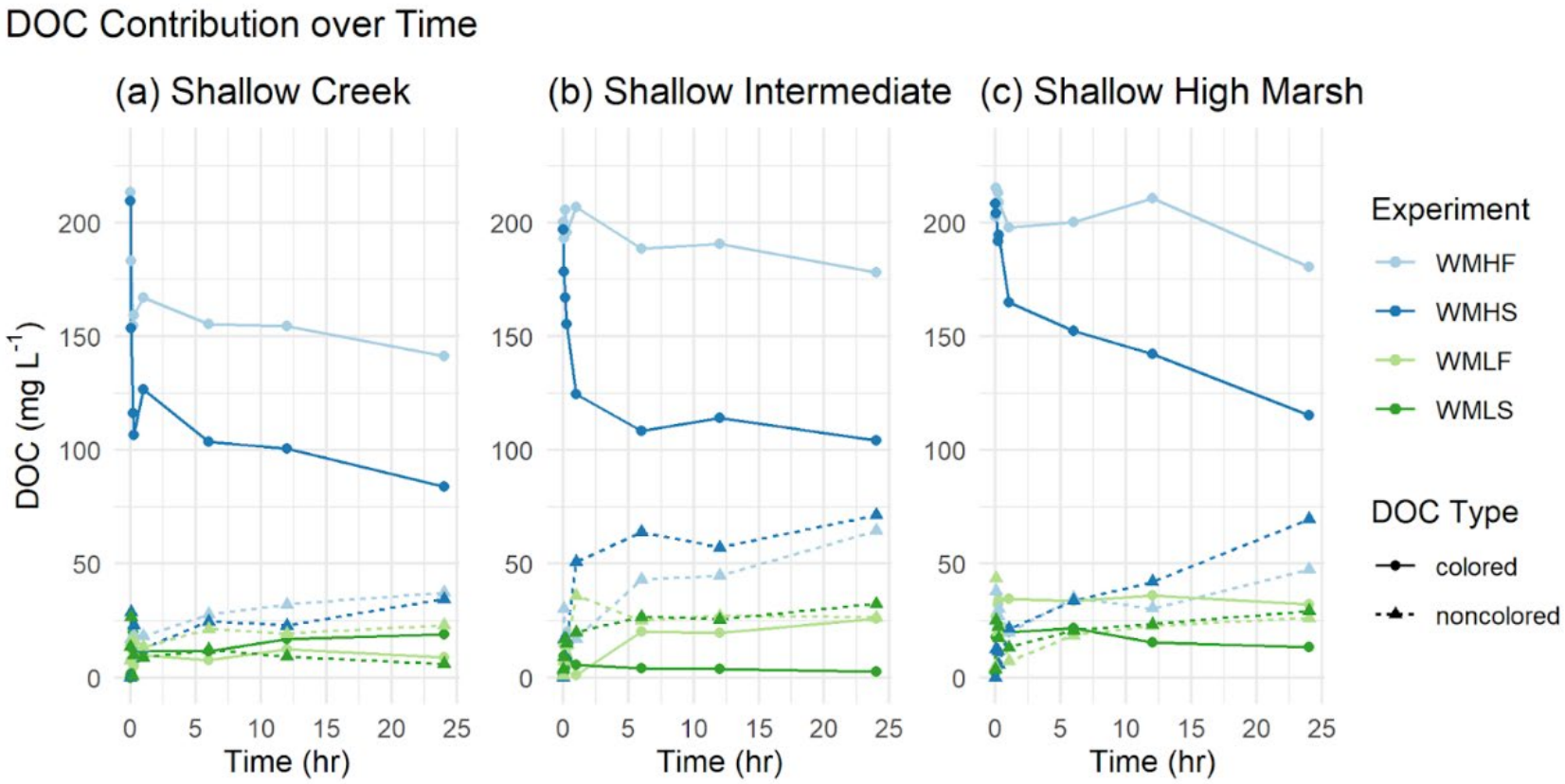

Figure 6.8. DOC concentrations of each pool at every incubation time point for the three shallow segments; a) WC, b) WI, and c) WM. Colors indicate one of the four sets of initial conditions (light blue = HF, dark blue = HS, light green = LF, dark green = LS), and the line type is associated with the DOC pool type (solid = colored, dashed = non-colored).

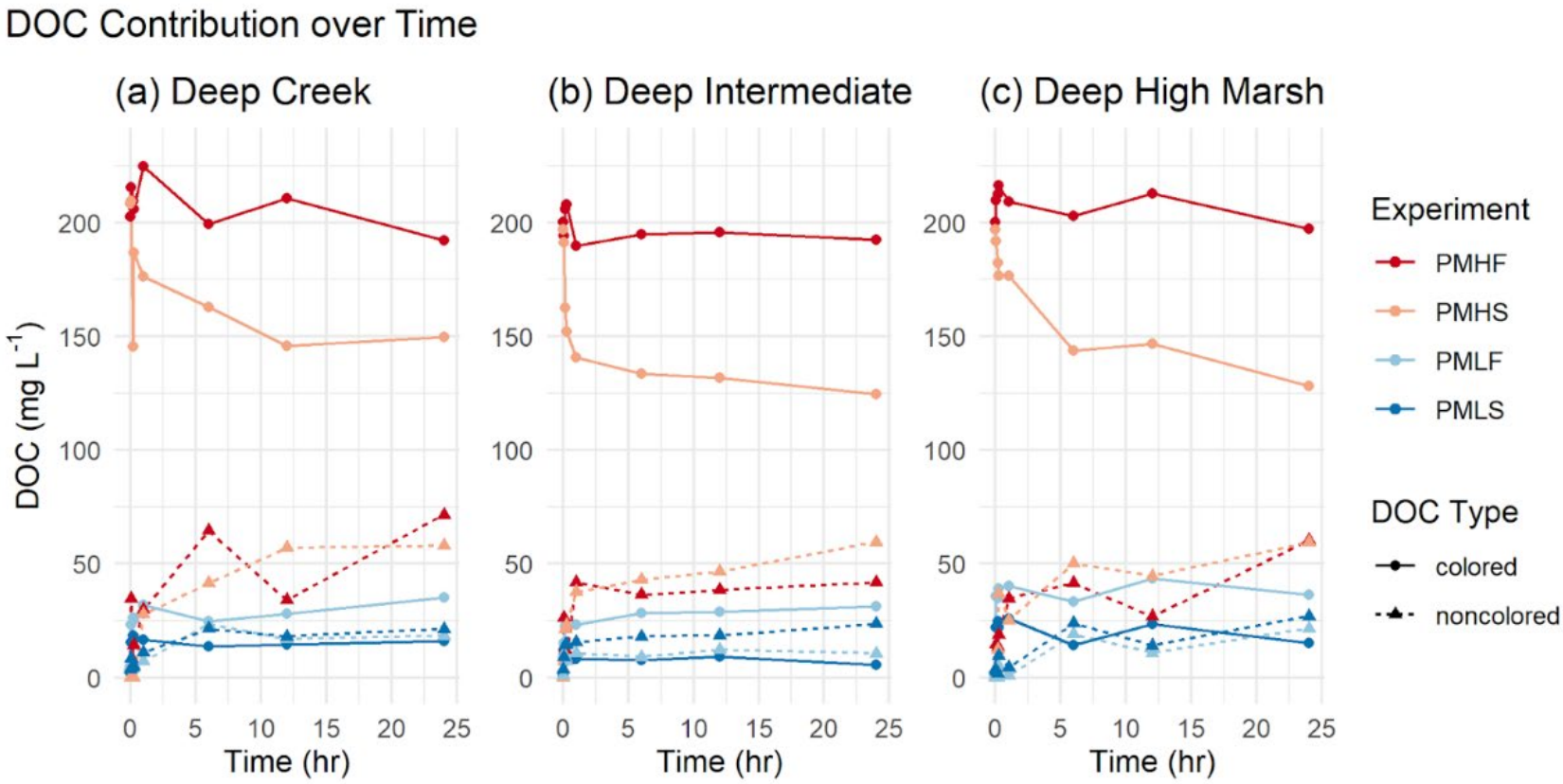

Figure 6.9. DOC concentrations of each pool at every incubation time point for the three deeper segments; a) PC, b) PI, c) PM. Colors indicate one of the four sets of initial conditions (red = HF, orange = HS, light green = LF, dark green = LS), and the line type is associated with the DOC pool type (solid = colored, dashed = non-colored).

The individual CDOC and NCDOC pools explained much of the movement seen in the bulk DOC sorption over time. Again, zooming into the first 30 minutes, Figures 6.10-11 show the same lateral gradient of decreasing adsorption of CDOC in the HF and HS experiments, increasing desorption of CDOC in the LF and LS experiments, and increasing NCDOC in solution over time as seen in the shallow bulk ΔDOC (Figure 6.2). More adsorption occurred in the HS incubations for the shallow segments of every core. The differences in sorption of the individual pools were not statistically significant (each with $p < 0.05$, two-sample t-test), matching the lack of significance in the bulk DOC, but sorption of the pools between the shallow and deep segments of the same core were statistically significant (each with $p < 0.05$, two-sample t-test). The speed of exchange for the CDOC pools in the shallow segments and NDOC in the deep segments decreases with distance from the creek edge. Over all sites and initial conditions, CDOC pools completed significantly more of the total sorption processes in a faster time frame, 15 minutes, than NCDOC ($p = 0.021$, three-way ANOVA, Table 6.5). After 1 hour, the percentages of completed sorption was no longer significantly different between the pools (Table 6.6). The difference in percent completed sorption between initial conditions was very marginally significant for 15 minutes only ($p = 0.03$, three-way ANOVA), but the difference of sorption completed between sites was significant for both the 15-minute ($p = 0.0023$, three-way ANOVA) and 1-hour ($p = 0.0001$, three-way ANOVA) time frames (Tables 6.5-6.6). Influence of interactions between initial conditions, type of DOC, and site were minor.

Table 6.4. Percent sorption completed 15 minutes and 1 hour into the incubations for the CDOC and NCDOC pools of each initial condition.

Site	Initial Conditions	DOC Pool	15 minutes	1 hour
WC	HF	CDOC	65.15%	73.23%
		NCDOC	55.09%	56.18%
	HS	CDOC	62.03%	74.16%
		NCDOC	64.17%	74.49%
	LF	CDOC	53.79%	68.32%
		NCDOC	56.22%	64.08%
	LS	CDOC	76.86%	78.20%
		NCDOC	81.42%	83.57%
WI	HF	CDOC	40.34%	55.52%
		NCDOC	48.58%	50.98%
	HS	CDOC	40.09%	69.54%
		NCDOC	31.64%	65.91%
	LF	CDOC	26.91%	53.54%
		NCDOC	32.94%	74.19%
	LS	CDOC	76.02%	87.21%
		NCDOC	43.77%	57.89%
WM	HF	CDOC	25.85%	41.08%
		NCDOC	52.04%	62.60%

	HS	CDOC	19.41%	49.63%
		NCDOC	23.54%	42.46%
	LF	CDOC	80.75%	81.88%
		NCDOC	65.19%	81.11%
	LS	CDOC	63.48%	63.62%
		NCDOC	59.90%	67.85%
PC	HF	CDOC	23.54%	43.14%
		NCDOC	36.73%	45.10%
	HS	CDOC	70.45%	77.35%
		NCDOC	16.62%	56.44%
	LF	CDOC	50.55%	63.96%
		NCDOC	15.83%	24.07%
	LS	CDOC	77.80%	78.05%
		NCDOC	28.86%	46.96%
PI	HF	CDOC	42.17%	80.71%
		NCDOC	38.54%	63.14%
	HS	CDOC	61.78%	77.55%
		NCDOC	55.41%	70.90%
	LF	CDOC	70.16%	73.66%
		NCDOC	56.23%	59.84%
	LS	CDOC	74.26%	74.51%

		NCDOC	23.25%	40.47%
PM	HF	CDOC	29.66%	42.83%
		NCDOC	39.29%	51.73%
	HS	CDOC	27.33%	27.40%
		NCDOC	12.93%	21.99%
	LF	CDOC	61.26%	62.98%
		NCDOC	16.74%	25.99%
	LS	CDOC	44.21%	50.81%
		NCDOC	55.09%	56.18%
	Average across conditions	**CDOC**	**52.78%**	**65.16%**
		NCDOC	**42.23%**	**58.16%**

Table 6.5 Three-way ANOVA results for percent completion of sorption processes within 15 minutes.

Source	**Sum Squares**	**degrees of freedom**	**Mean Squares**	**F-statistic**	**P-value**
Initial Condition	0.23807	3	0.07936	3.32	0.03
Colored vs. Non-colored	0.13979	1	0.13979	5.84	**0.0206**
Site	0.547	5	0.1094	4.57	**0.0023**
Error	0.90952	38	0.02393		
Total	1.83439	47			

Table 6.6 Three-way ANOVA results for percent completion of sorption processes within 1 hour.

Source	Sum Squares	degrees of freedom	Mean Squares	F-statistic	P-value
Initial Condition	0.0383	3	0.01277	0.72	0.5473
Colored vs. Non-colored	0.06225	1	0.06225	3.5	0.069
Site	0.59403	5	0.11881	6.68	**0.0001**
Error	0.67554	38	0.01778		
Total	1.37012	47			

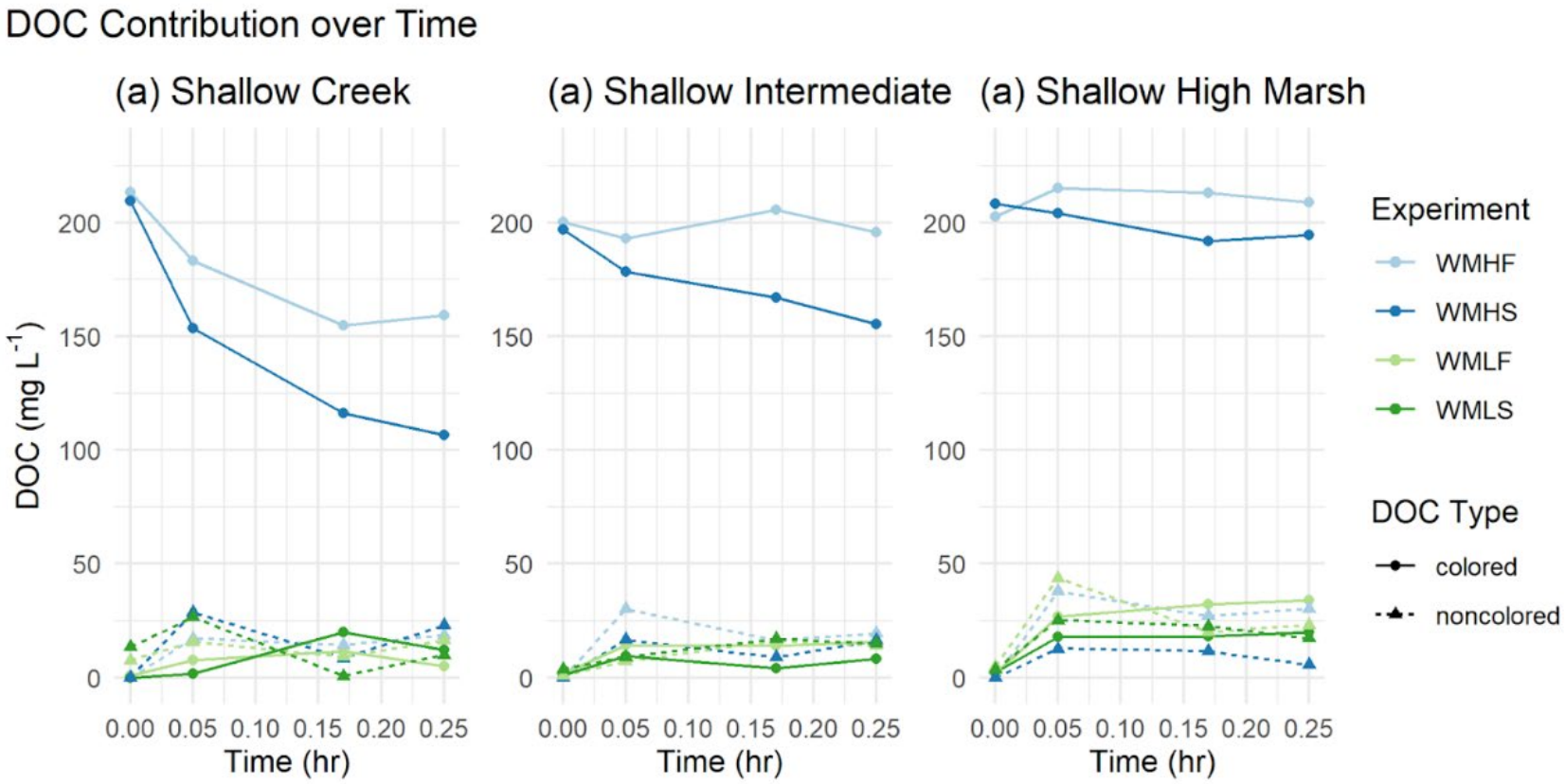

Figure 6.10. DOC concentrations of each pool during the first 30 minutes of the incubations for the three shallow segments; a) WC, b) WI, and c) WM. Colors indicate one of the four sets of initial conditions (light blue = HF, dark blue = HS, light green = LF, dark green = LS), and the line type is associated with the DOC pool type (solid = colored, dashed = non-colored).

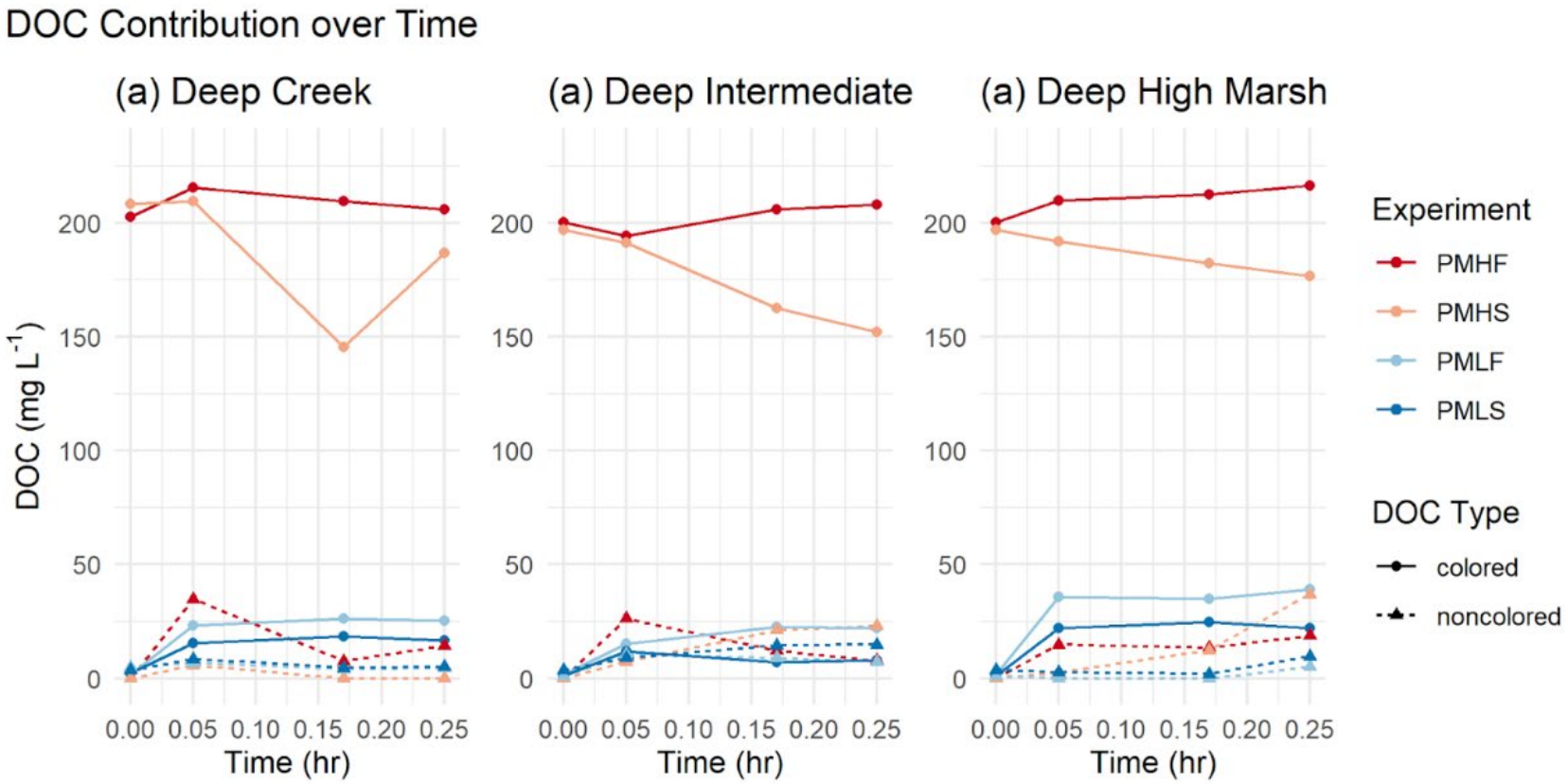

Figure 6.11. DOC concentrations of each pool during the first 30 minutes of the incubations for the three deeper segments; a) PC, b) PI, c) PM. Colors indicate one of the four sets of initial conditions (red = HF, orange = HS, light green = LF, dark green = LS), and the line type is associated with the DOC pool type (solid = colored, dashed = non-colored).

Figure 6.12-13 show the same patterns in percentage as the contribution of DOC type. Across almost all sets of initial conditions, with the exception of the WCLS and WMLF experiments, CDOC decreased and NCDOC increased in percentage of the total DOC in solution. Due to the closed, conservative nature of the experiments and only analyzing two pools, a decrease in one pool equaled the increase in the other pool, so percentages were presented as percent shifts. Over the whole set of experiments, HF and HS increased in NCDOC proportion by 22.80% and 33.24%. LF and LS increased in proportion of CDOC over time by 14.07% and 10.69%. Interestingly, the percent shifts between CDOC and NCDOC over time for the HF and HS incubations were never statistically significant between sites and initial conditions, even when the differences in the actual concentrations of each pool were significant, such as the HF and HS CDOC and NCDOC time series across shallow sites. For example, differences in CDOC change over time between WC, WI, and WM's HF experiments were significantly different ($p = 2.4 \times 10^{-4}$, $F = 12.72$, single factor ANOVA), but the percentage of CDOC at each time point between the three remained similar ($p = 0.925$, $F = 0.08$, single factor ANOVA). Higher total percentages of CDOC in the top panels match the relative higher amount of DOC placed into the incubation. Time 0 was removed from the low [DOC] (bottom panels) experiments because there was no DOC in solution.

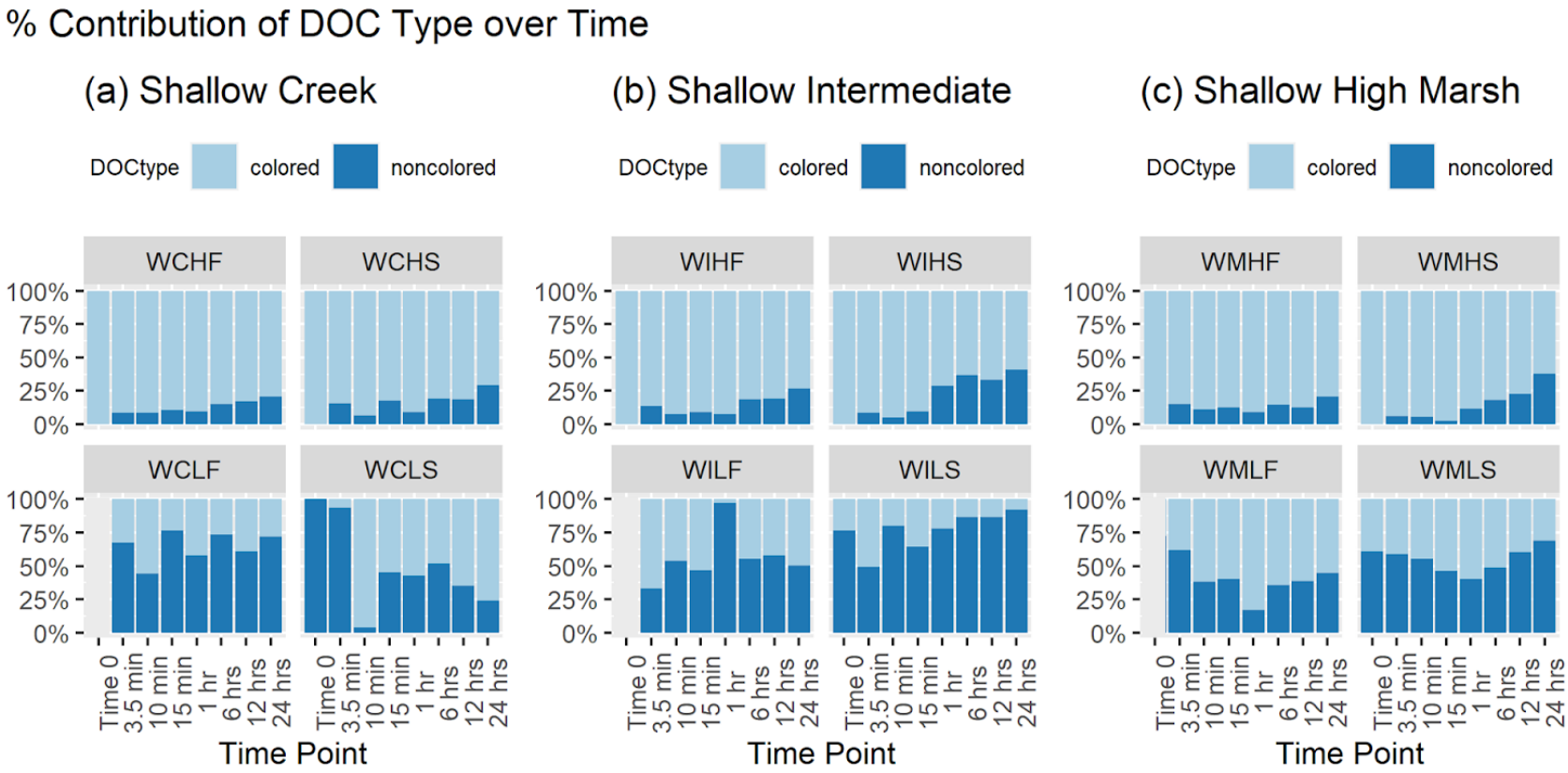

Figure 6.12. Percent contribution of DOC pools in each post-incubation solution for the shallow segments; a) WC, b) WI, and c) WM. Colors indicate DOC type (light blue = colored, dark blue = non-colored), and each of the four panels is a set of initial conditions (top left = HF; top right = HS, bottom left = LF; bottom right = LS).

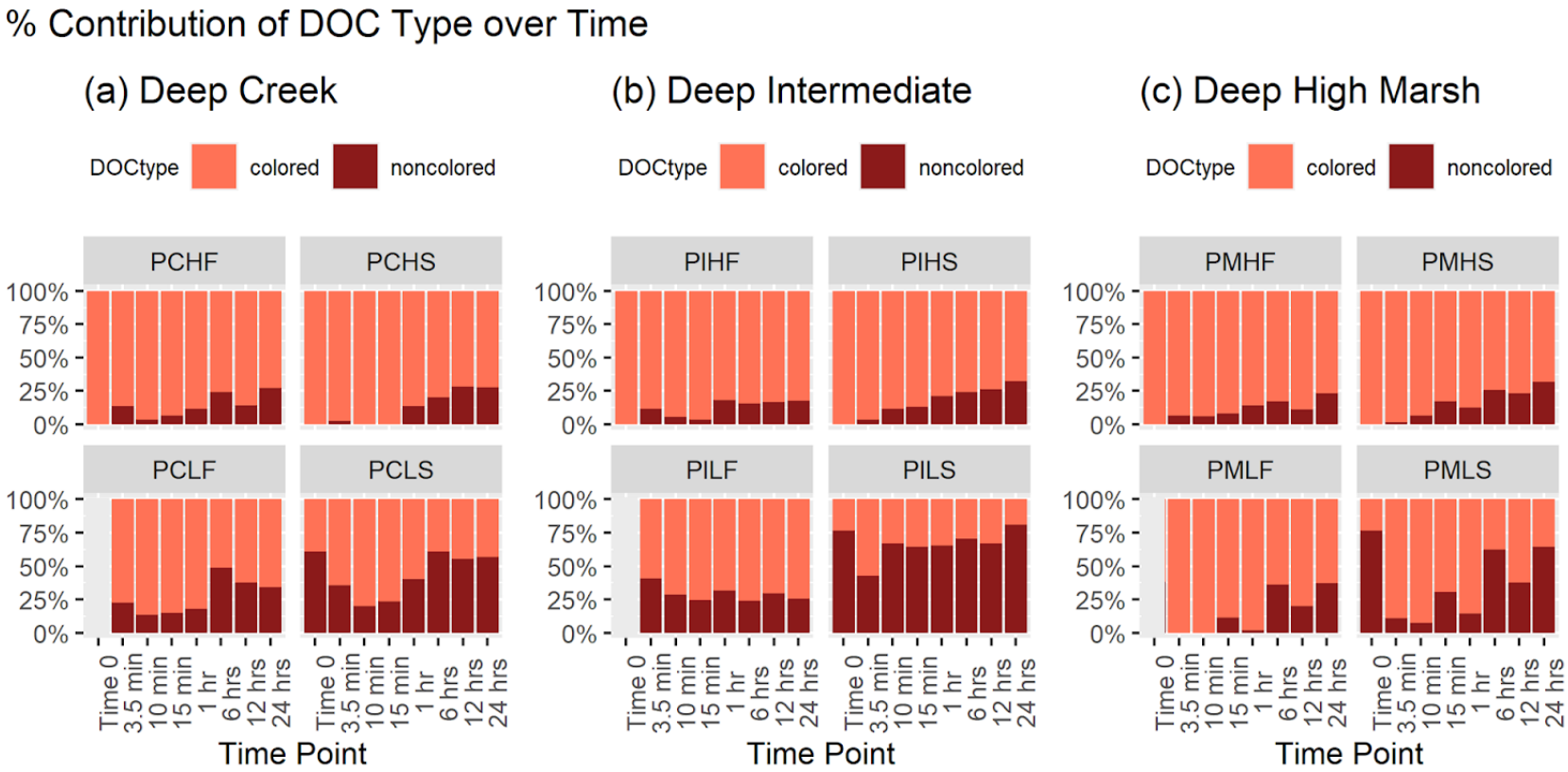

Figure 6.13. Percent contribution of DOC pools in each post-incubation solution for the deeper segments; a) PC, b) PI, c) PM. Colors indicate DOC type (orange = colored, dark red = non-colored), and each grouping of four panels is a set of initial conditions (top left = HF; top right = HS, bottom left = LF; bottom right = LS).

Sediment characteristics, measured for each of the six core samples separately and detailed further in Pinsonneault et al. (*in prep*) and Canuel & Pondell (unpublished data), are shown as a function of space in Figure 6.14. The sediment characteristics that increased laterally moving further away from the creek edge were %SOM (shallow segments by 137.50%; deep by 156.38%), %TN (shallow by 107.88%; deep by 115.27%), %TOC (shallow by 173.44%; deep by 185.52%), and C:N (shallow by 31.50%; deep by 32.66%). In contrast, bulk density and SSA decreased laterally moving away from the creek edge by 50.15% and 39.34% for the shallow segments and 60.89% and 56.16% for the deep segments, respectively. Grain size, NC-Al, and NC-Fe all spiked in increase or decrease at the intermediate core. The largest differences between depths occurred in NC-Fe (by an average of 80.00%) and SSA (by an average of 29.22%). %SOM, %TN, %TOC, C:N, and bulk density were all significantly different across cores ($p = 9.39 \times 10^{-9}$, $F = 124.63$; $p = 3.58 \times 10^{-7}$, $F = 65.22$; $p = 8.32 \times 10^{-8}$, $F = 84.81$; $p = 6.83 \times 10^{-4}$, $F = 14.22$; and $p = 0.014$, $F = 24.46$ respectively; single factor ANOVAs). NC-Fe was significantly different between depth segments ($p = 0.0268$, $F = 35.78$, two-way ANOVA).

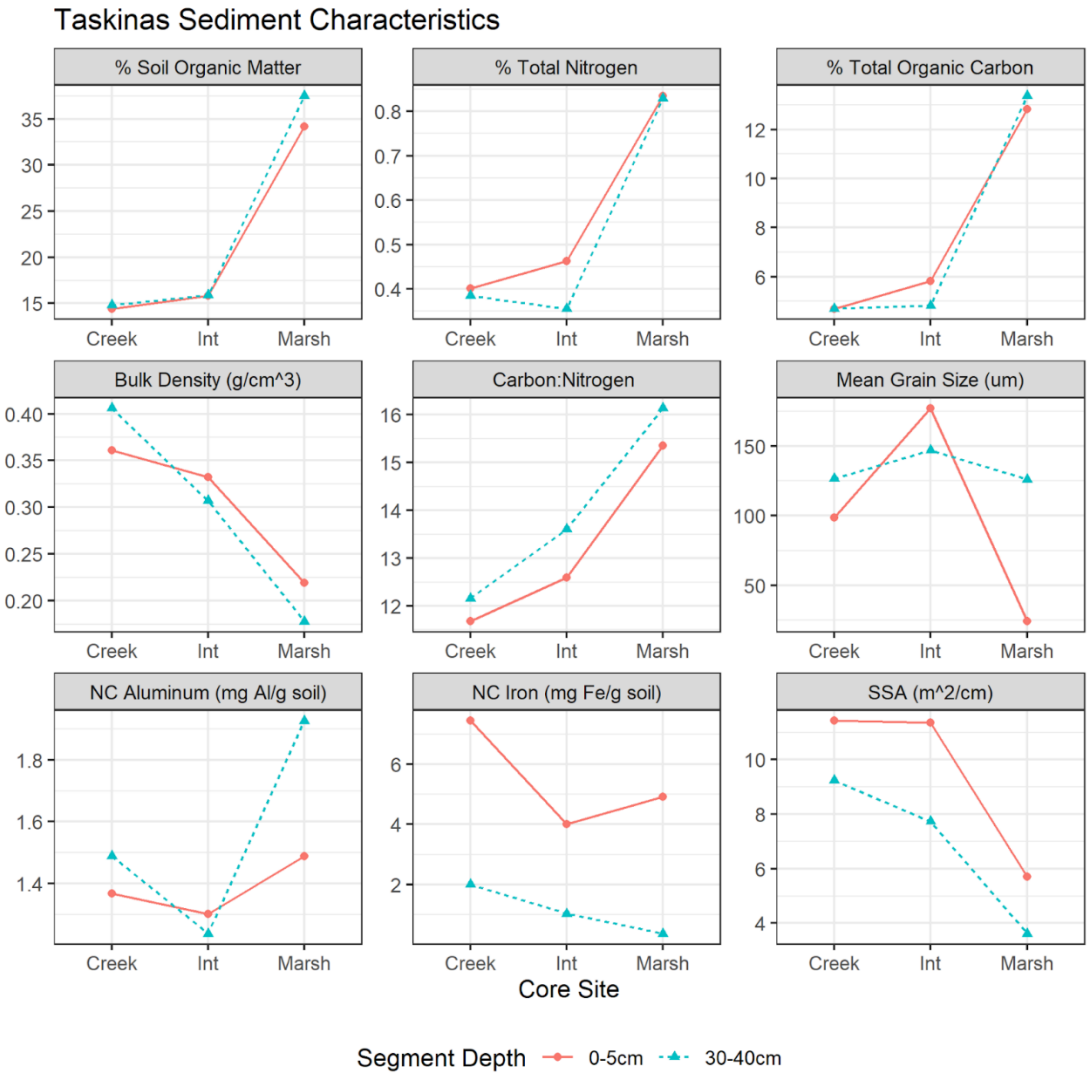

Figure 6.14. Summary of relevant sediment characteristics for the shallow (orange solid lines) and deep (blue dashed lines) segments of the three Taskinas Marsh spatial cores (Creek = Creek Edge; Int = Intermediate Plot; Marsh = High Marsh). (Pinsonneault et al. 2021; Canuel & Pondell (unpublished data)).

Discussion

Sorption has been studied in various ecosystems around the world, often focusing on the net abiotic release and capture of carbon in sediments, but this work

has mainly been done in forested, freshwater environments (Ahrens et al., 2015; Kaiser & Guggenberger, 2000; Kaiser & Zech, 1998; Kothawala et al., 2009; Qualls & Haines, 1992; Shaker et al., 2012). This study presented results from some of the first marsh sorption experiments, building on the marsh isotherm and kinetic incubation results reported in Pinsonneault et al. (2021) and [b]Morrissette et al. (*in prep*), which examined sorption processes over a broad range of sediment characteristics, including different marsh types, salinity levels, dominant vegetation, etc. In these previous studies, tidal marsh sites were chosen around the Chesapeake Bay to get a better understanding of how sorption properties change in different marshes and how these changes are controlled by differences in the biogeochemical properties of marsh soils. This study extended this understanding by providing new insights into the effects of spatial gradients and sediment characteristics on sorption kinetics, and it revealed, among other things, that sorption processes can vary as much within one marsh site as between multiple marsh sites due to within marsh spatial variability of sediment characteristics.

Bulk DOC

The magnitude of adsorption of the bulk DOC concentration decreased as the cores moved further away from the creek edge and in deeper core samples. In contrast, the amount of desorption increased further away from the creek edge. These patterns could potentially be largely explained by observed changes in the biogeochemical characteristics of the sediments. %SOM and TOC increased moving into the high marsh, which means that there was more available carbon on these sediments to desorb into solution and less sites for adsorption to occur. In addition,

there were decreases in NC-Fe, SSA, bulk density, and grain size moving away from the creek edge, which are known to be associated with higher amounts of adsorption (Groeneveld et al., 2020; Keil & Mayer, 2014; Kaiser et al., 1996; Kothawala et al., 2009, 2012; Pinsonneault et al., 2021), i.e., they are all associated with increasing the abundance of available adsorption sites to which DOC can attach.

Focusing on the first 30 minutes of the incubations revealed rapid sorption processes consistent with other published sorption experiments (Kaiser & Zech 1998; [b]Morrissette et al. *in prep*; Shaker et al., 2012), with over 62% of sorption occurring in the first 15 minutes, and over 75% in the first hour. The same peaks of NCDOC desorption in the first 2 time points were observed here, as in previous kinetic incubations ([c]Morrissette et al., *in prep*). The initial fluctuations in NCDOC were most likely due to a mixture of processes involving rapid dissolution of freeze-dried DOC from the core pore water, different reaction speeds for adsorption and desorption, and preferential adsorption of the highly humic, colored Dismal Swamp DOC from the solution replacing native DOC on the sediment.

Spectral Properties

Tracking the separate movements of CDOC and NCDOC revealed that these pools moved independent of one another, controlled by different initial conditions, as observed in previous isotherm and kinetic incubations ([c]Morrissette et al., *in prep*; Pinsonneault et al., *in prep*). The movement of the colored fraction was determined by the initial levels of [DOC] and salinity, with CDOC being adsorbed by the sediment with high initial DOC (compounded with high salinity), and desorbed from the sediments when there was low DOC. In contrast, NCDOC desorbed from the

sediments over time in almost all experiments regardless of the initial DOC concentration or salinity levels. The NCDOC movement, especially within the first few time points, mirrored the presence of a peak in bulk DOC flux, indicating that rates of change for these processes were independent and non-linear over time, and also revealing that the large peaks and initial fluctuations of DOC were dominated by movement of the NCDOC fraction, regardless of the process that controls that NCDOC flux.

The optical analysis of absorbance, CDOC vs. NCDOC fractionation, spectral slope, slope ratio, and SUVA 280 all pointed to shifts in DOC composition over time. While the quantity of DOC movement tended to be dictated by the initial DOC concentration, salinity, and the biogeochemical properties of the sediments that determine available adsorption sites, DOC quality was controlled by the dynamics of the individual DOC pools, i.e., highly humic, colored material from the Dismal Swamp was quickly adsorbed by the sediments and removed from solution, causing a shift to a lower molecular weight DOC in solution as revealed by the increased slope ratio and decreased absorbance spectra. In addition, an increase was observed in the native pools in solution as revealed by a net decrease in SUVA 280 over time. Combined, these measurements revealed that the sediment preferentially adsorbed the introduced CDOC while simultaneously releasing native NCDOC and CDOC pools (of lower molecular weight) into solution. This exchange of DOC pools may actually happen in natural marsh soils when highly humic CDOC from upland areas is introduced, resulting in the release of native NCDOC and CDOC into the surrounding

estuarine or coastal ocean environment, potentially affecting the biological activity downstream.

Implications

One of the most important takeaways from this study is that sorption processes have significant spatial variability, not only between marshes, but within a single marsh. This means that when tracking the transport and transformation of dissolved organic carbon through a marsh-estuarine ecosystem, it is not only essential to include sorption as a critical process controlling DOC flux, but also that measuring adsorption and desorption capacity at a single spot in a marsh will not necessarily be representative of the marsh's sorption capacity.

This is also most likely exacerbated by the marsh morphology. While these cores are taken from a transect moving deeper into the marsh perpendicular to the creek edge, the expanses of most marshes are characterized very differently depending on their creeks, channels, and extension. If a marsh has many channels running through its interior, that potentially increases the amount of tidal influence and lateral exchange with the sediments. Conversely, higher elevation marshes or sections of marsh are considered to export less organic material to adjacent environments (Taylor & Allanson, 1995). There is also a prevalent effect of sea level rise of the formation of ponds within the interior of the marsh when sediment accretion is not rapid enough to combat the rising waters (Burns et al., 2021; Qi et al., 2020). This could affect sorption in conflicting ways; reducing the amount of moving water and subsequent exchange via sorption through a standing pond, increasing the surface water area for wave fetch that would increase water movement and exchange,

and/or increasing the amount of "creek edge", which could increase the amount of lateral exchange.

These experiments also show less overall adsorption in most samples than in the 0-40 cm homogenized cores used in the kinetic incubations ([b]Morrissette et al., *in prep*), signaling that a homogenized sample is also not necessarily representative of the marsh's sorption capacity, and may overestimate how much DOC is retained in the sediments. This has implications for affecting neighboring or downstream environments from that tidal marsh ecosystem, and should be further explored.

Conclusion

Pinsonneault et al. (2021) reported the first marsh sediment isotherm incubations, providing important new information on the variability and biogeochemical controls of sorption processes and DOC exchanges in sediments from multiple Chesapeake Bay marshes. Building on this work, [b]Morrissette et al. (*in prep*; Chapter 3) showed how fast these sorption processes could occur and how the rates were influenced by the biogeochemistry of the sediments. In this study, the spatial variability in sorption kinetics within a single marsh was examined in relation to sediment biogeochemical properties, which provides further insight into the factors that affected sorption rates and ultimately net exchanges of DOC at the marsh-estuarine interface.

It is shown that sorption processes varied significantly with space, both horizontally across the marsh and vertically within the depth profile. This variability is comparable to that which has been observed between separate marshes with very different sediment characteristics, marsh plant composition, and morphology. This

suggests that efforts to incorporate sorption processes into sediment flux models, as recommended by [a]Morrissette et al. (*in prep*; Chapter 2), should be careful to consider spatial variability, recognizing that one sample or even one core is not representative of the entire marsh. Because the creek edge and shallow segments throughout the marsh are most influenced by water exchange (tides, inundation, precipitation, runoff), perhaps the sediment characteristics and sorption processes derived from them should be prioritized for incorporation into models that simulate marsh-estuary exchanges. However, it may be that the sediment characteristics and sorption processes derived from depth should be prioritized for incorporation into models that simulate carbon sequestration.

Chapter 7: Conclusion

As emphasized in Najjar et al. (2018), the spatial and temporal variability of the carbon cycle make it difficult to quantify coastal carbon budgets. The initial motivation for researching the specific processes of sorption was both its hypothesized ability to buffer tidal marsh DOC exchange, but also its observed dominance over other pathways of DOC transport into adjacent waters and sequestration. The results discussed in this dissertation support the hypothesis of sorption buffering capacity: through sorption, both DOC quality and quantity are altered between its import into and export from marsh sediments. Due to this ability, sorption confirms its importance in the regulation of carbon within the coastal cycle via preferential uptake and release of different compounds, the rapidness with which this occurs, and the transformation of the composition of DOC at the sediment-water interface. The research presented in this dissertation focused on quantifying rates and variability of sorption processes in marsh sediments and how the incorporation of these processes into models impacts model simulation results.

Chapter 2 incorporated adsorption and desorption processes into a highly studied and well-exercised sediment flux model (Di Toro, 2001) with increasing levels of complexity. Sediment flux models are very useful research and management tools for nutrient, oxygen, and organic matter fluxes between sediments and the overlying water column (Brady et al., 2013; Clark et al., 2017; Testa et al., 2013). The addition of adsorption and desorption significantly changed model behavior, with the presence of desorption in any capacity tending to drive DOC fluxes out of the sediments, which is consistent with the observational data that led marshes to be a

known source of DOC despite being a major sink for carbon overall (Cai, 2011; Herrmann et al., 2015; Najjar et al., 2018; Windham-Myers et al., 2018). Adding sorption processes not only increased the flux of bulk DOC out of the sediment, but it also increased the fluxes toward the water column in every lability pool in the model (labile, semilabile, and refractory) and in both the colored and non-colored DOC pools. The model was also significantly sensitive to changes in the sorption rate parameters, which can alter the fluxes by orders of magnitude with increased rates. Also, even though most of the model remained unchanged from its estuarine parameterization, the addition of the sorption processes resulted in DOC fluxes that are more consistent with existing knowledge of marsh sediment carbon flux behavior. It is therefore recommended that sorption processes be included in sediment flux models that aim to analyze coastal wetland carbon fluxes moving forward. It is also recommended that more in situ measurements and sorption kinetic experiments need to be done, especially related to nutrient and oxygen fluxes, to help with further development and validation of these models. Without these sorption processes and marsh-specific parameterizations, sediment flux models could be significantly incorrect in regard to simulation of dissolved organic carbon and nutrient fluxes.

Chapter 3 describes the results from a series of DOC sorption kinetics experiments. Motivations for this chapter were quite clear: adsorption and desorption have been theorized and observed to be rapid and important processes in sediments (Kaiser & Zech, 1998; Kleber et al., 2021; Kothawala et al., 2009; Pinsonneault et al., 2021; Qualls & Richardson, 2003; Shaker et al., 2021), yet measurements of these rates in marsh sediments are generally lacking, and new sediment flux models require

rates to inform their parameterization. The research conducted in this chapter built on the first isotherm results for marsh soils, which provided important information on net DOC exchange due to sorption and the biogeochemical influences on the processes (Pinsonneault et al., 2021). The results presented in this chapter provided crucial new information on sorption rate in marsh sediments - 76% of the processes occurring within 15 minutes, and 84% in the first hour. Many of the water-driven influences on marsh sediments happen quickly, e.g., due to tides storms, etc. Knowing that DOC exchange between the sediment and overlying water column happens rapidly means that these sorption-driven DOC fluxes could be occurring almost continuously over time with each new disturbance. This chapter also revealed how DOC concentrations and salinity, along with the biogeochemical properties of the marsh sediments, influence sorption kinetics. Compounding effects of high initial DOC concentrations and high salinity levels always led to an extremely rapid net adsorption. Low initial DOC concentrations always led to net desorption, regardless of salinity level, but with a lower magnitude of exchange. High initial DOC concentrations with low salinity levels, however, led to different net DOC flux outcomes, revealing that sediment characteristics also influenced the direction of these processes, such as the high mineral content of Jug Bay and the high soil organic matter percentage of Taskinas. It is recommended that more kinetic experiments should be conducted for a range of marsh types and sediment characteristics, as this research focused on end-member initial conditions.

Chapter 4 built upon the sorption kinetic measurements from Chapter 3 and the need for rate measurements to parameterize new sediment flux models that

include sorption processes that were formulated in Chapter 2. A series of simplified models were constructed that were specifically designed to simulate the laboratory sorption kinetic experiments, i.e., removing oxygen, diffusion, and biologically- and photochemically-mediated processes. These simplified models were fit to the kinetic curves to provide rate parameters for the full sediment flux model (Chapter 2). Three separate model versions provided specific information on 1) whether the equations could simulate the data, 2) whether adsorption saturation was present in the experimental data, and 3) how the addition of time-dependency for the sorption rates changed model behavior. The simplified model built from linear, first-order, ordinary differential equations was unable to simulate the majority of the non-linear sorption kinetic curves, though it did provide either an exponential decay (net adsorption-dominant) or hyperbolic saturation (net desorption-dominant) response. The saturation (Langmuir) kinetic model version was almost always drastically different, and mostly improved, from the first linear model version, which revealed that saturation was a concern. Finally, incorporation of a time-dependent desorption rate allowed the model to fit rapid initial oscillations in DOC concentrations that were observed in some of the experiments in the first few time points. This chapter not only provided a range of sorption rate parameters for the model developed in Chapter 2, but it also provided the information on what type of model might be needed for sediment flux simulations that focus on short versus longer time scales. It is recommended that for rapid, post-disturbance simulations of carbon exchange within the sediment flux models, a time-dependency for the sorption rate parameters should be used in order to capture oscillations of DOC exchange within the first few minutes.

However, in sediment flux models that are used to simulate long-term carbon storage within the sediments, Langmuir formulations with constant rates are probably more appropriate.

Chapter 5 was motivated, again, by the previous sorption studies. The isotherm incubations suggested that separate pools within the bulk DOC were moving independently of each other and were controlled by different initial conditions and the biogeochemical characteristics of the sediments (Pinsonneault et al., *in prep*). These separate pools, colored and non-colored DOC, were distinguished based on their distinct optical properties that could be tracked using absorbance and fluorescence data. It was shown that highly humic CDOC from the Great Dismal Swamp was rapidly adsorbed, especially under compounding effects of high initial DOC concentrations and salinity. The adsorption of CDOC was present, although less rapid with lower salinity, for any experiment with high initial DOC concentrations. Native marsh CDOC was always desorbed from the sediments over time, in a much lower magnitude, under low DOC initial conditions. The non-colored DOC fraction was not controlled by the initial conditions, desorbing from the sediments over time for every incubation, regardless of the initial DOC or salinity levels. As extensively discussed in previous chapters, the rapid release of DOC in the first few time points of some incubations was most likely a combination of desorption and immediate dissolution of dehydrated DOC. Nonetheless, the rapid increases in NCDOC in solution along with the rapid adsorption of CDOC under HS initial conditions controlled the oscillations seen in the first few moments of the bulk DOC incubations (<15 minutes). The CDOC flux drove the net processes seen in the bulk kinetics. The

displacement of native DOC with highly humic CDOC that was introduced to the system has interesting implications for coastal management, i.e., runoff of high CDOC water from upland areas might actually displace native DOC from marshes and subsequently impact downstream biogeochemistry. It is recommended that more research be carried out focusing on the fractionation of different pools within bulk DOC sorption kinetics, as these results are one of very few to provide this kind of information (Kaiser & Zech, 1998).

Finally, Chapter 6 examined spatial variability of marsh sediment DOC sorption kinetics and how this variability relates to sediment biogeochemical characteristics within one marsh location. Results from the other chapters and yet-to-be-published data on marsh sediment properties show that sorption varies significantly between marsh sites, determined by initial conditions and the biogeochemical characteristics of the sediments (Pinsonneault et al., *in prep*). In this chapter it was shown that these biogeochemical characteristics also vary significantly between samples collected at different locations and depths within one marsh site (Canuel & Pondell, unpublished data), and that this variability strongly influenced the sorption kinetics. Adsorption magnitude was highest for the shallow sample of the creek edge core, and decreased with depth and distance from the creek. Desorption was more consistent across cores in magnitude but increased with depth and distance from the creek edge. Patterns in sorption kinetics were the same as reported in Chapter 3: 1) HS conditions drove the highest magnitudes of adsorption, 2) LF and LS always led to net desorption, 3) bulk kinetics were rapid (62% in 15 minutes, 75% in the first hour), 4) CDOC decreased in solution over time with high DOC initial

conditions 5) CDOC increased in solution over time with low DOC initial conditions, and 6) NCDOC always desorbed from the sediments over time regardless of initial conditions. While it was interesting that patterns remained similar throughout all sorption incubations of all experimental chapters, the most important takeaway from this specific set of spatial incubations was the fact that sorption processes can vary just as much within one marsh location as between multiple marsh sites. It is recommended that this spatial variability be taken into consideration when utilizing sorption data in sediment flux models or scaling up for sediment carbon stock estimates, considering that one core will provide significantly different dissolved organic carbon exchange information depending on the location in the marsh from which it is taken.

Limitations of this research, due to experimental time frames, methodology, or depth of the measurements, led to more scientific questions and recommendations for future research. The implementation of sorption in the sediment flux model within the scope of this research was a sensitivity study; how an existing model's behavior changes with the addition of a single new process at a time between state variables in an established formulation. However, to be a widely applicable model, it would need to have additional sets of initial conditions and marsh-specific parameterizations added to the framework, such as tidal, salinity, and pore water influences, and subsequently be validated with matching OM and nutrient flux data from marsh sites. Also, throughout this research, idealized conditions were established for the isolation of parameters of interest. This included the use of highly concentrated Great Dismal Swamp water to force adsorption, the removal of biological influences to reduce

concurrent OM processing, the inoculations in anaerobic conditions to avoid high amounts of iron precipitation, and the processes of freeze-drying sediment cores to provide more uniform samples. All of this leads to the question of applicability in the real world. This research isolated the sorption of DOC, which, however interesting, is not necessarily mirrored in in situ environmental processing. A next step of this research would be to perform the kinetic and isotherm incubations with conditions closer to in the field: a water source adjacent to the marsh, full and intact cores, the inclusion of microbiological processes, and the ability of DOC to laterally diffuse. A larger scientific question that stems from this realm of research could assess how sorption processes compare between other types wetland sediments, as sorption kinetics are sparse and not quantified for other ecotypes such as mangrove forests. As mangroves are known to be even better at carbon sequestration than marsh sediments, but are being depleted rapidly worldwide, sorption processes could be critical in these changing ecosystems.

The results of this dissertation research will provide improved confidence in estimates of coastal carbon budgets, as requested in Windham-Myers et al. (2018), through the resolution of temporal and spatial variability of tidal marsh sorption kinetics. These chapters revealed the specifics of tidal marsh bulk and individual DOC sorption, their kinetics, and the biogeochemical controls on those kinetics. Tidal marshes provide important ecosystem services in the form of carbon sequestration and regulation, storing massive amounts of carbon in the upper sediments globally. Through the use of numerical models, field collections, and laboratory incubations, this research provided definitive information on the dominant abiotic adsorption and

desorption processes, rates, and patterns within marsh sediments that could affect the carbon pools in these sediments. The sorption rate measurements that were made in this dissertation can be used to inform sediment flux models that simulate the impacts of climate change on marsh DOC exchanges. Including these sorption processes in sediment flux models will provide more accurate simulations of marsh-specific DOC sediment and water column exchange, and can be applied over a wide range of marsh conditions due to the quantification of biogeochemical controls of these processes. The parameterization of sediment flux models to include sorption, and their subsequent validation, could also provide further information on DOC exchange from interannual to decadal time scales. This research could be used to inform marsh restoration efforts, coastal management decisions, and carbon budget analyses, providing a deeper understanding of biogeochemical interactions within wetland sediments and the implications for marsh sediment changes over time.

Appendices

Appendix A: Model Parameter Input Descriptions

Table A.1. List and description of the rate parameters used in the four new models of adsorption and desorption of organic matter. Models increase in the complexity of their description of adsorption and desorption processes. All parameter units are in d^{-1}. Test1 used minimum estimated rates; Test2 used elevated, maximum rates informed from the kinetic experiments in [e]Morrissette et al. (*in prep*) (described in methods).

Symbol	Description	Value Test1	Value Test2
Adsorption model			
$kDOCads_1$	adsorption of labile DOC to POC	0.1	5.184
$kDOCads_2$	adsorption of semi-labile DOC to POC	0.01	0.5184
$kDOCads_3$	adsorption of refractory DOC to POC	0.001	0.0518
$kDONads_1$	adsorption of labile DON to PON	0.1	0.1
$kDONads_2$	adsorption of semi-labile DON to PON	0.01	0.01
$kDONads_3$	adsorption of refractory DON to PON	0.001	0.001
$kDOPads_1$	adsorption of labile DOP to POP	0.1	0.1
$kDOPads_2$	adsorption of semi-labile DOP to POP	0.01	0.01
$kDOPads_3$	adsorption of refractory DOP to POP	0.001	0.001
Adsorption and desorption model (includes all above parameters plus the following)			
$kPOCdes_1$	desorption of labile POC to DOC	0.1	9.072
$kPOCdes_2$	desorption of semi-labile POC to DOC	0.01	0.9072
$kPOCdes_3$	desorption of refractory POC to DOC	0.001	0.0907
$kPONdes_1$	desorption of labile PON to DON	0.1	0.1
$kPONdes_2$	desorption of semi-labile PON to DON	0.01	0.01
$kPONdes_3$	desorption of refractory PON to DON	0.001	0.001
$kPOPdes_1$	desorption of labile POP to DOP	0.1	0.1
$kPOPdes_2$	desorption of semi-labile POP to DOP	0.01	0.01
$kPOPdes_3$	desorption of refractory POP to DOP	0.001	0.001
Bound DOM model (includes all above parameters plus the following)			

kDOCbads$_1$	adsorption of labile free DOC to bound DOC	0.1	5.184
kDOCbads$_2$	adsorption of semi-labile free DOC to bound DOC	0.01	0.5184
kDOCbads$_3$	adsorption of refractory free DOC to bound DOC	0.001	0.0518
kDONbads$_1$	adsorption of labile free DON to bound DON	0.1	0.1
kDONbads$_2$	adsorption of semi-labile free DON to bound DON	0.01	0.01
kDONbads$_3$	adsorption of refractory free DON to bound DON	0.001	0.001
kDOPbads$_1$	adsorption of labile free DOP to bound DOP	0.1	0.1
kDOPbads$_2$	adsorption of semi-labile free DOP to bound DOP	0.01	0.01
kDOPbads$_3$	adsorption of refractory free DOP to bound DOP	0.001	0.001
kDOCbdes$_1$	desorption of labile bound DOC to free DOC	0.1	9.072
kDOCbdes$_2$	desorption of semi-labile bound DOC to free DOC	0.01	0.9072
kDOCbdes$_3$	desorption of refractory bound DOC to free DOC	0.001	0.0907
kDONbdes$_1$	desorption of labile bound DON to free DON	0.1	0.1
kDONbdes$_2$	desorption of semi-labile bound DON to free DON	0.01	0.01
kDONbdes$_3$	desorption of refractory bound DON to free DON	0.001	0.001
kDOPbdes$_1$	desorption of labile bound DOP to free DOP	0.1	0.1
kDOPbdes$_2$	desorption of semi-labile bound DOP to free DOP	0.01	0.01
kDOPbdes$_3$	desorption of refractory bound DOP to free DOP	0.001	0.001
Inorganic and organic bound DOM model (includes adsorption and desorption parameters plus the following)			
kDOCbadso$_1$	adsorption of free labile DOC onto organics	0.1	5.184
kDOCbadso$_2$	adsorption of free semi-labile DOC onto organics	0.01	0.5184
kDOCbadso$_3$	adsorption of free refractory DOC onto organics	0.001	0.0518
kDOCbadsi$_1$	adsorption of free labile DOC onto inorganics	0.1	5.184

kDOCbadsi$_2$	adsorption of free semi-labile DOC onto inorganics	0.01	0.5184
kDOCbadsi$_3$	adsorption of free refractory DOC onto inorganics	0.001	0.0518
kDOCbdeso$_1$	desorption of labile bound DOC onto organics to free DOC	0.1	9.072
kDOCbdeso$_2$	desorption of semi-labile bound DOC onto organics to free DOC	0.01	0.9072
kDOCbdeso$_3$	desorption of refractory bound DOC onto organics to free DOC	0.001	0.0907
kDOCbdesi$_1$	desorption of labile bound DOC onto inorganics to free DOC	0.1	9.072
kDOCbdesi$_2$	desorption of semi-labile bound DOC onto inorganics to free DOC	0.01	0.9072
kDOCbdesi$_3$	desorption of refractory bound DOC onto inorganics to free DOC	0.001	0.0907
kDONbadso$_1$	adsorption of free labile DON onto organics	0.1	0.1
kDONbadso$_2$	adsorption of free semi-labile DON onto organics	0.01	0.01
kDONbadso$_3$	adsorption of free refractory DON onto organics	0.001	0.001
kDONbadsi$_1$	adsorption of free labile DON onto inorganics	0.1	0.1
kDONbadsi$_2$	adsorption of free semi-labile DON onto inorganics	0.01	0.01
kDONbadsi$_3$	adsorption of free refractory DON onto inorganics	0.001	0.001
kDONbdeso$_1$	desorption of labile bound DON onto organics to free DON	0.1	0.1
kDONbdeso$_2$	desorption of semi-labile bound DON onto organics to free DON	0.01	0.01
kDONbdeso$_3$	desorption of refractory bound DON onto organics to free DON	0.001	0.001
kDONbdesi$_1$	desorption of labile bound DON onto inorganics to free DON	0.1	0.1
kDONbdesi$_2$	desorption of semi-labile bound DON onto inorganics to free DON	0.01	0.01
kDONbdesi$_3$	desorption of refractory bound DON onto inorganics to free DON	0.001	0.001
kDOPbadso$_1$	adsorption of free labile DOP to organics	0.1	0.1
kDOPbadso$_2$	adsorption of free semi-labile DOP to organics	0.01	0.01
kDOPbadso$_3$	adsorption of free refractory DOP to organics	0.001	0.001
kDOPbadsi$_1$	adsorption of free labile DOP to inorganics	0.1	0.1

kDOPbadsi$_2$	adsorption of free semi-labile DOP to inorganics	0.01	0.01
kDOPbadsi$_3$	adsorption of free refractory DOP to inorganics	0.001	0.001
kDOPbdeso$_1$	desorption of labile bound DOP onto organics to free DOP	0.1	0.1
kDOPbdeso$_2$	desorption of semi-labile bound DOP onto organics to free DOP	0.01	0.01
kDOPbdeso$_3$	desorption of refractory bound DOP onto organics to free DOP	0.001	0.001
kDOPbdesi$_1$	desorption of labile bound DOP onto inorganics to free DOP	0.1	0.1
kDOPbdesi$_2$	desorption of semi-labile bound DOP onto inorganics to free DOP	0.01	0.01
kDOPbdesi$_3$	desorption of refractory bound DOP onto inorganics to free DOP	0.001	0.001

Appendix B: Sediment Flux Model Equations

B.1 Hydrolysis (Previous) Formulation

(a) $RHS_{TMP} = -Krx * DOMx_{1,t-1} * H_1 + KL_{12}(DOMx_{2,t-1} - DOMx_{1,t-1}) - KL_{01}(DOMx_{1,t-1} - DOMx_{0,t-1})$

(b) $DOMx_1 = DOMx_{1,t-1} + RHS_{TMP}\frac{DT}{H1}$

(c) $RHS_{TMP} = -Krx * DOMx_{2,t-1} * H_2 - KL_{12}(DOMx_{2,t-1} - DOMx_{1,t-1}) + Khx * POMx_{t-1} * H_2 - \omega_2 DOMx_{2,t-1}$

(d) $DOMx_2 = DOMx_{2,t-1} + RHS_{TMP}\frac{DT}{H2}$

(e) $RHS_{TMP} = J_{POCx} * f_{POCx} - Khx * POMx_{t-1} * H_2 - \omega_2 POMx_{t-1}$

(f) $POMx = POMx_{t-1} + RHS_{TMP}\frac{DT}{H2}$

(g) $Rx = Kx * \theta x^{T-20}$

(h) $\frac{d(H_1 C_{T1})}{dt} = \frac{K_1^2}{KL_{01}} C_{T1} + KL_{01}(f_{d0}C_{T0} - f_{d1}C_{T1}) + \omega_{12}(f_{p2}C_{T2} - f_{p1}C_{T1}) + KL_{12}(f_{d2}C_{T2} - f_{d1}C_{T1}) - \omega_2 C_{T1} + J_{T1}$

(i) $\frac{d(H_2 C_{T2})}{dt} = -K_2 C_{T2} - \omega_{12}(f_{p2}C_{T2} - f_{p1}C_{T1}) - KL_{12}(f_{d2}C_{T2} - f_{d1}C_{T1}) + \omega_2(C_{T1} - C_{T2}) + J_{T2}$

(j) $f_{di} = \frac{1}{1 + m_i \pi_i}$ where i = 1 or 2

(k) $f_{pi} = 1 - f_{di}$

(l) $KL_{01} = \frac{D_{O2}}{H_1} = \frac{SOD}{[O_2(0)]}$

(m) $KL_{12} = \frac{D_d \theta_{Dd}^{T-20}}{(H_1 + H_2)/2}$

(n) $\omega_2 = \frac{D_p \theta_{Dp}^{T-20}}{H_1 + H_2} \frac{POC_1}{POC_R} min_{eachyear}(1 - K_s S)$

Table B.1 Sediment flux model hydrolysis formulation parameters, descriptions, units and values if used as constant. Gx represents values for the three lability pools: 1 = labile, 2 = semilabile, 3 = refractory.

Term	Description	Units	Value (if constant)
RHS_{TMP}	Temporary variable for solver equations	g m^{-2} d^{-1}	--
[b]DOMx	Concentration of a DOM pool (CDOM or NCDOM)	g m^{-3}	--
$DOMx_{t-1}$	Concentration of a DOM pool (CDOM or NCDOM) at the previous time step	g m^{-3}	--
[a,c]K_1, K_2	Reaction rate for removal reaction constant in layers 2 and 2	m d^{-1}	--
[b]Krx	Remineralization rate	d^{-1}	G1 = 0.35 G2 = 0.03 G3 = 0.00
[a,c]H_1, H_2	Depth of layers 1 or 2	m	$H_1 + H_2 = 0.1$
[a,c]KL_{01}	Mass transfer coefficient between water column and layer 1	m d^{-1}	--
[a,c]KL_{12}	Mass transfer coefficient between layers 1 and 2	m d^{-1}	--
[a,c]Khx	Hydrolysis rate	d^{-1}	0.01, 1.8 x 10^{-4}, 5.0 x 10^{-6}
DT	Time step	d	0.0417
[a,c]ω_{12}	Particle mixing velocity	m d^{-1}	--
[a,c]ω_2	Sedimentation velocity	m d^{-1}	0.0025
[a,c]J_{POCx}	Depositional flux of POC into layer 2	gC m^{-2} d^{-1}	0.52 (Site R-64)
[a,c]f_{POCx}	Lability fractionation coefficient of POM	unitless	G1 = 0.65 G2 = 0.20 G3 = 0.15
[a,c]POMx	Concentration of the POM pool	g m^{-3}	--
$POMx_{t-1}$	Concentration of POM (layer 2 only) at the previous time step	g m^{-3}	--
[b]Rx	Generic reaction term	Dependent on reaction of interest	
[b]Kx	Specific reaction term	Dependent on reaction of interest	
[a,c]θx	Temperature coefficient	unitless	

[a,c]C_{T0}, C_{T1}, C_{T2}	Total concentration of non-DOM solutes in water column or layers 1 or 2	mmol m^{-3}	$\theta_{hyrdolysis}$ = 1.1-1.5 $\theta_{diffusion}$ = 1.08-1.12
[a,c]J_{T1}, J_{T2}	Source of non-DOM solutes to layer 1 or 2	mmol m^{-2} d^{-1}	--
[a,c]f_d	Dissolved fraction of total pool	unitless	G1 = 0.70 G2 = 0.05 G3 = 0.25
[a,c]f_p	Particulate fraction of total pool	unitless	G1 = 0.65 G2 = 0.20 G3 = 0.15
[a,c]m	Solids concentration	kg L^{-1}	0.36
[a,c]π	Partition coefficient	L kg^{-1}	--
[a,c]D_d, D_p	Diffusion coefficient	cm^2 d^{-1}	5.0, 0.6
[a,c]SOD	Sediment oxygen demand	mmol O_2 m^{-2} d^{-1}	--
[a,c]POC_1	Layer one POC concentration	mmol m^{-3}	--
[a,c]POC_R	Reference POC concentration	mg C g $solids^{-1}$	0.1
[a,c]Ks	Decay coefficient for benthic stress	d^{-1}	0.03
[a,c]S	Benthic stress term	d	--

[a]Brady et al. (2013) [b]Clark et al. (2017) [c]Testa et al. (2013)

B.2 Adsorption Formulation

DOM Concentration; Layer 2

(1) $$RHS_{TMP} = -Krx * DOMx_{2,t-1} * H_2 - KL_{12}\left(DOMx_{2,t-1} - DOMx_{1,t-1}\right) + Khx * POMx_{t-1} * H_2 - \omega_2 DOMx_{2,t-1} - KDOMadsx * DOMx_{t-1} * H_2$$

(2) $$DOMx_2 = DOMx_{2,t-1} + RHS_{TMP}\frac{DT}{H2}$$

POM Concentration; Layer 2

(3) $$RHS_{TMP} = J_{POCx} * f_{POCx} - Khx * POMx_{t-1} * H_2 - \omega_2 POMx_{t-1} + KDOMadsx * DOMx_{2,t-1} * H_2$$

(4) $POMx = POMx_{t-1} + RHS_{TMP}\frac{DT}{H2}$

Flux of DOM to Water Column

(5) $DOMx_{0,flux} = KL_{01}(DOMx_1 - DOMx_0) * DT$

Table B.2. New sediment flux model adsorption formulation parameters, descriptions, units and values if used as constant. x represents the three lability pools: 1 = labile, 2 = semilabile, 3 = refractory.

Term	Description	Units	Value (if constant)
KDOMadsx	Adsorption rate parameter	d^{-1}	See table A.1
$DOMx_{0,flux}$	Flux of DOM to the water column	$g\ m^{-2}\ d^{-1}$	--

B.3 Desorption Formulation

POM Concentration; Layer 2

(6) $RHS_{TMP} = J_{POCx} * f_{POCx} - Khx * POMx_{t-1} * H_2 - \omega_2 POMx_{t-1} - KPOMdesx * POMx_{t-1} * H_2 + KDOMadsx * DOMx_{2,t-1} * H_2$

(7) $POMx = POMx_{t-1} + RHS_{TMP}\frac{DT}{H2}$

DOM Concentration; Layer 2

(8) $RHS_{TMP} = -Krx * DOMx_{2,t-1} * H_2 - KL_{12}(DOMx_{2,t-1} - DOMx_{1,t-1}) + Khx * POMx_{t-1} * H_2 - \omega_2 DOMx_{2,t-1} - KDOMadsx * DOMx_{2,t-1} * H_2 + KPOMdesx * POMx_{t-1} * H_2$

(9) $DOMx_2 = DOMx_{2,t-1} + RHS_{TMP}\frac{DT}{H2}$

Table B.3. New sediment flux model desorption formulation parameters, descriptions, units and values if used as constant. x represents the three lability pools: 1 = labile, 2 = semilabile, 3 = refractory.

Term	Description	Units	Value (if constant)
KPOMdesx	Desorption rate parameter	d^{-1}	See Table A.1

B.4 Bound Formulation

DOM Concentration, Layer 1

(10) $RHS_{TMP} = -Krx * DOMx_{1.t-1} * H_1 - KDOMbadsx * DOMx_{1,t-1} * H_1 + KDOMbdesx * DOMbx_{1,t-1} * H_1 + KL_{12}(DOMx_{2,t-1} - DOMx_{1.t-1})$

(11) $DOMx_1 = DOMx_{1,t-1} + RHS_{TMP}\frac{DT}{H1}$

Bound DOM Concentration; Layer 1

(12) $RHS_{TMP} = KDOMbadsx * DOMx_{1,t-1} - KDOMbdesx * DOMbx_{1,t-1}$

(13) $DOMbx_1 = DOMbx_{1,t-1} + RHS_{TMP} * DT$

DOM Concentration; Layer 2

(14) $RHS_{TMP} = Khx * POMx_{t-1} * H_2 - Krx * DOMx_{2,t-1} * H_2 - KDOMbads * DOMx_{2,t-1} * H_2 - KDOMadsx * DOMx_{2,t-1} * H_2 + KDOMbdesx * DOMbx_{2,t-1} * H_2 + KPOMdesx * POMx_{t-1} * H_2 - KL_{12}(DOMx_{2,t-1} - DOMx_{1,t-1}) - \omega_2 * DOMx_{2,t-1}$

(15) $DOMx_2 = DOMx_{2,t-1} + RHS_{TMP}\frac{DT}{H_2}$

Bound DOM Concentration; Layer 2

(16) $RHS_{TMP} = KDOMbads * DOMx_{2,t-1} - KDOMbdesx * DOMbx_{2,t-1}$

(17) $DOMbx_2 = DOMbx_{2,t-1} + RHS_{TMP} * DT$

Table B.4. New sediment flux model bound formulation parameters, descriptions, units and values if used as constant. x represents the three lability pools: 1 = labile, 2 = semilabile, 3 = refractory.

Term	Description	Units	Value (if constant)
KDOMbadsx	Adsorption to bound pool parameter	d^{-1}	See Table A.1
KDOMbdesx	Desorption from bound pool parameter	d^{-1}	See Table A.1
DOMbx	Concentration of adsorbed DOM (CDOM or NCDOM)	$g\ m^{-3}$	--
$DOMbx_{t-1}$	Concentration of adsorbed DOM (CDOM or NCDOM) at the previous time step	$g\ m^{-3}$	--

B.5 Organic/Inorganic Formulation

DOM Concentration; Layer 1

(18) $$RHS_{TMP} = -Krx * DOMx_{1,t-1} * H_1 - KDOMoadsx * DOMx_{1,t-1} * H_1 + KDOModesx * DOMox_{1,t-1} * H_1 - KDOMiadsx * DOMx_{1,t-1} * H_1 + KDOMidesx * DOMix_{1,t-1} * H_1 + KL_{12}(DOMx_{2,t-1} - DOMx_{1,t-1})$$

(19) $$DOMx_1 = DOMx_{1,t-1} + RHS_{TMP}\frac{DT}{H_1}$$

Bound-to-Organics DOM Concentration; Layer 1

(20) $$RHS_{TMP} = -KDOModesx * DOMox_{1,t-1} + KDOMoadsx * DOMx_{1,t-1}$$

(21) $$DOMox_1 = DOMox_{1,t-1} + RHS_{TMP} * DT$$

Bound-to-Inorganics DOM Concentration; Layer 1

(22) $$RHS_{TMP} = -KDOMidesx * DOMix_{1,t-1} + KDOMiadsx * DOMx_{1,t-1}$$

(23) $$DOMix_1 = DOMix_{1,t-1} + RHS_{TMP} * DT$$

DOM Concentration; Layer 2

(24) $RHS_{TMP} = Khx * POMx_{t-1} * H_2 - Krx * DOMx_{2,t-1} * H_2 - KDOMoads * DOMx_{2,t-1} * H_2 - KDOMiadsx * DOMx_{2,t-1} * H_2 - KDOMads * DOMx_{2,t-1} * H_2 + KDOModesx * DOMox_{2,t-1} * H_2 + KDOMidesx * DOMix_{2,t-1} * H_2 + KPOMdesx * POMx_{t-1} * H_2 - KL_{12}(DOMx_{2,t-1} - DOMx_{1,t-1}) - \omega_2 * DOMx_{2,t-1}$

(25) $DOMx_2 = DOMx_{2,t-1} + RHS_{TMP}\frac{DT}{H_2}$

Bound-to-Organics DOM Concentration; Layer 2

(26) $RHS_{TMP} = -KDOModes * DOMox_{2,t-1} + KDOMoads * DOMx_{2,t-1}$

(27) $DOMox_2 = DOMox_{2,t-1} + RHS_{TMP}\frac{DT}{H_2}$

Bound-to-Inorganics DOM Concentration

(28) $RHS_{TMP} = -KDOMides * DOMix_{2,t-1} + KDOMiads * DOMx_{2,t-1}$

(29) $DOMix_2 = DOMix_{2,t-1} + RHS_{TMP}\frac{DT}{H_2}$

Table B.5. New sediment flux model organic/inorganic formulation parameters, descriptions, units and values if used as constant. x represents the three lability pools: 1 = labile, 2 = semilabile, 3 = refractory.

Term	Description	Units	Value (if constant)
KDOMoadsx	Adsorption to organics rate parameter	d^{-1}	See Table A.1
KDOMiadsx	Adsorption to inorganics rate parameter	d^{-1}	See Table A.1
KDOModesx	Desorption from organics rate parameter	d^{-1}	See Table A.1
KDOMidesx	Desorption from inorganics rate parameter	d^{-1}	See Table A.1
DOMox	Concentration of adsorbed DOM (CDOM or NCDOM) onto organic material	$g\ m^{-3}$	--
DOMix	Concentration of adsorbed DOM (CDOM or NCDOM) onto inorganic material	$g\ m^{-3}$	--

$DOMox_{t-1}$	Concentration of adsorbed DOM (CDOM or NCDOM) onto organic material at the previous time step	$g\ m^{-3}$	--
$DOMix_{t-1}$	Concentration of adsorbed DOM (CDOM or NCDOM) onto inorganic material at the previous time step	$g\ m^{-3}$	--

Appendix C: 20 Relevant Sorption Studies

Table C.1. Summary list of relevant sorption studies

Citation	Study overview	Relevance to this study
Chen, X. 2015. Modeling of Experimental Adsorption Isotherm Data. Information **6**, 14-22.	Tested three isotherm models to determine which matched experimental sorption data best.	- capacity of isotherm models (Langmuir, Freundlich, Dubinin-Radushkevich) - not directly relevant in sorption experiment process, but useful for assessing the model performance - showed validity of using Langmuir and importance of non-linear isotherms
Gu, B., Schmitt, J., Chen, Z., Llyuan, L., McCarthy, J.F. 1994. Adsorption and Desorption of Natural Organic Matter on Iron Oxide: Mechanisms and Models. Environ. Sci. Technol. **28**, 38-46.	Tested the interactions between natural organic matter and iron oxide surfaces with a NOM adsorption/desorption predictive model.	- importance of adsorption on iron - used modified Langmuir model - hysteresis coefficient for reversible/irreversible reactions - discussed adsorption mechanisms - modeling in SFM should consider sorption neither completely reversible or irreversible - attested to adsorption speed
Guggenberger, G., Kaiser, K. 2003. Dissolved organic matter in soil: challenging the paradigm of sorptive preservation. Geoderma **113**, 293-310.	Proved that sorptive stabilization while simultaneously showing the limits of sorption capacity.	- must keep limits in mind when scaling up - ask the question: does this apply to wetland soils? more flushing occurs than forest floors - great overview of the sorption processes and other ways DOM is retained, chemically/physically; all relevant studies - also ignored microbial activity/decomposer - biodegradation is so much slower than sorption - mineralization cannot be the reason that C is stored in forest soils since it's so slow - saw more available sorption sites w/ depth - higher ads capacity - capacity may increase by less ads happens w/ depth in Taskinas
Kaiser, K., Guggenberger, G. 2000. The role of DOM sorption to mineral surfaces in the preservation of organic matter in soils. Organic Chemistry **31**,711-725.	Proved that sorption was an important process in preserving OM in soils.	- relationship with DOM sorption and Al and Fe oxyhydroxides - not very reversible once DOM is sorbed to those minerals - important for modeling reactions rates (des could be much smaller) - usefulness of initial mass approach (Nodvin et al 1986) for samples with native OM to desorb - use of DRIFT spectroscopy - strong preference (as in other studies) to hydrophobic sorption, and

		hydrophilic (more labile) more likely to desorb - Fe and Al control DOM sorption (consistent with all studies)
Kaiser, K., Guggenberger, G. 2003. Mineral surfaces and soil organic matter. Eur. J. Soil Sci. **54**, 219-236.	Showed relationship between surface area and organic matter in mineral surfaces.	- importance of mineral soils to increasing adsorption - relationship with SSA - as adsorption occurs, SSA decreases - similar to other studies that coin the term "masking" the SSA w/ adsorption - adsorption and accumulation not limitless - SSA plays a huge role - mechanisms of sorption - saw an exchange; sorption of added OM and release of native OM - attested to the difficulty of desorption from iron oxides - suggested that OM modifies SSA of soils - agreed that adsorption could lead to stabilization of OM
Kaiser, K., Kaupenjohann, M., Zech W. 2001. Sorption of dissolved organic carbon in soils: effects of soil sample storage, soil-to-solution ratio, and temperature. Geoderma **99,** 317–328.	Compared how different experiment conditions affected DOC sorption.	- implications of freeze drying the soil - explanation for soil changing properties once DOC sorbs - "predominant portion of the released DOC was in the hydrophilic fraction" - same as other studies
Kaiser, K., Zech, W. 1998. Rates Of Dissolved Organic Matter Release And Sorption In Forest Soils. Soil Science **163**, 714-725.	Performed experiments for time-dependent DOM release and sorption on four forest soils for 24 hours.	- "properties controlling sorption are the content of organic carbon (OC), Al and Fe hydrous oxides, and clay minerals such as kaolinite" - the speed is the same as this study - mineral oxides also important in kinetics - various equations - also saw increase in [DOC] = increase in retention
Keil, R.G., Montlucon, D.B., Prahl, F.G., Hedges, J.I. 1994. Sorptive preservation of labile organic matter in marine sediments. Nature **370**, 549– 552.	Showed the effect that sorption to mineral surfaces might have in controlling either the lability or quantity of organic matter in the marine sedimentary record.	- anaerobic sediment analysis - study not focused on forest soils like so many others - importance of mineral surface area for sorption - limits extent of OM preservation - tested desorption - sorption of this OM leads to a stabilization of more labile material - degradation of desorbed material was 5 orders of mag faster than OM in the same section
Kothawala, D.N., Moore, T.R. 2009. Adsorption of dissolved nitrogen by forest mineral soils. Can. J. For. Res. **39**, 2381-2390.	Performed batch experiments to study which soil properties affect DON adsorption.	- soil characteristics that impact DOM sorption - similar methods, [DOC] = 200 mg/L - also used linear IM isotherm as other studies

		- importance of mineral oxides in adsorption (Fe and Al)
Kothawala, D.N., Moore, T.R., Hendershot, W.H. 2008. Adsorption of dissolved organic carbon to mineral soils: A comparison of four isotherm approaches. Geoderma **148**, 43-50.	Compared the theoretical limitations and modeling accuracy of four isotherm approaches to describe DOC partitioning to soil surfaces.	- description of four different ways to look at calculating sorption - which is best, most reliable, **equations** - Pinsonneault et al. followed methodology
Kothawala, D.N., Roehm, C., Blodau, C., Moore, T.R. 2012 Selective adsorption of dissolved organic matter to mineral soils. Geoderma **189-190**, 334-342.	Showed adsorption of DOC to forest soils, looking at concentration, molecular, and structural changes using fluorescence index, SUVA, high performance size exclusion chromatography (HPSEC), and Fourier transform infrared (FTIR) spectrophotometry.	- Langmuir equations, solving for Qmax/desorption potential - very similar methods as isotherms - uses optics also to look at internal changes - selective adsorption of aromatic compounds may be similar to results of adsorption of stock solution used in this study - addressed increase in adsorption capacity - preferential loss of DOC functional groups - importance of Fe in adsorption and overall retention
Lilienfein, J., Qualls, R.G., Uselman, S.M., Bridgham, S.D. 2004. Adsorption of Dissolved Organic Carbon and Nitrogen in Soils of a Weathering Chronosequence. Soil Sci. Soc. Am. J. **68**, 292-305.	Demonstrated which soil characteristics regulated DOC & DON adsorption.	- spatial variability w/ depth (0-10, 10-20, 30-40, 70-80, 140-150cm depths) - modified Langmuir isotherms - importance of adsorption site (Allophane is a aluminosilicate; "allophanic soils are known to accumulate organic matter rapidly...large surface area and positive surgace charge...adsorption of organic matter to allophane surfaces is probably by ligand exchange") - decreased adsorption w/ depth - what is seen in spatial
McKnight, D.M., Bencala, K.E., Zellweger, G.W., Aiken, G.R., Feder, G.L., Thorn, K.A. 1992. Sorption of Dissolved Organic Carbon at the Confluence of Deer Creek with the Snake River, Summit County, Colorado. Environ. Sci. Technol. **26**, 1388-1396.	Performed a freshwater study on DOC adsorption onto Fe and Al.	- [DOC] had more effect than Al and Fe precipitation, but importance of mineral oxides still abundantly clear - ligand exchange-surface complexation - did not see exactly the same as other studies - no dominance in hydrophobic preference for sorption - considered sorption to be quick
Pinsonneault, A.J., Megonigal, J.P., Neale, P.J., Tzortziou, M., Canuel, E.A., Pondell, C.R., Morrissette, H.K. Dissolved Organic Carbon Sorption Dynamics in Tidal Marsh Soils. 2021. Limnol. Oceanogr.	Compared adsorption/desorption isotherms between four different marsh soils, testing [DOC], mineralogy, and salinity.	- same methods/materials - provides part motivation for this study - importance of sorption, marsh characteristics, salinity, [DOC]i, Fe & Al oxides - experiments w/o soil showed no precipitation

		- first of these studies in tidal wetland environments - called for the importance of resolving spatial variability
Qualls, R. 2000. Comparison of the behavior of soluble organic and inorganic nutrients in forest soils. Forest Ecol. Managem. **138**, 29-50.	Performed encompassing experiments to build a conceptual model of all pools/processes affecting DOM.	- descriptive diagram of all DOM processes and pools in forest soils - similar methods; 30 mL DOC stock (3 or 5 diff concentrations) to 1 g soil - suppressed microbial activity (mercuric chloride) - also performed exp to determine precipitation and if HgCl2 affected DOC (no to both) - desorbable pool experiments (with and without microbial activity) - tested adsorption of OM on organic substrates and mineral soils - useful for 4th SFM formulation - attested to kinetic speed w/ sorption - importance of metal oxides for DOM retention
Qualls, R.G., Richardson, C.T. 2003 Factors Controlling Concentration, Export, and Decomposition of Dissolved Organic Nutrients in the Everglades of Florida. Biogeochemistry **62**, 197-229.	Detailed the most important aspects of the origin and fate of DOM & the processes controlling concentration/export.	- showed the importance of abiotic processes, microbial degradation slow - desorption series - overview of marsh DOM processes - complex - Figure 1, 9, 10 - explained isotherm incubations - presented idea of sorption as a buffer to regulate concentration - useful for SFM model analysis
Shaker, A.M., Komy, Z.R., Heggy, S.E.M., El-Sayed, M.E.A. 2012. Kinetic Study for Adsorption Humic Acid on Soil Minerals. J. Phys. Chem. **116**, 10889-10896.	Showed the kinetics of humic acid adsorption on two types of soil.	- one of just a few kinetic studies - more than one type of soil - very high concentrations tested - found adsorption capacity/saturation - tested until equilibrium - humic materials
Shields, M.R., Bianchi, T.S., Gelinas, Y., Allison, M.A., Twilley, R.R. 2016. Enhanced terrestrial carbon preservation promoted by reactive iron in deltaic sediments. Geophys. Res. Lett. **43**, 1149-1157.	Showed how iron affects OC preservation in Mississippi River Delta sediments.	- importance of iron relative to sorption of organic carbon - also freeze-dried sediments - relevance of age, differences in sediment characteristics - looked at depth (aka age) - redox important
Tavakkoli, E., Derrien, M., Rengasamy, P., McDonald, G. 2014. Adsorption of dissolved organic carbon to carbonate minerals and alkaline soils.	Showed effects of varying pH levels in soil on DOC adsorption.	- DOC adsorption increased with lower pH (kinetic soils were more acidic than alkaline) - agreed that adsorption is rapid relative to microbial decomposition and huge control on DOC retention in mineral soils - DOC sorption can be reversible; management implications

Wagai, R., Mayer, L.M. 2007. Sorptive stabilization of organic matter in soils by hydrous iron oxides. Geochim. Cosmochim. Acta **71**, 25-35.	Tested stabilization through sorption of OM to iron oxides.	- importance of iron relative to sorption of organic matter - different from other studies; showing that sorption play a role but other process were at play for OM preservation

Appendix D: Scenario Description

Table D.1. Experimental scenarios, IDs, and descriptions.

Scenario	ID	Description
1	JBHF	Jug Bay, high initial [DOC], low salinity, 0-40 cm homogenized sample
2	JBHS	Jug Bay, high initial [DOC], high salinity, 0-40 cm homogenized sample
3	JBLF	Jug Bay, low initial [DOC], low salinity, 0-40 cm homogenized sample
4	JBLS	Jug Bay, low initial [DOC], high salinity, 0-40 cm homogenized sample
5	TAHF	Taskinas, high initial [DOC], low salinity, 0-40 cm homogenized sample
6	TAHS	Taskinas, high initial [DOC], high salinity, 0-40 cm homogenized sample
7	TALF	Taskinas, low initial [DOC], low salinity, 0-40 cm homogenized sample
8	TALS	Taskinas, low initial [DOC], high salinity, 0-40 cm homogenized sample
9	WCHF	Taskinas, high initial [DOC], low salinity, 0-5 cm creek edge sample
10	WCHS	Taskinas, high initial [DOC], high salinity, 0-5 cm creek edge sample
11	WCLF	Taskinas, low initial [DOC], low salinity, 0-5 cm creek edge sample
12	WCLS	Taskinas, low initial [DOC], high salinity, 0-5 cm creek edge sample
13	WIHF	Taskinas, high initial [DOC], low salinity, 0-5 cm intermediate marsh sample
14	WIHS	Taskinas, high initial [DOC], high salinity, 0-5 cm intermediate marsh sample

15	WILF	Taskinas, low initial [DOC], low salinity, 0-5 cm intermediate marsh sample
16	WILS	Taskinas, low initial [DOC], high salinity, 0-5 cm intermediate marsh sample
17	WMHF	Taskinas, high initial [DOC], low salinity, 0-5 cm high marsh sample
18	WMHS	Taskinas, high initial [DOC], high salinity, 0-5 cm high marsh sample
19	WMLF	Taskinas, low initial [DOC], low salinity, 0-5 cm high marsh sample
20	WMLS	Taskinas, low initial [DOC], high salinity, 0-5 cm high marsh sample
21	WCHF	Taskinas, high initial [DOC], low salinity, 30-40 cm creek edge sample
22	WCHS	Taskinas, high initial [DOC], high salinity, 30-40 cm creek edge sample
23	WCLF	Taskinas, low initial [DOC], low salinity, 30-40 cm creek edge sample
24	WCLS	Taskinas, low initial [DOC], high salinity, 30-40 cm creek edge sample
25	WIHF	Taskinas, high initial [DOC], low salinity, 30-40 cm intermediate marsh sample
26	WIHS	Taskinas, high initial [DOC], high salinity, 30-40 cm intermediate marsh sample
27	WILF	Taskinas, low initial [DOC], low salinity, 30-40 cm intermediate marsh sample
28	WILS	Taskinas, low initial [DOC], high salinity, 30-40 cm intermediate marsh sample
29	WMHF	Taskinas, high initial [DOC], low salinity, 30-40 cm high marsh sample
30	WMHS	Taskinas, high initial [DOC], high salinity, 30-40 cm high marsh sample
31	WMLF	Taskinas, low initial [DOC], low salinity, 30-40 cm high marsh sample

32	WMLS	Taskinas, low initial [DOC], high salinity, 30-40 cm high marsh sample

Appendix E: Initial Values

Table E.1. Cs_{t0} & $DOCw_{t0}$ initial values for the analytical solution (C t_0 values) by scenario for all three model formulations, plus Q_{max} for the Langmuir model.

Scenario	**Cs_{t0} (mg)**	**$DOCw_{t0}$ (mg)**	**Q_{max} (mg)**
Description	Concentration of OC on sediment	Concentration of DOC in solution	Maximum sorption capacity
JBHF	4.284	8.867	5.967
JBHS	4.500	8.385	12.500
JBLF	4.242	0.077	5.909
JBLS	4.500	0.105	12.500
TAHF	2.030	8.780	2.254
TAHS	1.930	8.413	10.800
TALF	2.030	0.122	2.254
TALS	1.969	0.124	11.016
WCHF	1.015	3.003	1.127
WCHS	0.939	2.955	5.256
WCLF	0.995	0.042	1.105
WCLS	0.933	0.072	5.220
WIHF	1.048	3.103	1.164
WIHS	0.984	2.955	5.508
WILF	1.022	0.069	1.134
WILS	0.952	0.084	5.328
WMHF	0.968	3.003	1.076
WMHS	0.971	2.955	5.436
WMLF	1.002	0.042	1.112
WMLS	0.991	0.072	5.544

PCHF	0.982	3.038	1.090
PCHS	0.920	3.125	5.148
PCLF	0.995	0.101	1.105
PCLS	0.920	0.086	5.148
PIHF	0.988	3.103	1.098
PIHS	0.933	2.955	5.220
PILF	0.988	0.069	1.098
PILS	0.971	0.084	5.436
PMHF	0.962	3.003	1.068
PMHS	0.926	2.955	5.184
PMLF	0.982	0.042	1.090
PMLS	0.939	0.072	5.256

Appendix F: Model Rates

Table F.1. Optimized Linear, Langmuir, and Time-Dependent model rates. Linear and Langmuir outputs are using the reduced data sets, and Time-Dependent outputs are using the full data sets (with peaks).

	Linear (hr $^{-1}$)		**Langmuir (hr $^{-1}$)**		**Time-Dependent (hr $^{-1}$)**		
Scenario	kdes	kads	kdes	kads ($kads_2$*Q_{max})	kdes _max	kdes _min	kads
JBHF	0.383	0.925	0.527	4.520	51.25	28.62	20.88
JBLF					5.07	4.85	17.58
JBHS	1.107	0.927	2.43	11.703	12.86	8.01	13.21
JBLS					4.73	4.80	17.69
TAHF	-0.001	-0.010	1.841	1.176	6.64	0.44	0.08
TALF					15.49	14.38	8.18
TAHS	0.688	1.957	0.969	0.750	2.43	1.06	0.57
TALS					9.03	5.40	5.75
WCHF	0.269	1.016	0.992	6.501	39.48	1.50	0.71
WCLF					69.80	39.67	65.44
WCHS	0.902	0.841	0.361	0.790	41.26	1.18	1.26
WCLS					868.96	4.93	10.10
WIHF	-0.020	0.298	0.665	0.285	1.14	0.29	0.04
WILF					2.40	0.35	0.20
WIHS	1.364	3.833	2.544	1.076	0.79	1.66	0.90
WILS					6.69	9.44	14.16
WMHF	-0.010	0.227	12.456	4.183	124.61	56.40	7.51
WMLF					402.11	18.82	6.85

WMHS	0.620	2.534	0.851	0.500	9.12	2.21	0.92
WMLS					20.35	8.55	7.65
PCHF	-577.48	3417.05	1.000	1.091	50.00	2.81	0.16
PCLF					7.10	10.59	8.07
PCHS	0.228	1.809	0.502	0.235	1.80	7.46	2.35
PCLS					17.87	25.79	31.72
PIHF	-0.782	12.564	2.200	18.311	2.99	3.18	0.55
PILF					11.54	14.59	14.15
PIHS	0.465	2.149	0.309	0.211	23.54	18.62	8.64
PILS					18.19	22.73	41.30
PMHF	-5.526	39.390	65.475	11.694	130.11	238.13	23.32
PMLF					25.78	55.70	23.55
PMHS	0.673	2.939	0.765	0.385	0.61	0.00	0.01
PMLS					16.14	25.85	24.64

Appendix G: Statistics

Table G.1. Ranked RMSE outputs for each model, lowest to highest values. Linear and Langmuir outputs are using the reduced data sets, and Time-Dependent outputs are combined H & L values using the full data sets (with peaks).

Analytical/Linear		**Langmuir**		**Time-Dependent**	
Scenario	RMSE	Scenario	RMSE	Scenario	RMSE
PIS	0.1296	WMS	0.103	PIS	0.0508
WIS	0.1316	PMS	0.1136	WIS	0.0520
WCS	0.1363	PCS	0.1209	PIF	0.0560
WCF	0.1862	WIS	0.1230	WIF	0.0693
PCS	0.2374	WMF	0.1255	PMS	0.0709
PMS	0.2627	WIF	0.1292	PMF	0.0907
WMS	0.2641	JBS	0.1552	WMF	0.1092
JBF	0.3192	PIS	0.1571	WMS	0.1177
TAS	0.3706	PMF	0.1648	PCS	0.1200
PIF	0.3967	TAF	0.2056	JBS	0.1837
WIF	0.4716	TAS	0.2139	JBF	0.2521
PCF	0.5578	WCF	0.2183	PCF	0.2636
WMF	0.5765	WCS	0.2957	TAS	0.2715
PMF	0.5785	JBF	0.3398	TAF	0.2860
TAF	0.9532	PIF	0.3478	WCF	0.6853
JBS	1.3656	PCF	0.4119	WCS	0.7212

Appendix H: Analytical Fitting Process

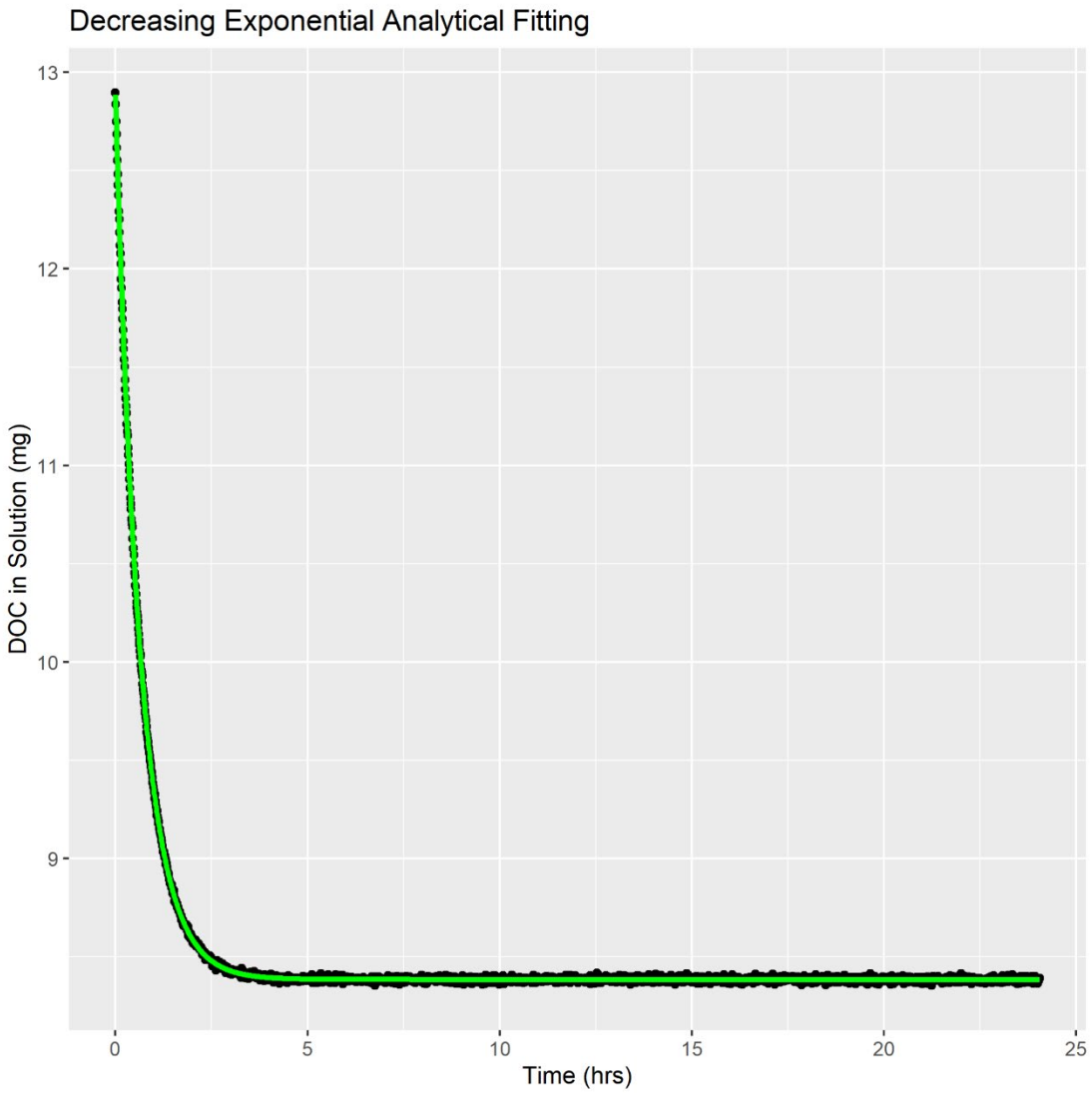

Figure H.1. Analytical fitting (green line) to a decreasing exponential set of data (black points).

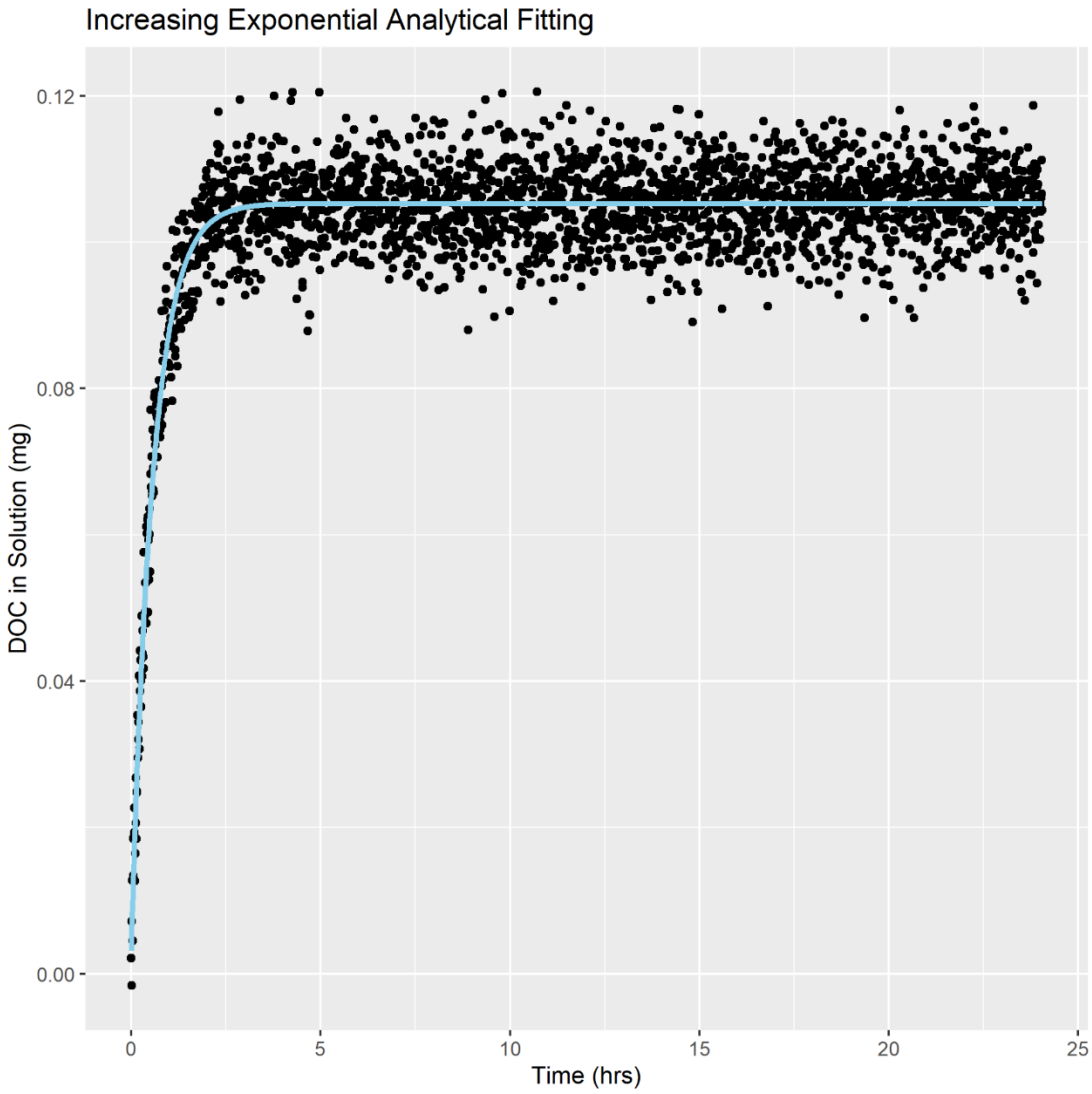

Figure H.2. Analytical fitting (blue line) to an increasing saturation set of data (black points).

Appendix I: Linear Model (Analytical) Fits

Figures I.1-7 show the remaining *Linear* model fits for all other experiments. Points are the observed DOC mass over time, and the dashed lines are the corresponding model outputs. The two panels are a) fresh or b) saline initial conditions, and the colors represent either high [DOC] (pink) or low [DOC] (red) initial conditions.

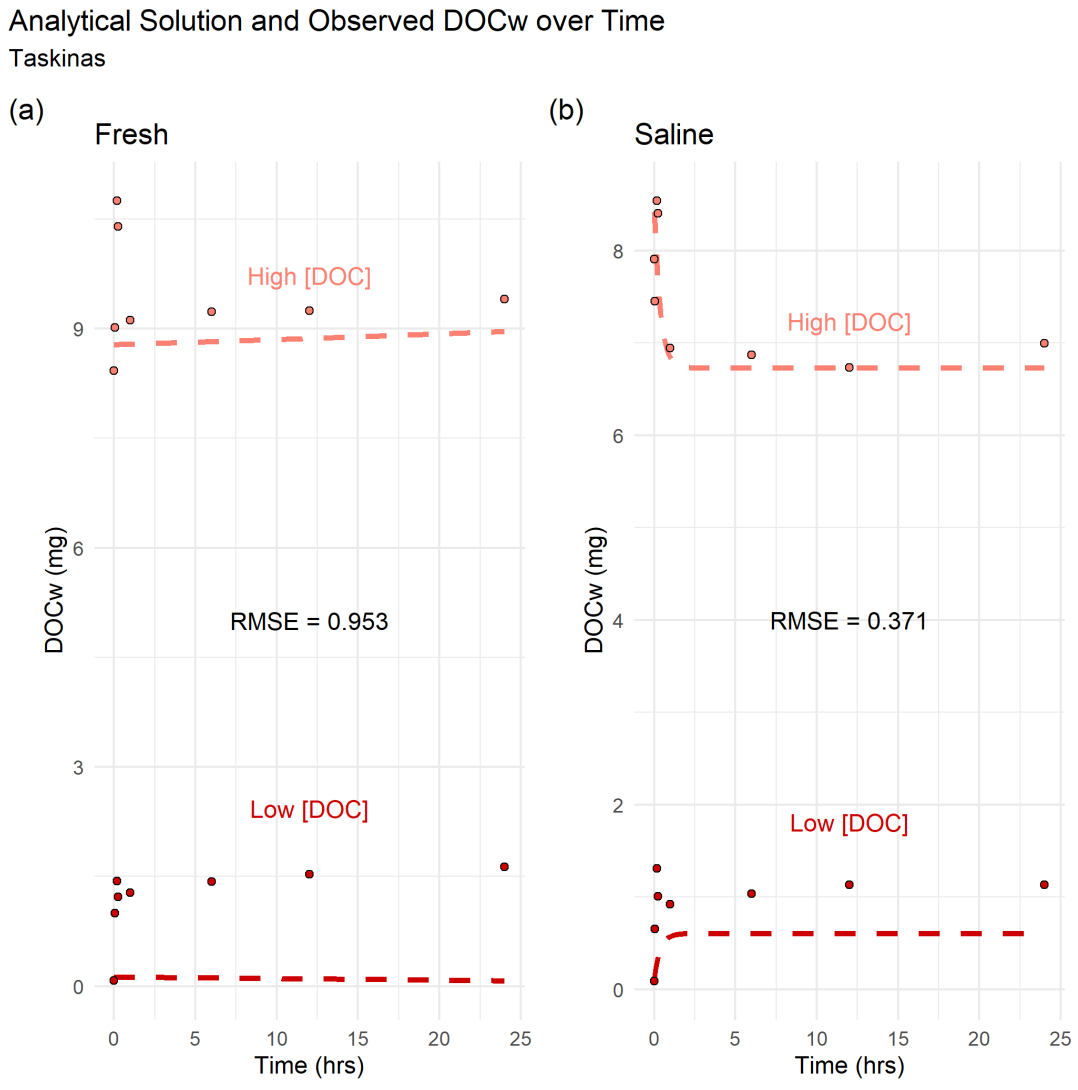

Figure I.1. Taskinas Creek, bulk kinetic experiments.

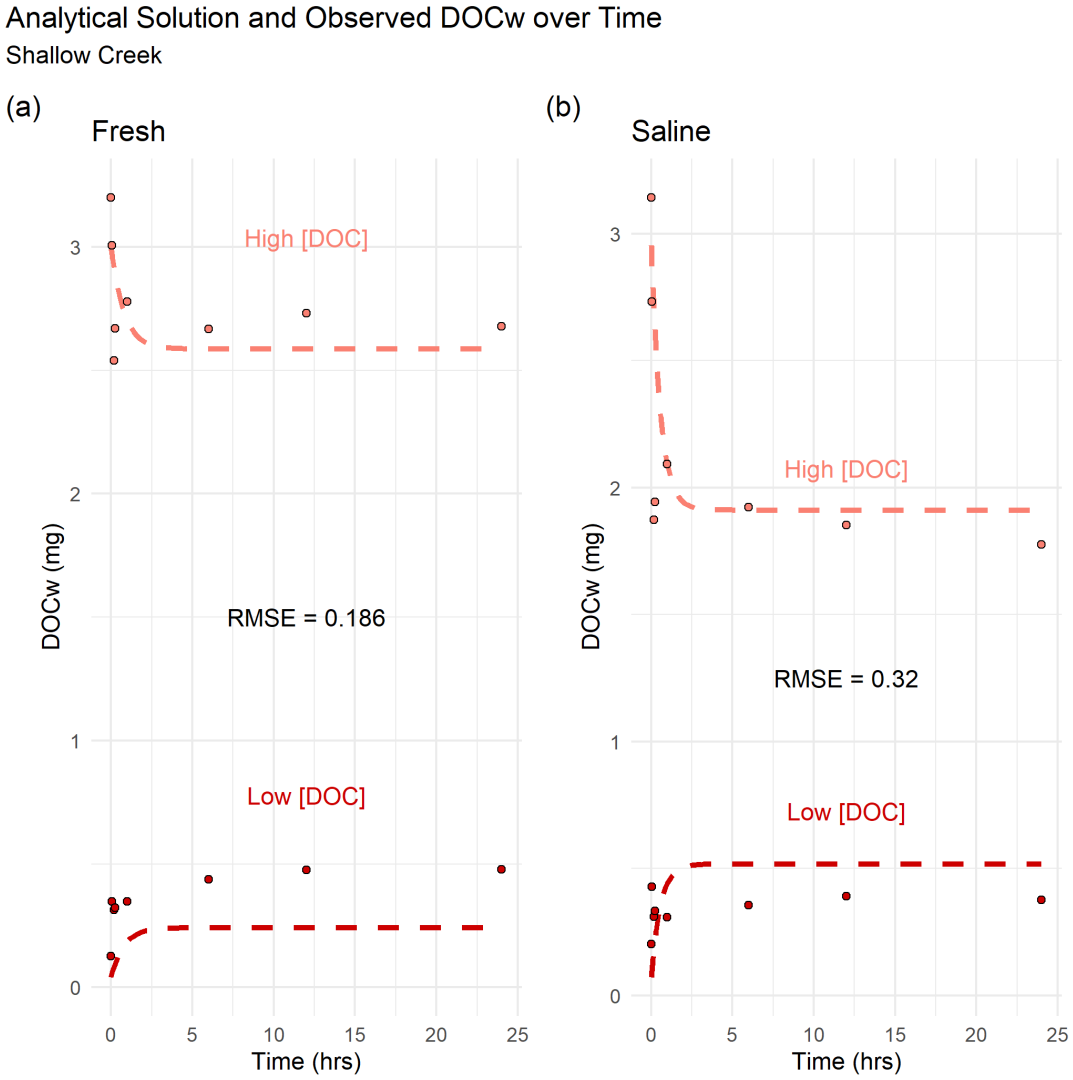

Figure I.2. Shallow Creek Edge, spatial experiments.

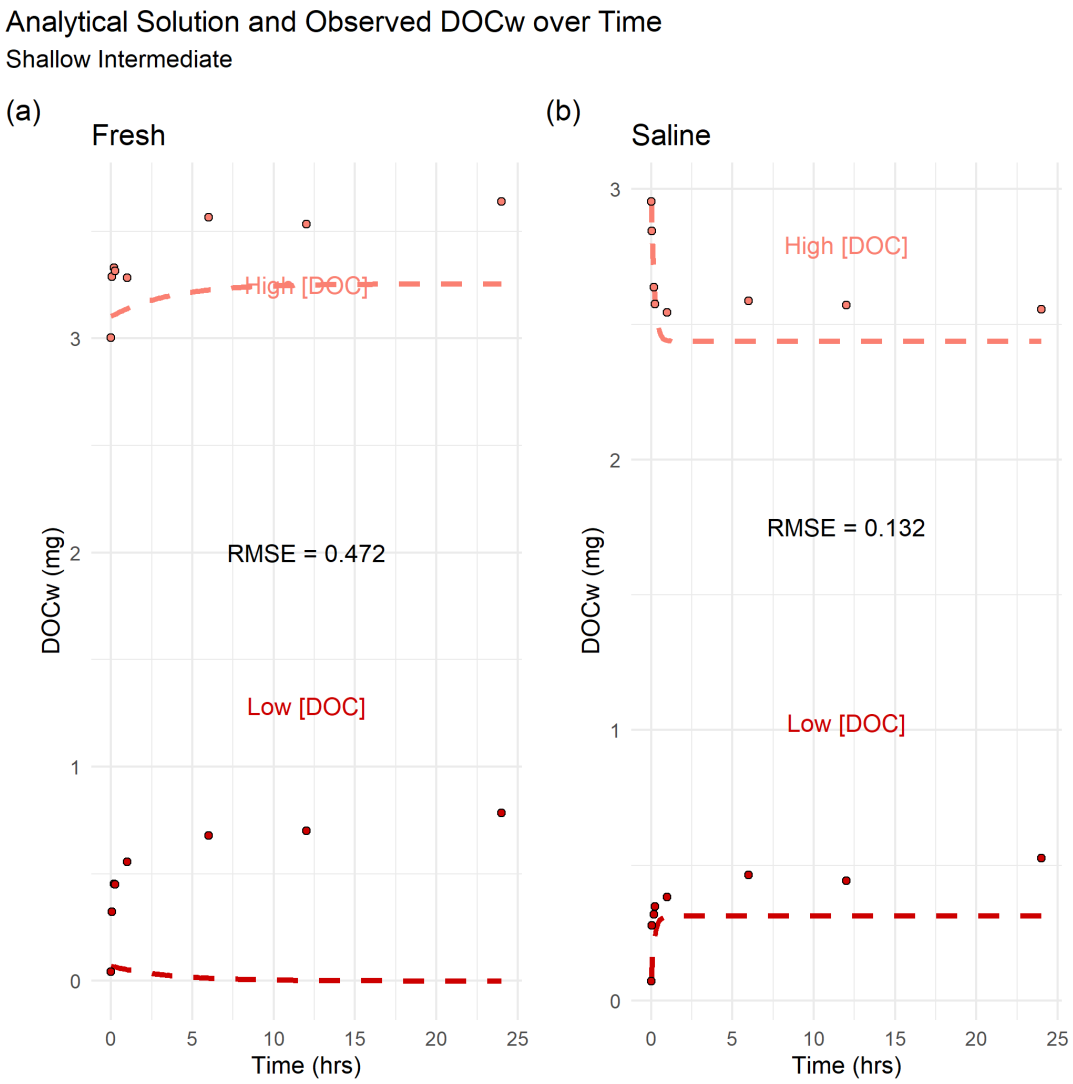

Figure I.3. Shallow Intermediate Plot, spatial experiments.

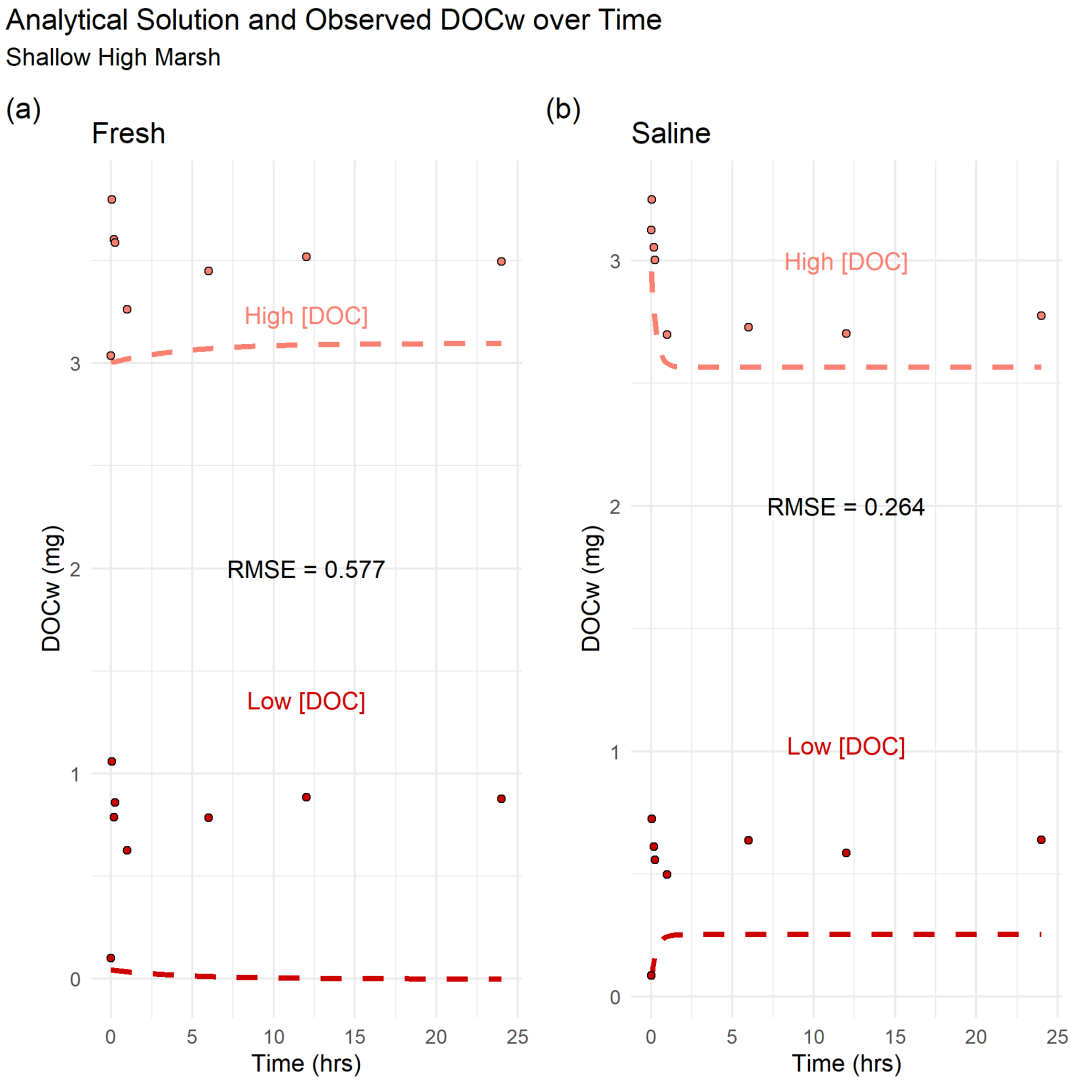

Figure I.4. Shallow High Marsh, spatial experiments.

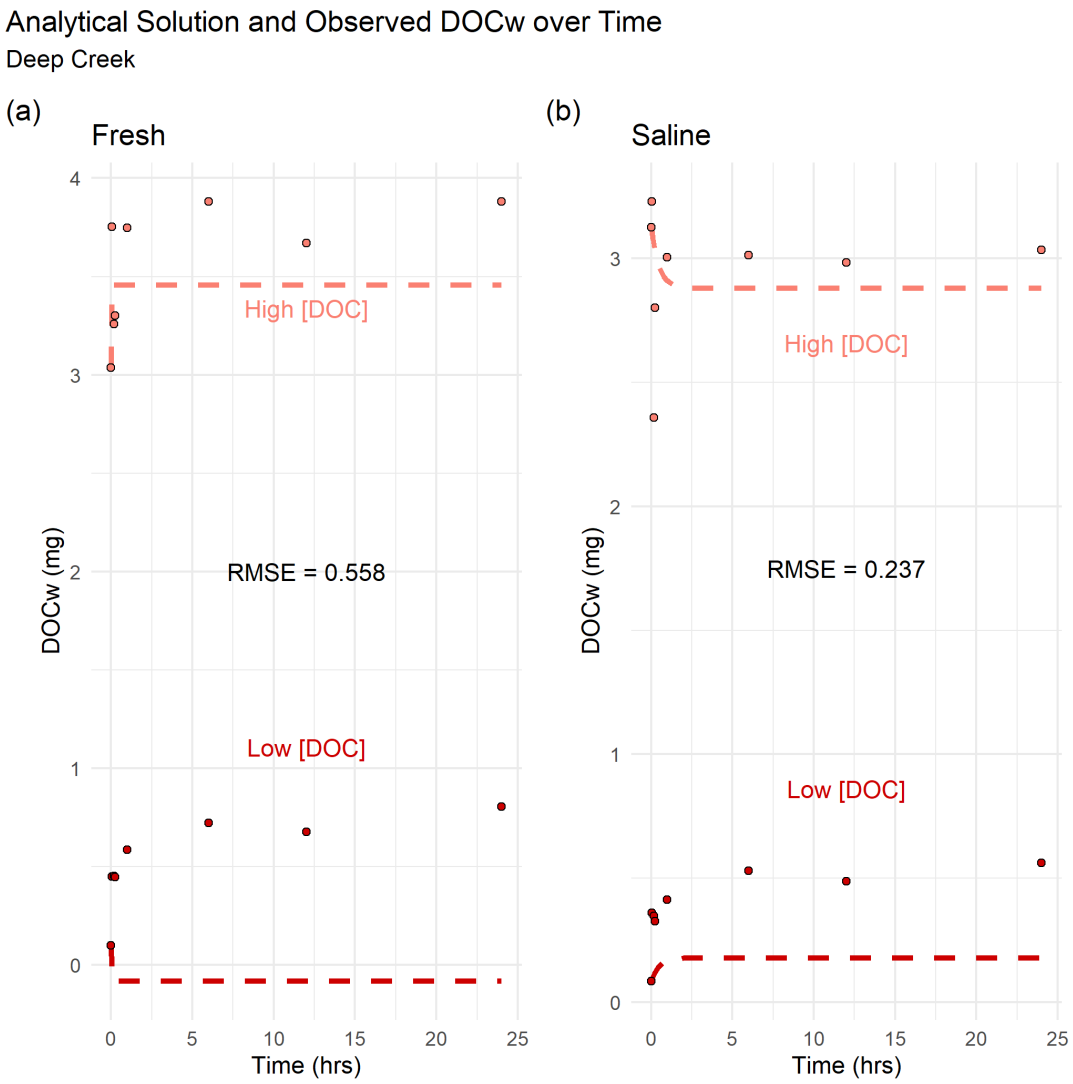

Figure I.5. Deep Creek Edge, spatial experiments.

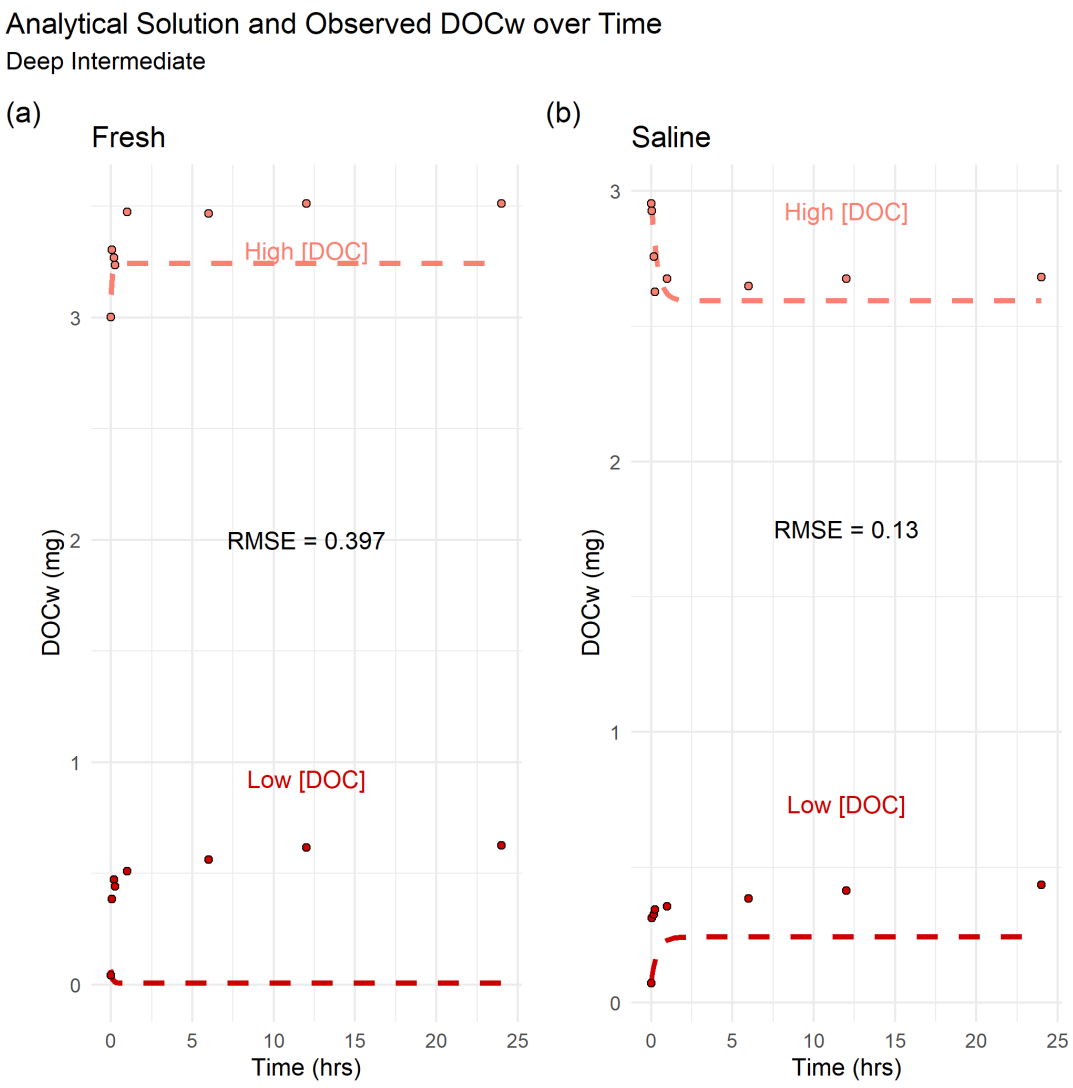

Figure I.6. Deep Intermediate Plot, spatial experiments.

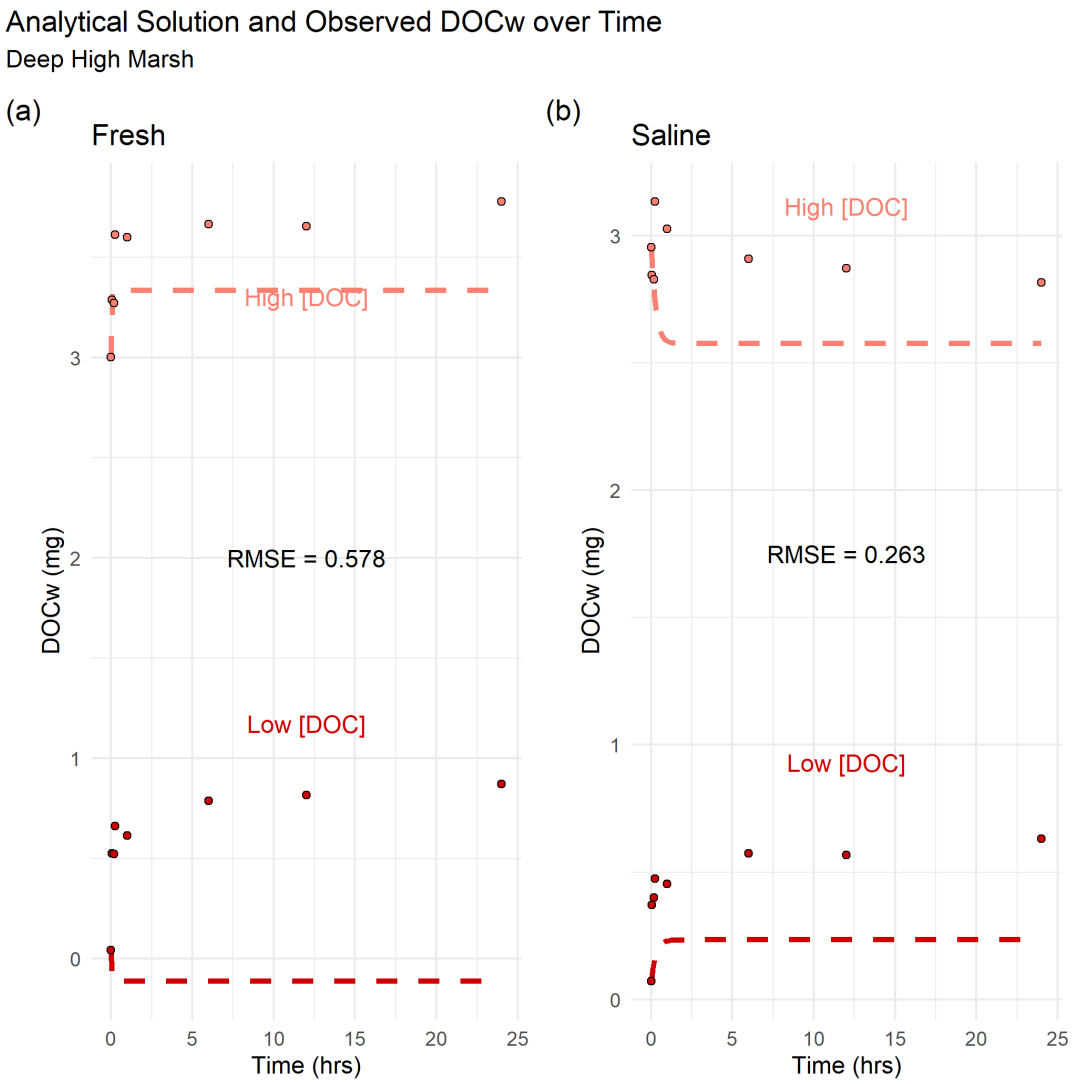

Figure I.7. Deep High Marsh Plot, spatial experiments.

Appendix J: Langmuir Model Fits

Figures J.1-7 show the remaining *Langmuir* model fits for all other experiments. Points are the observed DOC mass over time, and the solid lines are the corresponding model outputs. The two panels are a) fresh or b) saline initial conditions, and the colors represent either high [DOC] (light green) or low [DOC] (dark green) initial conditions.

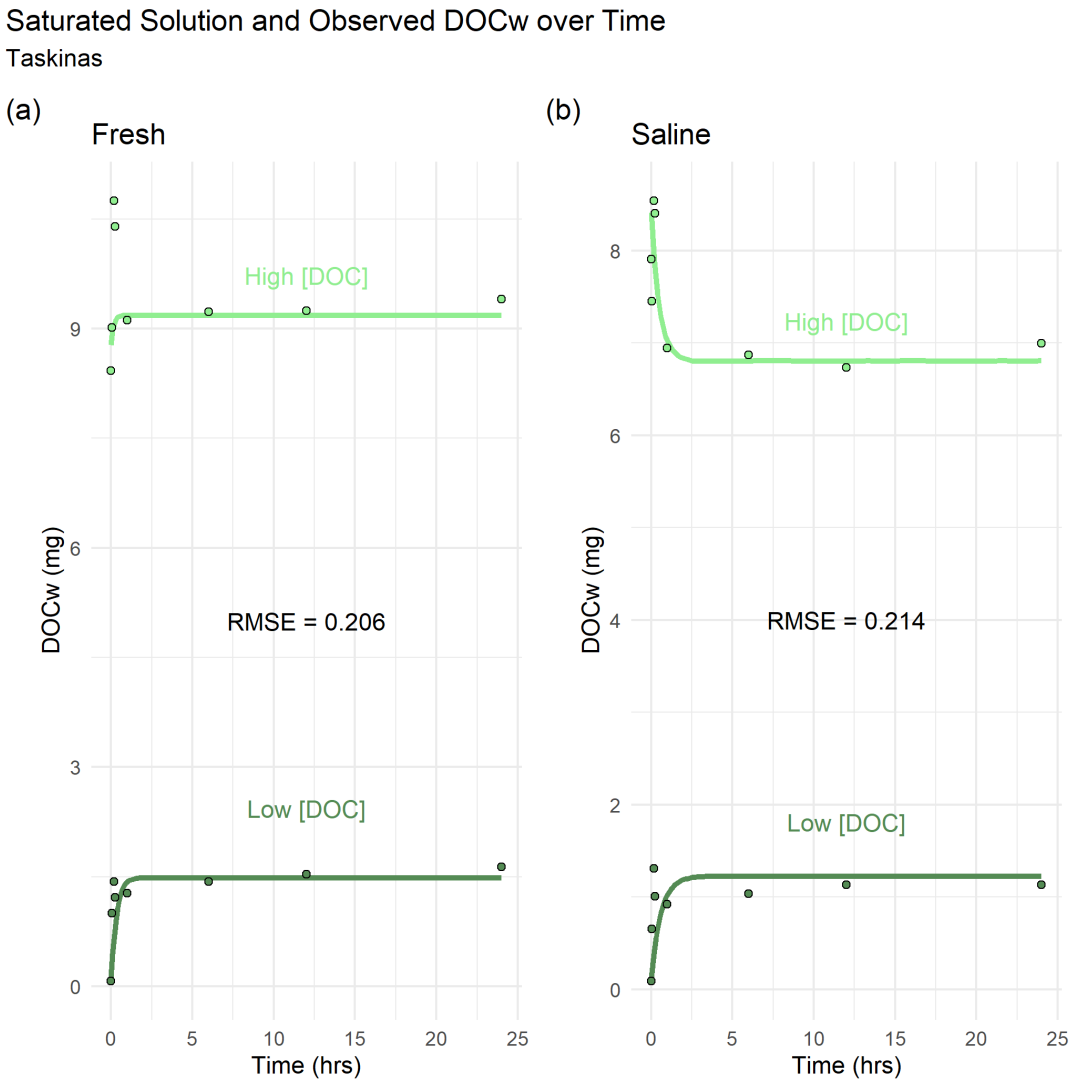

Figure J.1. Taskinas Creek, bulk kinetic experiments.

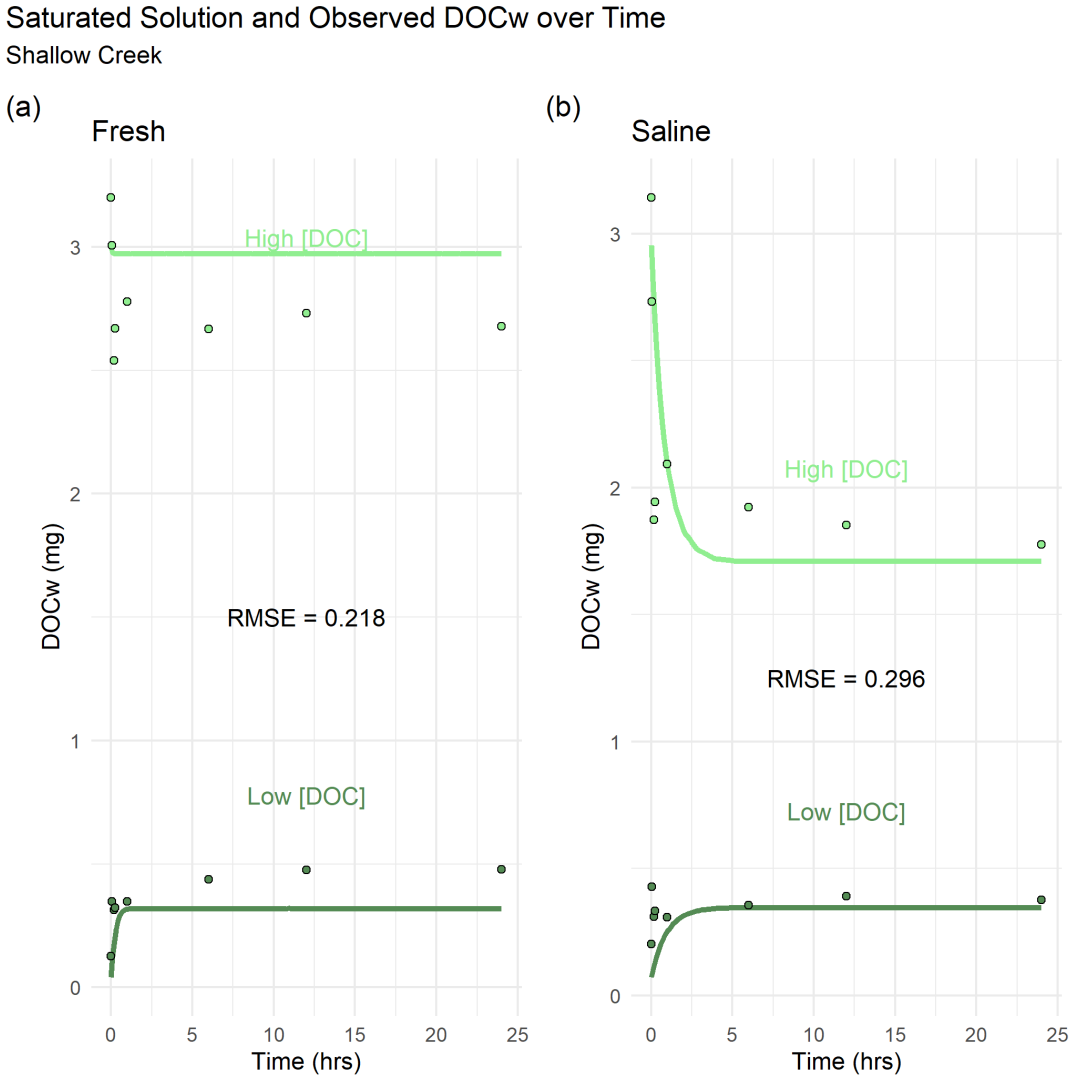

Figure J.2. Shallow Creek Edge, spatial experiments.

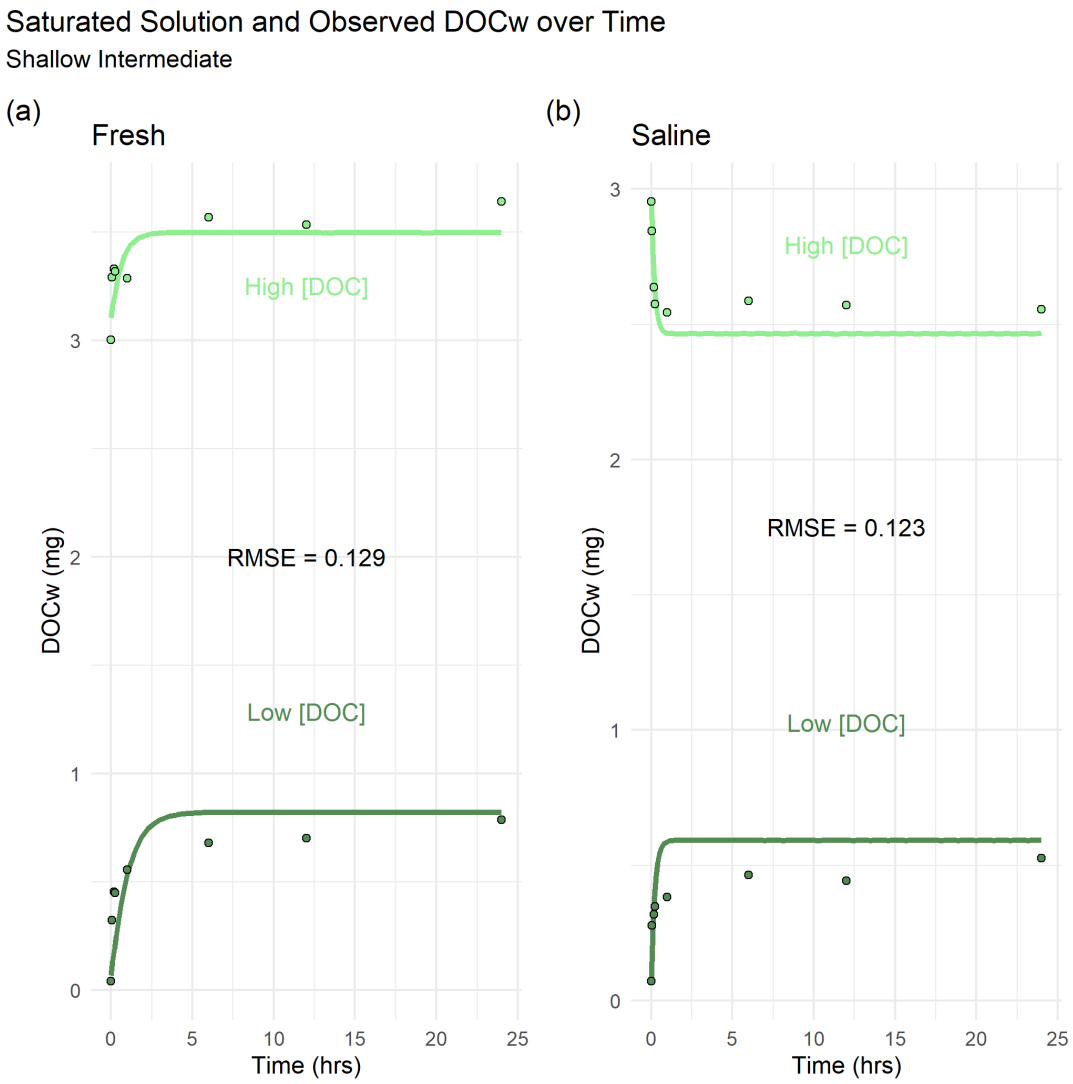

Figure J.3. Shallow Intermediate Plot, spatial experiment.

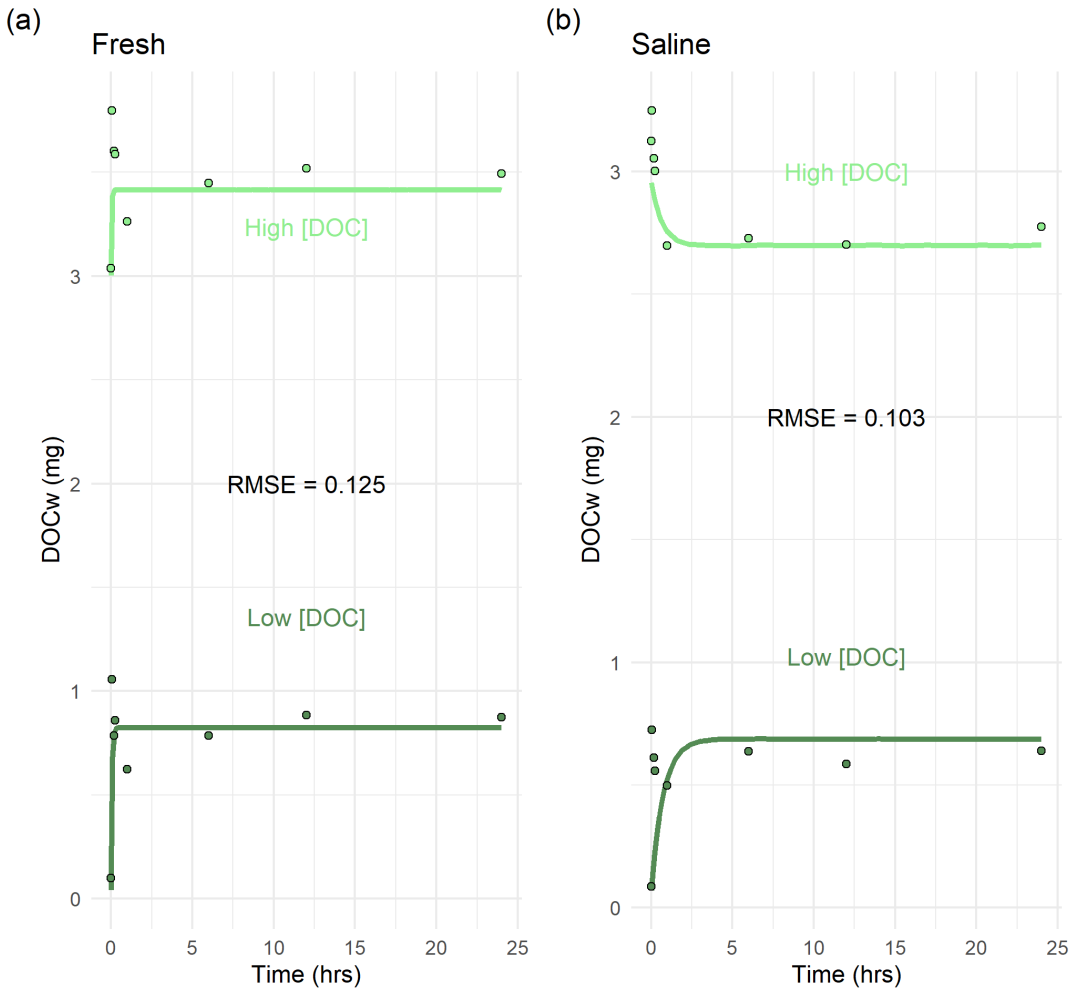

Figure J.4. Shallow High Marsh, spatial experiments.

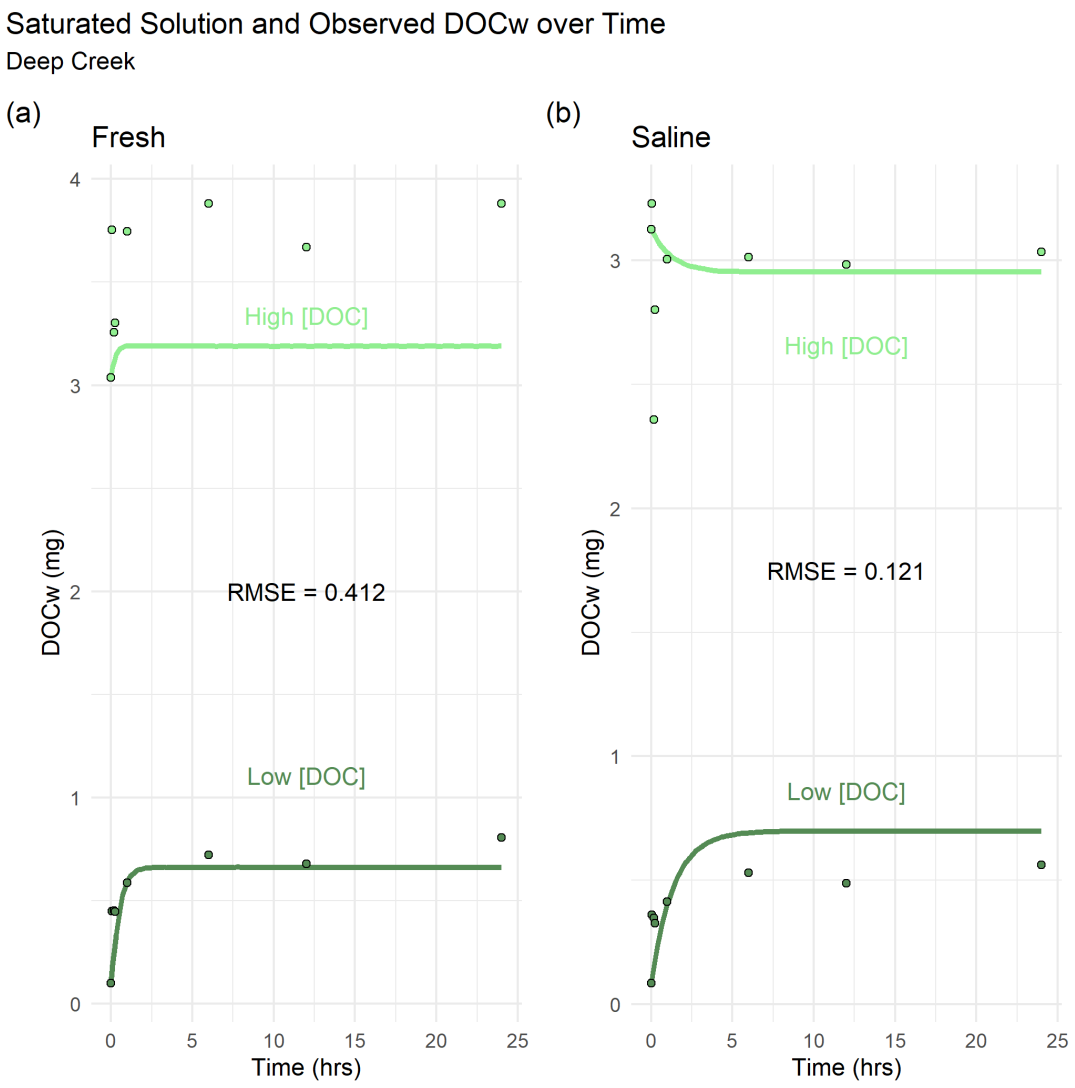

Figure J.5. Deep Creek Edge, spatial experiments.

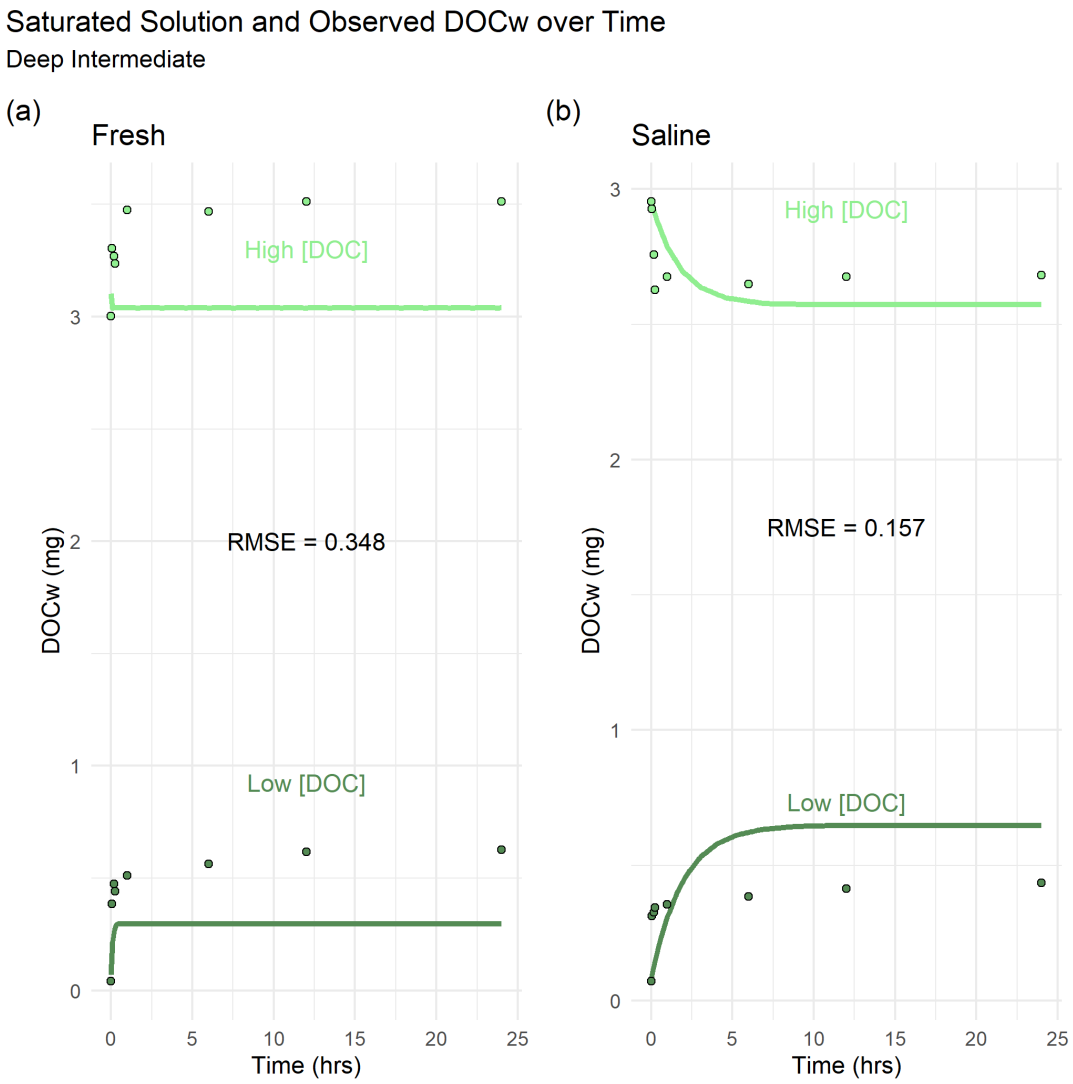

Figure J.6. Deep Intermediate Plot, spatial experiments.

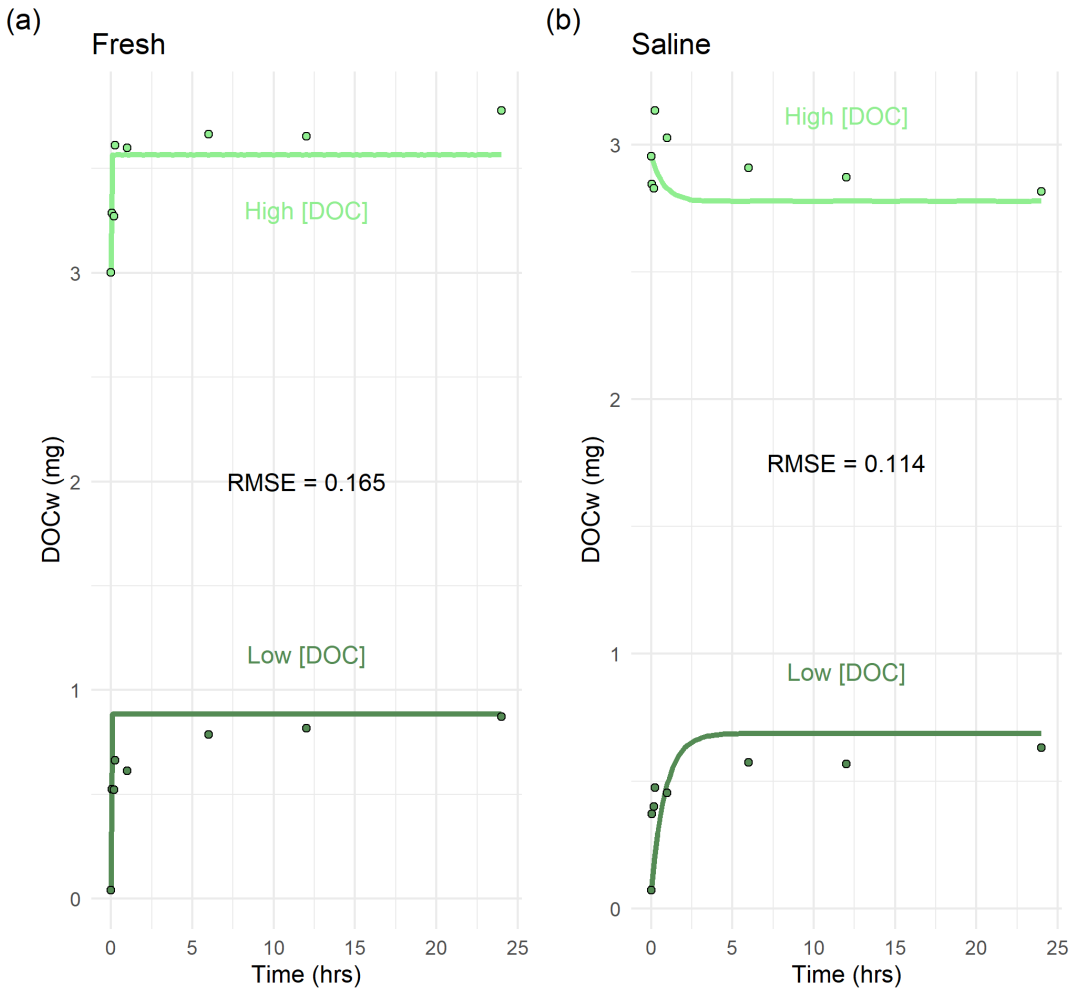

Figure J.7. Deep High Marsh, spatial experiments.

Appendix K: Time-Dependent Model Fits

Figures K.1-7 show the remaining *Time-Dependent* model fits for all other experiments. Points are the observed DOC mass over time, and the dashed lines are the corresponding model outputs. The four panels are the four sets of initial conditions: a) HF; b) HS; c) LF; d) LS.

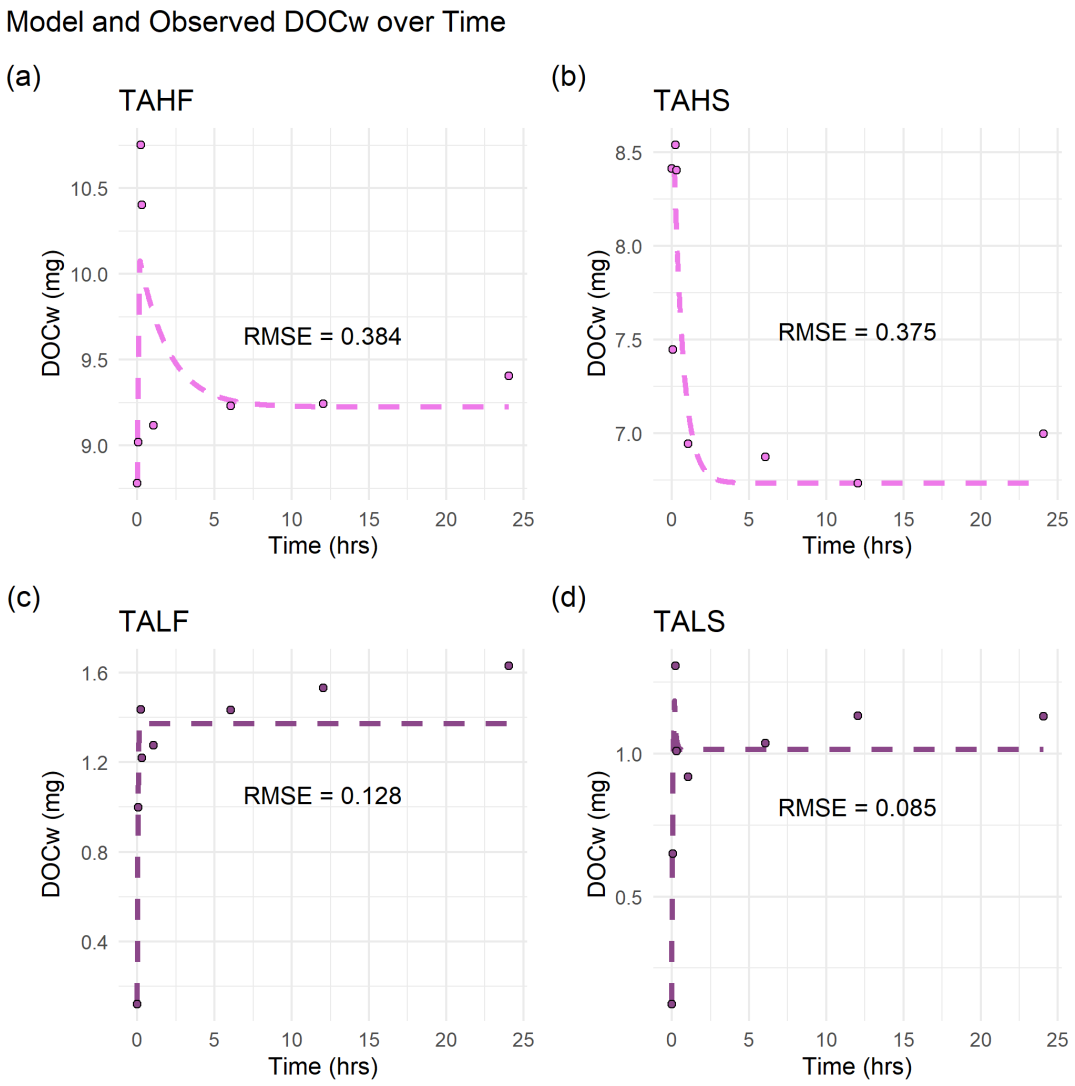

Figure K.1. Taskinas Creek, bulk kinetic experiments.

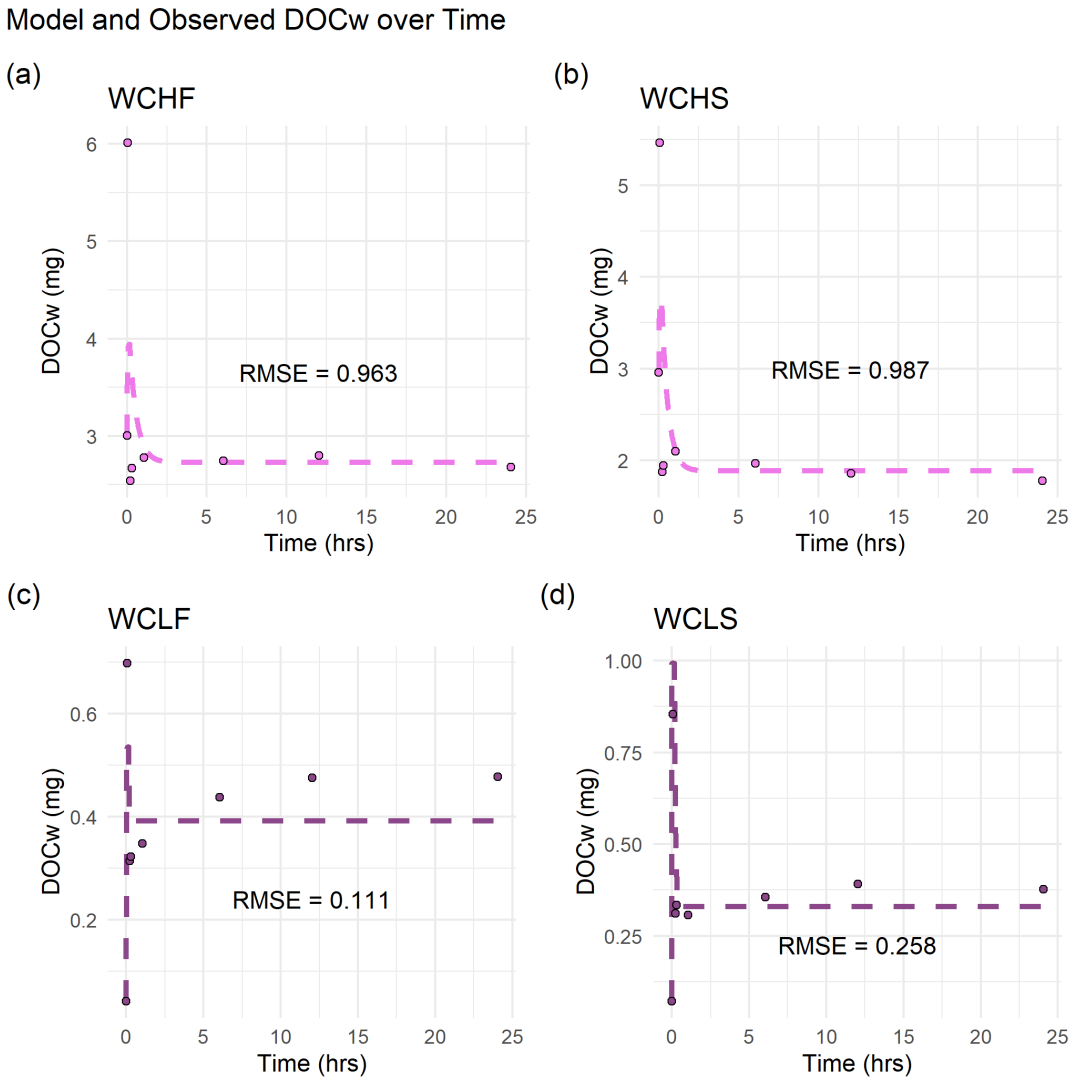

Figure K.2. Shallow Creek Edge, spatial experiments.

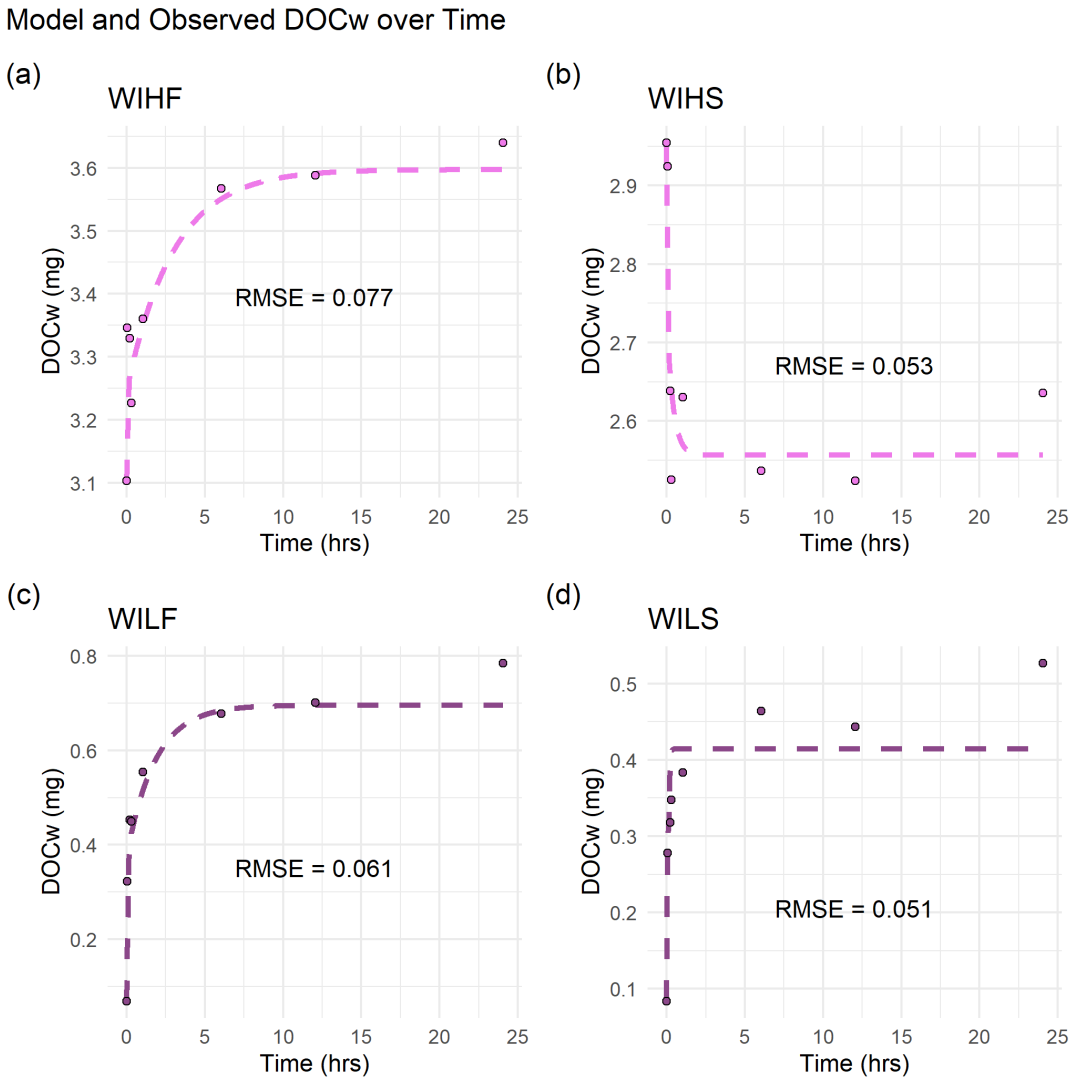

Figure K.3. Shallow Intermediate Plot, spatial experiments.

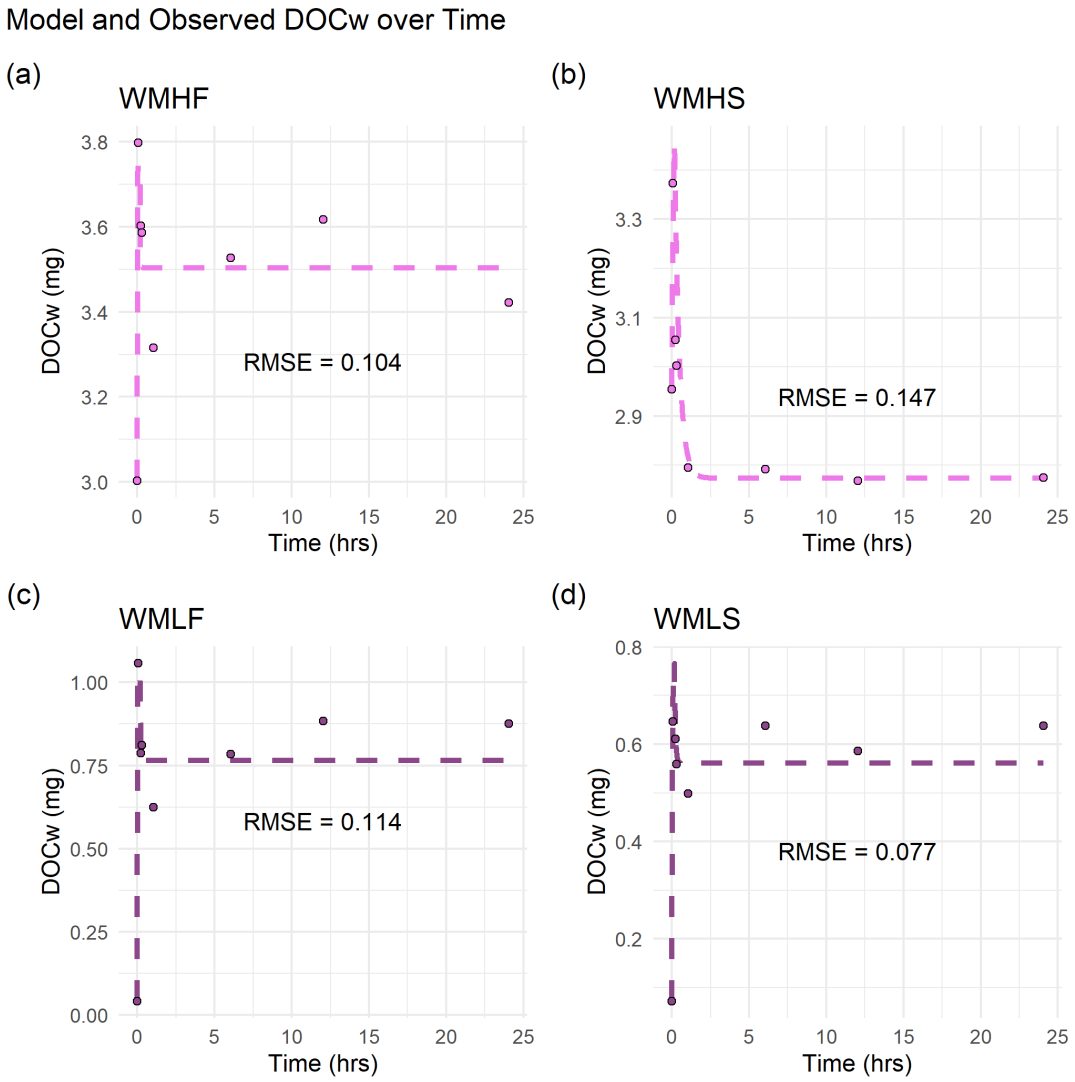

Figure K.4. Shallow High Marsh, spatial experiments.

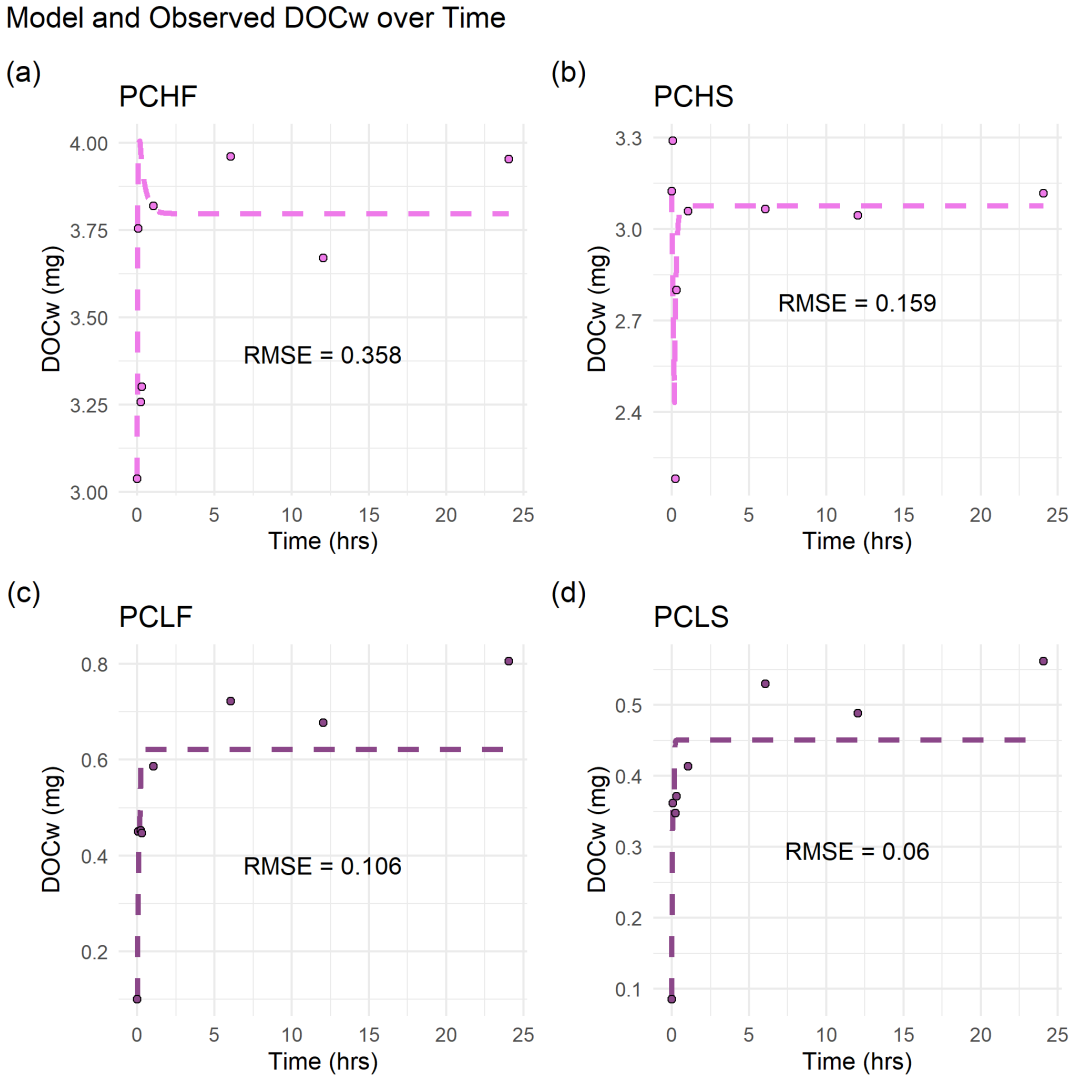

Figure K.5. Deep Creek Edge, spatial experiments.

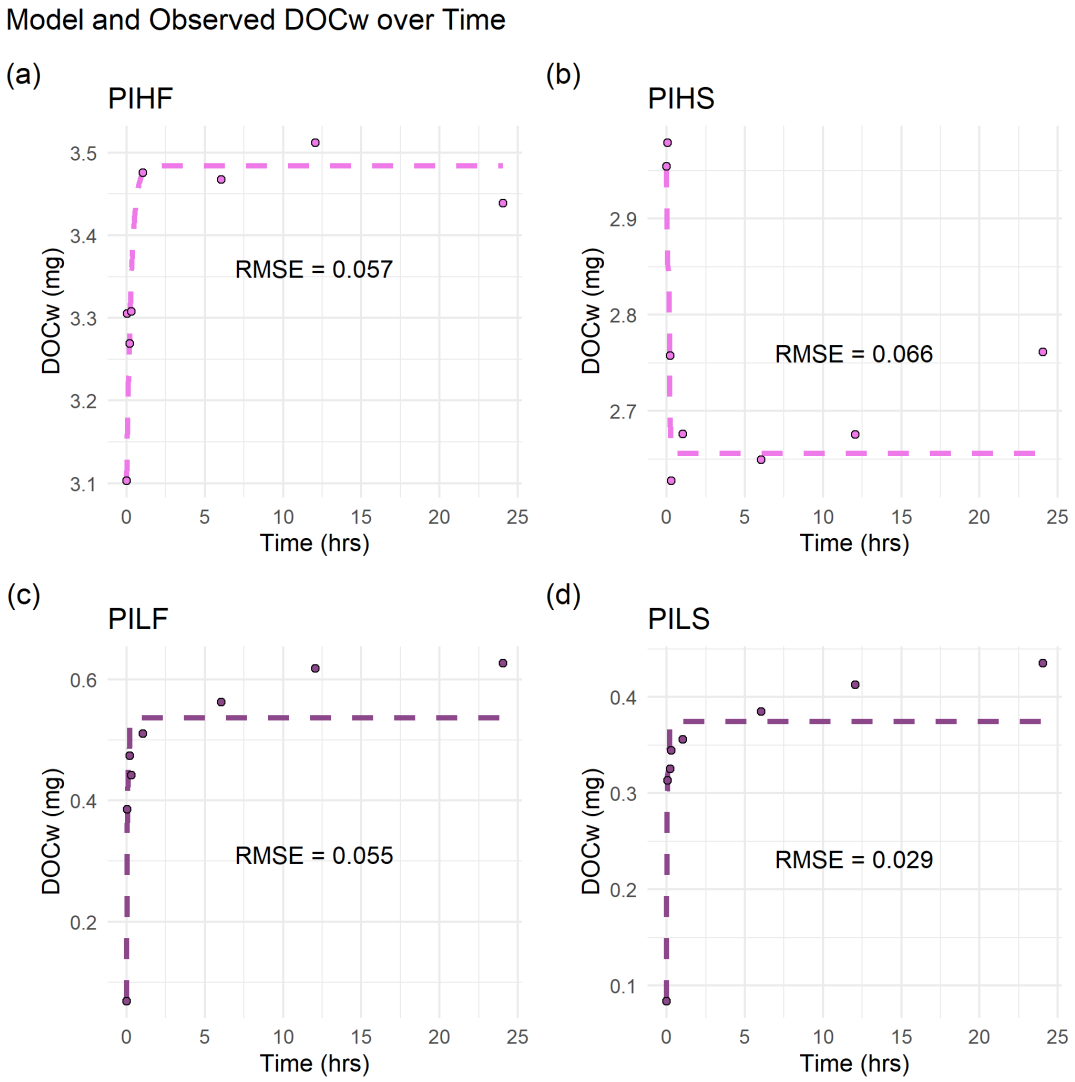

Figure K.6. Deep Intermediate Plot, spatial experiments.

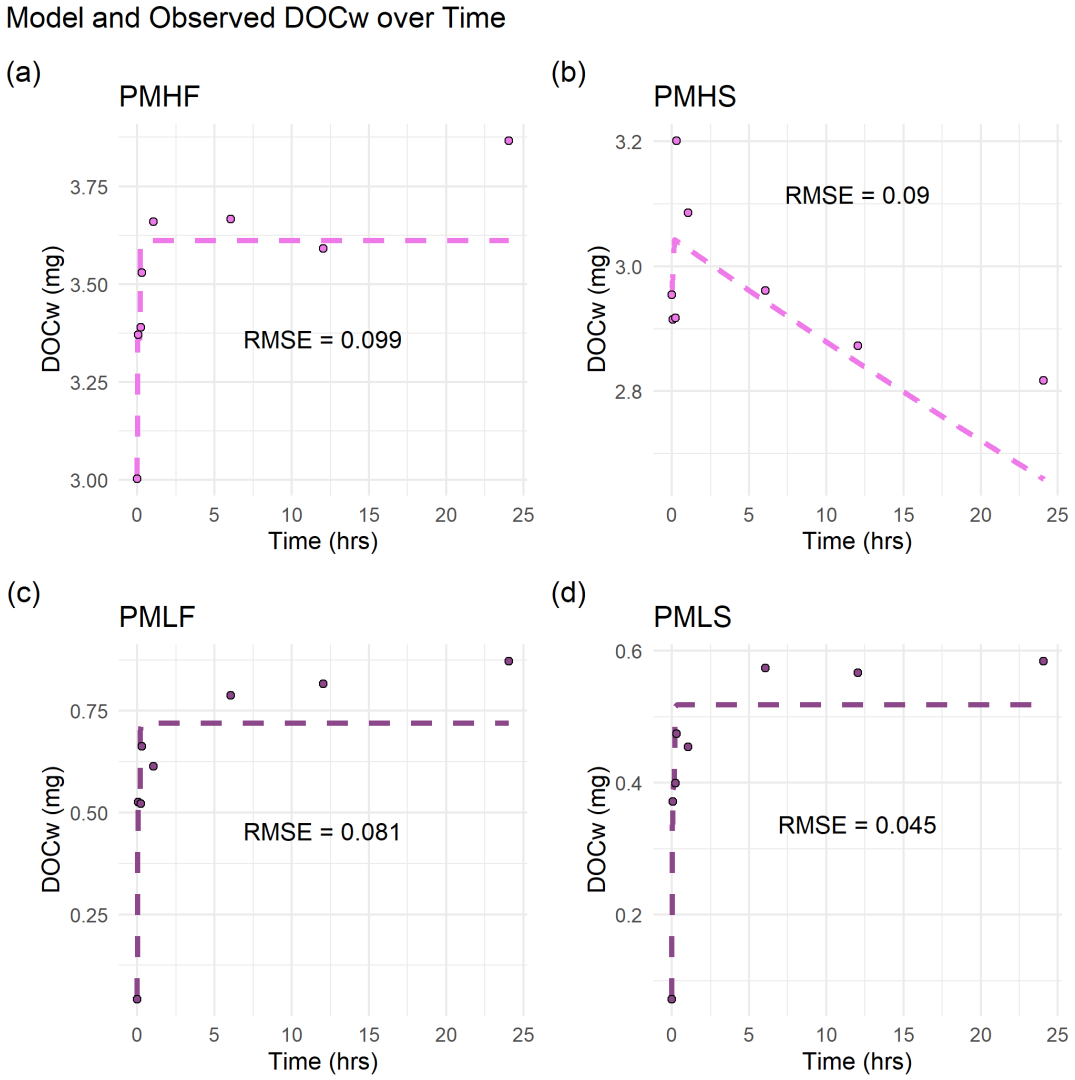

Figure K.7. Deep High Marsh, spatial experiments.

Appendix L: Model Comparisons

Figures L.1-7 show the remaining model comparisons for all other experiments. Black dots are the observed DOC mass over time, while the lines are the corresponding model outputs: *Linear* (orange dot-dashed); *Langmuir* (green solid); *Time-dependent* (purple dashed). The four panels are the four sets of initial conditions: a) HF; b) HS; c) LF; d) LS.

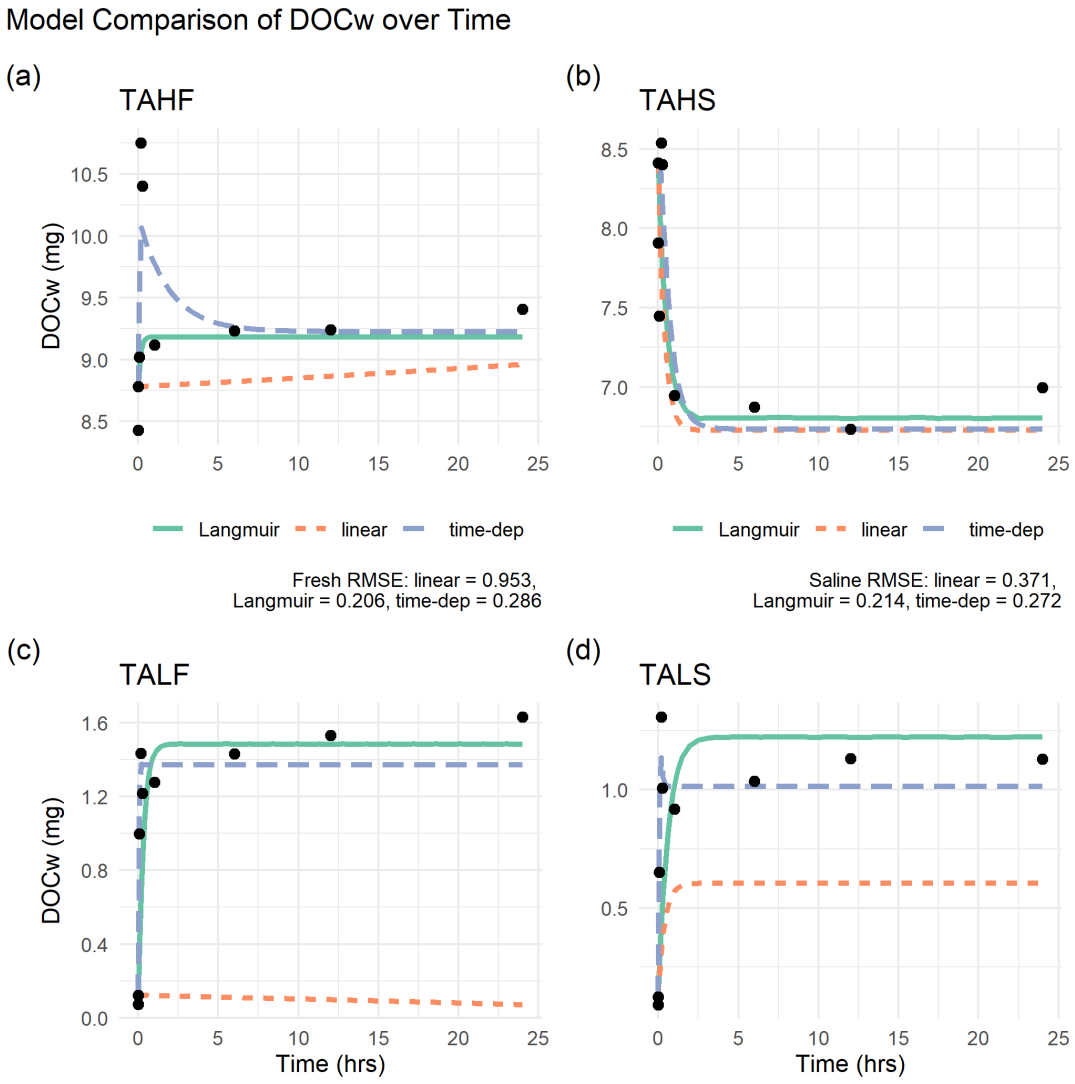

Figure L.1. Taskinas Creek, bulk kinetic experiments.

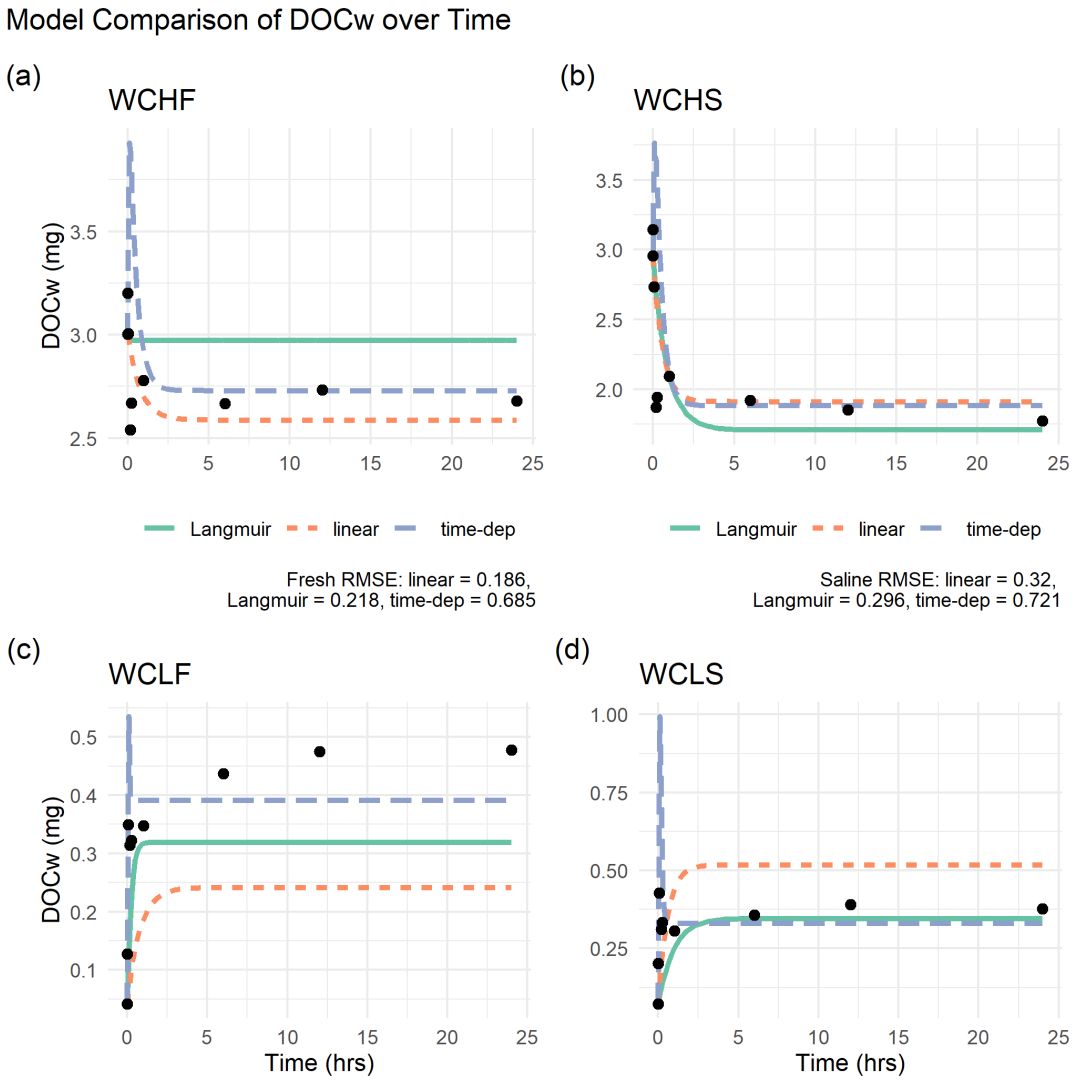

Figure L.2. Shallow Creek Edge, spatial experiments.

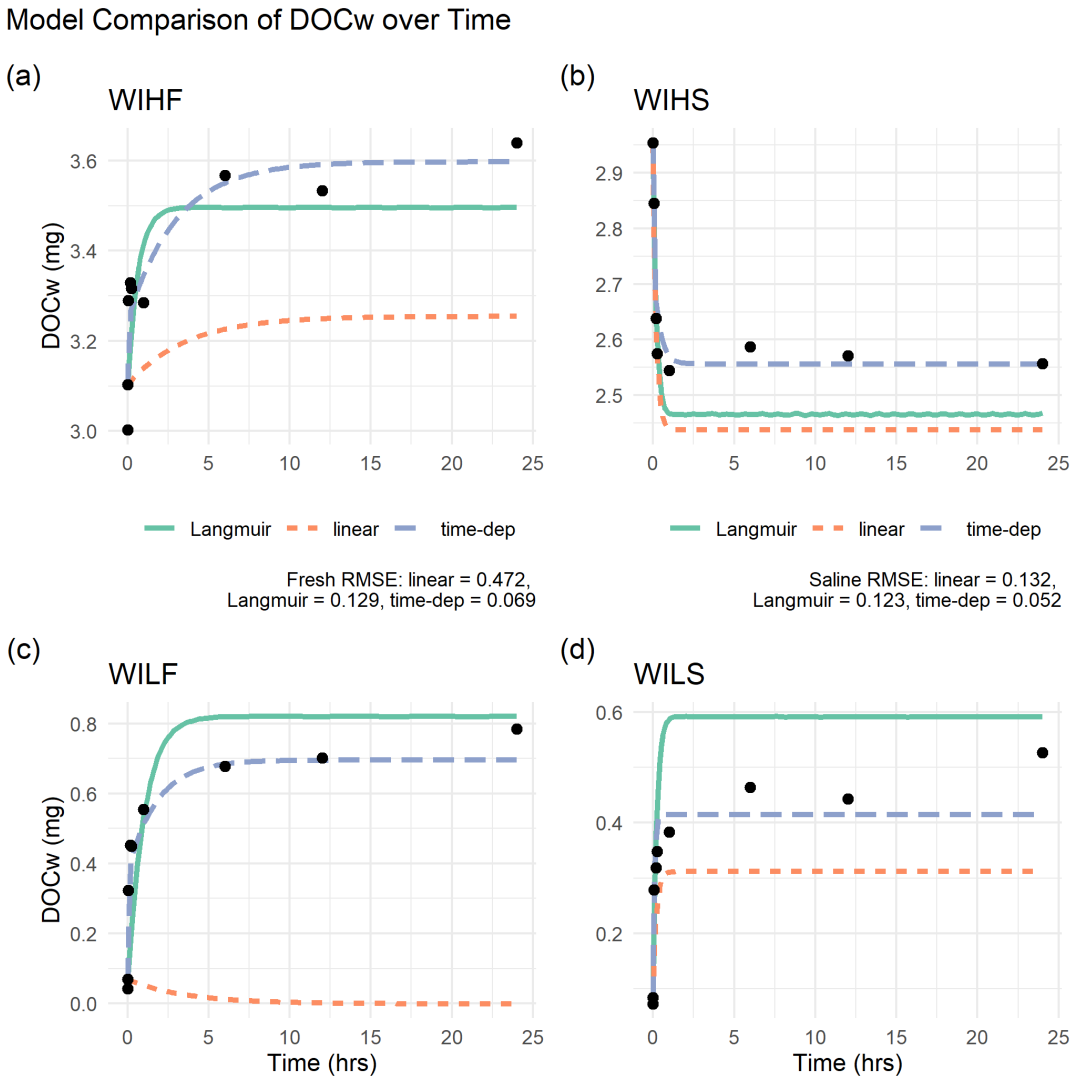

Figure L.3. Shallow Intermediate Plot, spatial experiments.

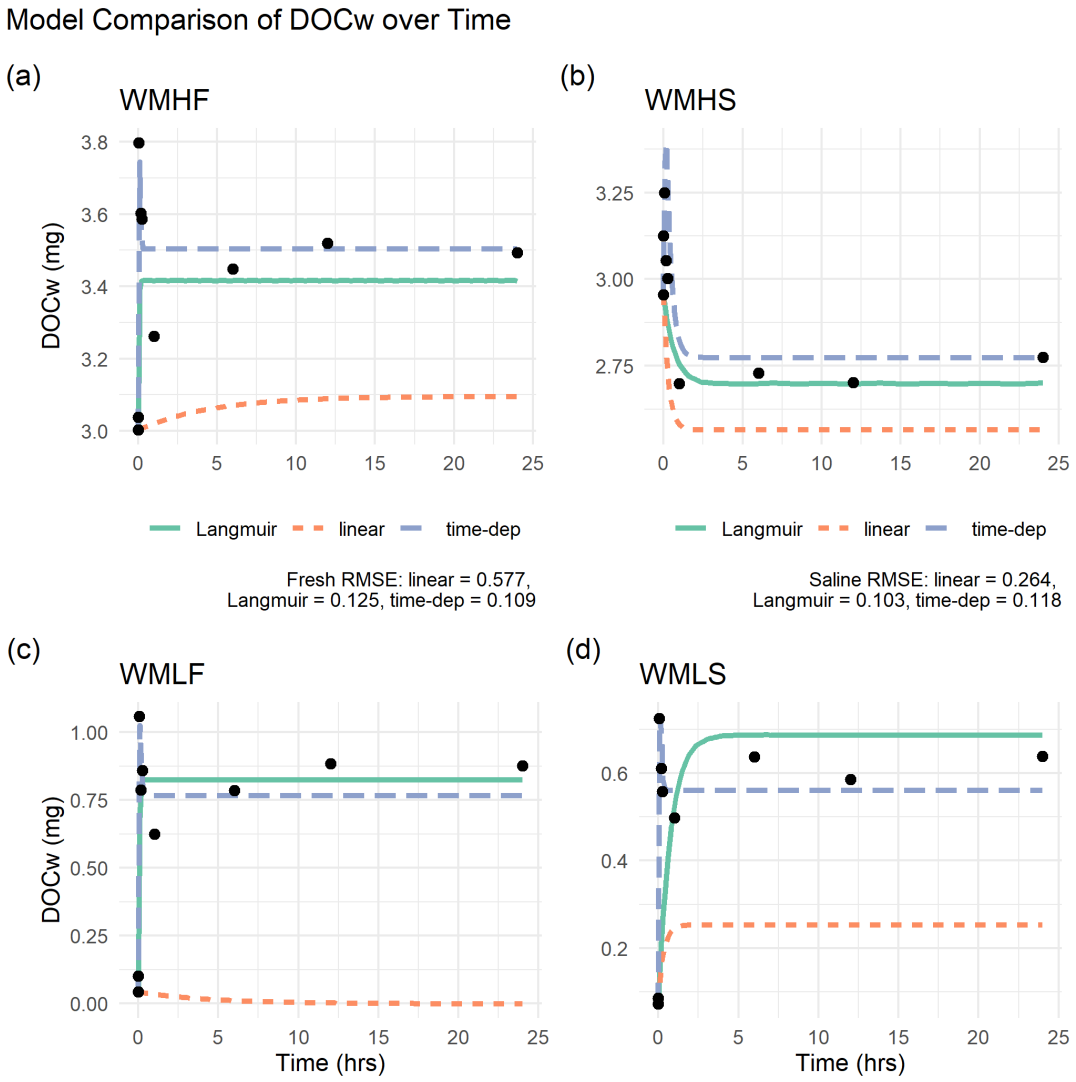

Figure L.4. Shallow High Marsh, spatial experiments.

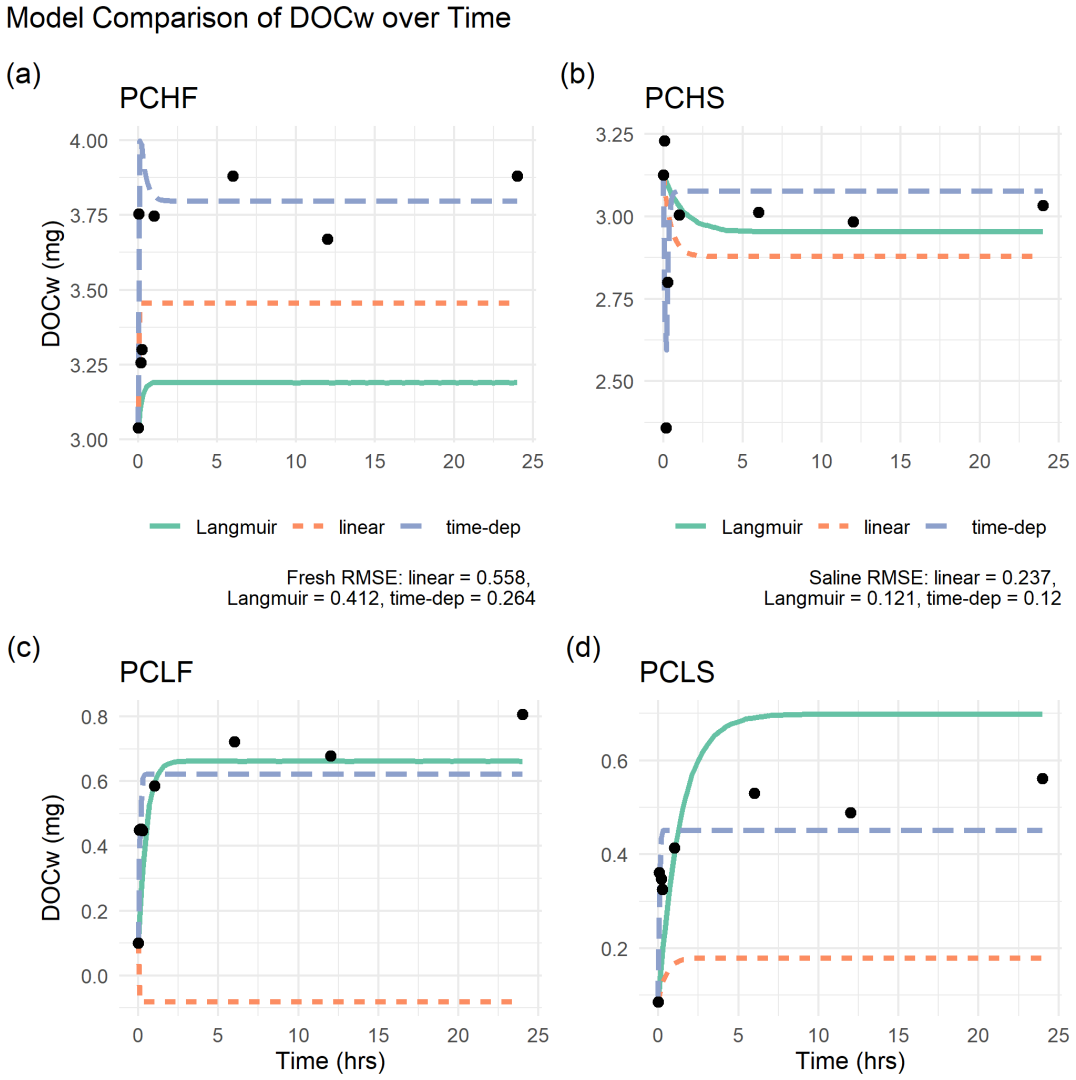

Figure L.5. Deep Creek Edge, spatial experiments.

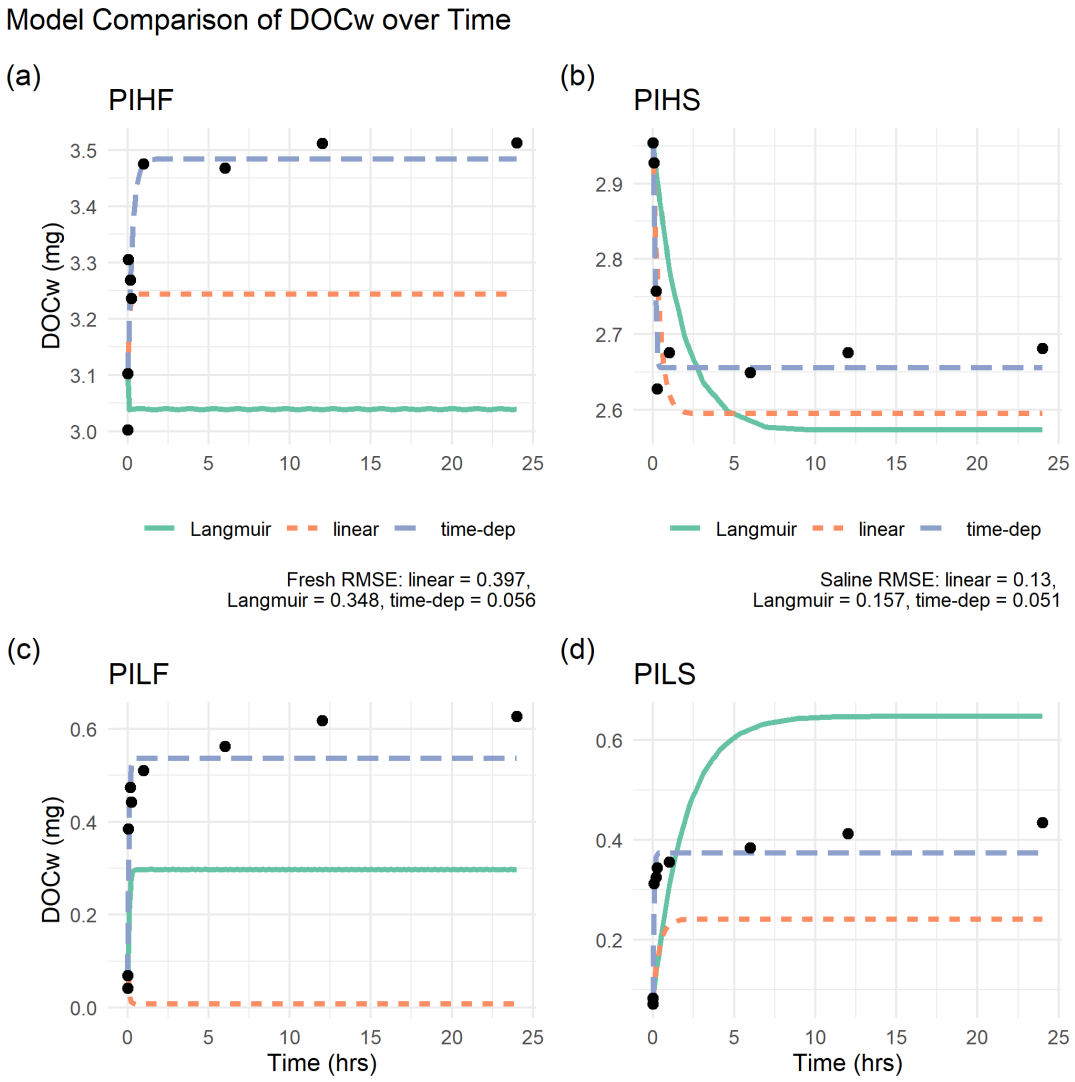

Figure L.6. Deep Intermediate Plot, spatial experiments.

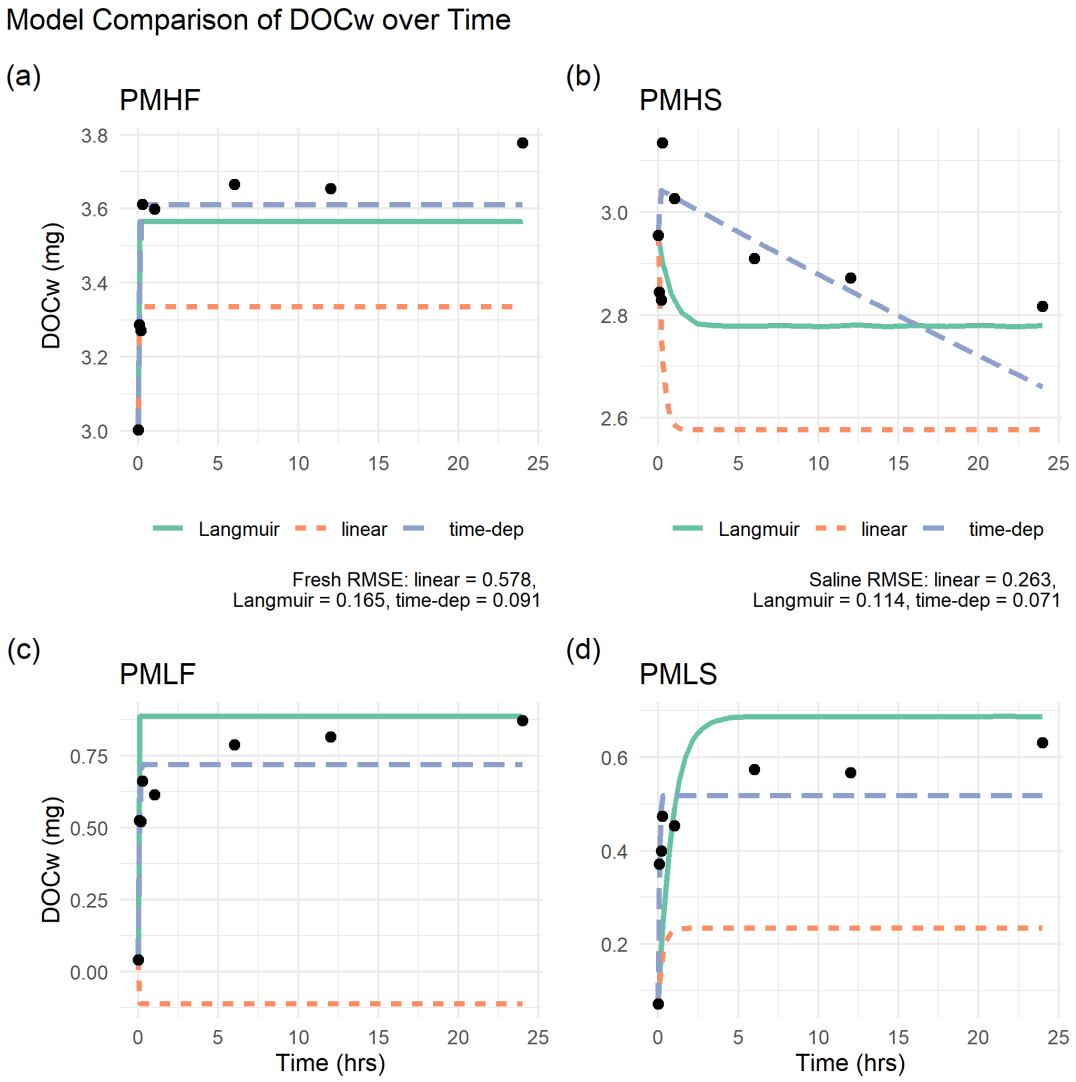

Figure L.7. Deep High Marsh, spatial experiments.

Appendix M: Site Locations

Figure M.1. Taken from Pinsonneault et al. (2021). Locations for the marsh sites of sediment cores and the Great Dismal Swamp from which stock surface water was collected. Only Jug Bay Marsh (J), Taskinas Marsh (T), and the Great Dismal Swamp (star) were used in this manuscript's incubations.

Appendix N: Relevant kinetic incubation information from previous manuscripts

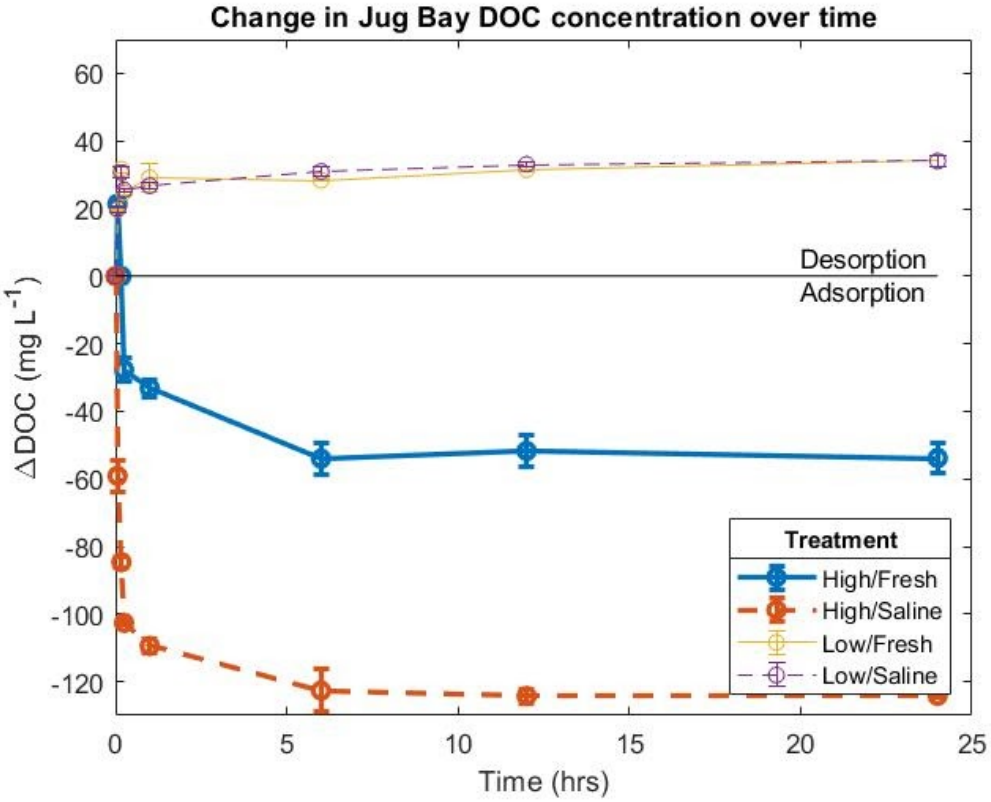

Figure N.1. Taken from [b]Morrissette et al. (*in prep*). The above figure shows Jug Bay Δ[DOC] (final-initial) over time. Negative indicated net adsorption for that time point, while positive values indicated net desorption had occurred. The four different colors were each of the four stock solutions: HF (blue, solid line); HS (red, dashed line); LF (yellow, solid line); LS (purple, dashed line).

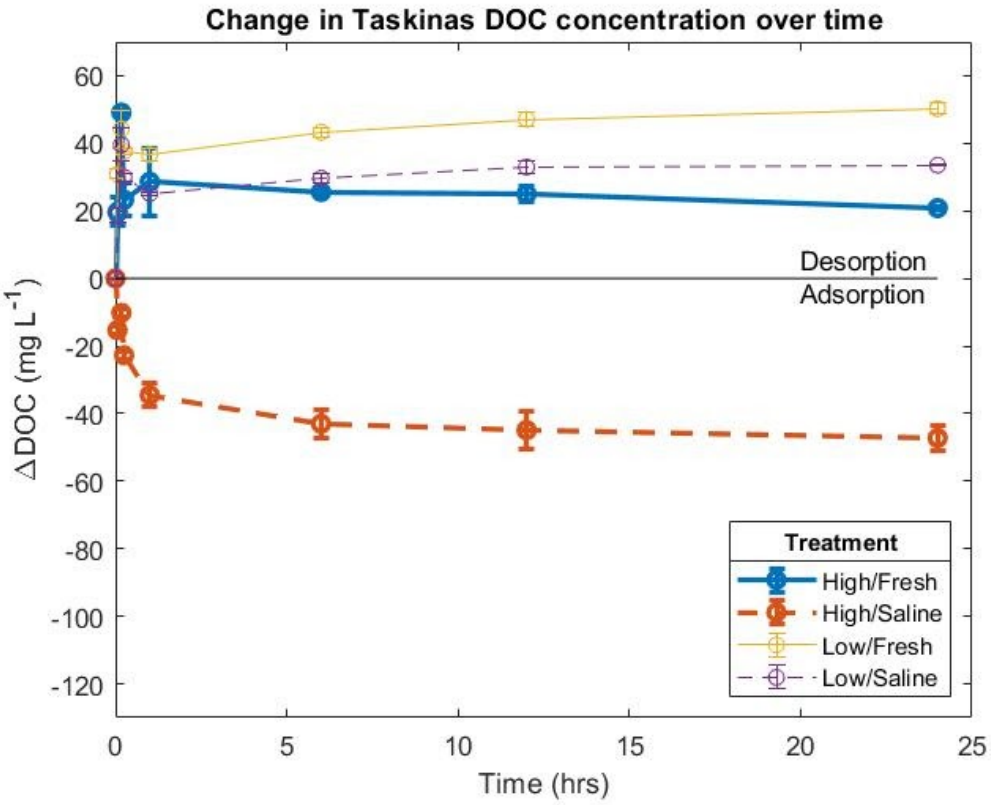

Figure N.2. Taken from [b]Morrissette et al. (*in prep*). The above figure shows Taskinas Δ[DOC] (final-initial) over time. Negative indicated net adsorption for that time point, while positive values indicated net desorption has occurred. The four different colors were each of the four stock solutions: HF (blue, solid line); HS (red, dashed line); LF (yellow, solid line); LS (purple, dashed line).

Appendix O: Spectral Slope

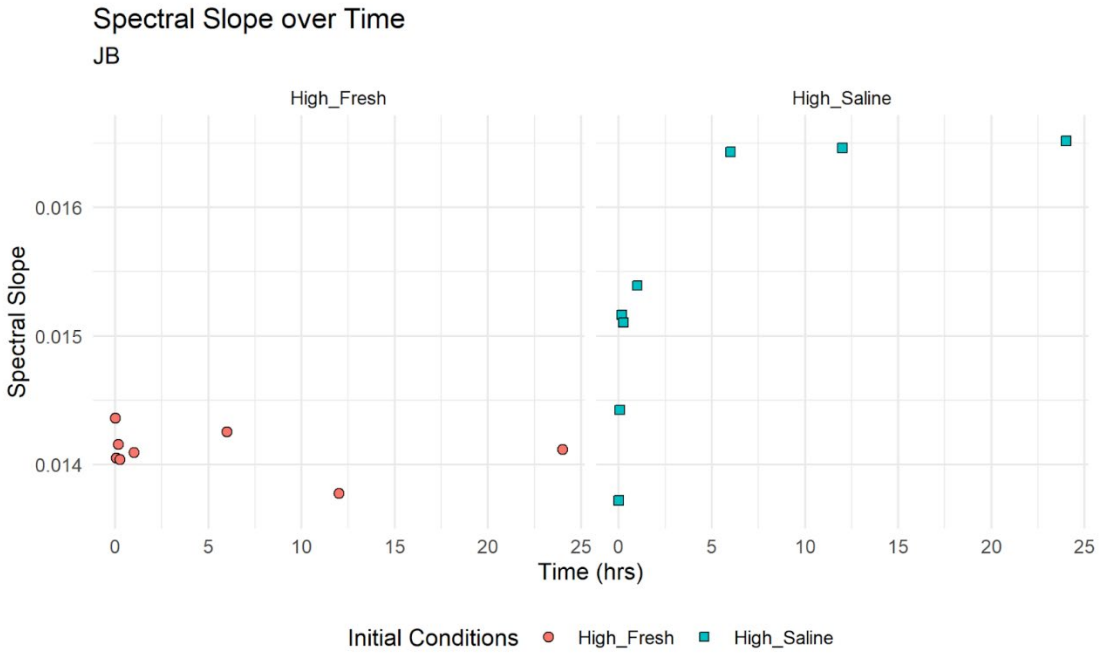

Figure O.1. Jug Bay spectral slope over time for HF (orange circles) and HS (blue squares) initial conditions.

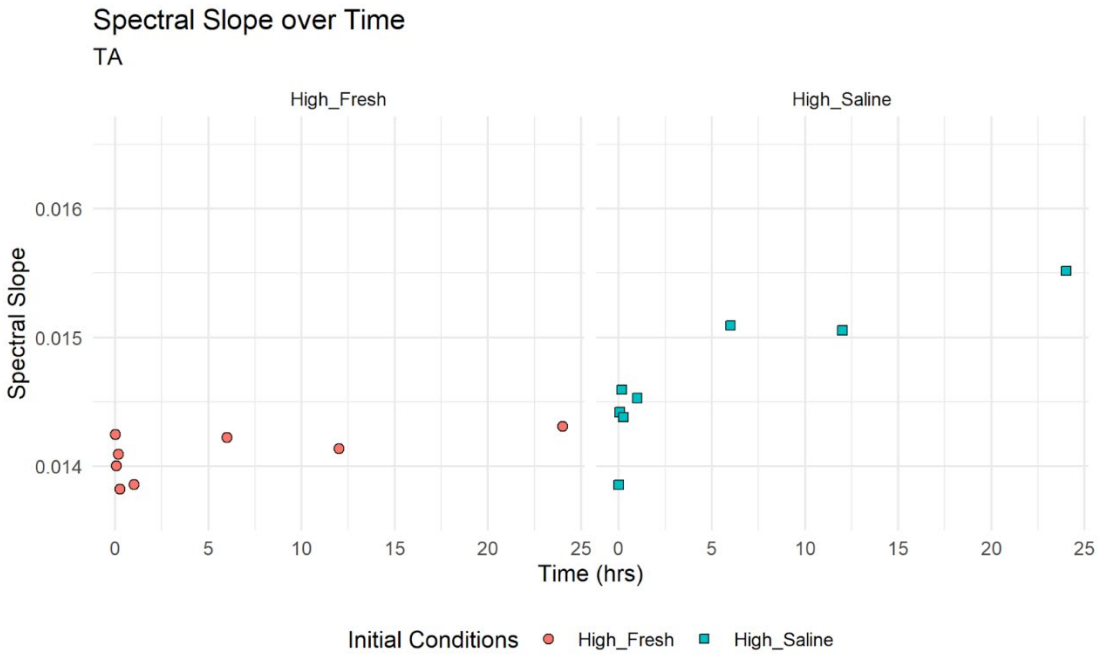

Figure O.2. Taskinas slope ratio over time for HF (orange circles) and HS (blue squares) initial conditions.

Appendix P: R^2 values for least squares non-negative optical fitting

Table P.1. Jug Bay and Taskinas average post CDOC concentration, std. deviation, and R^2 values for least squares non-negative optical fitting for every time point.

Sample	Average Post CDOC (mg L^{-1})	Standard Deviation	Average R^2
JBHF0	272.833	0.474	1.000
JBHS0	273.067	0.362	1.000
JBLF0	1.478	0.052	0.536
JBLS0	1.208	0.017	0.902
JBHF1	231.806	9.942	1.000
JBHS1	185.701	3.750	0.999
JBLF1	3.988	0.377	0.969
JBLS1	3.687	0.585	0.972
JBHF2	251.974	4.854	1.000
JBHS2	145.666	4.999	0.997
JBLF2	3.713	0.208	0.812
JBLS2	1.298	0.310	0.442
JBHF3	241.056	5.544	1.000
JBHS3	123.386	2.759	0.999
JBLF3	4.532	0.110	0.969
JBLS3	4.914	0.122	0.971
JBHF4	231.330	5.219	1.000
JBHS4	110.731	2.938	0.998
JBLF4	4.375	0.105	0.967
JBLS4	4.832	0.257	0.970
JBHF5	198.472	4.851	1.000
JBHS5	86.381	3.295	0.995

JBLF5	4.977	0.487	0.947
JBLS5	6.531	0.782	0.976
JBHF6	195.468	6.330	0.999
JBHS6	80.698	3.021	0.995
JBLF6	5.661	0.114	0.959
JBLS6	5.705	0.067	0.965
JBHF7	197.771	5.206	1.000
JBHS7	77.145	2.328	0.994
JBLF7	5.451	0.297	0.978
JBLS7	5.328	0.329	0.975
TAHF0	280.900	0.055	1.000
TAHS0	263.567	0.036	1.000
TALF0	1.356	0.024	0.565
TALS0	0.720	0.037	0.492
TAHF1	295.314	5.137	1.000
TAHS1	223.633	7.219	1.000
TALF1	17.786	0.950	0.999
TALS1	6.774	2.497	0.971
TAHF2	339.176	5.320	1.000
TAHS2	235.061	3.130	0.999
TALF2	22.803	0.951	0.995
TALS2	13.135	0.651	0.979
TAHF3	349.481	0.451	1.000
TAHS3	244.625	4.499	0.999
TALF3	26.629	1.530	0.997
TALS3	12.006	1.124	0.986
TAHF4	267.073	13.213	1.000

TAHS4	180.399	0.923	0.999
TALF4	20.288	0.691	0.999
TALS4	9.530	0.430	0.996
TAHF5	257.212	3.635	1.000
TAHS5	171.177	3.728	0.998
TALF5	24.158	0.277	0.999
TALS5	9.186	0.301	0.988
TAHF6	262.488	1.378	1.000
TAHS6	157.948	2.352	0.997
TALF6	24.183	0.873	0.999
TALS6	8.529	0.760	0.987
TAHF7	279.891	1.324	1.000
TAHS7	100.982	0.214	0.996
TALF7	30.443	1.235	0.998
TALS7	7.060	0.859	0.973

Appendix Q: S_R and $S_{275-295}$ measurements for the remaining spatial sites

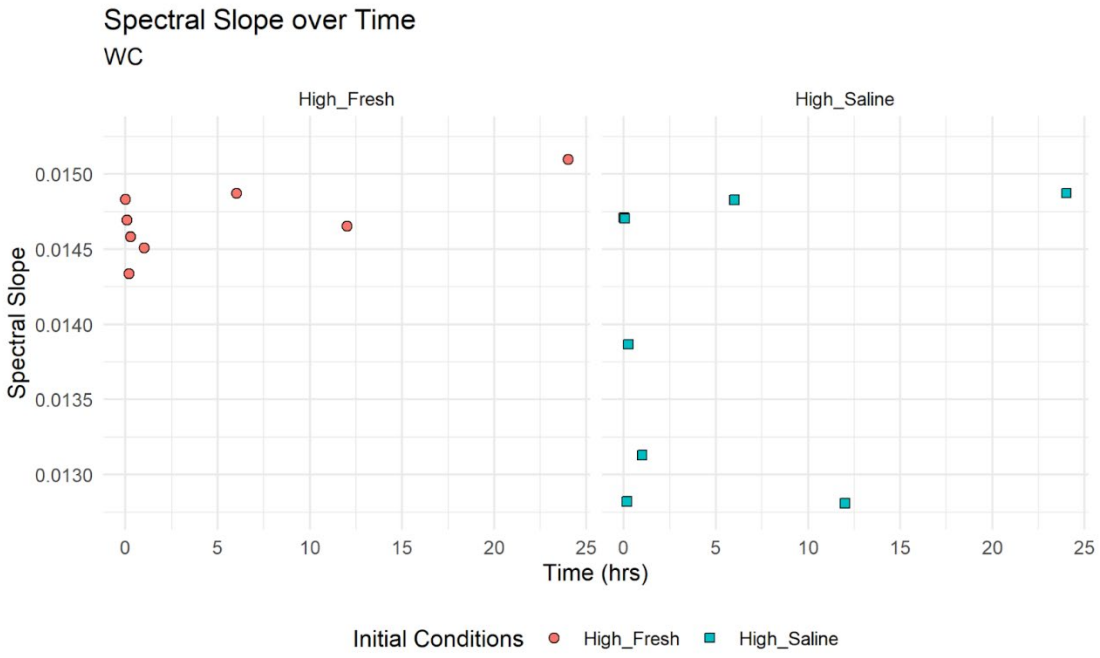

Figure Q.1. WC spectral slope over time for HF (orange circles) and HS (blue squares) initial conditions.

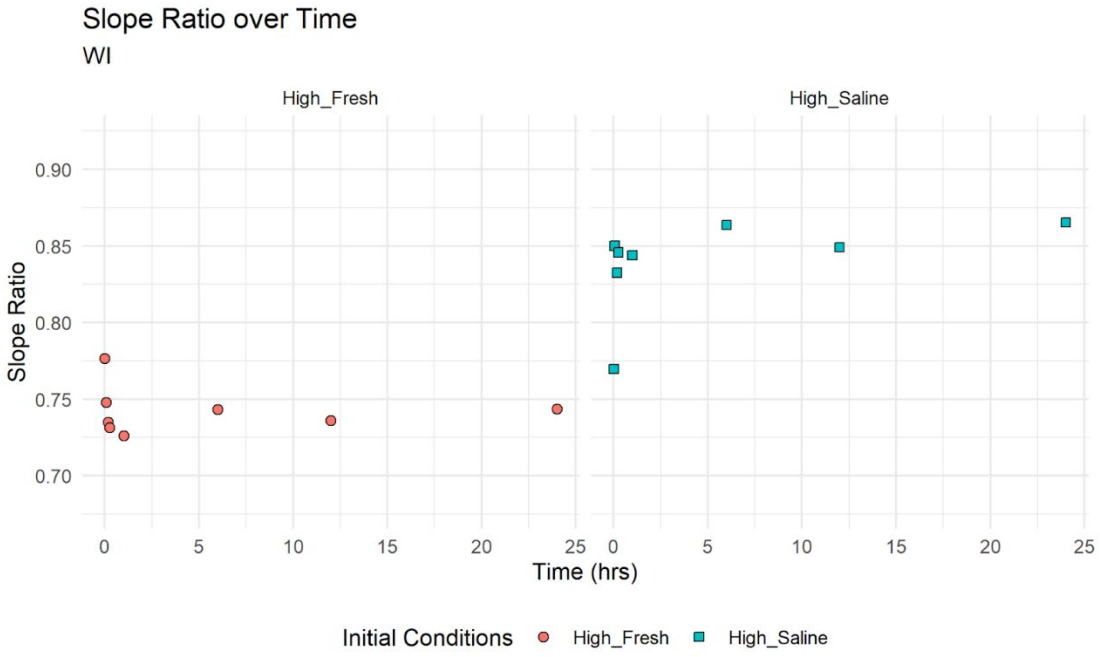

Figure Q.2. WI slope ratio over time for HF (orange circles) and HS (blue squares) initial conditions.

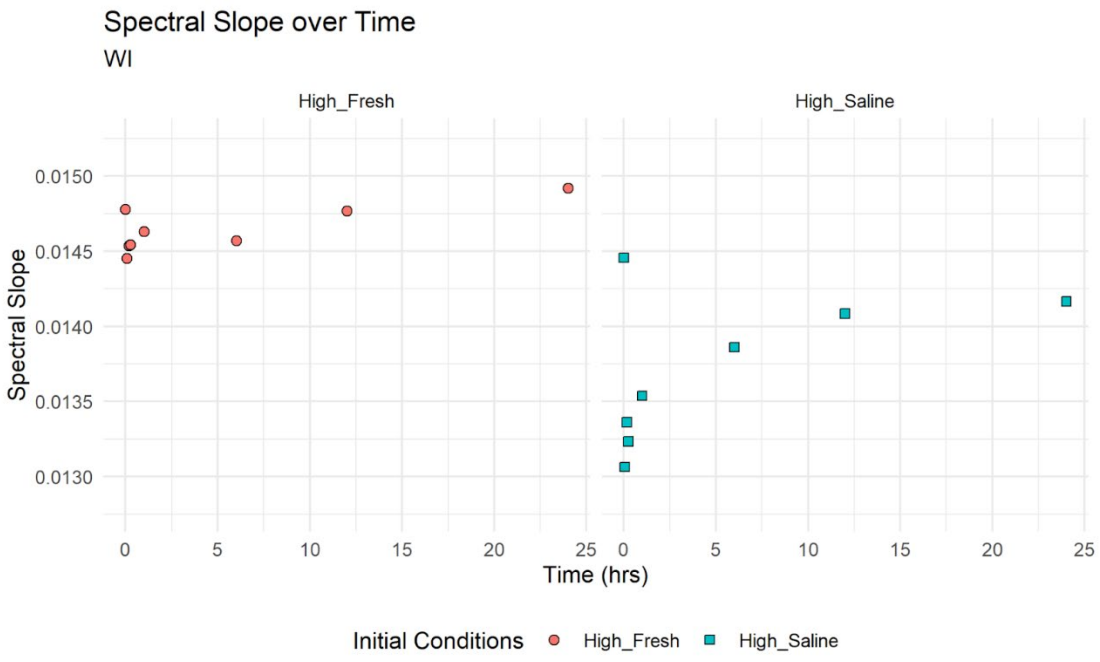

Figure Q.3. WI spectral slope over time for HF (orange circles) and HS (blue squares) initial conditions.

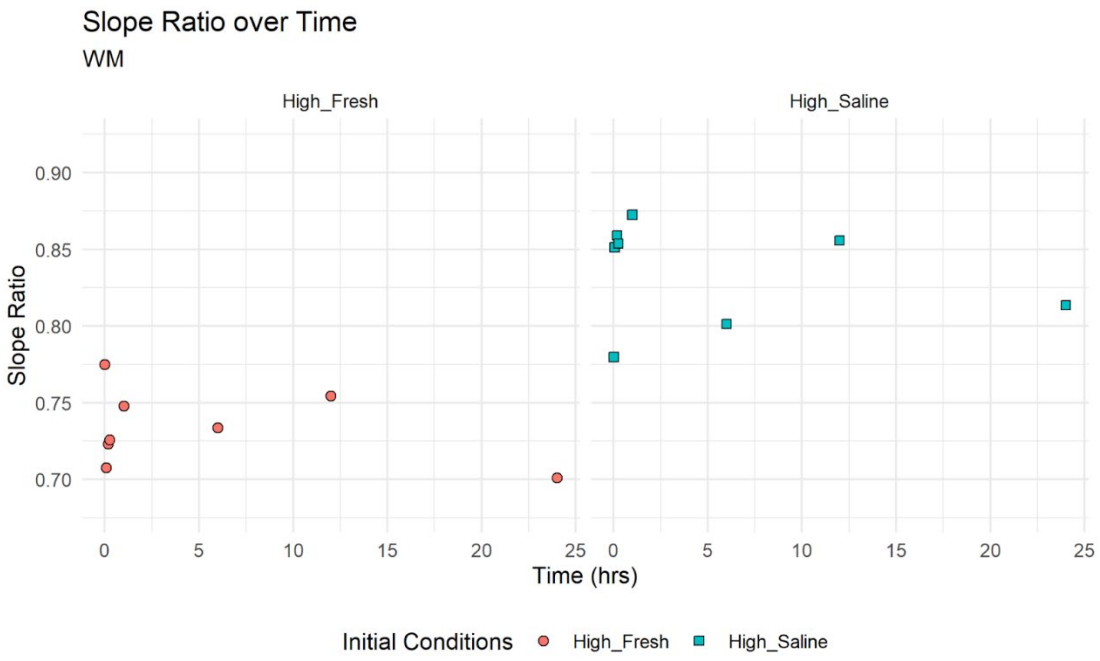

Figure Q.4. WM slope ratio over time for HF (orange circles) and HS (blue squares) initial conditions.

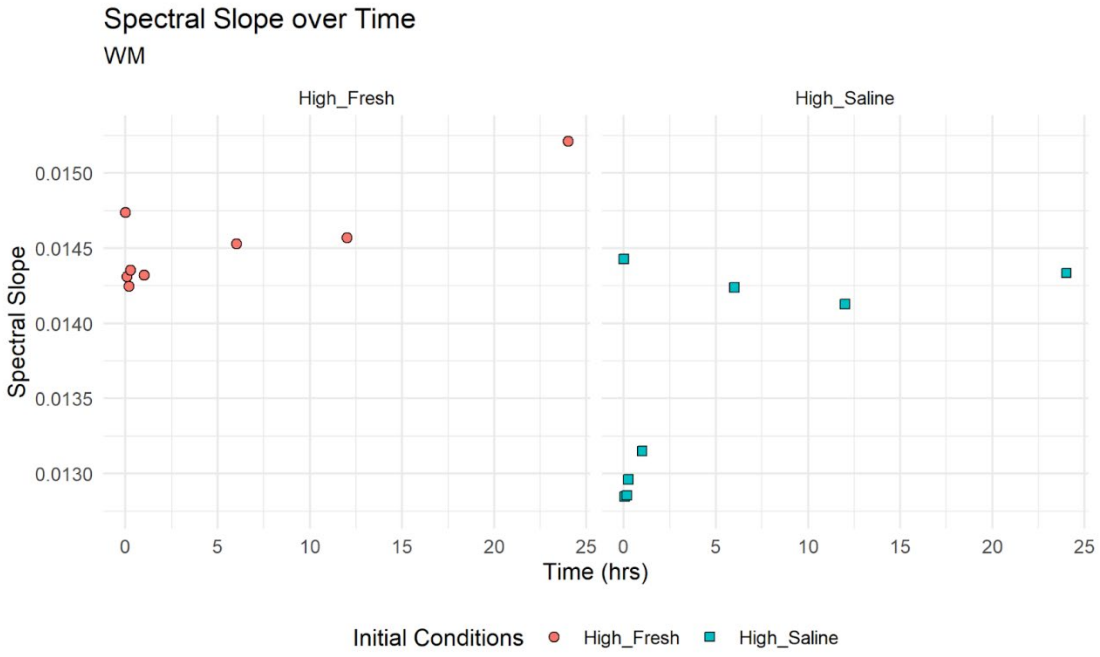

Figure Q.5. WM spectral slope over time for HF (orange circles) and HS (blue squares) initial conditions.

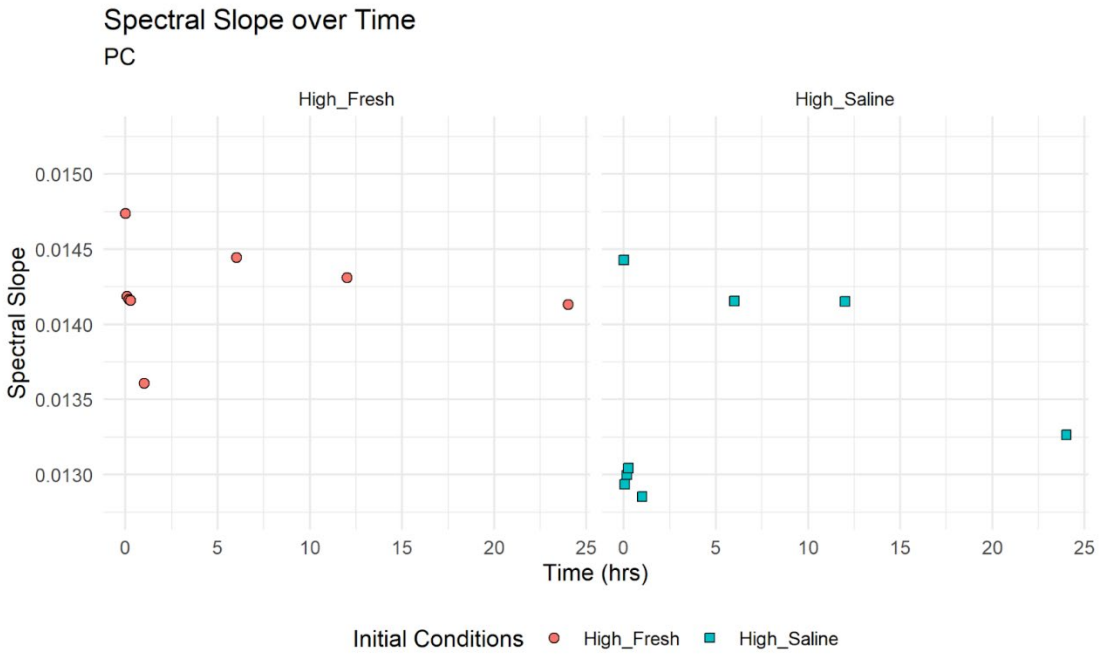

Figure Q.6. PC spectral slope over time for HF (orange circles) and HS (blue squares) initial conditions.

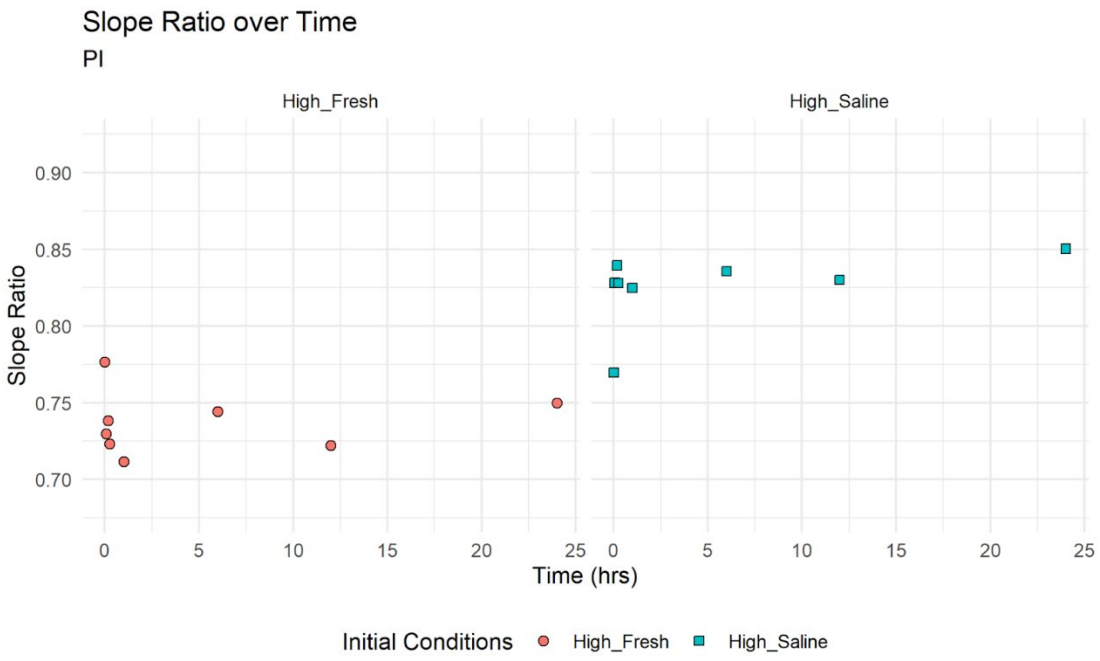

Figure Q.7. PI slope ratio over time for HF (orange circles) and HS (blue squares) initial conditions.

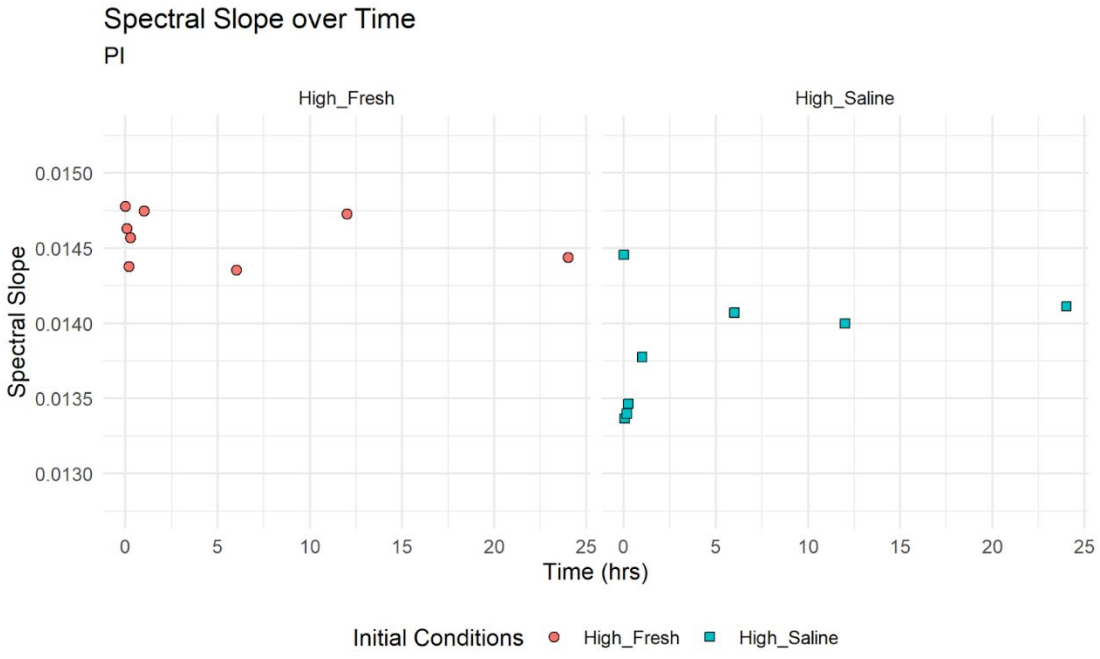

Figure Q.8. PI spectral slope over time for HF (orange circles) and HS (blue squares) initial conditions.

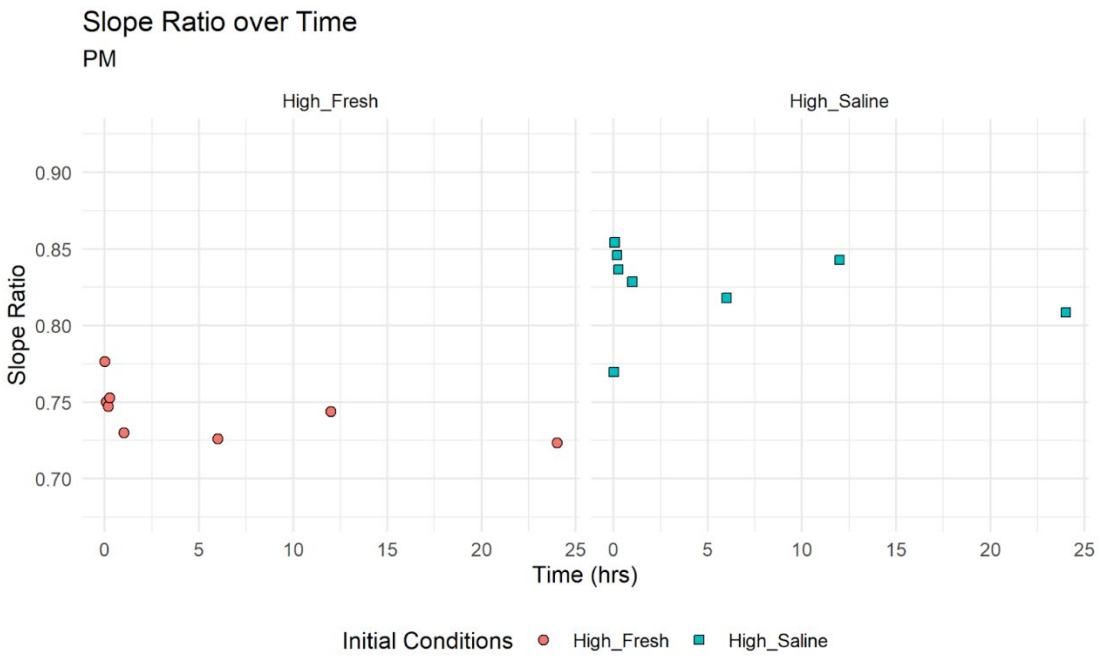

Figure Q.9. PM slope ratio over time for HF (orange circles) and HS (blue squares) initial conditions.

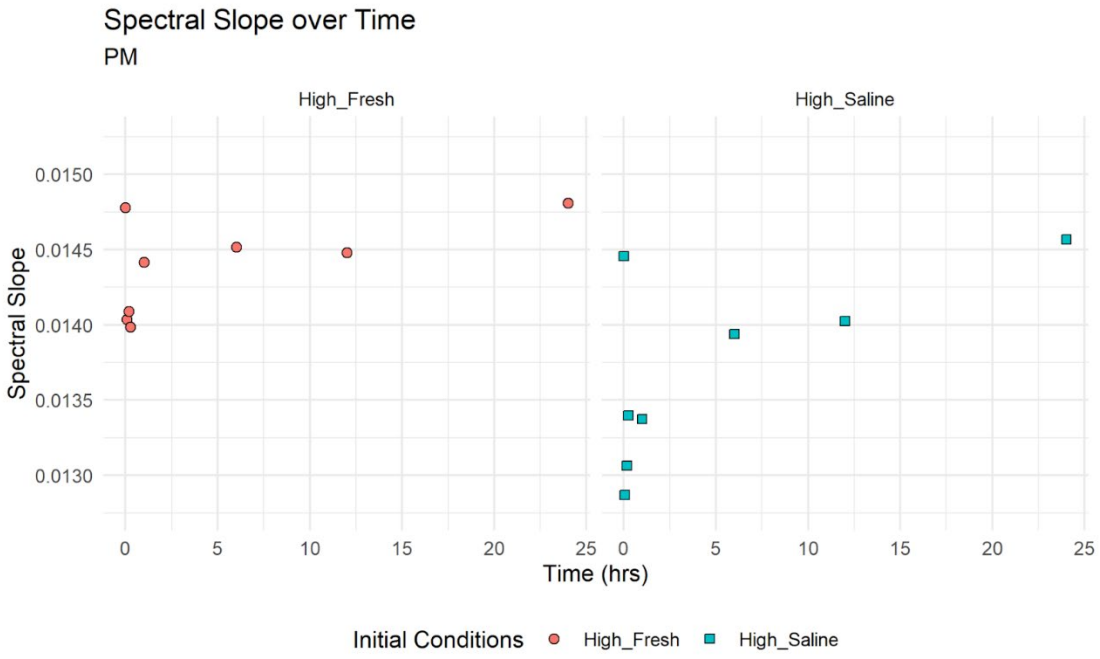

Figure Q.10. PM spectral slope over time for HF (orange circles) and HS (blue squares) initial conditions.

Appendix R: R^2 values for least squares non-negative optical fitting (spatial)

Table R.1. Spatial average post CDOC concentration, std. deviation, and R^2 values for least squares non-negative optical fitting for every time point.

Sample	Average Post CDOC (mg L^{-1})	Standard Deviation	Average R^2
WCHF0	214.158	5.170	1.000
WCHS0	209.567	2.896	1.000
WCLF0	0.932	0.814	0.374
WCLS0	0.000	0.000	0.000
WCHF1	183.296	5.736	1.000
WCHS1	153.547	0.208	1.000
WCLF1	7.593	1.918	0.951
WCLS1	1.809	1.491	0.583
WCHF2	154.851	0.176	1.000
WCHS2	116.348	4.501	0.994
WCLF2	11.680	0.430	0.819
WCLS2	19.951	1.342	0.905
WCHF3	159.258	2.702	1.000
WCHS3	106.628	2.212	0.998
WCLF3	5.071	0.804	0.974
WCLS3	12.178	1.075	0.972
WCHF4	167.066	3.430	1.000
WCHS4	126.758	3.184	0.997
WCLF4	9.759	0.133	0.989
WCLS4	11.696	1.820	0.971
WCHF5	155.310	5.363	1.000
WCHS5	103.572	2.995	0.996

WCLF5	7.756	0.738	0.926
WCLS5	11.449	1.558	0.948
WCHF6	154.515	3.436	1.000
WCHS6	100.686	4.382	0.996
WCLF6	12.449	0.554	0.972
WCLS6	16.866	3.826	0.957
WCHF7	141.216	5.166	1.000
WCHS7	83.886	8.154	0.997
WCLF7	8.920	1.058	0.968
WCLS7	19.066	3.380	0.958
WIHF0	200.167	0.028	1.000
WIHS0	196.967	0.378	1.000
WILF0	1.727	0.155	0.535
WILS0	1.131	0.025	0.589
WIHF1	192.910	3.976	1.000
WIHS1	178.310	0.330	0.996
WILF1	14.356	3.942	0.980
WILS1	9.447	5.050	0.965
WIHF2	205.557	3.517	1.000
WIHS2	166.905	3.782	0.997
WILF2	13.903	1.740	0.998
WILS2	4.221	2.497	0.899
WIHF3	195.644	1.629	1.000
WIHS3	155.270	3.012	0.997
WILF3	15.874	1.623	0.997
WILS3	8.265	2.635	0.977
WIHF4	206.867	0.075	1.000

WIHS4	124.635	1.882	0.997
WILF4	0.982	0.069	0.294
WILS4	5.677	2.393	0.952
WIHF5	188.614	0.631	1.000
WIHS5	108.545	1.444	0.998
WILF5	20.197	4.049	0.998
WILS5	4.201	1.834	0.912
WIHF6	190.722	7.342	1.000
WIHS6	114.190	3.655	0.999
WILF6	19.678	1.832	0.992
WILS6	3.960	2.123	0.807
WIHF7	178.201	0.384	1.000
WIHS7	104.241	10.081	0.998
WILF7	25.929	2.115	0.998
WILS7	2.718	1.985	0.684
WMHF0	202.500	0.550	1.000
WMHS0	208.333	0.123	1.000
WMLF0	1.836	0.035	0.555
WMLS0	2.223	0.029	0.680
WMHF1	215.216	3.734	0.999
WMHS1	203.954	3.182	0.994
WMLF1	26.773	1.838	0.977
WMLS1	17.855	1.548	0.937
WMHF2	212.922	3.174	0.999
WMHS2	191.923	10.126	0.995
WMLF2	32.358	2.815	0.994
WMLS2	18.193	0.504	0.988

WMHF3	209.004	7.472	1.000
WMHS3	194.591	10.160	0.996
WMLF3	34.108	0.741	0.992
WMLS3	19.980	2.052	0.989
WMHF4	197.856	3.829	0.999
WMHS4	164.879	2.345	0.997
WMLF4	34.560	2.343	0.989
WMLS4	19.940	2.826	0.988
WMHF5	200.103	1.923	1.000
WMHS5	152.271	4.409	0.998
WMLF5	33.691	4.075	0.998
WMLS5	21.697	2.301	0.992
WMHF6	210.761	7.964	1.000
WMHS6	142.358	1.534	0.999
WMLF6	36.159	1.923	0.999
WMLS6	15.595	2.625	0.983
WMHF7	180.530	5.869	0.999
WMHS7	115.365	4.389	0.999
WMLF7	32.254	4.186	0.996
WMLS7	13.277	0.784	0.982
PCHF0	202.500	0.550	1.000
PCHS0	208.333	0.123	1.000
PCLF0	1.836	0.035	0.555
PCLS0	2.223	0.029	0.680
PCHF1	215.477	5.636	0.999
PCHS1	209.515	0.862	0.995
PCLF1	23.302	3.014	0.981

PCLS1	15.552	1.241	0.975
PCHF2	209.504	4.850	0.999
PCHS2	193.211	3.842	0.996
PCLF2	26.124	1.182	0.982
PCLS2	18.578	0.630	0.978
PCHF3	205.753	4.862	0.999
PCHS3	192.726	3.983	0.996
PCLF3	25.334	2.122	0.984
PCLS3	16.634	2.045	0.970
PCHF4	224.647	7.130	0.998
PCHS4	176.228	1.843	0.995
PCLF4	31.984	3.206	0.966
PCLS4	16.575	2.745	0.945
PCHF5	199.444	3.958	1.000
PCHS5	162.824	0.557	0.997
PCLF5	24.720	1.311	0.997
PCLS5	13.767	5.405	0.985
PCHF6	210.539	5.352	0.999
PCHS6	145.864	4.488	0.998
PCLF6	28.077	1.153	0.993
PCLS6	14.539	2.389	0.987
PCHF7	192.017	14.697	0.999
PCHS7	149.756	3.432	0.997
PCLF7	35.338	2.849	0.977
PCLS7	16.121	1.353	0.962
PIHF0	200.167	0.028	1.000
PIHS0	196.967	0.378	1.000

PILF0	1.727	0.155	0.535
PILS0	1.131	0.025	0.589
PIHF1	194.143	1.083	1.000
PIHS1	191.252	4.228	0.997
PILF1	15.207	1.345	0.998
PILS1	11.943	4.008	0.979
PIHF2	205.754	2.848	1.000
PIHS2	162.578	0.369	0.997
PILF2	22.579	2.717	0.998
PILS2	7.220	2.229	0.967
PIHF3	207.978	2.882	1.000
PIHS3	152.199	6.572	0.997
PILF3	22.172	3.327	0.996
PILS3	8.122	2.294	0.975
PIHF4	189.828	1.012	1.000
PIHS4	140.772	1.160	0.998
PILF4	23.232	1.065	0.998
PILS4	8.176	2.988	0.943
PIHF5	194.670	6.536	0.999
PIHS5	133.565	6.079	0.998
PILF5	28.427	3.592	0.998
PILS5	7.617	2.753	0.967
PIHF6	195.671	4.765	1.000
PIHS6	131.765	1.539	0.999
PILF6	28.931	3.597	0.996
PILS6	9.105	3.011	0.979
PIHF7	192.431	1.821	1.000

PIHS7	124.502	4.444	0.999
PILF7	31.213	3.946	0.996
PILS7	5.510	1.839	0.931
PMHF0	200.167	0.028	1.000
PMHS0	196.967	0.378	1.000
PMLF0	1.727	0.155	0.535
PMLS0	1.131	0.025	0.589
PMHF1	209.907	2.624	0.999
PMHS1	191.765	6.049	0.995
PMLF1	35.776	0.550	0.992
PMLS1	22.033	0.981	0.989
PMHF2	212.501	7.744	0.999
PMHS2	182.160	3.381	0.996
PMLF2	40.727	1.468	0.991
PMLS2	24.688	1.294	0.986
PMHF3	216.372	5.270	0.999
PMHS3	176.500	5.693	0.997
PMLF3	39.076	5.503	0.993
PMLS3	21.919	0.982	0.986
PMHF4	209.171	3.542	1.000
PMHS4	176.550	0.771	0.997
PMLF4	40.165	3.566	0.993
PMLS4	25.853	2.950	0.984
PMHF5	202.917	2.163	1.000
PMHS5	143.783	0.388	0.999
PMLF5	33.456	1.113	0.998
PMLS5	14.308	1.397	0.987

PMHF6	212.607	3.477	1.000
PMHS6	146.827	7.409	0.999
PMLF6	43.488	3.241	0.995
PMLS6	23.568	3.625	0.989
PMHF7	197.314	3.999	1.000
PMHS7	128.278	10.903	0.999
PMLF7	36.478	1.755	0.997
PMLS7	15.082	0.696	0.997

References

Aguinaga, O.E., Wakelin, J.F.T., White, K.N., Dean, A.P., Pittman, J.K. 2019. The association of microbial activity with Fe, S and trace element distribution in sediment cores within a natural wetland polluted by acid mine drainage. *Chemosphere* 231, 432-441.

Ahrens, B., Braakhekke, M.C., Guggenberger, G., Schrumpf, M., Reichstein, M. 2015. Contribution of sorption, DOC transport and microbial interactions to the 14C age of a soil organic carbon profile: Insights from a calibrated process. *Soil Biology & Biochemistry* 88, 390-402

Alongi, D. 2020. Carbon balance in salt marsh and mangrove ecosystems: A global synthesis. *Journal of Marine Science and Engineering* 8(10), 1-21.

Armitage, A.R., Weaver, C.A., Kominoski, J.S., Pennings, S.C. 2019. Resistant to Hurricane Effects Varies Among Wetland Vegetation Types in the Marsh-Mangrove Ecotone. *Estuaries and Coasts* 43, 960-970.

Aurin, D.A., Dierssen, H.M. 2012. Advantages and limitations of ocean color remote sensing in CDOM-dominated, mineral-rich coastal and estuarine waters. *Remote Sensing of the Environment.* 125, 181-197.

Avneri-Katz, S., Young, R.B., McKenna, A.M., Chen, H., Corilo, Y.E., Polubesova, T., Borch, T., Chefetz, B. 2017. *Org. Geochem.* 103, 113-124.

Bader, R.G., et al. 1960. Recovery of dissolved organic matter in sea-water and organic sorption by particulate material. *Geochimica et Cosmochimica Acta* 19, 236-243.

Bai, J., Jia, J., Zhang, G., Zhao, Q., Lu, Q., Cui, B., Liu, X. 2016. Spatial and temporal dynamics of heavy metal pollution and source identification in sediment cores from the short-term flooding riparian wetlands in a Chinese delta. *Environmental Pollution* 219, 379-388.

Barrõn, C., Duarte, C.M. 2015. Dissolved organic carbon pools and export from the coastal ocean. *Global Biogeochemical Cycles* 29, 1725-1738.

Bates, D. M. and Watts, D. G. (1988) Nonlinear Regression Analysis and Its Applications, Wiley.

Bauer, JE., Cai, W-J., Raymond, P.A., Bianchi, T.S., Hopkinson, C.S., Regnier, P.A.G. 2013. The changing carbon cycle of the coastal ocean. *Nature* 61, 61-70.

Bedford, B.L., Walbridge, M.R., Aldous, A. 1999. Patterns in nutrient availability and plant diversity of temperate North American wetlands. *Ecology* 80, 2151-2169.

Bernal, B., Mitsch, W.J. 2008. A comparison of soil carbon pools and profiles in wetlands in Costa Rica and Ohio. *Ecologial Engineering* 34, 311-323.

Bolan, N., Adriano, D.C., Kunhikrishnan, A., James, T.K., Mcdowell, R., Senesi, N. 2011. Dissolved organic matter: biogeochemistry, dynamics, and environmental significance in soils. *Advances in Agronomy* 110. doi: 10.1013/F978-0-12-385531-2.00001-3.

Boynton, W.R., Bailey, E.M., 2008. Sediment Oxygen and Nutrient Exchange Measurements from Chesapeake Bay, Tributary Rivers and Maryland Coastal Bays: Development of a Comprehensive Database & Analysis of Factors Controlling Patterns and Magnitude of Sediment-Water Exchanges. University of Maryland Center for Environmental Science Technical Report Series No. TS-542-08, Solomons, MD.

Brady, D.C., Testa, J.M., Di Toro, D.M., Boynton, W.R., Kemp, W.M., 2013. Sediment flux modeling: Calibration and application for coastal systems. *Estuarine, Coastal and Shelf Science*. 117, 107-124.

Brezonik, P.L., Olmanson, L.G., Finlay, J.C., Bauer, M.E. 2015. Factors affecting the measurement of CDOM by remote sensing of optically complex inland waters. *Remote Sensing of the Environment* 157, 199-215.

Bullock, A., Acreman, M. 2003. The role of wetlands in the hydrological cycle. *Hydrology and Earth System Sciences* 7(3), 358-389.

Burdige, D.J. 2007. Preservation of Organic Matter in Marine Sediments: Controls, Mechanisms, and an Imbalance in Sediment Organic Carbon Budgets? *Chem. Rev.* 107, 467-485.

Burdige, D.J., Komada, T., Cedric, M., Chanton, J.P. 2016. Modeling studies of dissolved organic matter cycling in Santa Barbara Basin (CA, USA) sediments. *Geochimica et Cosmochimica Acta* 195, 100-119.

Burns, C.J., Alber, M., Alexander, C.R. 2021. Historical Changes in the Vegetated Area of Salt Marshes. *Estuaries and Coasts* 44,162-177.

Cai, W-J. 2011. Estuarine and coastal ocean carbon paradox: CO2 sinks or sites of terrestrial carbon incineration? *Annual Review: Marine Science* 3, 123-145.

Cai, R., Zhou, W., He, C., Tang, K., Guo, W., Shi, Q., Gonsior, M., Jiao, N. 2019. Microbial Processing of Sediment-Derived Dissolved Organic Matter: Implications for Its Subsequent Biogeochemical Cycling in Overlying Seawater. *Journal of Geophysical Research: Biogeosciences* 124, 3479-3490.

Callaway, J., Delaune, R., Patrick Jr, W. 1998. Heavy Metal Chronolgies in Selected Wetlands from Northern Europe. *Marine Pollution Bulletin* 36(1), 82-96.

Canuel, E., Cammer, S.S., McIntosh Marcek, H.A., Pondell, C.R. 2012. Climate Change Impacts on the Organic Carbon Cycle at the Land-Ocean Interface. *Annual Review Earth Planetary Sciences* 40, 685-711.

Charles, S., Kominoski, J.S., Troxler, T.G., Gaiser, E.E., Servais, S., Wilson, B.J., Davis, S.E., Sklar, F.H., Coronado-Molina, C., Madden, C.J., Kelly, S., Rudnick, D.T. 2019. Experimental Saltwater Intrusion Drives Rapid Soil Elevation and Carbon Loss in Freshwater and Brackish Everglades Marshes. *Estuaries and Coasts*. doi:10.1077/s12237-019-00620-3.

Chen, X. 2015. Modeling of Experimental Adsorption Isotherm Data. *Information* 6, 14-22.

Chen, M., Hur, J. 2015. Pre-treatments, characteristics, and biogeochemical dynamics of dissolved organic matter in sediments: A review. *Water Research* 79, 10-25.

Childers, D. L., Day, J. W. Jr., & McKellar, N. Jr. 2000. Twenty more years of marsh and estuarine flux studies: Revisiting Nixon (1980). In M. Weinstein & D. A. Kreeger (Eds.), Concepts and controversies in tidal marsh ecology (pp. 391–423). Dordrecht: Kluwer Academic Publishing.

Chmura, G. 2013. What do we need to assess the sustainability of the tidal salt marsh carbon sink? *Ocean and Coastal Management* 83, 25-31.

Chmura, G.L. Anisfeld, S.C., Cahoon, D.R., Lynch, J.C. 2003. Global carbon sequestration in tidal, saline wetland soils. *Global Biogeochemical Cycles* 17(4).

Clark, C.D., Litz, L.P., Grant, S.B. Salt marshes as a source of chromophoric dissolved organic matter (CDOM) to Southern California coastal waters. *Limnology and Oceanography* 53(5), 1923-1933.

Clark, J.B., Long, W., Hood, R.R., 2017. Estuarine sediment dissolved organic matter dynamics in an enhanced sediment flux model. *Journal of Geophysical Research: Biogeosciences* 122, 2669-2682. https://doi.org/10.1002/2017JG003800.

Clark, J.G., Neale, P.J., Tzortziou, M., Cao, F., Hood, R.R. 2019. A mechanistic model of photochemical transformation and degradation of colored dissolved organic matter. *Marine Chemistry* 214, 103666.

Costanza, R. R., d'Arge, R., de Groot, R., Farber, S., Grasso, M., Hannon, B., Limburg, K., Naeem, S., O'Neill, R.V., Paruelo, J., Raskin, R.G., Sutton, P., van der Belt, M. 1997. The value of the world's ecosystem services and natural capital. *Nature* 387, 253-260.

Czapla, K.M., Anderson, I.C., Currin, C.A. 2020. Net Ecosystem Carbon Balance in a North Carolina, USA, Salt Marsh. *Journal for Geophysical Research: Biogeosciences* 125(10), doi: 10.1029/20019JG005509.

Dahlgreen, R., Marrett, D. 1991. Organic Carbon Sorption in Arctic and Subalpine Spodosol B Horizons. *Soil Science of America Journal* 55(5), 1382-1390.

Dalva, M., Moore, T.R. 1991. Sources and Sinks of Dissolved Organic Carbon in a Forested Swamp Catchment. *Biogeochemistry* 15(1), 1-19.

Day, J., Kemp, W., Yanez-Arancibia, A., Crump, B.C. 2013. *Estuarine Ecology, 2nd edition*. Wiley-Blackwell, 568 pp.

Davidson, N.C., Finlayson, C.M. 2018. Extent, regional distribution and changes in area of different classes of wetland. *Marine and Freshwater Research* 69, 1525-1533.

Di Toro, D.M., 2001. Sediment Flux Modeling. Wiley-Interscience, New York.

Fellman, J.B., Hood, E., Spencer, R.G.M. 2010. Fluorescence spectroscopy opens new windows into dissolved organic matter dynamics in freshwater ecosystems: A review. *Limnology and Oceanography* 55, 2452-2462.

French, J.R., Stoddart, D.R. 1992. Hydrodynamics of salt marsh creek systems: Implications for marsh morphological development and material exchange. *Earth Surface Processes and Landforms* doi: 10.1002/esp.3290170304.

Gao, L., Fan, D., Sun, C., Li, D., Cai, J. 2011. Optical characterization of CDOM in a marsh-influenced environment in the Changjiang (Yangtze River) Estuary. *Environmental Earth Sciences* 64(3), 643-658.

Glick, P., Clough, J., Polaczyk, A., Couvillion, B., Nunley, B. 2013. Potential Effects of Sea-Level Rise on Coastal Wetlands in Southeastern Louisiana. *Journal of Coastal Research* 63, 211-233.

Goni, M.A., Gardner, L.R. 2003. Seasonal Dynamics in Dissolved Organic Carbon Concentrations in a Coastal Water-Table Aquifer at the Forest-Marsh Interface. *Aquatic Geochemistry* 9, 209-232.

Grace, J.B., Ford, M.A. 1996. The Potential Impact of Herbivores on the Susceptibility of the Marsh Plant *Sagittaria lancifolia* to Saltwater Intrusion in Coastal Wetlands. *Estuaries* 19(1), 13-20.

Groeneveld, M., Catalan, N., Attermeyer, K., Hawkes, J., Einarsdottir, K., Kothawala, D., Bergquist, J., Tranvik, L. 2020. Selective adsorption of terrestrial dissolved organic matter to inorganic surfaces along a boreal inland water continuum. *Journal of Geophysical Research: Biogeosciences* 125(3), doi: 10.1029/2019JG005236.

Groffman, P., Hanson, G., Kiviat, E., Stevens, G. 1996. Variation in Microbial Biomass and Activity in Four Different Wetland Types. *Soil Science of America Journal* 60(2), 622-629.

Gu, B., Schmitt, J., Chen, Z., Llyuan, L., McCarthy, J.F. 1994. Adsorption and Desorption of Natural Organic Matter on Iron Oxide: Mechanisms and Models. *Environmental Science and Technology* 28, 38-46.

Guggenberger, G., Kaiser, K. 2003. Dissolved organic matter in soil: challenging the paradigm of sorptive preservation. *Geoderma* 113, 293-310.

Guo, X-J., Li, Q., Jiang, J-Y., Dai, B-L. 2013. Investigating Spectral Characteristics and Spatial Variability of Dissolved Organic Matter Leached from Wetland in Semi-Arid Region to Differentiate Its Sources and Fate. *Clean-Soil, Air, Water* 42(8), 1076-1082.

Han, J.Y., Kim, D-H., Oh, S., Moon, H.S. 2020. Effects of water level and vegetation on nitrate dynamics at varying sediment depths in laboratory-scale wetland mesocosms. *Science of the Total Environment* 703, 134741.

Hansen, A.M., Kraus, T.E.C., Pellerin, B.A., Fleck, J.A., Downing, B.D., Bergamaschi, B.A. 2016. Optical properties of dissolved organic matter (DOM): Effects of biological and photolytic degradation. *Limnology and Oceanography* 61, 1015-1032.

Herbert, E.R., Schubauer-Berigan, J., Craft, C.B. 2018. Differential effects of chronic and acute simulated seawater intrusion on tidal freshwater marsh carbon cycling. *Biogeochemistry* 138, 137-154.

Herman, Russell L. 2018. A First Course in Differential Equations for Scientists and Engineers. http://people.uncw.edu/hermanr/mat361/ODEBook/ODE1.pdf

Herrmann, M., Najjar, R. G., Kemp, W. M., Alexander, R. B., Boyer, E. W., Cai, W.-J., et al. 2015. Net ecosystem production and organic carbon balance of U.S. East Coast estuaries: A synthesis approach. *Global Biogeochemical Cycles* 29, 96–111. https://doi.org/10.1002/2013GB004736

Holden, J. 2005. Peatland hydrology and carbon release: why small-scale process matters. *Phil. Trans. R. Soc. A.* 363, 2891-2913.

Hunt, J.F., Ohno, T. 2007. Characterization of Fresh and Decomposed Dissolved Organic Matter Using Excitation-Emission Matrix Fluorescence Spectroscopy and Multiway Analysis. *Journal of Agricultural Food Chemistry* 55, 2121-2128.

Jaffe, R., Boyer, J.N., Lu, X., Maie, N., yang, C., Scully, N., Mock, S. 2004. Sources characterization of dissolved organic matter in a mangrove-dominated estuary by fluorescence analysis. *Marine Chemistry* 84, 195-210.

Jardine, P., Weber, N., McCarthy, J. 1989. Mechanisms of dissolved organic carbon adsorption on soil. *Soil Science of America Journal* 53(5), 1378-1385.

Johnston, C., Bridgham, S., Schubauer-Berigan, J. 2001. Nutrient Dynamics in Relation to Geomorphology of Riverine Wetlands. *Soil Science of America Journal* 65(2), 557-577.

Jordan, T.E., Correll, D.L. 1991. Continuous Automated Sampling of Tidal Exchanges of Nutrients by Brackish Marshes. *Estuarine, Coastal, and Shelf Science* 32, 527-545.

Kaiser, K., Guggenberger, G. 2000. The role of DOM sorption to mineral surfaces in the preservation of organic matter in soils. *Organic Chemistry* 31,711-725.

Kaiser, K., Guggenberger, G. 2003. Mineral surfaces and soil organic matter. *European Journal of Soil Science.* 54, 219-236.

Kaiser, K., Kaupenjohann, M., Zech W. 2001. Sorption of dissolved organic carbon in soils: effects of soil sample storage, soil-to-solution ratio, and temperature. *Geoderma* 99, 317–328.

Kaiser, K., Guggenberber, G., Zech, W. 1996. Sorption of DOM and DOM fractions to forest soils. *Geoderma* 74(3-4), 281-303.

Kaiser, K., Zech, W. 1998. Rates Of Dissolved Organic Matter Release And Sorption In Forest Soils. *Soil Science* 163, 714-725.

Kalbitz, K., Solinger, S., Park, J. H., Michalzik, B., and Matzner, E. 2000. Controls on the dynamics of dissolved organic matter in soils: a review. *Soil Science* 165, 277–304. doi: 10.1097/00010694-200004000-00001

Karstens, S., Buczko, U., Jurasinski, G., Peticzka, R., Glatzel, S. 2016. Impact of adjacent land use on coastal wetland sediments. *Science of the Total Environment* 550, 337-348.

Keil, R.G., Mayer, L.M. 2014. "Mineral matrices and organic matter," in Treatise on Geochemistry, Vol. 12, 2nd Edn., eds H. Holland and K. Turekian (Amsterdam: Elsevier), 337–359.

Keil, R.G., Montlucon, D.B., Prahl, F.G., Hedges, J.I. 1994. Sorptive preservation of labile organic matter in marine sediments. *Nature* 370, 549– 552.

Kirwan, M.L., Megonigal, J.P. 2013. Tidal wetland stability in the face of human impacts and sea-level rise. *Nature* 504, 53-60.

Kleber, M., Bourg, I., Coward, E., Hansel, C., Myneni, S., Nunan, N. 2021. Dynamic interactions at the mineral-organic matter interface. *Nature Reviews Earth & Environment.* doi: 10.1038/s43017-021-00162-y.

Knobloch, A., Reay, W., Canuel, E. 2021. Carbon Pools Differ in Source and Temporal Patterns in a Tidal Marsh Creek System of the York River, VA. *Estuaries and Coasts.* doi: 10.1007/s12237-020-00878-y.

Kroeger, K.D., Crooks, S., Moseman-Valtierra, S., Tang, J. 2017. Restoring tides to reduce methane emissions in impounded wetlands: A new and potent Blue Carbon climate change intervention. *Nature Scientific Reports* 7(1), 11914.

Koopal, L., Tan, W., Avena, M. 2019. Mixed ad/desorption kinetics unraveled with the equilibrium adsorption isotherm. *Colloid Surfaces A: Physicochemical Engineering Aspects* 577, 709-722.

Kothawala, D.N., Moore, T.R. 2009. Adsorption of dissolved nitrogen by forest mineral soils. *Canadian Journal for Research* 39, 2381-2390.

Kothawala, D.N., Moore, T.R., Hendershot, W.H. 2008. Adsorption of dissolved organic carbon to mineral soils: A comparison of four isotherm approaches. *Geoderma* 148, 43-50.

Kothawala, D.N., Roehm, C., Blodau, C., Moore, T.R. 2012 Selective adsorption of dissolved organic matter to mineral soils. *Geoderma* 189-190, 334-342.

Laffoley, D.d'A. & Grimsditch, G. (eds). 2009. The management of natural coastal carbon sinks. IUCN, Gland, Switzerland. 53 pp

Levin, L.A., Boesch, D.F., Covich, A., Dahm, C., Erseus, C., Ewel, K.C., Kneib, R.T., Moldenke, A., Palmer, M.A., Snelgrove, P., Strayer, D., Weslawski, J.M. 2001. The Function of Marine Critical Transition Zones and the Importance of Sediment Biodiversity. *Ecosystems* 4, 430-451.

Lilienfein, J., Qualls, R.G., Uselman, S.M., Bridgham, S.D. 2004. Adsorption of Dissolved Organic Carbon and Nitrogen in Soils of a Weathering Chronosequence. *Soil Science Society of America Journal* 68, 292-305.

Liu, Z., Lee, C. 2006. Drying effets on sorption capacity of coastal sediment: The importance of architecture and polarity of organic matter. *Geochimica et Cosmochimica Acta* 70(13), 3313-3324.

Logozzo, L., Tzortziou, M., Neale, P., Clark, J. 2021. Photochemical and Microbial Degradation of Chromophoric Dissolved Organic Matter Exported From Tidal Marshes. *Journal of Geophysical Research: Biogeosciences* 126(4), doi: 10.1029/2020JG005744.

Maher, D., Eyre, B. 2010. Benthic fluxes of dissolved organic carbon in three temperate Australian estuaries: Implications for global estimates of benthic DOC fluxes. *Journal of Geophysical Research: Biogeosciences* 115(4), doi: 10.1029/2010JG001433.

McKnight, D.M., Bencala, K.E., Zellweger, G.W., Aiken, G.R., Feder, G.L., Thorn, K.A. 1992. Sorption of Dissolved Organic Carbon at the Confluence of Deer Creek with the Snake River, Summit County, Colorado. *Environmental Science and Technology* 26, 1388-1396.

Mcleod, E., Chmura, G., Bouillon, S., Salm, R., Bjork, M., Duarte, C., Lovelock, C., Schlesinger, W., Silliman, B. 2011. A blueprint for blue carbon: toward an improved understanding of the role of vegetated coastal habitats in sequestering CO_2. *Frontiers in Ecology and the Environment* 9(10), 552-560.

Mitsch, W., Bernal, B., Nahlik, A., Mander, U., Zhang, L., Anderson, C., Jorgensen, S., Brix, H. 2013. Wetlands, carbon, and climate change. *Landscape Ecology* 28(4), 583-597.

Moffett, K., Nardin, W., Silvestri, S., Wang, C., Temmerman, S. 2015. Multiple stable states and catastrophic shifts in coastal wetlands: Progress, challenges, and opportunities in validating theory using remote sensing and other methods. *Remote Sensing* 7(8), 10184-10226.

Morris, J., Barber, D., Callaway, J., Chambers, R., Hagen, S., Hopkinson, C., Johnson, B., Megonigal, Pl, Neubauer, S., Troxler, T., Wigand, C. 2016. Contributions of organic and inorganic matter to sediment volume and accretion in tidal wetlands at steady state. *Earth's Future* 4(4), 110-121.

Morris, J., Sundareshwar, P., Nietch, C., Bjo, B., Kjerfve, B., Cahoon, A. 2002. Responses of Coastal Wetlands to Rising Sea Level. *Ecology* 83(10), 2869-2877.

[a]Morrissette, H.K., Long, W., Hood, R.R. Effect of increasing sorption complexity on a Sediment Flux Model for dissolved organic matter interactions. *in prep.*

[b]Morrissette, H.K., Pinsonneault, A.J., Neale, P.J., Tzortziou, M., Hood, R.R. Wetland soil biogeochemistry influences the kinetics of dissolved organic carbon sorption. *in prep.*

[c]Morrissette, H.K., Pinsonneault, A.J., Neale, P.J., Tzortziou, M., Hood, R.R. Optical properties as tools to track wetland dissolved organic carbon transformation and movement via sorption over time. *in prep.*

[d]Morrissette, H.K., Pinsonneault, A.J., Neale, P.J., Tzortziou, M., Hood, R.R. Resolving the spatial variaibility in tidal marsh sediment dissolved organic matter sorption kinetics. *in prep.*

[e]Morrissette, H.K., Tay, J., Neale, P.J., Tzortziou, M., Hood, R.R. Simplified model to track dissolved organic carbon sorption. *in prep.*

Nahlik, A., Fennessy, M. 2016. Carbon storage in US wetlands. *Nature Communications* 7, doi: 10.1038/ncomms13835.

Najjar, R. G., Herrmann, M., Alexander, R., Boyer, E. W., Burdige, D. J., Butman, D., et al. 2018. Carbon budget of tidal wetlands, estuaries, and shelf waters of eastern North America. *Global Biogeochemical Cycles* 32, 389–416. https://doi.org/10.1002/2017GB005790

Neubauer, S.C. 2013. Ecosystem Responses of a Tidal Freshwater Marsh Experiencing Saltwater Intrusion and Altered Hydrology. *Estuaries and Coasts* 36, 491-507.

Neubauer, S.C., Anderson, I.C. 2003 Transport of dissolved inorganic carbon from a tidal freshwater marsh to the York River estuary. *Limnology and Oceanography* 48(1), 299-307.

Neubauer, S.C., Franklin, R.B., Berrier, D.J. 2013. Saltwater intrusion into tidal freshwater marshes alters the biogeochemical processing of organic carbon. *Biogeosciences Discusssion* 10, 10685-10720.

Nicholls, R.J., Hoozemans, F.M.J., Marchand, M. 1999. Increasing flood risk and wetland losses due to global sea-level rise: regional and global analyses. *Global Environmental Change* 9, S69-S87.

Nuttle, W.K. 1988. The Extent of Lateral Water Movement in Sediments of a New England Salt Marsh. *Water Resources Research* 24(12), 2077-2085.

Ohno, T. 2002. Fluorescence Inner-Filtering Correction for Determining the Humification Index of Dissolved Organic Matter. *Environmental Science and Technology* 36, 742-746.

Osburn, C., Mikan, M., Etheridge, J., Burchell, M., Birgand, F. 2015. Seasonal variabion in the quality of dissolved and particulate organic matter exchanged between a salt marsh and its adjacent estuary. *Journal of Geophysical Research: Biogeosciences* 120(7), 1430-1449.

Ouyang, X., Lee, S. 2014. Updated estimates of carbon accumulation rates in coastal marsh sediments. *Biogeosciences* 11(18), 5057-5071.

Pendleton, L., Donato, D. C., Murray, B. C., Crooks, S., Jenkins, W. A., Sifleet, S., et al. 2012. Estimating global "blue carbon" emissions from conversion and degradation of vegetated coastal ecosystems. *PLoS One* 7(9), e43542. https://doi.org/10.1371/journal.pone.0043542

Pinsonneault, A.J., Neale, P.J., Tzortziou, M., Canuel, E.A., Pondell, C.R., Morrissette, H.K., Lefcheck, J.S., Megonigal, J.P. 2021. Dissolved organic carbon sorption dynamics in tidal marsh soils. *Limnology and Oceanography* 66(1), 214-225.

Pinsonneault, A.J., Neale, P.J., Megonigal, J.P., Tzorztiou, M., Canuel, E.A., Pondell, C.R., Morrissette, H.K. Sorption Processes Alter Dissolved Organic Carbon Composition in Tidal Marsh Soils. *in prep.*

Pinsonneault, A.J., Megonigal, J.P., Neale, P.J., Tzortziou, M., Canuel, E.A., Pondell, C.R., Morrissette, H.K. Soils and Tides Regulate Spatiotemporal Patterns in Tidal Marsh Dissolved Organic Carbon. *In prep.*

Portnoy, J.W. 1999. Salt Marsh Diking and Restoration: Biogeochemical Implications of Altered Wetland Hydrology. *Environmental Management* 24(1), 111-120.

Portnoy, J.W., Giblin, A.E. 1997. Effects of historic tidal restrictions on salt marsh sediment chemistry. *Biogeochemistry* 36, 275-303.

Pratolongo, P., Leonardi, N., Kirby, J., Plater, A. 2018. Temperate coastal wetlands. In *Coastal Wetlands: An Integrated Ecosystem Approach* (pp. 105-152).

Pumpanen, J., Linden, A., Miettinen, H., Kolari, P., Ilvesniemi, H., Mammarella, I., Hari, P., Nikinmaa, E., Heinonsalo, J., Back, J., Ojala, A., Berninger, F., Vesala, T. 2014. Precipitation and net ecosystem exchange are the most important drivers of DOC flux in upland boreal. *Journal of Geophysical Research: Biogeosciences* 119(9), 1861-1878.

Qi, M., MacGregor, J., Gedan, K. 2021. Biogeomorphic patterns emerge with pond expansion in deteriorating marshes affected by relative sea level rise. *Limnology and Oceanography* 66, 1036-1049.

Qualls, R.G. 2000. Comparison of the behavior of soluble organic and inorganic nutrients in forest soils. *Forest Ecological Management* 138, 29-50.

Qualls, R.G., Haines, B.L. 1992. Measuring adsorption isotherms using continuous, unsaturated flow through intact soil cores. *Soil Science Society of America* 56, 456-460.

Qualls, R.G., Richardson, C.T. 2003 Factors Controlling Concentration, Export, and Decomposition of Dissolved Organic Nutrients in the Everglades of Florida. *Biogeochemistry* 62, 197-229.

Raymond, P.A., Spencer, R.G.M. 2015. "Riverine DOM" in *Biogeochemistry of Marine Dissolved Organic Matter* (Elsevier), 509-533.

Shaker, A.M., Komy, Z.R., Heggy, S.E.M., El-Sayed, M.E.A. 2012. Kinetic Study for Adsorption Humic Acid on Soil Minerals. *Journal of Physical Chemistry* 116, 10889-10896.

Reay, W.G., Moore, K.A. 2009. Introduction to the Chesapeake Bay National Estuarine Research Reserve in Virginia. *Journal of Coastal Research* 57, 1-9.

Shields, M.R., Bianchi, T.S., Gelinas, Y., Allison, M.A., Twilley, R.R. 2016. Enhanced terrestrial carbon preservation promoted by reactive iron in deltaic sediments. *Geophysical Research Letters* 43, 1149-1157.

Soetaert, K., Petzoldt, T., Setzer, R.W. (2010). Solving Differential Equations in R: Package deSolve. *Journal of Statistical Software* 33(9), 1-25. URL http://www.jstatsoft.org/v33/i09/ DOI 10.18637/jss.v033.i09

Spivak, A., Sanderman, J., Bowen, J., Canuel, E., Hopkinson, C. 2019. Global-change controls on soil-carbon accumulation and loss in coastal vegetated ecosystems. *Nature Geoscience* 12(9), doi: 10.1038/s41561-019-0435-2.

Stedmon, C., Nelson, N. 2015. The Optical Properties of DOM in the Ocean. In *Biogeochemistry of Marine Dissolved Organic matter: Second Edition*, D.A. Hansell and C.A. Carlson, eds. Cambridge, MA: Academic Press. (pp. 481-508). doi: 10.1016/B978-0-12-405940-5.00010-8.

Steinmuller, H.E., Dittmer, K.M., White, J.R., Chambers, L.G. 2019. Understanding the fate of soil organic matter in submerging coastal wetland soils: A microcosm approach. *Geoderma* 337, 1267-1277.

Stow, C.A., Jolliff, J., McGillicuddy, D.J., Doney, S.C., Allen, J.I., Friedrichs, M.A., Wallhead, P. 2009. Skill assessment for coupled biological/physical models of marine systems. *Journal of Marine Systems* 76(1-2), 4-15.

Tavakkoli, E., Derrien, M., Rengasamy, P., McDonald, G. 2014. Adsorption of dissolved organic carbon to carbonate minerals and alkaline soils. Soil Science 2014 Conference.

Taylor, D.I., Allanson, B.R. 1995. Organic carbon fluxes between high marsh and estuary, and the inapplicability of the Outwelling Hypothesis. *Marine Ecology Progress Series* 120, 263-270.

Testa, J.M., Brady, D.C., Di Toro, D.M., Boynton, W.R., Cornwell, J.C., Kemp, W.M., 2013. Sediment flux modeling: Simulating nitrogen, phosphorus, and silica cycles. *Estuarine, Coastal, and Shelf Science* 131, 245-263.

Thomas, C., Miao, S., Sindjoj, E. 2009. Environmental factors affecting temporal and spatial patterns of soil redox potential in Florida everglades wetlands. *Wetlands* 29(4), 1133-1145.

Tobias, C., Neubauer, S. 2018. Salt marsh biogeochemistry - An overview. doi: 10.1016/B978-0-444-63893-9.00016-2.

Tzortziou, M., Neale, P.J., Megonigal, J.P., Pow, C.L., Butterworth, M. 2011. Spatial gradients in dissolved carbon due to tidal marsh outwelling into a Chesapeake Bay estuary. *Marine Ecology Progress Series* 426, 41-56.

Tzortziou, M., Neale, P.J., Osburn, C.L., Megonigal, J.P., Maie, N., Jaffe, R. 2008. Tidal marshes as a source of optically and chemically distinctive colored dissolved organic matter in the Chesapeake Bay. *Limnology and Oceanography* 53, 148-159.

Tzortziou, M., Zeri, C., Dimitriou, E., Ding, Y., Jaffe, R., Anagnostou, E., Pitta, E., Mentzafou, A. 2015. Colored dissolved organic matter dynamics and anthropogenic influences in a major transboundary river and its coastal wetland. *Limnology and Oceanography* 60(4), doi: 10.1002/lno.10092?sid=worldcat.org.

Vantrepotte, V., Danhiez, F-P., Loisel, H., Ouillon, S., Meriaux, X., Cauvin, A., Dessailly, D. 2015. CDOM-DOC relationship in contrasted coastal waters: implication for DOC retrieval from ocean color remote sensing observation. *Optical Society of America* 23(1), doi: 10.1364/OE.23.000033.

Wagai, R., Mayer, L.M. 2007. Sorptive stabilization of organic matter in soils by hydrous iron oxides. *Geochimica and Cosmochimica Acta* 71, 25-35.

Wang, Z.A., Cai, W.-J. 2004. Carbon dioxide degassing and inorganic carbon export from a marsh-dominated estuary (the Duplin River): A marsh CO2 pump. *Limnology and Oceanography* 49, 341-354.

Wang, Z.A., Kroeger, K.D., Ganju, N.K., Gonneea, M.E., Chu, S.N. 2016. Intertidal salt marshes as an important source of inorganic carbon to the coastal ocean. *Limnology and Oceanography* 61, 1916-1931.

Wang, S., Jin, X., Zhao, H., Zhou, X., Wu, F. 2007. Effect of organic matter on the sorption of dissolved organic and inorganic phosphorus in lake sediments. *Colloids and Surfaces A: Physiochemical Engineering Aspects* 297, 154-162.

Ward, N.D., Bianchi, T.S., Medeiros, P.M., Seidel, M., Richey, J.E., Keil, R.G., Sawakuchi, H.O. 2017. Where Carbon Goes When Water Flows: Carbon Cycling across the Aquatic Continuum. *Frontiers of Marine Science* 4. doi: 10.3389/fmars.2017.00007.

Wattel-Koekkoek, E.J.W., Buurman, P. 2004. Mean Residence Time of Kaolinite and Smectite-Bound Organic Matter in Mozambiquan Soils. *Soil Science Society of America Journal* 68(1), 154-161.

Weston, N.B., Vile, M.A., Neubauer, S.C., Velinsky, D.J. 2011. Accelerated microbial organic matter mineralization following salt-water intrusion into tidal freshwater marsh soils. *Biogeochemistry* 102, 135-151.

Wilson, A., Moore, W., Joye, S., Anderson, J., Schutte, C. 2011. Storm-driven groundwater flow in a salt marsh. *Water Resources Research* 47(2), 2535. doi: 10.1029/2010WR009496.

Windham-Myers, L., W.-J. Cai, S. R. Alin, A. Andersson, J. Crosswell, K. H. Dunton, J. M. Hernandez-Ayon, M. Herrmann, A. L. Hinson, C. S. Hopkinson, J. Howard, X. Hu, S. H. Knox, K. Kroeger, D. Lagomasino, P. Megonigal, R. G. Najjar, M.-L. Paulsen, D. Peteet, E. Pidgeon, K. V. R. Schäfer, M. Tzortziou, Z. A. Wang, and E. B. Watson. 2018. Chapter 15: Tidal wetlands and estuaries. In Second State of the Carbon Cycle Report (SOCCR2): A Sustained Assessment Report [Cavallaro, N., G. Shrestha, R. Birdsey, M. A. Mayes, R. G. Najjar, S. C. Reed, P. Romero- Lankao, and Z. Zhu (eds.)]. U.S. Global Change Research Program, Washington, DC, USA, pp. 596-648, https://doi.org/10.7930/SOCCR2.2018.Ch15.

Worrall, F., Burt, T., Jaeban, R., Warburton, J., Shedden, R. 2002. Release of dissolved organic carbon from upland peat. *Hydrological Processes* 16(17), 3487-3504.

Xing, B., Pignatello, J.J. 1996. Time-dependent isotherm shape of organic compounds in soil organic matter: Implications for sorption mechanism. *Environmental Toxicology and Chemistry* 15(8), 1282-1288.

Xu, M. 2016. Exponential model fitting. http://stats.stackexchange.com/questions/32824/how-to-minimize-residual-sum-of-squares-of-an-exponential-fit/32832

Yang, S., Li, H., Yzebaert, T., Bouma, T., Zhang, W., Wang, Y., Li, P., Li, M., Ding, P. 2008. Spatial and temporal variations in sediment grain size in tidal

wetlands, Yangtze Delta: On the role of physical and biotic controls. *Estuarine, Coastal and Shelf Science.* 77(4), 657-671.

Yelverton, G.F., Hackney, C.T. 1986. Flux of dissolved organic carbon and pore water through the substrate of a *Spartina alterniflora* marsh in North Carolina. *Estuarine, Coastal and Shelf Science* 22(2), 255-267.

Yurova, A., Sirin, A., Buffam, I., Bishop, K., Laudon, H. 2008. Modeling the dissolved organic carbon output from a boreal mire using the convection-dispersion equation: Importance of representing sorption. *Water Resources Research* 44(7), 7411. doi: 10.1029/2007WR006523.

Zhou, Z., Meng, H., Liu, Y., Gu, J., Li, M. 2017. Stratified bacterial and archaeal community in mangrove and intertidal wetland mudflats revealed by high throughput 16S rRNA gene sequencing. *Frontiers in Microbiology* 8(NOV), 2148.

Zhuang, W., Yang, L. 2018. Impacts of global changes on the biogeochemistry and environmental effects of dissolved organic matter at the land-ocean interface: a review. *Environmental Science and Pollution Research* 25(5), 4165-4173.